Reconstructing the Plio – Pleistocene evolution of the water mass exchange and climate variability in the Nordic Seas and North Atlantic Ocean

Dissertation
zur Erlangung des Doktorgrades
Dr.rer.nat.

der Mathematisch-Naturwissenschaftlichen Fakultät der
Christian-Albrechts Universität
zu Kiel

vorgelegt von
Claudia Teschner

Kiel, 2013

1. Gutachter und Betreuer:	Prof. Dr. Martin Frank
2. Gutachter:	Prof. Dr. Anton Eisenhauer

Tag der Disputation:	10.01.2014
Zum Druck genehmigt:	13.01.2014

Gez. Prof. Dr. Wolfgang J. Duschl, Dekan

Erklärung

Hiermit versichere ich an Eides statt, dass ich diese Dissertation selbstständig und nur mit Hilfe der angegebenen Quellen und Hilfsmittel erstellt habe. Ferner versichere ich, dass der Inhalt dieses Dokuments weder in dieser, noch in veränderter Form einer weiteren Prüfungsbehörde vorliegt. Die Arbeit ist unter Einhaltung der Regeln guter wissenschaftlicher Praxis der Deutschen Forschungsgemeinschaft entstanden.

Kiel, 06.05.2013

Claudia Teschner

Contents

Abstract

Global climate of the Plio-Pleistocene has been largely impacted by changes of the Atlantic Meridional Overturning Circulation (AMOC), which has most likely to a large extent been controlled by the formation of North Atlantic Deep Water (NADW) ventilating the entire Atlantic Ocean. The main areas contributing to the formation of NADW have been the Labrador Sea, the Nordic Seas, and North Atlantic Ocean. The circulation pattern in these areas underwent dramatic changes during the Plio – and Pleistocene, in particular during the onset and intensification of the Northern Hemisphere Glaciation (NHG) at 2.7 Ma and the Mid Pleistocene Transition (MPT) 1.5 – 0.6 Ma. The main goal of this study is to improve the understanding of the role of changes in ocean circulation in these key areas and their relationships to glaciations controlling and responding to climate. To investigate the past water mass mixing and erosional input between the climatically important areas of Nordic Seas and North Atlantic Ocean, the radiogenic isotope signatures of neodymium (Nd), lead (Pb) and strontium (Sr) of seawater-derived ferromanganese coatings on sediment particles, as well as of detrital material have been analyzed.

Sediments obtained from six ODP (Ocean Drilling Program) Sites covering intermediate to deep waters in the Nordic Seas and North Atlantic Ocean are the basis of this study. Two Sites are located in the North Atlantic Ocean on Bjørn Drift (Site 984) in 1648 m water depth and on Rockall Plateau (Site 982) in 1135 m water depth. The sites in the Nordic Seas are located in the region influenced by Arctic Intermediate Water on Iceland Plateau (Site 907, 1800 m water depth) and of the inflowing Atlantic waters on Vøring Plateau (Site 644, 1220 m water depth), on the Svalbard margin (Site 986, 2051 m deep) and on Yermak Plateau in the Fram Strait (Site 911, 906 m water depth). The extraction of seawater Nd and Pb isotope compositions from authigenic ferromanganese coatings, as well as Nd isotope composition from the calcitic foraminiferal shells from locations in the western part of the study area (Sites 907 and 984) gave no reliable results as compared to the present seawater signatures in this area [*Lacan and Jeandel*, 2004b], mainly as a consequence of partial dissolution of basaltic ash particles during the extraction procedures. In contrast, for the sites (982, 644, 986, 911) in the eastern part of the Nordic Seas and in the North Atlantic Ocean reliable past

bottom water signatures were extracted using different leaching methods and allow paleoreconstructions for the past 3 - 5 Ma.

The Nd and Pb isotope records of ferromanganese coatings of Site 911 on the Yermak Plateau were extracted with a leach method based on studies by *Haley et al.* [2008a, 2008b] without a preceding decarbonation step. These records show only small variations prior to 2.7 Ma pointing to a continuous Atlantic inflow under generally warmer climatic conditions. In contrast, since the intensification of the Northern Hemisphere Glaciation the Nd isotope composition has shown a high variability as a consequence of the waxing and waning of ice sheets on Svalbard, the Barents Sea and Eurasia. The Pb record at the same time reveals a trend to more radiogenic values as a result of increasing glacial weathering inputs from old continental landmasses after 2 Ma. A similar evolution is evident from the Nd and Pb isotope records of Sites 986, 644 and 982, which were extracted from seawater derived ferromanganese coatings applying the leaching method of *Gutjahr et al.* [2007]. Comparison of the Nd isotope records of these three ODP sites shows periods of a warmer climate, moderate glacial conditions and an enhanced Atlantic inflow into the Nordic Seas prior to the onset of the NHG at 2.7 Ma and between 2.2 Ma and 1.5 Ma. In contrast, at the beginning of the MPT between 1.5 and 1.2 Ma the Atlantic inflow was significantly reduced, expressed as marked differences between the Nd isotope records in the Nordic Seas and North Atlantic Ocean.

Sediment provenance obtained from Nd and Pb isotope compositions of the detrital material shows a dominant influence of Svalbard, Barents Sea and Eurasian shelf at the sites on the Svalbard margin and Yermak Plateau. The Vøring Plateau has been dominated by sediment input from Scandinavia to which material from the Barents Sea via icebergs and sea ice was added during glaciations. In contrast, the Rockall Plateau shows the lowest erosional influence due to its location distant from land. However, the Pb isotope evolution obtained from ferromanganese coating of sediment of Site 982 nevertheless points to a slightly increased erosional input from Greenland and Iceland after 1.2 Ma. The results of this study provide a deeper insight into the overall climate control mechanisms of the past 5 Myr and will contribute to improve the understanding of future climatic change.

Zusammenfassung

Das globale plio-pleistozäne Klima ist in hohem Maße durch die atlantische thermohaline Zirkulation beeinflusst worden, die wahrscheinlich hauptsächlich durch die Bildung von Nordatlantischem Tiefenwasser angetrieben wurde, das heute den gesamten Atlantischen Ozean belüftet. Hauptgebiete für die Entstehung des Nordatlantischen Tiefenwassers sind die Labrador See, die Grönländisch-Norwegische See und der Nordatlantische Ozean. Das Zirkulationsmuster in diesen Gebieten unterlag während des Plio-Pleistozäns signifikanten Änderungen, besonders während der Intensivierung der Nordhemisphärenvereisung vor 2.7 Millionen Jahren und des Mittelpleistozänen Klimawandels vor 1.5 bis 0.6 Millionen Jahren. Das Hauptziel dieser Studie ist die Verbesserung des Verständnisses der Zusammenhänge zwischen Änderungen der Zirkulation und der kontinentalen Vereisung und des Klimas. Um die Wassermassenverteilung und den Verwitterungseintrag zwischen den klimarelevanten Gebieten der Grönländisch-Norwegischen See und dem Atlantischen Ozean zu untersuchen, wurden die radiogenen Isotopenverhältnisse von Neodym (Nd), Blei (Pb) und Strontium (Sr) aus dem authigenen Mangan-Eisenoxidcoating der Partikel und die Isotopensignaturen der Sedimentpartikel selbst analysiert.

Sechs Sedimentkerne des Ocean Drilling Programms (ODP) aus intermediären und tiefen Wasserschichten in der Grönländisch-Norwegischen See und dem Atlantischen Ozean waren die Basis dieser Studie. Zwei Kerne wurden im Atlantischen Ozean auf dem Bjørn Drift (Site 984) in 1648 m Wassertiefe und auf dem Rockall Plateau (Site 982) in 1135 m Wassertiefe gewonnen. Die Kerne in der Grönländisch-Norwegischen See befinden sich im Einflussbereich des Arktischen Zwischenwassers auf dem Island Plateau (Site 907, 1800 m tief) und des einströmenden Atlantikwassers auf dem Vøring Plateau (Site 644, 1220 m tief), auf dem Svalbard-Schelf (Site 986, 2051 m tief) und auf dem Yermak Plateau in der Framstraße (Site 911, 906 m tief). Die Nd- und Pb- Isotopenverhältnisse aus dem authigenen Mangan-Eisenoxidcoating, sowie die Nd-Isotopenverhältnisse aus Foraminiferenkalzit an den Kernlokationen im westlichen Teil des Gebiets (Site 907 und 984) wurden verglichen mit den heutigen Wassermassenzusammensetzungen in

diesem Gebiet [*Lacan und Jeandel*, 2004b] und ergaben keine verlässlichen Daten, hauptsächlich durch die teilweise Lösung von basaltischen Aschepartikeln. Für die Kerne (982, 644, 986 und 911) im östlichen Teil der Grönländisch-Norwegischen See und dem Nordatlantischen Ozean war es möglich, verlässliche Tiefenwassersignaturen unter Verwendung verschiedener Laugungsmethoden zu gewinnen, die die Erstellung weitergehender Paläorekonstruktionen über die vergangenen 3 bis 5 Millionen Jahre erlaubte.

Die Nd- und Pb-Isotopenzeitserien der Mangan-Eisenoxidcoatings von Site 911 auf dem Yermak Plateau wurden durch Anwendung der Laugungsmethode von *Haley et al.* [2008a, 2008b] ohne einen vorherigen Entkarbonatisierungsschritt gewonnen. Diese Daten zeigen nur geringe Schwankungen im Zeitraum vor 2.7 Millionen Jahren, was auf einen kontinuierlichen Zufluss von Atlantikwasser unter generell wärmeren Klimabedingungen hindeutet. Seit dem Beginn der Nordhemisphären-Vereisung zeigten die Neodym-Isotopendaten eine höhere Variabilität als Folge der wachsenden und schrumpfenden Eisschilde auf Svalbard, der Barents See und dem Eurasischen Schelf. Die Blei-Isotopenzeitserien zeigen einen Trend zu radiogeneren Werten als Konsequenz des zunehmenden glazialen Verwitterungseintrags von den alten kontinentalen Landmassen im Zeitraum nach 2 Millionen Jahren. Eine ähnliche Entwicklung konnte in den Nd- und Pb-Isotopenzeitserien von Site 986, 644 und 982, die nach der Laugungsmethode von *Gutjahr et al.* [2007] extrahiert wurden, beobachtet werden. Der Vergleich der Nd-Isotopendaten dieser drei ODP Kerne zeigt Perioden von wärmerem Klima, moderaten Vereisungsbedingungen und einem verstärktem Atlantikwassereinflusses in die Grönländisch-Norwegische See vor dem Einsetzen der Nordhemisphären-Vereisung (2.7 Millionen Jahre vor heute) sowie zwischen 2.2 und 1.5 Ma. Zu Beginn des mittelpleistozänen Klimawandels zwischen 1.5 und 1.2 Millionen Jahren hingegen war der Atlantikwassereinfluss vermindert, was sich in einer signifikant unterschiedlichen Nd-Isotopie in der Grönländisch-Norwegischen See und dem Nordatlantischen Ozean ausdrückte.

Die Rekonstruktion der Quellen der detritischen Sedimente selbst, die auf der Basis der Nd- und Pb- Isotopenverhältnisse des detritischen Materials erstellt wurde, zeigt einen dominanten Einfluss von Svalbard, der Barents See und des Eurasischen

Schelfs auf die Kerne am Svalbard-Schelf und auf dem Yermak Plateau. Das Vøring Plateau war bestimmt durch den Sedimenteintrag von Skandinavien und teilweise von der Barents See durch den Transport durch Eisberge und Meereis während der zunehmenden Vereisung. Das Rockall Plateau hingegen zeigt einen geringeren Verwitterungseintrag aufgrund der größeren Entfernung zum Land. Dennoch deuten die Blei-Isotopenverhältnisse auf einen leichten Anstieg des Erosionseintrags von Grönland und Island in den letzten 1.2 Millionen Jahren hin. Die Ergebnisse dieser Studie öffnen einen tieferen Einblick in die übergeordneten Klimakontrollmechanismen der letzten 5 Millionen Jahre und werden das Verständnis der zukünftigen Klimaentwicklungen verbessern.

CHAPTER 1

Introduction

1.1. MOTIVATION AND PREVIOUS WORK

The Nordic Seas and the northernmost Atlantic Ocean are key areas for the interaction of deep water formation with global climate (Fig. 1.1). There, North Atlantic Deep Water (NADW) is formed and plays a crucial role for the global climate system as it affects the Atlantic Meridional Overturning Circulation (AMOC), which is responsible for the ventilation of the entire Atlantic Ocean [*Broecker et al.*, 1985; *Rahmstorf*, 2002; *Kuhlbrodt et al.*, 2007].

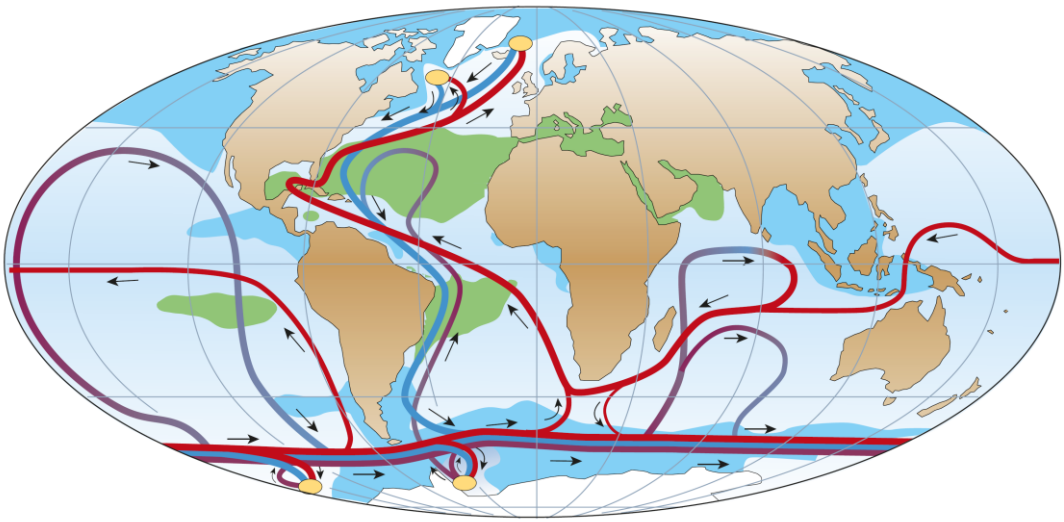

Figure 1.1: Simplified map of the thermohaline circulation system [Rahmstorf, 2002]. *The yellow circles present the areas of deep water formation in the Labrador Sea, Nordic Seas, Ross Sea and Weddell Sea. The warm surface currents are displayed in red, deep currents in blue, bottom currents in purple and the direction of the currents as black arrows.*

The relevance of this area is to balance heat gain at low latitudes and heat loss at high latitudes. Heat is sent polewards as warm ocean currents and through the atmosphere, and in turn freshwater from rivers and ice melt is exported from high latitudes. The anthropogenic impact contribute significantly to the global warming and

influence the atmospheric and circulation system between the Arctic and Atlantic Ocean negatively. It leads to a greater temperature increase in the Arctic Ocean during the last 100 yrs, hence climate models predict an amplified warming for the Arctic Ocean in the future. Several studies document the increased warming of the Atlantic inflow through the Fram Strait [*Spielhagen et al.*, 2011] and further along the Siberian shelf [*Dmitrenko et al.*, 2008, 2010, 2012] during the past 100 yrs. The input of warm Atlantic water into the Arctic Ocean in turn strongly affects the sea ice distribution due to enhanced melting, caused by the warm inflow waters. This could have a large impact on the circulation in the Atlantic Ocean, because huge amounts of freshwater, which could be released and cause a significant rise in sea level, are stored in the Arctic Ocean. *Aagaard and Carmack* [1989] assumed 80,000 km^3 of freshwater, mainly stored in the form of sea ice and icebergs in the Arctic Ocean and additionally 50,000 km^3 in the marginal seas of the Arctic Ocean. Increased freshwater export from the Arctic Ocean into the Nordic Seas and North Atlantic can cause a reduction of the deep water formation [e.g., *Ganopolski and Rahmstorf,* 2001; *Peltier et al.*, 2006; *Clark et al.*, 2002], which has had a large impact on the regional and global climate. Hence, it is of major importance to investigate the changes in the balance between deep water formation and freshwater export, which controls the strength of the global thermohaline circulation today. This balance underwent changes as a consequence of extreme climate phases, e.g. by the large glaciations over the Plio – and Pleistocene. Hence, to get an idea about the future evolution of the circulation change in this important area, it is of main importance to understand the climate and circulation variability during the past.

Since the Plio – Pleistocene the North Atlantic Ocean and Nordic Seas experienced major changes. During the past 5 Myrs, the largest shifts of the global climate occurred through the onset and intensification of the Northern Hemisphere Glaciation (NHG) at ~2.7 Ma as well as during the Mid Pleistocene Glaciation (MPT) between ~1.5 to 0.6 Ma. Prior to 3 Ma the Northern Hemisphere was relatively warm and forests grew along the shores around the Arctic Ocean [*Knies et al.*, 2002]. After the onset, of both the NHG and MPT, the circulation patterns and sediment transport pathways underwent drastic changes in these areas due to the glacial/interglacial alternations between build up and regression of huge ice sheets on the Northern Hemisphere. The adjacent oceans were affected through enhanced glacial sea-ice

formation and changes in deep water formation. This study provides new insights into the future climate by reconstructing the climatic evolution of the past 5 Myr and by a deeper understanding of its controlling factors.

Numerous studies to reconstruct the paleoceanographic evolution of the Nordic Seas and the North Atlantic Ocean were performed on the basis of micropaleontological and sedimentological proxies, such as stable oxygen and carbon isotopes and the abundances of ice rafted debris (IRD) [e.g. *Jansen et al.*, 1989, *Jansen and Sjøholm*, 1991; *Raymo and Ruddiman*, 1992; *Raymo et al.*, 2004; *Kleiven et al.*, 2002, 2003; *Knies et al.*, 2002, 2009]. The common stable isotope methods are problematic in the high latitudes because the sediments, especially in the Northern Nordic Seas and the Arctic Ocean are barren of foraminifera. Therefore, the reconstruction of water mass exchange and sediment input on the basis of radiogenic isotopes as Nd and Pb was applied in this study. Furthermore, studies using radiogenic isotopes (neodymium, lead, strontium) in ferromanganese crusts, foraminifera and authigenic ferromanganese coatings on sediment particles as well as on bulk sediment were carried out in the Arctic Ocean [*Winter et al.*, 1997; *Haley et al.*, 2008a, 2008b] and the North Atlantic Ocean [e.g. *Burton et al.*, 1997, *Reynolds et al.*, 1999, *Crocket et al.*, 2010; *Roberts et al.*, 2010; *Elmore et al*., 2011]. The aim of this study was to understand the long term variations of the regional intermediate and deep water circulation patterns in the Nordic Seas and North Atlantic Ocean and its linkage to the climate variability based on radiogenic isotopes extracted from the authigenic ferromanganese coatings on sediment particles as well as of the detrital section of the bulk sediments during Plio (5.33 – 2.58 Ma) – and Pleistocene (2.58 – 0.0117 Ma) focusing on the major climate shifts (NHG and MPT). In particular the goals were:

- *Verification of different leach methods to extract seawater radiogenic isotope ratios from ferromanganese oxyhydroxide coatings on sediment particles and their application to different areas in the Nordic Seas and North Atlantic Ocean*. For this purpose a total of six sediment cores were sampled. Radiogenic isotopes from ferromanganese coatings on sediment particles were extracted and the core top values were compared to seawater neodymium (Nd) isotope data from nearby water profiles.

- *Reconstruction of changes in the water mass circulation between the Nordic Seas and North Atlantic Ocean over the past 3 Myrs*. To achieve this, down core records of the Nd and Pb isotope composition of past seawater were obtained from sediment coatings and were compared to previous paleoceanographic studies from the Arctic and Atlantic Ocean.

- *Changes in the sediment provenance and transport mechanisms in the Nordic Seas* based on Nd and Pb isotope compositions of the bulk sediment, were reconstructed from the sediment cores.

Concerning the NHG this study aims to answer the questions:

- *Were the circulation patterns between North Atlantic Ocean, Nordic Seas and Arctic Ocean similar to and as stable as today or did they undergo drastic changes? Were these changes drivers of past environmental and climatic changes or did they change as a consequence of climatic changes?*

- *Did the sediment regime change in a particular basin? Which ice sheets were the main contributors of sediment during glacial times (Laurentide ice sheet, Eurasian, or Fennoscandian ice sheet)?*

Concerning the MPT this study aims to answer the questions:

- *Were changes in ocean circulation recorded by the Nd- isotopes related to changes in the volume and extent of the continental ice sheets as reflected by the IRD content of the sediments? Was the MPT accompanied by any significant changes in ocean circulation?*

- *How did changes in weathering inputs and sediment provenances (from North Canada, Greenland and Siberia), as reflected by paleo seawater Pb and Nd isotopes in the Arctic Ocean, affect the Nordic Seas and North Atlantic Ocean?*

1.2. HYDROGRAPHIC SETTING

1.2.1. Circulation in the North Atlantic Ocean

The Atlantic Meridional Overturning Circulation (AMOC) is one of the main components of the global ocean circulation [*Broecker et al*., 1985]. It is the most important mechanism for the ventilation of the deep Atlantic Ocean and hence a critical feature for the modern climate system. It is characterized by wind-driven surface currents (Gulf Stream, North Atlantic current – NAC) flowing northwards into the Nordic Seas, Labrador Sea and northernmost Atlantic Ocean. There, these warm and saline surface waters cool and sink due to increasing density and form North Atlantic Deep Water (NADW). Labrador Sea Water (LSW) and Nordic Sea Overflow Water with small contributions by Mediterranean Outflow Water (MOW) are the North Atlantic sources of the NADW. Labrador Sea Water (1500 – 2000 m water depth) is formed in the Labrador basin by deep convection from the overlying waters [*Lacan and Jeandel*, 2005b]. This water mass then continues south into the deep North Atlantic Ocean and northwards into the Irminger Basin and Iceland Basin [*Lacan and Jeandel*, 2005b] (Fig. 1.2).

The Nordic Seas Overflow waters, influencing the Atlantic Ocean are formed through convection to intermediate depth dominantly in the Greenland Sea. These water masses can be traced at three different locations between Greenland and the Shetland Islands: Between Greenland and Iceland the East Greenland Current flows through the Denmark Strait (620 m depth), one branch of the Overflow Waters crosses the Iceland – Faroer ridge (300 – 500 m depth) and lastly one branch between Faroer and the Shetland Islands passes the Faroer – Shetland channel (420 – 480 m depth) [*Hansen and Østerhus*, 2000]. This overflow process can be reduced by an enhanced outflow of fresh Arctic waters, ultimately resulting in a reduction of the oceanic heat flux to the northern high latitudes [*Loeng et al.*, 2005].

Several studies indicate that the modern AMOC experienced dramatic changes in the past with a large impact on climate caused e.g. by freshwater inputs and decreased surface ocean salinity [*Knies et al.*, 2007; *Brinkhuis et al*., 2006; *Spielhagen et al.*, 2004]. As a consequence, these water masses did not sink and hence the AMOC

was reduced or even shut down in the past [e.g. *Ganopolski and Rahmstorf*, 2001; *Peltier et al.*, 2006; *Clark et al.*, 2002].

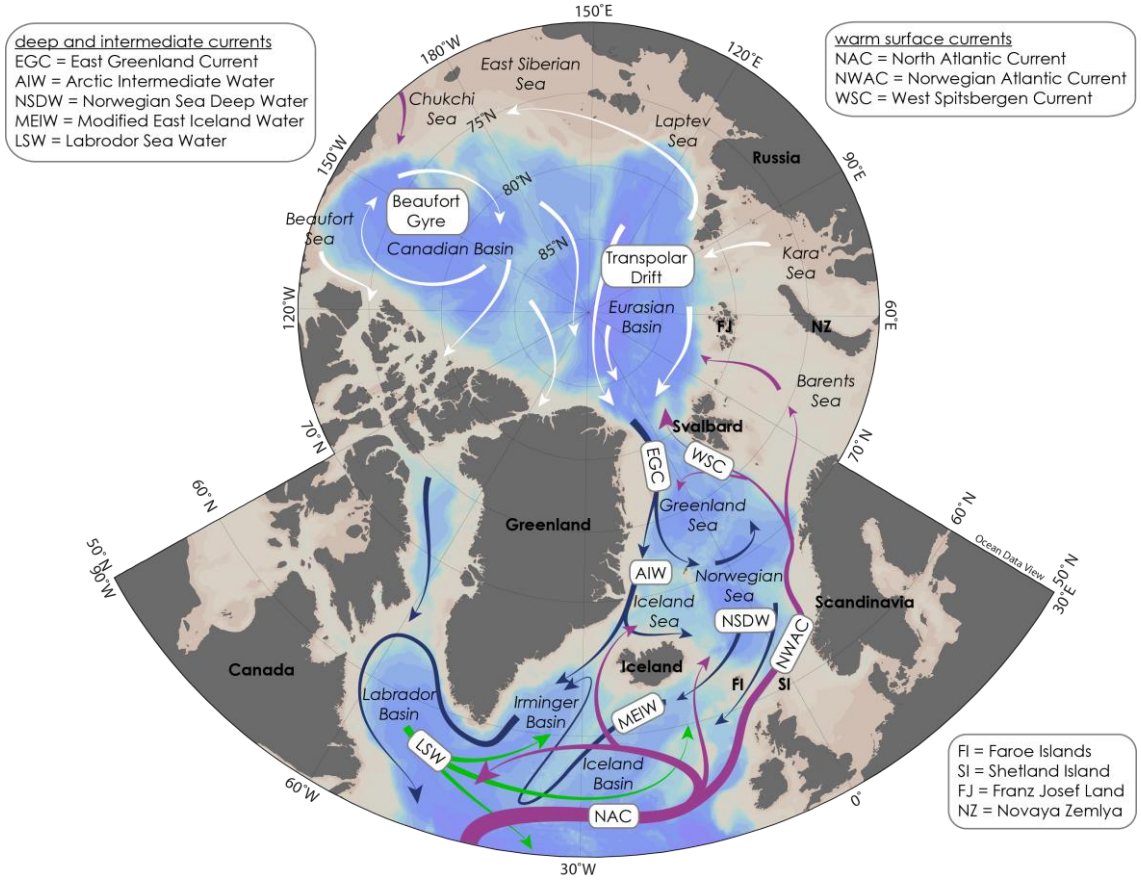

Figure 1.2: Map of the Arctic Ocean, Nordic Seas and northernmost Atlantic Ocean with schematic surface, intermediate and deep currents [after Hansen and Østerhus, 2000; Rahmstorf 2002; Loeng et al., 2005]. *Purple arrows indicate warm, saline Atlantic surface water inflow into the Nordic Seas and the Arctic Ocean, as well as surface water inflow from the North Pacific Ocean through Bering Strait. White arrows mark the surface currents in the Arctic Ocean, including the Beaufort Gyre and the Transpolar Drift, supplying sea ice and freshwater to the Fram Strait and Nordic Seas. The dark blue arrows represent the cold intermediate and deep waters flowing out of the Arctic Ocean and Nordic Seas. The green arrows mark the intermediate water originated in the Labrador basin and its flow directions north in the Irminger and Iceland basin as well as south in the North Atlantic Ocean.*

1.2.2. The Nordic Seas

The Nordic Seas comprise the three ocean basins of the Norwegian Sea in the southeast, the Greenland Sea in the north and the Iceland Sea in the southwest, which are separated from each other by submarine ridges [*Hansen and Østerhus*, 2000]. The area receiving most of the heat input from the warm Atlantic Ocean is the so called Arctic Mediterranean, which includes the eastern part of the Nordic Seas and Arctic Ocean (see 1.2.3) [*Aagaard et al.*, 1985, *Loeng et al.*, 2005]. Warm and saline Atlantic Water flows through the Barents Sea and Fram Strait into the Arctic Ocean forming the Norwegian Atlantic Current (NWAC) and continues further north along the Svalbard margin as West Spitsbergen Current (WSC) (Fig. 1.2). The Atlantic inflow in the Nordic Seas occurs in three branches: The Iceland branch with volume fluxes of 1 Sv (10^6 m^3/s), and the Faroer and Shetland branches each with 3.5 Sv [*Hansen and Østerhus*, 2000]. The Iceland branch having passed Iceland flows eastwards towards the Norwegian Sea, where it mixes with polar waters from the Arctic Ocean and freshwaters from the surrounding landmasses. The Norwegian Sea Deep Water (NSDW), found in the Norwegian Seas, is dominantly formed by a mixing of cold and fresh waters from the Greenland Sea with warmer, saltier Eurasian Basin Deep Water from the Arctic Ocean (see 1.2.3) [*Swift and Koltermann*, 1988]. The Faroer and Shetland branches flow directly into Norwegian Sea, from where they continue as Norwegian Atlantic Current (NWAC) (Fig. 1.2) [*Loeng et al.*, 2005].

The thermohaline circulation in the Nordic Seas results from the increasing density of surface waters by cooling and freezing of the surface waters, which causes convection and sinking to depth. The thermohaline convection is the main driving force of the Atlantic inflow [*Hansen and Østerhus*, 2000] and occurs as a two-step process [*Loeng et al.*, 2005]: Firstly cooling and brine rejection during sea-ice formation lead to an increasing density [*Aagaard et al.*, 1985] and secondly near surface waters are subducted to deeper layers. Atlantic Water enters the Nordic Seas at a temperature close to 8°C, where cooling and brine rejection takes place resulting in a rapid temperature decrease, which is largest in the southern Norwegian Sea. Besides the mainly atmospheric heat loss in ice-free areas, this temperature decrease is caused by the admixture of colder and less saline water masses [*Simonsen and Haugan*, 1996].

The vertical transfer of surface waters in the Nordic Seas is mainly driven by open-ocean convection [*Swift and Aagaard*, 1981], shelf convection [*Rudels*, 1986, *Rudels et al.*, 1994] and other ventilation processes. The boundary current of the NWAC enters the Nordic Seas and continues as an upper-layer flow along the continental slope of Norway and Svalbard to Fram Strait and divides into one branch moving westward towards Greenland and one continuing into the Arctic Ocean (see 1.2.3). There, it continues as a sub-surface current along the Arctic continental slope before leaving the Arctic Ocean again through Fram Strait, from where it continues to flow south as sub-surface boundary current through Denmark Strait [*Rudels et al.*, 2002]. This boundary current sinks mainly due to the large temperature decrease accompanied by a salinity decrease, which occurs during its flow through the Nordic Seas and Arctic Ocean by the isopycnal mixing with surrounding waters (see 1.2.3) [*Loeng et al.*, 2005]. In contrast to the deepening of the boundary current, water masses in the open-ocean sink due to convection after cooling and mixing. Highest vertical velocities occur in the form of plumes or eddies on comparably small horizontal scales on the order of a few kilometers [*Budéus et al.*, 1998; *Gascard et at*, 2002]. Open-ocean convection of water masses reaches mid-depth levels in the Iceland Sea [*Swift and Aagaard*, 1981] and down to 2000 m in the Greenland Seas [*Gascard et al.*, 2002]. Shelf convection as a result of brine rejection producing highly saline and very cold waters sinking to abyssal depths are restricted to the Arctic basin and are the only deep-reaching thermohaline ventilation process, which is however, at present volumetrically not important compared to the other processes described above [*Loeng et al.*, 2005].

The overflow exiting the Nordic Seas consists of a near-bottom flow of cold, dense water from the Arctic Mediterranean. The volume of outflow waters from the Nordic Seas is estimated at 3 Sv through the Denmark Strait [*Dickson and Brown*, 1994], as well as 3 Sv of overflow through the Faroer Bank Channel and the Iceland Faroer ridge via the Modified East Icelandic Water (MEIW) [*Hansen and Østerhus*, 2000; *Saunders*, 2001] (Fig. 1.2).

1.2.3. The Arctic Ocean

The Arctic Ocean consists of the Eurasian basin, the Canadian basin and the surrounding extensive shelf seas (Barents, White, Kara, Laptev, East Siberian and Chukchi Sea) (Fig. 1.2). The Arctic Ocean receives most of its heat input by the warm and saline Atlantic water masses, which enter the Arctic Ocean via the Fram Strait and Barents Sea. A very shallow branch enters the Arctic Ocean from the Pacific Ocean via the Bering Strait (Fig. 1.2). Surface currents, such as the clockwise Beaufort Gyre of the Canadian basin and the counter clockwise Transpolar Drift (TPD) of the Eurasian basin, both influenced by wind forcing [*Loeng et al., 2005*] control the water masses leaving the Arctic Ocean through the Fram Strait and the Canadian Archipelago. Most of the Arctic waters exit as Eurasian Basin Deep Water and Polar Surface Water via Fram Strait, from where they are further transported southwards along East Greenland as the East Greenland Current (EGC) and leaving the Nordic Seas via the Denmark Strait (Fig. 1.2).

The dominant physical feature in the Arctic Ocean is sea ice, which covers the Central Arctic Ocean year-round and controls the heat exchange between the ocean and the atmosphere. It also transports sediments (ice rafted debris, IRD), which had been incorporated on the shelves surrounding the Arctic Ocean during sea ice formation. Sediments from the Laptev/Kara Sea and Barents Sea are therefore transported across the Fram Strait via the Siberian branch of the Transpolar Drift and are released upon melting. In addition, the river runoff plays an important role in the Arctic Ocean. 11% of global river runoff contributes into Arctic Ocean, which represents only 5% of global surface area of the ocean and only 1% of its volume [*Shiklomanov et al.*, 2000]. Riverine and sea-ice derived freshwater inputs influence the stratification and stability of the water column in the Arctic Ocean. A reduction in the freshwater input would possibly induce less freezing, less ice cover and less brine rejection [*Rudels*, 1989]. Hence, the North Atlantic Ocean, Nordic Seas and Arctic Ocean have influenced global circulation and climate substantially and experienced remarkable changes during the Plio – and Pleistocene.

1.3. PLIO – PLEISTOCENE EVOLUTION OF THE NORTH ATLANTIC OCEAN

The past five million years witnessed drastic changes of the global climate, which represented the final stages of the Cenozoic transition from a "greenhouse" to an "icehouse" world. The Pliocene was significantly warmer than today and is thus often seen as a possible analogue for present and future anthropogenic climate changes. The most important climatic changes were the Northern Hemisphere Glaciation starting at ~ 2.7 Ma and the Mid Pleistocene Transition from ~ 1.5 to 0.6 Ma, which are the main focus of this thesis.

1.3.1. The Northern Hemisphere Glaciation

The onset and intensification of the Northern Hemisphere Glaciation at 2.75 Ma was one of the most significant shifts in global climate during the past 5 Ma. First evidence of a glaciation of the Northern Hemisphere was found already during the late Miocene and involved a first build-up of an ice sheet on southern Greenland [*Wolf and Thiede*; 1991; *Jansen and Sjøholm*, 1991; *Wolf-Welling et al.*, 1995], but was rather insignificant until 3.3 to 3 Ma. At 3.3 Ma, *Jansen et al.* [2000] described a pronounced increase in the Greenland ice sheet size, when it started to expand. The enhancement of the glaciation beyond Greenland occurred after 2.8 Ma. At 2.74 Ma a rapid glaciation covered the Eurasian Arctic and Northeast Asia, at 2.7 Ma Alaska followed and by 2.54 Ma a major glaciation on the North American continent had developed [*Tiedemann et al.*, 1994, *Shackleton et al.*, 1995].

The processes that caused the onset of the Northern Hemisphere Glaciation are not yet fully understood. The uplift of Himalayan-Tibetan Plateau [*Raymo*, 1994, *Raymo and Ruddiman*, 1992] causing a decrease in the CO_2 concentration as a consequence of the enhanced chemical weathering has been attributed to a global cooling related to the NHG. *Cane and Molnar* [2001] explained changes of climate related to NHG by the gradual closure of the Indonesian gateways at 4 Ma, which is, however, one million years too early to account for the changes of the climate related to the NHG and has possible only been a prerequisite for the NHG. Another hypothesis

was developed by *Maslin* [1995, 1996] and further tested by *Huybers and Molnar* [2007], who attributed the NHG to the influence of changes in orbital forcing with increasing amplitudes of the orbital obliquity cycles between ~3 to 2.5 Ma. The best examined and most accepted hypothesis involves the closure of the Panama Isthmus [*Keigwin*, 1982; *Driscoll and Haug*, 1998; *Haug and Tiedemann*, 1998; *Bartoli et al.*, 2005, *Frank et al.*, 1999], which most likely resulted in a stronger heat transport and moisture supply to the Northern Hemisphere thereby leading to increased river discharge from Siberia resulting in enhanced sea ice formation and a greater albedo over the Arctic ocean [*Driscoll and Haug*, 1998]. Major changes in $\delta^{18}O$ records [*Driscoll and Haug*, 1998; *Haug and Tiedemann*, 1998; *Bartoli et al*., 2005], and of the radiogenic isotope compositions of deep waters [*Burton et al*., 1997, *Frank et al.*, 1999; *Reynolds et al.*, 1999; *Frank et al.*, 2002] documented a significant change of the Atlantic Ocean circulation and a stimulation of enhanced ice sheet build-up in the high northern latitudes.

Sarnthein et al. [2009] concluded that a first pulse of enhanced poleward heat transport to the due to the final closing of the Panamanian gateway near 3.25 – 3.15 Ma followed by a second pulse between 3 to 2.85 Ma. A strong cooling and freshening of the EGC and an expansion of perennial Arctic sea ice, as well as increasing albedo at ~3.2 to 3.0 Ma may have caused a thermal isolation of Greenland and supported a persistent glaciation of Greenland. Recently, the major onset of this first climatic change was defined at 2.82 Ma by *Sarnthein et al.* [2009], which has been supported by studies of IRD deposition in the Nordic Seas [e.g., *Kleiven et al.*, 2002; *Jansen and Sjøholm*, 1991; *Jansen et al.*, 2000; *Knies et al.*, 2002, 2009]. Additionally, this period is characterized by an enhanced ice-sheet build-up in the northern high latitudes reflected in an increase of benthic $\delta^{18}O$ by 0.4 ‰ between 2.93 – 2.82 Ma and a decrease of the global sea level on the order of 43 m [*Ravelo et al.*, 2004; *Mudelsee and Raymo*, 2005].

1.3.2. The Mid Pleistocene Transition

The Mid Pleistocene Transition (MPT) was characterized by a shift in the dominant frequency of glacial-interglacial cycles from 41 kyrs to 100 kyrs. This shift between the major orbital Milankovitch frequencies occurred between ~1.5 to ~0.6 Ma

[*Hays et al.*, 1976; *Shackleton and Opdyke*, 1976; *Pisias and Moore*, 1981; *Lisiecki & Raymo*, 2005; *Raymo and Huybers*, 2008]. *Clark et al*. [2006] characterized the start of this gradual transition defining the MPT at 1.25 Ma on the basis of an increase in the mean benthic $\delta^{18}O$ by 0.64‰ Myr^{-1}. The end is described by a maximum benthic $\delta^{18}O$ value at 700 ka, which then remained almost unchanged until present [*Clark et al*., 2006]. The onset of the MPT was accompanied by decreases in sea surface temperatures in the North Atlantic Ocean, as well as by an increase in African [*Tiedemann et al.*, 1994] and Asian aridity and monsoonal intensity [*Clemens et al.*, 1996; *Williams et al*., 1997; *Sun et al.*, 2006].

Most hypotheses attribute the cause of the MPT to a decrease in atmospheric pCO_2 [*Raymo*, 1997; *Paillard*, 1998; *Berger et al.*, 1999]. Other theories ascribe the MPT shifts to, e.g. increased glaciation on the North American continent exposing the bedrocks of the Precambrian Shield due to glacial erosion [*Clark and Pollard*, 1998] or to a $\delta^{18}O$ signal of a shift between northern and southern hemispheric ice dynamics [*Raymo et al.*, 2006].

The Mid Pleistocene Transition was characterized by a gradual increase of the intensities of glaciations and consequently by increasing ice volume, which caused a regression of the sea level of ~50m and a decrease in the global deep water temperature [*Clark et al*., 2006]. Several studies [*Pisias and Moore*, 1981; *Mudelsee and Schulz*, 1997; *Elderfield et al.*, 2012] describe an abrupt transition at 900 ka by the first long glaciation of about 80 kyrs, accompanied by a reduction of substantial melting of ice during MIS23, which was followed by a new ice growth in MIS 22, causing a sealevel decrease of 120 m. At that time a general cooling of deep water in the North Atlantic Ocean coincided with a reduction of the deep ocean circulation. Furthermore *Clark et al*. [2006] state that, ice sheets have been the only part of the climate system to reveal constant low-frequent variability since 900 ka.

Carbon isotope data suggest changes in the water mass structure in the northernmost North Atlantic Ocean during the MPT [*Raymo et al.*, 2004]. These changes may also have initiated the present day mode of water mass exchange between the Nordic Seas and Arctic Ocean. In addition, the climatic rearrangement in the Nordic Seas during the MPT is expressed by an increase in IRD deposition [e.g. *Jansen and Sjøholm*, 1991; *Helmke et al.*, 2003, 2005; *Knies et al.*, 2009]. In the Nordic Seas, the

formation of intermediate and deep water has been explained by brine formation during the MPT, which implies that the Nordic Seas have been largely ice-covered during that time [*Raymo et al.*, 2004; *Henrich and Baumann, 1994*]. This is in contrast to the present day mode of dense waters forming through cooling of saline waters.

1.4. RADIOGENIC ISOTOPE SYSTEMS IN SEAWATER

Over the past decades several proxies were developed to reconstruct changes of the water mass circulation processes and the structure of the water column of the past 20 million years, e.g. stable carbon isotopes ($\delta^{13}C$) [*Raymo et al.*, 1992; *Ravelo and Andreasen*, 2000; *Raymo et al*., 2004], cadmium to calcium ratios (Cd/Ca) [*Boyle and Keigwin*, 1985] or radiogenic neodymium, lead and hafnium isotope compositions. These radiogenic isotope systems have been applied to reconstruct the mixing processes between water masses, as well as continental weathering inputs into the ocean [e.g. *Grousset et al.*, 1988; *Fagel et al.*, 2002, 2004, *Haley et al.*, 2008a, 2008b; *Crocket et al.*, 2010;]. The radiogenic isotope signatures are extracted from different archives, e.g. ferromanganese crusts [e.g. *Burton et al.*, 1997; *Reynolds et al.*, 1999], planktonic and benthic foraminifera [e.g. *Roberts et al.*, 2012; *Elmore et al.*, 2011], fish teeth [e.g. *Martin et al.*, 2000, 2010, 2012] and authigenic ferromanganese oxyhydroxide coatings of sediment particles [e.g. *Rutberg et al.*, 2000; *Piotrowski et al.*, 2005; *Gutjahr et al.*, 2007, 2008; *Haley et al.*, 2008a, 2008b]. A great advantage of the radiogenic isotopes is their independence from the fractionation by biological processes or evaporation.

Due to weathering and erosional processes the trace metals with distinct isotope compositions are transferred into the ocean either as particles via riverine or eolian input or in dissolved or colloidal form via rivers [*Goldstein et al.*, 1984; *Grousset et al.*, 1988; *Bayon et al.*, 2004; *Grousset and Biscaye*, 2005]. Additional sources releasing trace metals to the ocean are boundary exchange processes at the continental margins and hydrothermal inputs at mid-ocean ridges [*Frank et al.*, 2002; *Lacan and Jeandel*, 2005a; *Arsouze et al*., 2009].

1.4.1. Neodymium isotopes

Neodymium belongs to the light Rare Earth Elements (REE) and has seven naturally occurring isotopes with the masses: 142 (27.1%), 143 (12.2%), 144 (23.9%), 145 (8.3%), 146 (17.2%), 148 (5.7%) and 150 (5.6%). ^{143}Nd is a product of the α-decay of samarium (^{147}Sm) with a half-life of 106 Gyrs:

$$^{147}_{62}Sm \rightarrow {}^{143}_{60}Nd + \alpha + Q$$

with *Q* being the total decay energy. The abundance of ^{143}Nd is normalized to that of primordial ^{144}Nd. Natural isotopic variations of the ^{143}Nd/^{144}Nd are small in different rocks types and are therefore expressed as the relative deviation of the ^{143}Nd/^{144}Nd ratio of a sample to the Nd isotope ratio of the chondritic Earth (**Ch**ondritic **U**niform **R**eservoir **CHUR** with a ^{143}Nd/^{144}Nd ratio of 0.512638 [*Jacobsen and Wasserburg*, 1980]) in parts per 10,000:

$$\varepsilon_{Nd} = \left[\frac{^{143}Nd/^{144}Nd_{sample}}{^{143}Nd/^{144}Nd_{CHUR}} - 1\right] * 10000$$

Sm and Nd are both REEs and show similar chemical behaviour due to similar ionic radii (Nd^{3+} = 0.0983 nm, Sm^{3+} = 0.0958 nm), but Nd is slightly more incompatible than Sm, which causes a fractionation during partial melting. In this case, Nd is concentrated in the liquid phase (partial melts), while Sm remains in the residue. This leads to higher Sm/Nd ratios in basic to ultrabasic mantle derived rocks, such as as tholeiitic basalts and gabbros compared to acidic rocks as granites, granulites, sandstones and shales, which show a lower Sm/Nd ratio.

In general, ε_{Nd} values in the continental crust vary between -56 and +12. Old cratons are characterized by a low Sm/Nd and a low ε_{Nd}, e.g. rocks from Greenland, Canada, the Scandinavian shield as well as parts of Antarctica and West and Southeast Africa. In contrast, younger mantle derived volcanic rocks, e.g. rocks surrounding the Pacific Ocean, as well as Iceland and the East African Rift system, have a higher Sm/Nd

ratio and high (radiogenic) ε_{Nd} values [*Goldstein and Hemming*, 2003; *Jeandel et al.*, 2007].

The most likely dominant source of Nd in the ocean besides the riverine and eolian input is boundary exchange at the continental margin/seawater interface in areas with pronounced shelf regions, e.g. the Arctic Ocean and the Nordic Seas [*Lacan and Jeandel*, 2005a]. In comparison to the Rb/Sr system (for details see 1.4.2.), Nd and Sm mostly show no significant fractionation during sedimentary processes. In seawater, Nd behaves quasi conservatively due to its moderate particle reactivity resulting in a residence between 360 to 2000 yrs [*Tachikawa et al.*, 1999; *Arsouze et al.*, 2009] and can be therefore be used as a water mass tracer. To reconstruct the bottom water signature throughout the Quaternary the extraction of Nd from ferromanganese coatings of sediment particles has been applied in all ocean basins [e.g. *Crocket et al.*, 2011 (North Atlantic Ocean); *Haley et al.*, 2008a (Arctic Ocean); *Piotrowski et al.*, 2008 (Southern Ocean); *Piotrowski et al.*, 2009 (Indian Ocean); *Martin et al.*, 2010 (Pacific Ocean)].

1.4.2. Strontium isotopes

The basis of the Rb/Sr isotope system is the β^--decay of ^{87}Rb to ^{87}Sr with a half-life of 48.8 Gyrs:

$$^{87}_{37}Rb \rightarrow {}^{87}_{38}Sr + \beta^- + \bar{\upsilon} + Q$$

with $\bar{\upsilon}$ = antineutrino and Q = total decay energy. Strontium belongs to the Alkaline Earth Metals and has four naturally occurring isotopes with the masses: 84 (82.5%), 86 (7.0%), 87 (9.9%), and 88 (0.6%). The abundance of ^{87}Sr is normalized to the primordial ^{86}Sr. In contrast, Rb belongs to the Alkali Metals and compared to Sr (1.13 Å), has a much larger ionic radius (1.48 Å). Thus it behaves geochemically very differently from Sr, which results in a strong fractionation during magmatic, metamorphic and sedimentary processes. This in turn causes a large variation of the Rb/Sr ratios between ultrabasic/basic rocks and acidic rocks. Weathering processes cause a separation of Rb and Sr due to faster weathering of minerals with a lower Rb/Sr

ratio (pyroxene, An-rich feldspar, amphibolites) than of minerals with a higher Rb/Sr ratio (mica, K-rich feldspar).

During the evolution of the Earth, the continental crust developed by differentiation processes from the Earth`s mantle. During this process Rb has become enriched in the rocks of the continental crust, because it is more compatible and thus builds up in liquids during mantle melting and crust formation. As a result the Rb/Sr ratio in the continental crust is much higher than in the mantle, leading to lower $^{87}Sr/^{86}Sr$ ratios in young mantle-derived rocks and higher and more variable $^{87}Sr/^{86}Sr$ ratios in old continental rocks.

Dissolved Sr enters the oceans dominantly via riverine input and has a high concentration in seawater (8100µg/l, for comparison: Rb = 120 µg/l, Nd = 0.0028 µg/l, Sm = 0.00045 µg/l, Pb = 0.03 µg/l). Sr is not particle reactive and the $^{87}Sr/^{86}Sr$ is independent from biological processes. Compared to Nd and the ocean mixing time, Sr behaves conservative and has a large ocean residence time in the order of several million years, which leads to a homogenous distribution in the oceans and a present day global $^{87}Sr/^{86}Sr$ ratio of 0.70916 [*Palmer and Edmond*, 1989; *McArthur et al.*, 2001]. In addition to the riverine input, Sr can be strongly influenced by 1) old carbonates, which are dissolved very easily and have an isotopic signature similar to seawater or 2) to a smaller rate by hydrothermal inputs at the mid-ocean ridges, which releases a generally less radiogenic $^{87}Sr/^{86}Sr$ ratio into the ocean [*Palmer and Edmond*, 1989]. The $^{87}Sr/^{86}Sr$ ratio in the ocean changed significantly throughout the Phanerozoic as a consequence of phases in the earth history, when a higher weathering intensity prevailed as function of orogenies leading to enhanced the input of rocks of the continental crust, such as since mid Jurassic times or at the Ordovician/Silurian boundary [*Qing et al.*, 1998] or during periods of increased hydrothermal input during continental break up phases.

In contrast to Nd, the Sr isotope ratio changes with grain size e.g. during incongruent weathering and erosional processes [*Tütken et al.*, 2002]. Higher Rb/Sr and $^{87}Sr/^{86}Sr$ ratios are found in fine-grained weathering products, where Rb is enriched in clay minerals and substitutes potassium. These clay-size particles are distributed by ocean currents over large distances. Due to the homogenous distribution of Sr in the ocean and its long residence time, Sr cannot be used as a water mass tracer. However, the Sr isotope composition in detrital particles is a useful tracer for the reconstruction of

sediment provenance, providing insight into both the regional subaerial erosive regime and sediment transport pathways.

1.4.3. Lead isotopes

Lead has three stable radiogenic isotopes with the masses: 206 (23.6%), 207 (22.6%) and 208 (52.3%), which are produced by the radioactive decay of uranium (U) and thorium (Th) and are generally normalized to primordial ^{204}Pb (1.48%). The simplified decay of U and Th to Pb can be described as follows:

$$^{238}U \rightarrow {}^{206}Pb + 8\,{}^{4}He + 6\beta^{-}$$

with a half-life of 4.468 Gyrs;

$$^{235}U \rightarrow {}^{207}Pb + 7\,{}^{4}He + 4\beta^{-}$$

with a half-life of 703.8 Myrs and

$$^{232}Th \rightarrow {}^{208}Pb + 6\,{}^{4}He + 4\beta^{-}$$

with a half-life of 14.01 Gyrs.

Uranium and thorium behave geochemically very different to lead. Lead has a much higher ionic radius (1.19 - 1.29Å) than U and Th, but all elements are highly incompatible for the paragenesis of the Earth`s mantle and are therefore enriched in the rocks of the continental crust compared to the upper mantle. The dominant sources of dissolved Pb into the ocean are riverine input from continents, eolian input and the input from hydrothermal sources, although the Pb isotope signature weathering products released to the ocean do not necessarily represent the Pb isotope signature of the source rocks due to significant incongruent weathering effects [e.g. *von Blanckenburg and Nägler*, 2001]. During this process the lattice structure of the different minerals are damaged by progressive radioactive decay of U and Th, which leads to enhanced mobilization and release of the radiogenic Pb isotopes compared to primordial ^{204}Pb.

Pb is highly particle reactive and has a residence time of only 20 – 50 yrs in the Atlantic Ocean [*Henderson and Maier-Reimer*, 2002] and 200 yrs in the Pacific Ocean [*Schaule and Patterson*, 1981; *von Blanckenburg and Nägler*, 2001]. Hence it is more sensitive to local variations in continental weathering sources and can be used as an indicator for changes of the continental inputs into the ocean and short distance water mass mixing, especially in shallow waters near the location of subduction.

1.5. OUTLINE OF THE THESIS

Radiogenic isotopes were commonly used to reconstruct past exchange processes of water masses in most ocean basins as well as for the reconstruction of the weathering input and sediment source [e.g. *Frank et al.*, 2002; *Crocket et al.*, 2011 (North Atlantic Ocean); *Haley et al*., 2008a (Arctic Ocean)]. So far no studies were established in the Nordic Seas using radiogenic isotopes extracted from seawater derived ferromanganese coatings on sediment particles during the Plio – and Pleistocene.

Thus, after a short introduction, the methodology part (Chapter 2) gives insights into the extraction of past seawater Nd and Pb isotope compositions from sediments on the basis of different leach methods for two sites in the North Atlantic Ocean (Site 984 and 982) and four sites in the Nordic Seas (Site 911, 986, 644 and 907). The Nd isotope composition from foraminiferal calcite was obtained from two sites in the western part of the study area (Site 907 and 984). In this chapter the chemical procedures to extract neodymium, lead and strontium from the ferromanganese-oxyhydroxides as well as the analyses of their isotope ratio were described. Additionally, the difficulties and differences of the applied leach methods on the basis of the studies of *Gutjahr et al.* [2007] and *Haley et al.* [2008a, 2008b] were examined.

Chapter 3 investigates the evolution of water mass exchange and erosional input on the Yermak Plateau in the Fram Strait during the Plio – and Pleistocene (past 5 Myrs). The results of the core top and down core samples were compared to the present seawater Nd isotope composition and to the Nd isotope composition of previous studies in the Arctic and North Atlantic Ocean with regards to changes in past circulation patterns, sediment sources and transport processes. The Nd and Pb isotope compositions

of the detrital material of Site 911 in the Yermak Plateau give insight into the sediment origin.

Chapter 4 examines changes of the inflow of the Atlantic water into the Nordic Seas during the past 3 Myrs. To get a better understanding about the evolution of the Atlantic inflow with regards to climatic changes, sediment cores from the Northern Atlantic Ocean (Site 982) and the Nordic Seas (Site 986 and 644) were compared to each other and to previous studies. Additionally, the erosional input, influenced by the increasing glaciation, was investigated on the basis of Nd and Pb isotope composition of ferromanganese coatings and detrital fraction of the bulk sediment.

Finally, Chapter 5 concludes the general findings and gives an outlook for future research.

CHAPTER 2

Methodology – Extracting past seawater Nd isotope compositions from sediments in the Nordic Seas and the northernmost Atlantic Ocean

Abstract

The reconstruction of past water mass exchange on the basis of the Nd isotope composition extracted from ferromanganese coatings, as well as foraminiferal calcite has become a valuable tool used in every ocean basin. Here we test different leaching methods to extract the seawater derived Nd and Pb isotope composition from authigenic coatings on sediment particles and Nd isotope signature on shells of foraminifera obtained from core top and down core sediments of different ODP Sites in the Nordic Seas (Site 907 (leg 151), 644 (leg 104), 986 (leg 162) and 911 (leg 151)) and northernmost Atlantic Ocean (Site 984 and 982 (leg 162)).

Site locations in the western part of the study area near Iceland (984 and 907) show no reliable results for attempts to extract the Nd isotope compositions of past bottom waters due to contamination originating from small ash particles. These particles cause more radiogenic values than expected from nearby seawater measurements for the leachates extracted by both methods as well as for cleaned planktonic foraminifera from Site 984. For sites (982, 644, 986, 911) in the eastern part of the Nordic Seas and in the North Atlantic Ocean it was possible to extract reliable past bottom water signatures using different leaching methods. One method is based on the established method of *Gutjahr et al.* [2007], while the second methods ignores the prepend decarbonation step, based on studies by *Haley et al.* [2008a, 2008b]. However, we observed a systematic offset of the ε_{Nd} signatures between these different leaching methods, with more radiogenic values produced by the method of *Gutjahr et al.* [2007].

This chapter is going to be submitted as:

Teschner, C., M. Frank and B.A. Haley. Extracting past seawater Nd isotope compositions from sediments in the Nordic Seas and the northernmost Atlantic Ocean.

This offset increases with decreasing mean carbonate content, and therefore with latitude, most likely caused by dissolution of an unidentified phase carrying a non-radiogenic signature, which is removed during the carbonate removal step prior to leaching of the ferromanganese coatings. This demonstrates that the leaching methods need to be carefully checked and adjusted for each new location. In contrast to the Nd and Sr isotope composition, the leach method seems to play no role for the Pb isotope composition.

2.1. INTRODUCTION

2.1.1. Radiogenic isotopes as water mass tracers

The radiogenic neodymium isotopic composition extracted from foraminifera and authigenic iron-manganese oxyhydroxide coatings on sediment particles is a common tool to reconstruct water mass exchange in the past [*Frank et al.*, 1999; *Haley et al.*, 2008; *Martin et al.*, 2010; *Roberts et al.*, 2010]. This utility is based on the dissolved Nd isotope signature behaving quasi-conservatively in the deep ocean, with a residence time of 360 – 2000 years [*Arsouze et al.*, 2009; *Tachikawa et al.*, 2003; *Frank et al.*, 2002; *Rempfer et al.*, 2011] compared to the global ocean mixing time of about 1500 yr [*Broecker and Peng*, 1982]. In addition, the Nd isotope composition is independent from fractionation by biological and low temperature processes [e.g. *Piotrowski et al.*, 2005] and is thus potentially amenable to straightforward interpretation. Neodymium isotope compositions are expressed as $\varepsilon_{Nd} = [(^{143}Nd/^{144}Nd)_{Sample}/(^{143}Nd/^{144}Nd)_{CHUR} -1] * 10.000$, where *CHUR (Chondritic Uniform Reservoir) is 0.512638* [*Jacobsen and Wasserburg*, 1980].

The fundamental source of dissolved Nd in the ocean is the weathering of the continents, through eolian [*Tachikawa et al.* 1997, 1999] or riverine inputs [*Bayon et al.*, 2004], as well as boundary exchange processes with the ocean margins and shelves [*Lacan and Jeandel*, 2004a, 2005a]. In the Nordic Seas, Arctic and North Atlantic Ocean the Nd isotope compositions of the water masses are influenced by the surrounding cratonic terrane rocks, such as those exposed on Greenland, which release a highly unradiogenic Nd (ε_{Nd} = -40) [*Taylor et al.*, 1992], and younger basaltic rocks,

such as those of Iceland, which release highly radiogenic Nd signature (ε_{Nd} = +5 to +10) [*O`Nions and Grönvold*, 1973].

Extracting bottom water Nd isotope signatures from sediments through leaching is a widely done, and has been demonstrated to work in most ocean basins [*Crocket et al.*, 2011 (North Atlantic Ocean); *Haley et al*., 2008a (Arctic Ocean); *Piotrowski et al*., 2008 (Southern Ocean); *Piotrowski et al*., 2009 (Indian Ocean); *Martin et al.*, 2010 (Pacific Ocean)]. In the Nordic Seas, by contrast, the extraction of bottom water Nd isotope compositions and their interpretation in terms of water mass mixing is complicated by: boundary exchange processes [*Lacan & Jeandel*, 2004a, 2004b]; contamination of the Nd isotope signal in situ or in the lab by partial dissolution of often abundant volcanic material [*Elmore et al*., 2011]; or preformed coatings delivered by sea ice or ice bergs [*Bayon et al.*, 2004; Chen et al., 2012].

Several studies in the Arctic [*Winter et al.*, 1997; *Haley et al.*, 2008a, 2008b] and Atlantic Ocean [*Roberts et al.*, 2010; *Crocket et al*., 2011; *Elmore et al*., 2011] have determined the Nd isotopic composition from seawater as derived from ferromanganese coatings of bulk sediments and of foraminiferal calcite in order to reconstruct past water mass exchange on different time scales. Ferromanganese coatings precipitate on sediment particles at the sediment water interface [*Palmer and Elderfield*, 1985; *Piotrowski et al.*, 2005] and can be influenced by the presence of anoxic pore waters, which can cause the reduction of solid Fe-oxides and the subsequent release of Nd [*Haley et al.*, 2004]. To support the seawater origin of the Nd isotopes extracted from this authigenic fraction and to assure no contamination of the clay fraction occurred several studies have used the Sr isotope composition of the leachates, given that the Sr isotope composition of seawater is homogenously distributed and well known over time [e.g. *Palmer and Edmond*, 1989; *McArthur et al.*, 2001; *Piotrowski et al.*, 2005]. The isotopic composition of the detrital phase, which consists of the weathered products from the continents, serves as an indicator for sediment provenance and input mechanisms into the Ocean.

Reductively cleaned planktonic foraminiferal shells have been suggested to be robust archives of the Nd isotope signature of the surface ocean, [*Vance and Burton*, 1999; *Scrivner et al*., 2004; *Vance et al*., 2004]. For core top foraminifera in the North Atlantic Ocean, *Roberts et al.* [2010] argue that after the removal of clay and detrital

silicate, the signatures extracted from the foraminifera represent bottom water signatures. This fact is based on high Nd concentrations and thus dominating signature of the ferromanganese coatings precipitated on the foraminiferal shells. They also showed that cleaned and uncleaned planktonic foraminiferal samples of three North Atlantic sites are the same within error and therefore 90 – 98% of the ferromanganese coating must be removed in order to get a reliable surface ocean signature. The analysis of benthic foraminifera clearly reflects bottom water isotopic signatures [*Klevenz et al.*, 2008].

Additionally, we extracted the Pb isotope composition from the ferromanganese coatings, which can provide information about changes of the past sediment sources and transport mechanisms into the ocean basin. The low residence time of around 50 yrs in the Atlantic Ocean [*Schaule and Patterson*, 1981, *Erel et al.*, 1994; *Henderson and Maier-Reime*r, 2002] implicate a very local Pb isotope signal, reflecting the surrounding rocks. The dominant sources of Pb into the Nordic Seas and North Atlantic Ocean are mainly riverine and glacial input. Whereby the Pb signal is modified and does not mirror the exact isotope signature of the nearby rocks due to the incongruent weathering, especially during glacial periods [*Foster and Vance*, 2006]. This process is a consequence of the radioactive decay inside the lattice of the minerals, leading to a preferential mobilization of the radiogenic Pb isotopes (^{206}Pb, ^{207}Pb, ^{208}Pb), which causes a shift to more radiogenic Pb isotope compositions in seawater [*Erel et al.*, 1994; *von Blanckenburg and Nägler*, 2001].

To test the reliability of different leaching methods, we analyzed Nd and Pb isotope compositions extracted from authigenic ferromanganese coating, as well as Nd isotope composition from foraminiferal tests at Site 907 on the Iceland Plateau und Site 984 south of Iceland on Bjørn Drift. Additionally we measured Nd and Pb isotopic composition of the authigenic coatings of Site 911, 986, 644 and 982. We tried to extract the bottom water Nd isotope signatures from the sediment for six sediment cores drilled during ODP legs 151, 162, and 104 in the North Atlantic Ocean, Nordic Seas and in the Fram Strait from water depths between 900 and 2000 m. We focused on the deep and intermediate water mass exchange in the North Atlantic and Nordic Seas, because these are two of the most important areas for the formation of deep waters and therefore for the ventilation of the entire Atlantic Ocean.

2.1.2. Study area and hydrographic setting

The Nordic Seas include the Greenland Sea, the Iceland Sea and the Norwegian Sea in a hydrographically complex area. On the one hand, the Nordic Seas are influenced by outflowing relatively fresh Arctic waters, the Arctic Intermediate Water (AIW: ~0.5°C < T < 3°C; 34.87 < S < 34.90), also called 'Norwegian Sea Intermediate Water', flowing through Denmark Strait or is advected east of Iceland as Modified East Icelandic Water (MEIW) over the Iceland-Faroer ridge and through the Faroer Bank Channel [*Hansen and Østerhus*, 2000] (Fig. 2.1). The intermediate waters in the Greenland Sea are characterized by $\varepsilon_{Nd} \approx -11.1$ and in the Icelandic sea by $\varepsilon_{Nd} \approx -8.1$.

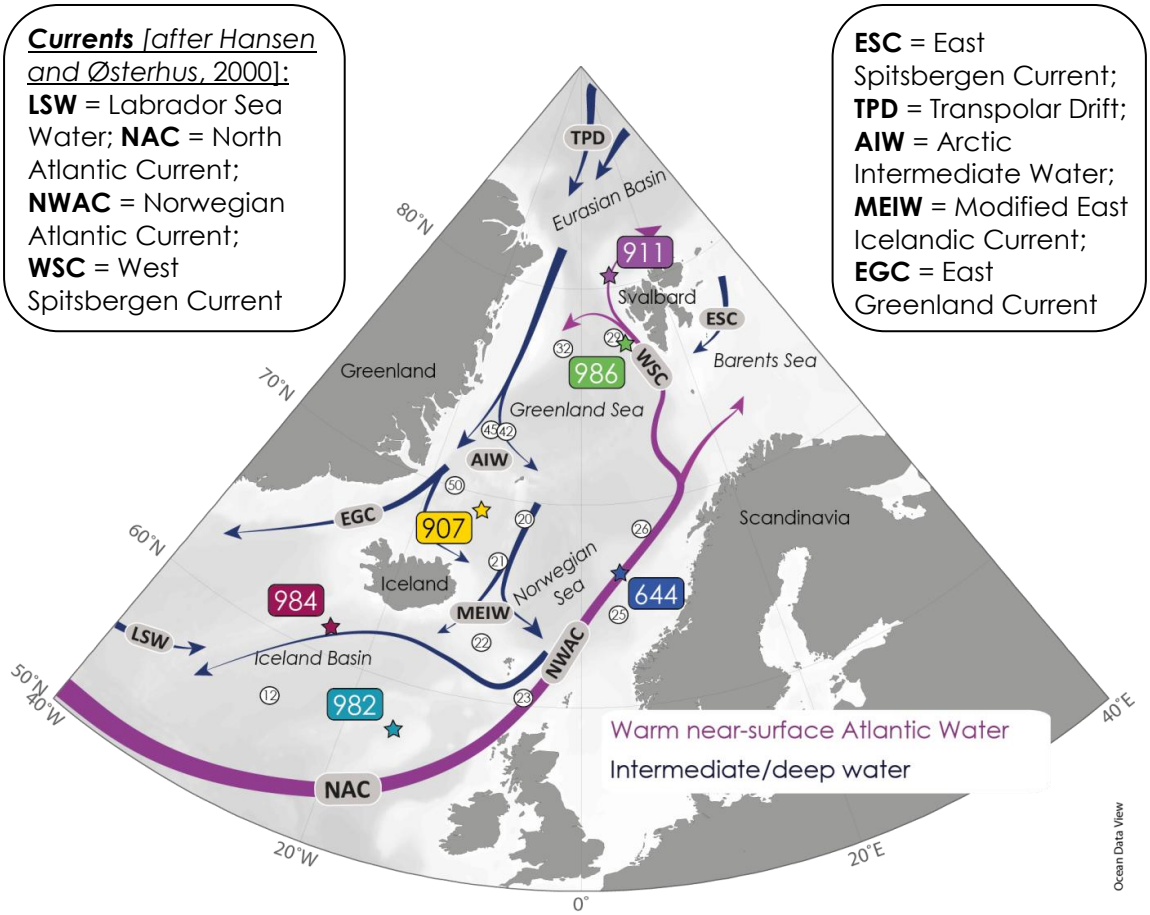

***Figure 2.1: Map of the study area**. The Nordic Seas with the location of the ODP Sites subject to this study (colored stars), and schematic dominant near-surface, intermediate and deep water currents, as well as locations of available water column Nd isotope measurements (numbers according to [Lacan and Jeandel, 2004b, 2005b]).*

The Norwegian Sea Deep Water leaving the Nordic Seas is characterized by an ε_{Nd} = ~ -9.8, leaving further northeast of Iceland ε_{Nd} around -8.9 and leaving the Faroe – Shetland channel reach at -8.2 [*Lacan and Jeandel*, 2004b]. The Denmark Strait Overflow Water shows ε_{Nd} values between -11.1 to -10.8 at 70°N and -7.9 further south in the Denmark Strait at 66°N [*Lacan and Jeandel*, 2004a] due to the influence of the exchange with the basaltic margins of southeast Greenland and Iceland. Similar processes impart a significantly more radiogenic signature of -8.2 ε_{Nd} on the Iceland Scotland Overflow Water [*Lacan and Jeandel*, 2004b] through interaction with the Iceland-Scotland Ridge. Site 907 located in 1800 m water depth on the Iceland Plateau, as well as Site 984 in 1600 m water depth are dominated by Arctic Intermediate Water. Site 984, located on the Bjørn Drift in the northernmost Atlantic Ocean is also influenced by Labrador Sea Water (LSW) flowing north towards Iceland in 1000 to 1600 m water depth [*Lacan and Jeandel*, 2005b].

The Nordic Seas are strongly influenced from the south by warm and saline Atlantic water masses characterized by Nd isotope composition near -13. The Atlantic water enters the Nordic Seas in two branches across the Greenland-Iceland Ridge and the Iceland-Faroe Ridge. The North Atlantic Current (NAC) crosses the Rockall Plateau influencing Site 982 and flowing further north as Norwegian Atlantic Current (NWAC) along the Norwegian shelf and across the Vøring Plateau that is the location of Site 644 (1220 m deep). When reaching the Barents Sea shelf the NWAC divides into two branches: one enters the Barents Sea and one continues to flow along the western shelf of Svalbard and reaches the Yermak Plateau (Site 911; 900 m deep) before entering the Arctic Ocean. Site 986 (2050 m deep), located on the deep Svalbard shelf, is mainly influenced by Norwegian Sea Deep Water [*Hansen and Østerhus*, 2000].

2.2. MATERIAL AND METHODS

2.2.1. Site locations and age models

To test the extraction of the different leaching methods, six ODP sediment cores located in intermediate and deep water masses, two of them in the North Atlantic Ocean and four in the Nordic Seas were chosen. The northernmost Site 911 (80°28.466'N,

8°13.640'E) located on the Yermak Plateau in the Fram Strait at 906 m water depth [*Myhre et al.*, 1995] (Fig. 2.1, Tab. A.1) was drilled during ODP Leg 151. Previous studies provide the stratigraphy and the composition of the sediment of the core [*Knies et al.*, 2002, 2009]. For the interval prior to 2.7 Ma we applied the new stratigraphic framework established by *Mattingsdal et al.* [in review] based on seismo-, magneto-, and biostratigraphic correlations. After 2.7 Ma the age model of *Knies et al.* [2009] was applied, which is based on magnetostratigraphy and calcareous nanofossils. Besides a sedimentation rate between 8.7 cm/kyr and 19.2 cm/kyr, this sediment core is characterized by a carbonate content of 1% and 6% [*Myhre et al.*, 1995].

The second site in the influence area of Svalbard is ODP Site 986 (77°20.431' N, 09°04.664' E), located on the western Svalbard margin between Bellsund and Isfjorden fans at 2050 m water depth [*Jansen et al.*, 1996] was drilled during Leg 162 and is the deepest core of this study (Fig. 2.1, Tab. A.1). This site was subject to numerous previous studies, which generate the stratigraphic framework [*Channell et al.*, 1999; *Eidvin and Nagy*, 1999; *Forsberg et al.*, 1999; *Butt et al.*, 2000; *Knies et al.*, 2009]. For this study we applied the age model of *Knies et al.* [2009] based on magnetostratigraphic and micropaleontological evidence [*Channell et al.*, 1999; *Eidvin and Nagy*, 1999; *Smelror et al.*, 1999]. Samples were chosen on the basis of IRD abundance provided by *Knies et al.* [2009] given that foraminiferal carbonate is barren in this record, especially in the part older ~1 Myr [*Jansen et al.*, 1996]. The total carbonate content is similar to Site 911 very low around 0.7 – 10% [*Jansen et al.*, 1996].

ODP Site 907 (69°14,989' N, 12°41,894' W), drilled during Leg 151 (revisited Leg 162) is located on the Iceland Plateau in the Icelandic Sea in a water depth of 1800 m, (Fig. 2.1, Tab. A.1). We applied the age model and stratigraphic framework of *Jansen et al.* [2000], based on magnetostratigraphic and micropaleontological evidence. The sample selection is based on the IRD record established by *Jansen et al.* [2000] over the past 3.5 Ma. In the Nordic Seas this site provides the highest total carbonate content of 26 – 62% [*Myhre et al.*, 1995], but a low content in foraminifera.

The southernmost site in the Nordic Seas is Site 644 (66°40.700'N, 04°34.600'E) and was drilled during Leg 104 [*Eldholm et al.*, 1987]. It is located on the Vøring Plateau on the Norwegian shelf at a water depth of 1220 m [*Eldholm et al.*,

1987] (Fig. 2.1, Tab. A.1). The age model of Site 644 is based on magnetostratigraphy [*Bleil,* 1989] recalculated by *Cande and Kent* [1995] with a base of the core at ~ 3 Ma. Sampling intervals were chosen based on oxygen isotope stratigraphy of the benthic species *Cassidulina teretis* and *Melonis barleeanum* analyzed by *Jansen et al.* [1989].

ODP Site 984 (61°25,517' N, 24°04,949' W) is the westernmost site, located on the Bjørn Drift on the eastern flank of the Reykjanes Ridge in the North Atlantic Ocean at a water depth of 1648 m [*Jansen et al.*, 1996] (Fig. 2.1, Tab. A.1). This site was subject to many studies [*Raymo et al.*, 2004; *Bartoli et al.*, 2005]. The age model and sample selection is based on $\delta^{18}O$ isotope records of benthic *Cibicidoides wuellerstorfi* for the period prior to 1.8 Ma [*Raymo et al.*, 2004] and $\delta^{18}O$ isotope records of *Neogloboquadrina atlantica* for the period between 2.5 and 3 Ma [*Bartoli et al.*, 2005].

The southernmost site, ODP Site 982 (57°30,992'N, 15°52,001'W) is located at an intermediate water depth of 1145 m [*Jansen et al.*, 1996] in the Hatton – Rockall basin on Rockall Bank (Fig. 2.1, Tab. A.1), which is a shallow platform between Iceland and Ireland. Here, the age model of *Venz et al.* [1999] and *Venz and Hodell* [2002] was applied. It is based on benthic and planktonic foraminiferal oxygen isotope records. The samples were chosen on the basis of the benthic oxygen record of the foraminifera *Cibicidoides wuellerstorfi* and *Cibicidoides kullenbergi* for the samples younger than 1 Myrs [*Venz et al.*, 1999] and the benthic oxygen record of the foraminifera *Cibicidoides wuellerstorfi* of *Venz and Hodell* [2002] for the record older than 1 Myrs.

2.2.2. Extraction of the radiogenic isotope composition of the bulk sediment leach and total dissolution of the residual fraction

Two different leaching methods were applied to extract the Nd isotope signature of the authigenic Fe-Mn oxyhydroxide coatings ("leach" fraction), as well as of the residual detritus. The first method applied was published by *Gutjahr et al.* [2007] to extract the Nd, Pb, and Sr isotope composition of past bottom water incorporated in authigenic ferromanganese oxyhydroxide coatings of the sediment particles, (*Method A*, Fig. 2.2). The first step of this method was a double rinsing of 2 to 3g dried sediment

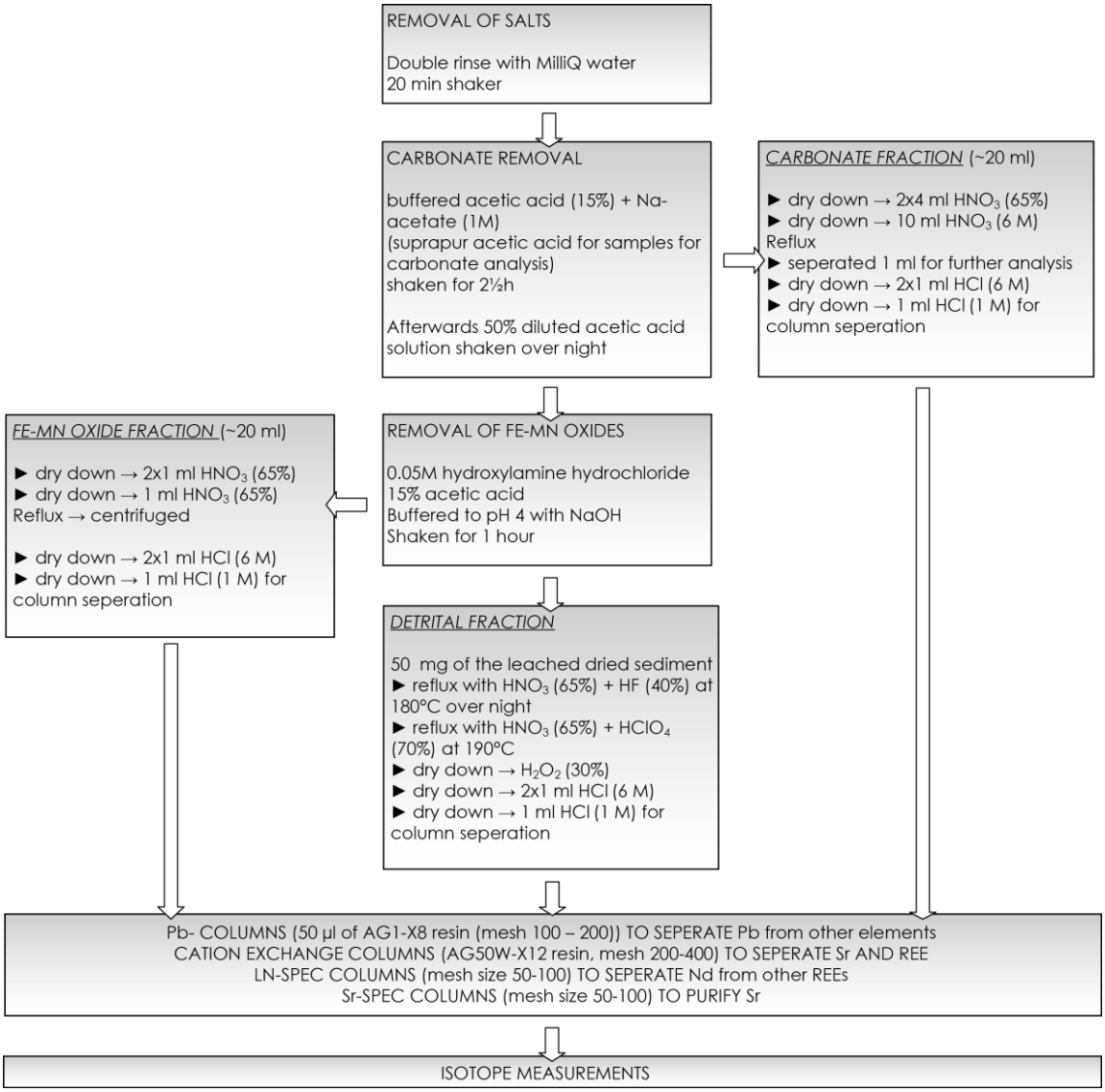

Figure 2.2: Schematic diagram of the leaching methods and further treatment of the separated fractions*. Leaching method A includes the first steps of double rinsing and carbonate removal. Leaching method B starts directly with the leaching of the Fe-Mn-oxides.*

with *MilliQ*© (ultra pure water 18.2 MΩ/cm) water accomplished by shaking for 20 minutes followed by centrifuging. Afterwards the carbonate fraction was removed with a buffered acetic acid solution (15% acetic acid/1M Na-acetate) followed again by a triple rinse with *MilliQ*© water. For selected samples this "carbonate" fraction was collected to analyze its Nd isotopic composition, using ultra-pure acetic acid (*supra pur*) to avoid contamination. Due to the high carbonate content, this solution was dried down

and then taken up in 10 ml of concentrated HNO_3 and 1 ml of this solution was separated for isotopic analyses. The subsequent leaching of the de-carbonated sediment was carried out for 1 hour with a 0.05 M Hydroxylamine HCl and 15% acetic acid mixture, buffered to pH ~ 3.5 to 4.0. The centrifuged supernatant, containing the dissolved authigenic fraction was pipetted into Teflon vials and evaporated to dryness. Afterwards it was taken up in 1 ml concentrated HNO_3 twice and dried each time to destroy the matrix of the hydroxylamine solution and prepare for further element separation and purification.

The second leaching procedure (*method B*) is based on results of a previous study of Central Arctic sediments [*Haley et al.,* 2008a, 2008b]. Due to the very low carbonate contents of the sediments at the northernmost Sites (Site 911 only reaching between 1% and 6% [*Myhre et al.,* 1995]; Site 986 between 0.7 and 10% [*Jansen et al.*, 1996]), the carbonate removal step was omitted from the leaching procedure. Hence, after double rinsing with *MilliQ*© water *method B* directly started with extracting the seawater signal from the coatings using the hydroxylamine leach solution. For both methods the initial $MgCl_2$ treatment to remove adsorbed metals from the particle surface [*Gutjahr et al.*, 2007] was omitted because *Haley et al*. [2008a, 2008b] found no significant differences in the isotopic composition of Nd, Pb and Sr extracted from Arctic Ocean sediments with or without this step.

After leaching, the sediment with a new batch of hydroxylamine solution was allowed to react for at least another 12 hours to guarantee complete removal of any authigenic coating. The detrital fraction was then rinsed three times with *MilliQ*© water, dried and ground for total digestion (Fig. 2.2). To accomplish this, 50 mg of sediment was weighed and dissolved in a mixture of concentrated HNO_3 + HF at 180°C over three days. If there was still minor amounts of clay left, the samples were evaporated and treated with a mixture of HNO_3 + $HClO_4$ at 190°C , prior to chromatographic separation and purification steps.

Chromatography began with separation of Pb from the other elements. It was purified on an anion exchange column filled with 50 µl of AG1-X8 resin (mesh 100 – 200) following the method of *Lugmair and Galer* [1992]. As second step the Rare Earth Elements (REEs) and Sr in the original solution using 0.8 ml AG50W-X12 cation exchange resin (mesh 200 – 400) were separated. The Sr cut was further purified on

columns with 50µl Sr-Spec resin (mesh 50 – 100) following the method of *Horwitz et al.* [1992] and *Bayon et al.* [2002]. Nd was separated from the other REEs using 2 ml Ln Spec resin (50 – 100mesh) [*Cohen et al.*, 1988; *Barrat et al.*, 1996; *Le Fèvre and Pin*, 2005].

2.2.3. Cleaning of foraminiferal calcite

For the extraction of the Nd from foraminifera of Sites 984 and 907 the samples were washed and sieved. Foraminifera >63 µm were handpicked and gently cracked to open all chambers [*Scrivner et al.*, 2004; *Roberts et al.*, 2010]. The cleaning procedure of the foraminifera followed the method established by *Boyle* [1981], which was later modified by *Vance and Burton* [1999] and *Vance et al.* [2004] (Tab. 1). For application of this method approximately 20 mg of foraminifera were put into 15 ml polypropylene/polyethylene (PP/PE) centrifuge vials and in a first step the clays were removed by multiple rinsing with *MilliQ*© water and methanol, followed by an oxidative cleaning step (with H_2O_2 (30%) and NaOH (0.1 N)) and a reductive cleaning step (with a solution containing ammonium hydroxide, citric acid and hydrazine hydroxide) to remove the ferromanganese coatings on the shells [*Vance et al.*, 2004]. After this, the shells were rinsed with *MilliQ*© water and then transferred to 1.5 ml centrifuge tubes. For final dissolution we used nitric acid (0.5 M) and added stepwise 100 µl to the sample (in 0.5 ml *MilliQ*© water). To enhance the dissolution the samples were sonicated after each addition of acid until the entire material was dissolved. The solution was then dried and prepared for Nd purification. For the "uncleaned" foraminifera (corresponding to those of *Roberts et al.* [2010]) we omitted the reductive and oxidative cleaning step and only removed the clays before dissolving the sample.

Tab. 1: Steps of the cleaning method of foraminifera calcite *(after Vance and Burton 1999; Vance et al., 2004).The "cleaned" foraminifera procedure includes all steps (with reductive and oxidative step), for the "uncleaned" foraminifera only the clays were removed.*

step	chemical solution	repetition	treatment
clay removal	5 ml *Milli Q*© water 2 to 5 ml methanol	3 times twice	20 to 60 sec ultrasonic bath 20 sec ultrasonic bath
sample rinse	5 to 10 ml *Milli Q*© water	3 times	-
reductive cleaning	10 ml of a cleaning solution (50 ml) containing: 30.5 ml ammonium hydroxid (25%) + 2.4 g citric acid + 2.43 ml hydraziniumhydroxid + 17 ml *Milli Q*© water	-	30 min water bath (90°C) + for 20 sec every 2 min ultrasonic bath
sample rinse	10 to 15 ml *Milli Q*© water	3 times	-
oxidative cleaning	10 ml of a cleaning solution containing: 500 µl H_2O_2 (30%) + 50 ml NaOH (0.1 N)	-	30 min water bath (90°C) + 1 min every 10 min ultrasonic bath
sample rinse	10 to 15 ml *Milli Q*© water	3 times	afterwards transfer in 1.5 ml safe lock tubes
dissolution	0.5 to 1 ml 0.5 M HNO_3	-	add in 100 µl steps ultrasonic for few min until dissolution is completed

PREPARATION FOR Nd COLUMNS (in 0.1 M HCl)
LN-SPEC COLUMNS (mesh size 50-100) TO SEPERATE Nd from other REEs

$^{143}Nd/^{144}Nd$ MEASUREMENT

2.2.4. Isotope analysis

All isotopic measurements were carried out on a *Nu Plasma* Multicollector ICP-MS at GEOMAR, Kiel. Prior to the isotope batch runs of all elements a concentration test was performed to ensure the same concentration and consequently the same beam size for all samples of one element during the isotope batch run. Hence, the Nd samples were diluted in 1 ml HNO_3 (2%) to concentrations around 120 ppb. Samples with a very low Nd concentration, e.g. the foraminifera calcite, were measured in the time – resolved mode, where the sample was diluted with 250 – 500 ml HNO_3 (2%) to generate a concentration as high as possible. Mass bias corrections used a value of

0.7219 for the $^{146}Nd/^{144}Nd$ and all $^{143}Nd/^{144}Nd$ data were normalized to the accepted value of the JNdi-1 standard of 0.512115 [*Tanaka et al.*, 2000]. Repeated measurements of this standard gave a long term reproducibility for the JNdi-1 standard solution of ±0.3 ε_{Nd} (2σ). The procedural Nd blanks were ≤ 85 pg.

The Sr samples were diluted to 80 ppb with 1 ml HNO_3 (2%) prior to the isotope measurement. Sr mass bias correction used an exponential fractionation law ($^{86}Sr/^{88}Sr$ = 0.1194 [*Steiger & Jäger*, 1977]) after correcting for interferences on ^{86}Kr and ^{87}Rb. The krypton (Kr) background noise, produced by the inconsistent krypton concentrations in the argon carrier gas, was determined by measuring an additional zero cycle prior to the standard and sample analysis. The Sr isotope results were normalized to $^{87}Sr/^{86}Sr$ = 0.710245, which is the accepted value of the NIST NBS987 standard and which was also used to derive the long term reproducibility of the radiogenic Sr isotope measurements of ±0.000032 (2σ) over one year. The Sr procedural blanks were below 2 ng.

Similarly to Sr, all purified Pb samples were diluted with 1 ml HNO_3 (2%) to a concentration of around 70 ppb. The analysis of the Pb ratios are based on the standard bracketing method of Albarède et al. [2004] using the NIST NBS981 standard with values of $^{206}Pb/^{204}Pb$ = 16.9405, $^{207}Pb/^{204}Pb$ = 15.4963 and $^{208}Pb/^{204}Pb$ = 36.7219 [*Abouchami et al.*, 1999]. The long term reproducibility (2σ) for this standard was ± 0.0062 for $^{206}Pb/^{204}Pb$, ± 0.0071 for $^{207}Pb/^{204}Pb$, ± 0.024 for $^{208}Pb/^{204}Pb$, ± 0.0005 for $^{208}Pb/^{206}Pb$ and ± 0.0001 for $^{207}Pb/^{206}Pb$. The Pb procedural blanks were below 1.5 ng.

2.3. RESULTS

2.3.1. Comparison of core top data with water data

2.3.1.1. Locations under the influence of Arctic outflow water

The Nd isotope compositions from the different leaching methods, as well as from cleaned and uncleaned foraminifera of core top sediments from ODP Sites 984 and 907 proximal to Iceland are more radiogenic than expected compared to corresponding seawater (Fig. 2.3, Tab. A.2). In contrast, the $^{87}Sr/^{86}Sr$ signatures of the same samples

(Tab. A.2) closely reflect the present seawater signal of 0.70916 [*McArthur et al.*, 2001]. At Site 984 (water depth 1648m), *leaching method A* produced an ε_{Nd} value of +4.7, 12 ε_{Nd} units more radiogenic than the isotopic signal of Arctic Intermediate Water (AIW) (ε_{Nd} = -8 to -9) northeast of Iceland (station 21) [*Lacan & Jeandel*, 2004b] and 19 ε_{Nd} units more radiogenic than the Labrador Sea Water (ε_{Nd} = -14) further the south in the Iceland basin (station 12) [*Lacan & Jeandel*, 2005b].

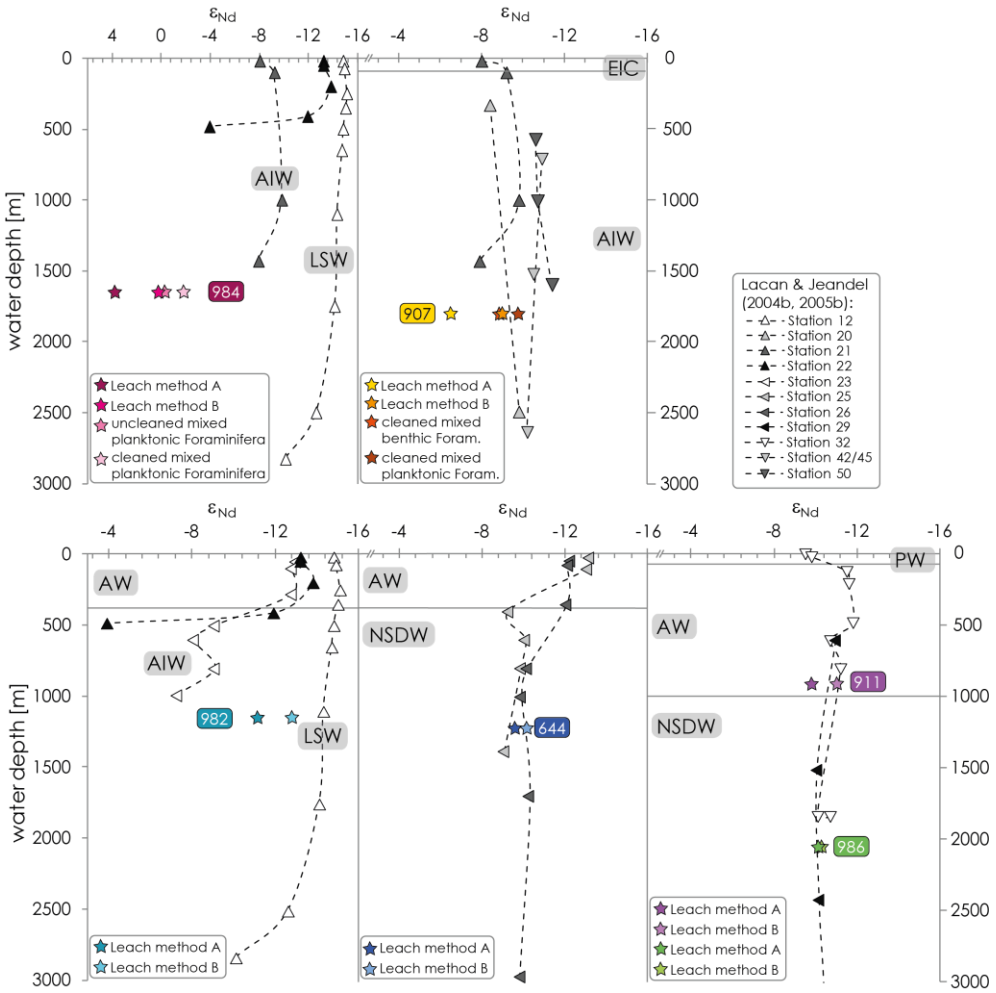

Figure 2.3: Water column Nd isotope profiles *of locations in the Nordic Seas and northernmost Atlantic Ocean [Lacan and Jeandel, 2004b, 2005b] in proximity to the ODP sites used in this study and core top Nd isotope composition extracted by different leaching methods of all sites and from foraminiferal calcite of Site 984 and 907. AIW: Arctic Intermediate Water, LSW: Labrador Sea Water, EIC: East Icelandic current, AW: Atlantic Water, NSDW: Norwegian Sea Deep Water, PW: Polar Water [Hansen and Østerhus, 2000].*

These differences are indicative of overprinting of the seawater signature by partial dissolution of volcanic ash from Iceland (ε_{Nd} = +5 [*O`Nions and Grönvold*, 1973]). However, we also point out that both these water column data cannot be considered fully representative of the location of Site 984 given that they are too far away (Fig. 2.1) and that the water column Nd isotope distribution west and southwest of Iceland is essentially unknown. The application of *leaching method B* yielded a less radiogenic ε_{Nd} value of -0.1 ± 0.3, which is however, most likely still more radiogenic than the bottom water at this site (Fig. 2.3). The Nd isotopic composition of calcitic shells of cleaned and uncleaned planktonic foraminifera varied between ε_{Nd} values of -1.3 and -1.6 units, which is also significantly more radiogenic than the expected seawater signal.

The leachates of Site 907 (water depth 1800m) (*method A*) show a somewhat more radiogenic signal (ε_{Nd} = -6.5) than AIW (station 20 and 21 [*Lacan & Jeandel*, 2004b]), while results of *leaching method B* with ε_{Nd} = -8.9 reflect the present seawater accurately. In contrast to Site 984, however, the core top cleaned planktonic and benthic foraminifera (ε_{Nd} = -8.8 to -9.8) exactly reflect the present day deepwater measured close to Site 907. Unfortunately, Site 907 is essentially barren of foraminifera below the surface.

2.3.1.2. Locations under the influence of inflowing Atlantic water

The Nd isotope composition of the leachates extracted with *leaching method A* (ε_{Nd} = -11) and *leaching method B* (ε_{Nd} = -13) of the core top sediment of southernmost Site 982 (1135m water depth) reflect a mixture of AIW from the north and LSW from the south. Here, the ε_{Nd} core top data reflect an increased influence of LSW, in particular the result of *leaching method B*. The core top data from Site 644 on Vøring Plateau (1220 m water depth) closely reflect Norwegian Sea Deep Water (ε_{Nd} = -9.1 to -10.1), independent of the leaching method used (ε_{Nd} = -9.6 and -9.9 for Method A and B, respectively). Similar to Site 644, the leachates (*method A and B*) of Site 986 on the western shelf of Svalbard (2050 m water depth) reproduced the Nd isotopic composition of NSDW (Fig. 2.3). In contrast, the leached core top data of Site 911 (ε_{Nd} = -11)

extracted with *method B* from a shallower water depth (900 m) on the Yermak Plateau reflects the modified inflowing Atlantic water entering the Nordic Seas.

In summary, the sites located under the influence of the modified Atlantic waters and at a distance from any volcanic sedimentary component reflect the present seawater signal and are thus suitable for further paleoceanographic reconstructions.

2.3.2. Comparison of the down core data

2.3.2.1. Neodymium isotope composition

The volcanic contamination from Iceland at Site 984 is confirmed by the down core Nd isotopic signal extracted from the sediments applying different leaching methods, as well as from cleaned and uncleaned foraminiferal shells (Fig. 2.4). *Leaching method A* yielded the most radiogenic ε_{Nd} values between +0.5 and +4.8, close to the Nd isotope composition of the detrital fraction (ε_{Nd} = +5.5 ± 0.17) that reflects the dominant contribution of basaltic ash and glasses from Iceland volcanoes. Results of *leaching method B* to sediments of Site 984 are less radiogenic, although still too radiogenic (ε_{Nd} = -1.9 to 1.7) compared to the expected seawater signal. These results are within error the same as those of the carbonate fraction determined for selected samples (ε_{Nd} = -1.6 to 1.5). Furthermore, the foraminiferal ε_{Nd} data range between -3.7 and +1.2 and also do not reflect the expected seawater signal (Fig. 2.4). At Site 984, the different leaching methods (*A* and *B*) yield a mean offset of 3 ε_{Nd} units and the mean difference between *leaching method B* and the cleaned and uncleaned foraminifera is 1.2 ε_{Nd} units. The Nd isotope composition of the "cleaned" and "uncleaned" foraminifera reveals the same value within error with no significant offset.

For Site 907 a mean offset of 1.5 ε_{Nd} units is observed between *leaching method A* and *B*, whereby *leaching method A* (ε_{Nd} = -6.5 to +4.5) yielded more radiogenic signatures than the bottom water signal extracted with *leaching method B* (ε_{Nd} = -8.9 to -0.2) (Fig. 2.4). Overall both signatures are also more radiogenic than expected bottom water values, but, in contrast to Site 984, the detrital fraction of Site 907 is much less

radiogenic (ε_{Nd} = -8.6) and can thus not serve as the source of contamination with too radiogenic signatures.

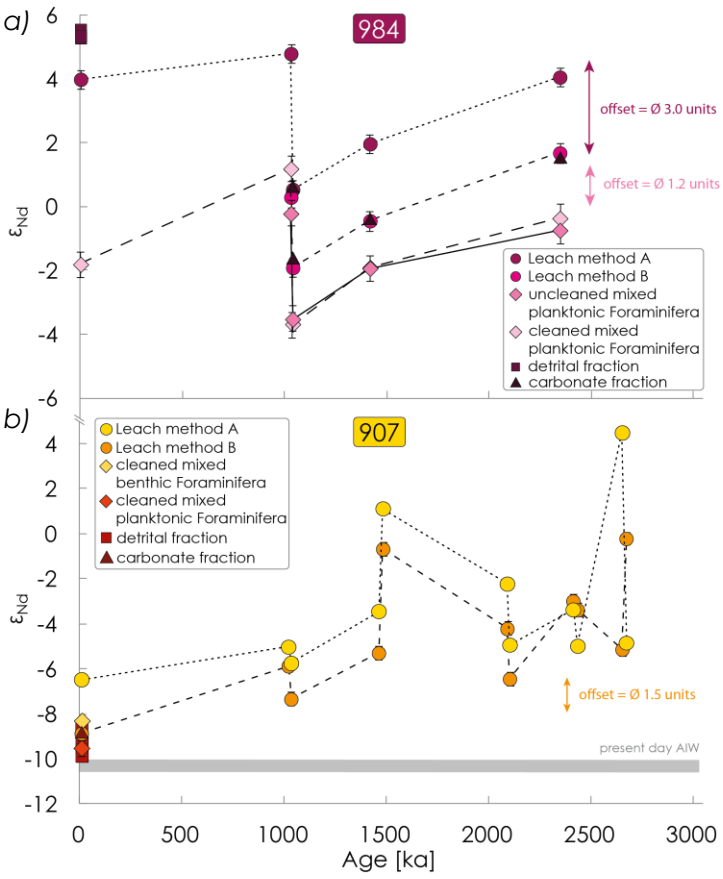

Figure 2.4: Down core Nd isotope data of a) Site 984 and b) 907 of the leach fractions extracted with the different leach methods, of the carbonate fraction, of the detrital fraction and of the foraminifera. *The gray bar indicates the present day seawater. The present day seawater near Site 984 varies between ε_{Nd} = -9 (AIW) and ε_{Nd} = -14 (LSW) [Lacan and Jeandel, 2004b, 2005a] and is therefore not displayed in this figure.*

In contrast to Sites 984 and 907, leachates of the sediments of the sites under the influence of the inflow Atlantic waters (982, 644, 986, and 911) appear to accurately reflect the bottom water (Fig. 2.5), and show similar differences between both leaching methods. The smallest offset between the different leaching methods is observed on Rockall Plateau (Site 982) (*A*: ε_{Nd} = -12.7 to -9.1; *B*: ε_{Nd} = -12.5 to -9.5) with a difference of less than 0.5 ε_{Nd} units. The offset of the Nd isotopic composition between *leaching method A* and *leaching method B* increases with latitude towards the north. At Site 644 on the Vøring Plateau difference between *leaching methods A* (ε_{Nd} = -11.7 to -7.2) and *B* (ε_{Nd} = -12.2 to -9.4) is 1.4 ε_{Nd} units, again with less radiogenic values using *leaching method B.*

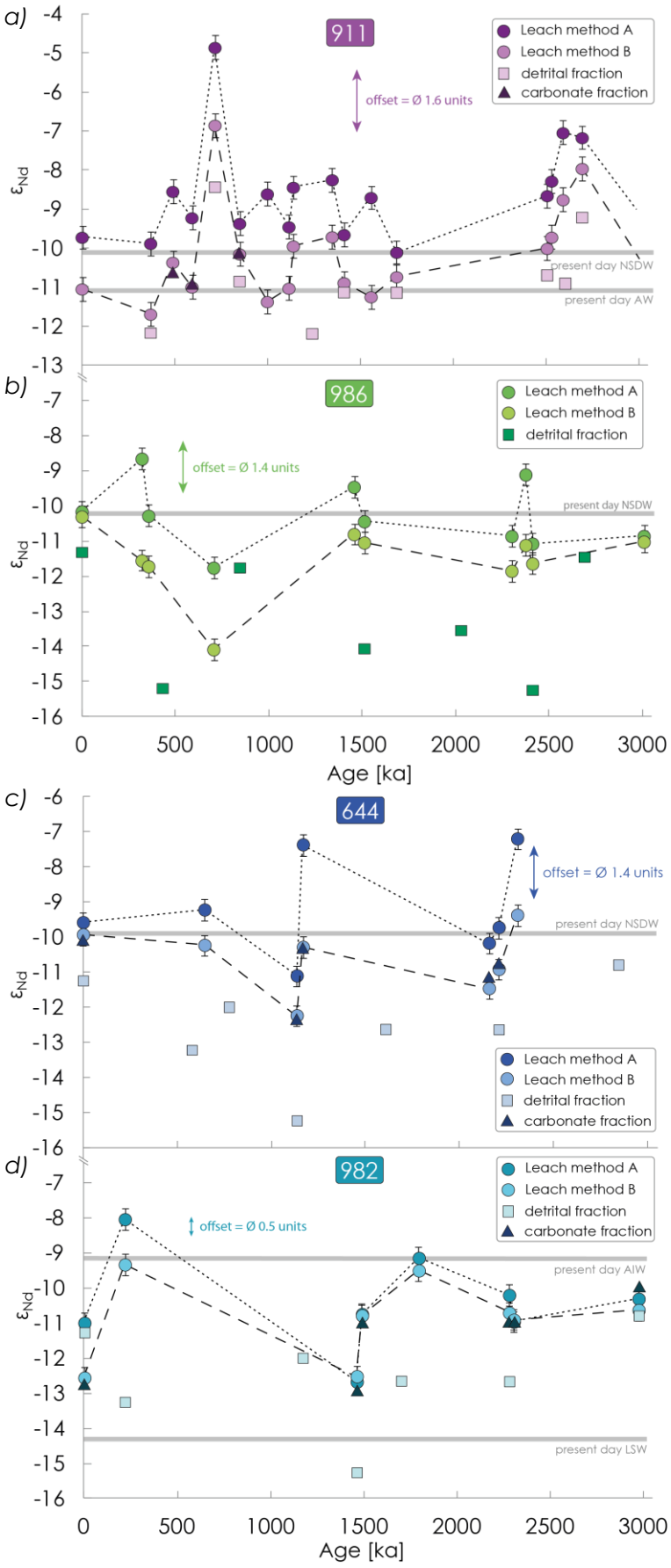

***Figure 2.5: Down core Nd isotope data extracted by leaching method A and B**, detrital fraction and carbonate fraction compared with present day seawater from the nearest locations (gray lines [Lacan and Jeandel, 2004b, 2005b]) from the north to the south: a) Site 911, b) Site 986, c) Site 644 and d) 982.*

A similar pattern is observed on the western shelf of Svalbard, where also an offset of 1.4 ε_{Nd} units is seen between both leaching methods (*A*: ε_{Nd} = -11.8 to -8.7; *B*: ε_{Nd} = -14.1 to -10.3). Further north on Yermak Plateau, this offset is also similar at 1.6 ε_{Nd} units despite the essentially negligible amount of biogenic carbonate in the samples of Site 911. The Nd isotope compositions of Site 911 using *method A* range between -10.1 and -4.9 and between -11.7 and -6.9 using *method B*.

For all sites in the Nordic Seas and the North Atlantic Ocean the Nd isotopic compositions obtained with *leaching method B* are indistinguishable from the results extracted from the carbonate fraction. The Nd isotope compositions of the detrital fraction of all sites under the influence of Atlantic waters in the eastern part of the North Atlantic Ocean and the Nordic Seas (Site 911, 986, 644, 982) are less radiogenic than those of the authigenic coatings or of foraminiferal carbonate (ε_{Nd} = -15.2 to -8.4) (see Chapter 4). In addition, despite the significant offsets between the different leaching methods and between the leach fractions and the foraminiferal record, all records show the same patterns of maxima and minima independent of the applied method.

2.3.2.2. Strontium and lead isotope composition

Contamination by partial dissolution of the detrital fraction may bias the seawater signal extracted. Despite being a qualitative, and possibly unambiguous measure of detrital Nd contamination [*Gutjahr et al.*, 2007], the radiogenic $^{87}Sr/^{86}Sr$ ratio in the solutions containing the seawater derived extracted metals were monitored to identify major deviations from the expected seawater signatures.

Leachates extracted from the sediment of the sites near Iceland (Site 907 and 984) closely reflect the seawater Sr isotope evolution [*McArthur et al.*, 2001]. The $^{87}Sr/^{86}Sr$ signature from leachates of Site 984 yields a very low difference between the two methods, but *leaching method A* (average $^{87}Sr/^{86}Sr$ = 0.708942) reveals slightly less radiogenic values than *leaching method B* (average $^{87}Sr/^{86}Sr$ = 0.709005), which is closer to the contemporaneous seawater (Fig. 2.6a). The $^{87}Sr/^{86}Sr$ ratio of the leach fractions, however, show a offset to the less radiogenic values of the detrital fraction (average $^{87}Sr/^{86}Sr$ = 0.704971).

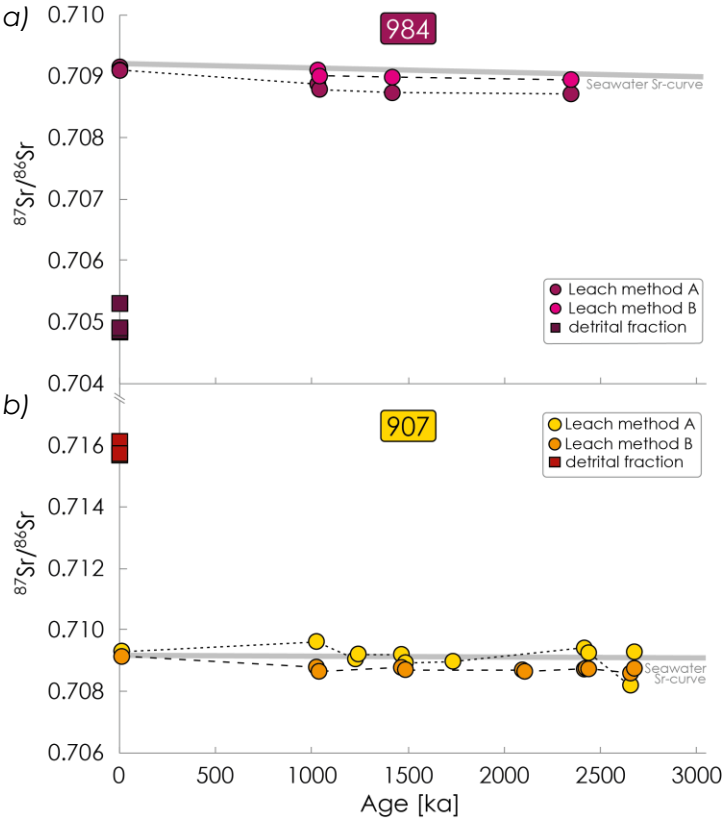

Figure 2.6: Down core $^{87}Sr/^{86}Sr$ data *of a) Site 984 and b) 907 of the leach fraction extracted with the two different leaching methods and of the detrital fraction. The gray line indicates the seawater $^{87}Sr/^{86}Sr$ evolution [McArthur et al., 2001].*

The Sr isotopic composition of Site 907 north of Iceland is close to the seawater signal although *leaching method A* (average $^{87}Sr/^{86}Sr$ = 0.709184) shows slightly more radiogenic values than the expected seawater values while *leaching method B* (average $^{87}Sr/^{86}Sr$ = 0.708742) shows slightly less radiogenic values than seawater. Similar to Site 984 the leach fractions are clearly distinct from the detrital fraction, which at Site 907 is more radiogenic (average $^{87}Sr/^{86}Sr$ = 0.715883) (Fig. 2.6b).

The Sr isotopic composition of the leachates from sites located on Rockall Plateau (Site 982) and Vøring Plateau (Site 644) reflect the seawater signal closely with no significant difference between the leaching methods (Fig. 2.7a+b). Site 982 has an average $^{87}Sr/^{86}Sr$ = 0.709149 for *leaching method A* and 0.709128 for *method B*. The data of Site 644 show a slight difference between both methods ($^{87}Sr/^{86}Sr$ = 0.709568 for leaching *method A*; $^{87}Sr/^{86}Sr$ = 0.709231 for leaching *method B*). The detrital fractions of both sites ($^{87}Sr/^{86}Sr$ = 0.713512 for Site 982; $^{87}Sr/^{86}Sr$ = 0.724634 for Site 644) show more radiogenic signatures than the leach fractions (Fig. 2.7a,b).

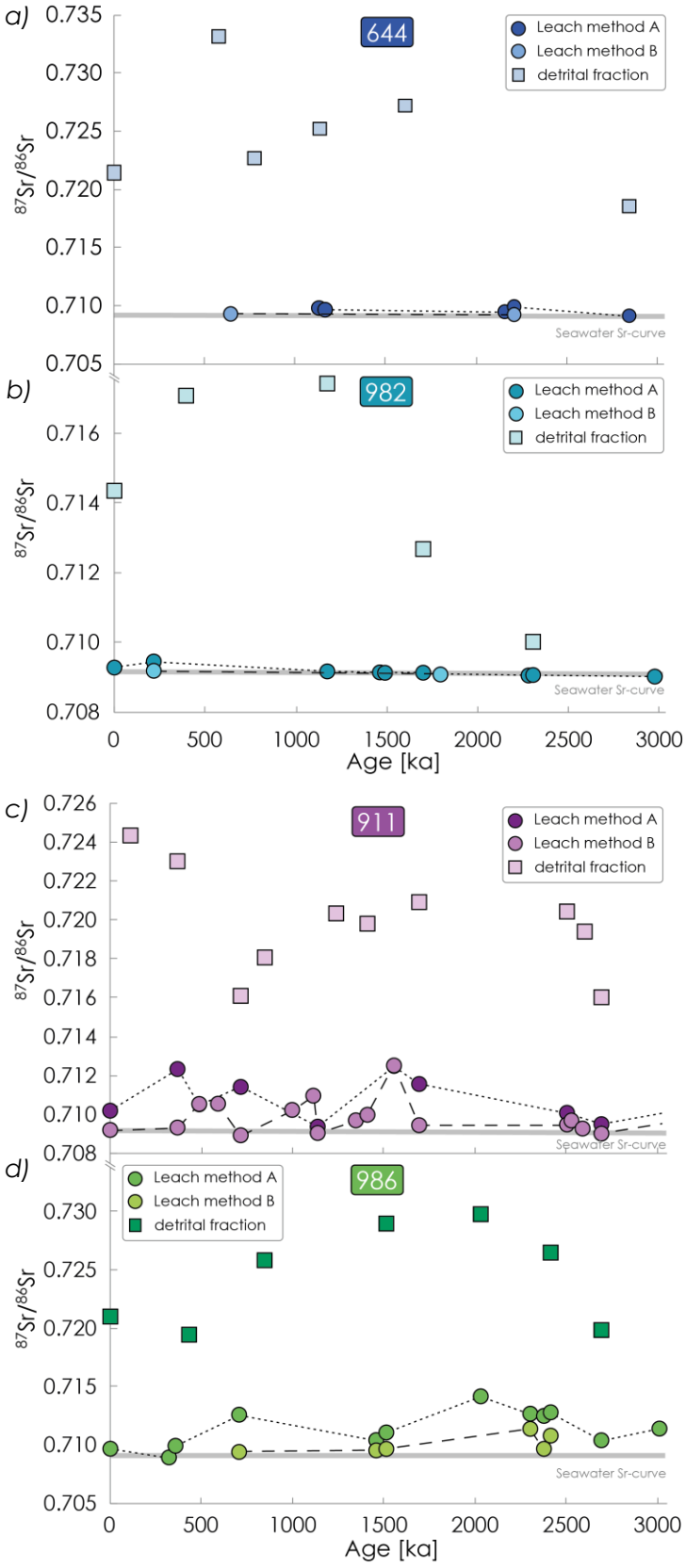

Figure 2.7: Down core $^{87}Sr/^{86}Sr$ data *of a) Site 644, b) Site 982, c) Site 911 and d) 986 of the leach fraction extracted applying leaching methods A and B and of the detrital fraction. The gray line indicates the seawater $^{87}Sr/^{86}Sr$ evolution [McArthur et al., 2001].*

In contrast to the four southern sites, the leachates of the northernmost sites on the western shelf of Svalbard (Site 911 and 986) show a significant difference to the Sr isotope evolution of seawater and between both leaching methods. Site 986 has an average Sr isotopic composition of 0.711360 for *leaching method A*, 0.710054 for *leaching method B* and 0.724459 for the detrital fraction. Accordingly *leaching method B* offers better fits with the seawater signal over this period, but is still slightly more radiogenic than seawater. A similar behavior is apparent at Site 911, for which both leaching methods produce a shift of the leachates to more radiogenic values ($^{87}Sr/^{86}Sr$ = 0.710837 for *leaching method A*; $^{87}Sr/^{86}Sr$ = 0.709870 for *leaching method B*) (Fig. 2.7 c,d). In summary we found that the offset from the expected seawater signal is always higher in *leaching method A* (with carbonate removal), which not surprising is given the high seawater-derived Sr concentrations contained in foraminiferal carbonate.

The down core isotope signal of Pb for selected samples of Site 911, 986, 644 and 907 in the Nordic Seas as well as Site 984 in the North Atlantic Ocean are displayed in Fig. 2.8. Generally, the lowest $^{206}Pb/^{204}Pb$ ratios occur in the influence of Svalbard at Site 911 ($^{206}Pb/^{204}Pb$ = 18.57) and Site 986 ($^{206}Pb/^{204}Pb$ = 18.49), whereas Site 644 reveals the most radiogenic composition of $^{206}Pb/^{204}Pb$ = 19.24 (Tab. A.3). The Pb isotope composition of the detrital fraction of the bulk sediment ranges around similar values as the leached fraction data. Additionally, the down core Pb isotope composition extracted from the ferromanganese coatings of all sites show no significant disagreement (except a few exceptions) between the different leaching methods.

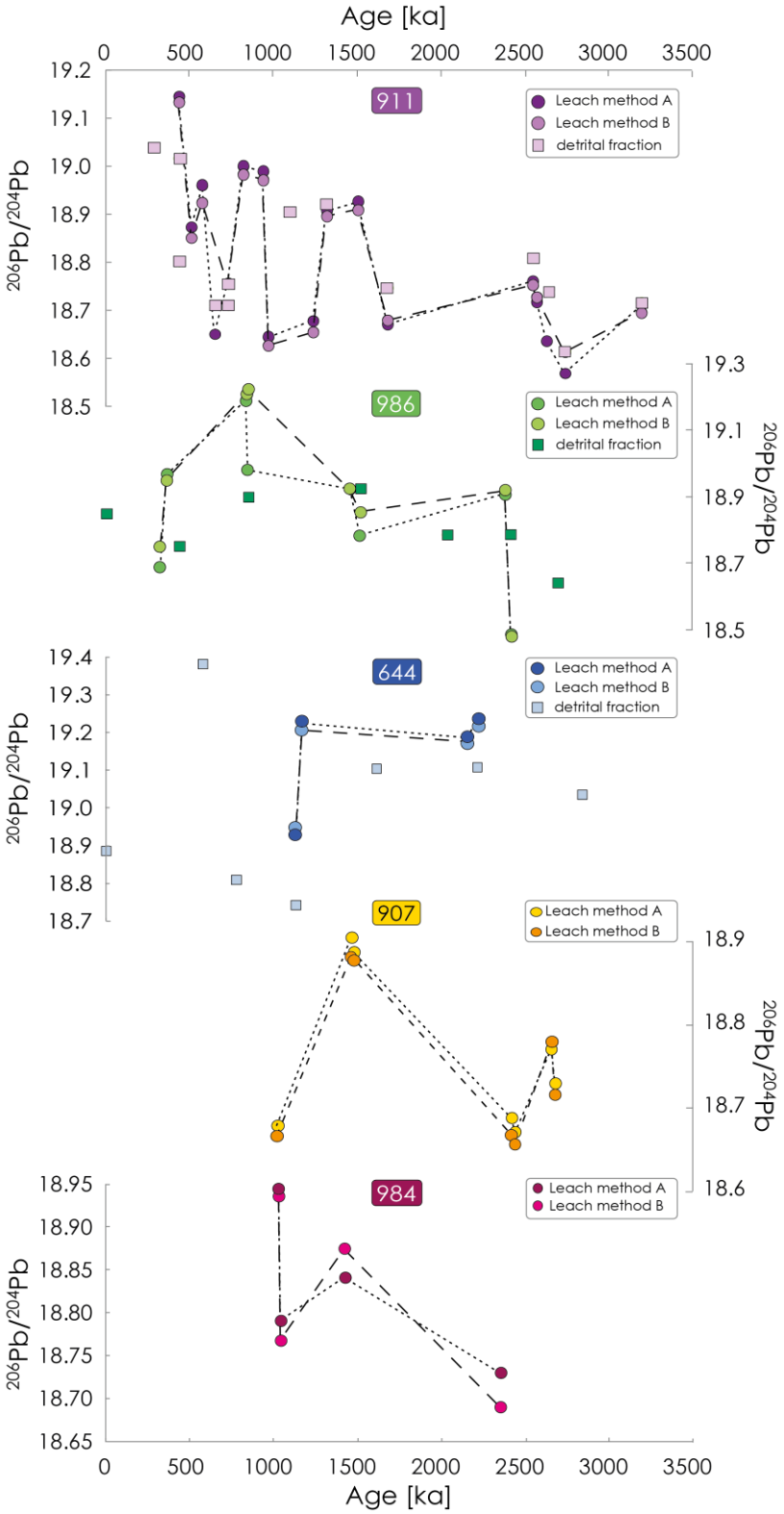

Figure 2.8: Down core $^{206}Pb/^{204}Pb$ data *of Site 911, Site 986, Site 644, Site 907 and Site 984 of the leach fraction extracted applying leaching methods A and B and the detrital fraction over the past 3.2 Ma.*

2.4. DISCUSSION

2.4.1. Influence of Icelandic basalts on the extracted Nd isotope compositions

Comparison of present seawater data in the northernmost Atlantic Ocean and Nordic Seas [*Lacan and Jeandel*, 2004b, 2005b; *Andersson et al.*, 2008] and the core top leachates of the different sites show that the western locations under the influence of Iceland and of Arctic intermediate water (AIW) do not reflect the present seawater signal. The core top Nd isotope results of Site 907 and Site 984 were too radiogenic compared with deep water values at the nearest location of known water column composition (Fig. 2.1). It is most likely that basaltic ash particles with highly radiogenic Nd isotope signatures originating from Iceland were partially dissolved and responsible for the positive offset. The contamination by volcanic material, especially ash, originates from 1) partial dissolution of the ash particles in the laboratory during the leaching procedure or 2) in the pore waters of the sediments during the early diagenetic formation of Fe-Mn oxides [*Elmore et al.*, 2011]. Here, the first mechanism is more likely, because volcanic ash is highly labile and dissolves readily in contact with seawater [*Gislason and Oelkers*, 2003] and is therefore easy leachable in the leach solution containing a pH of only 4. The dissolution of even a small amount of the highly radiogenic Icelandic material (ε_{Nd} = +5 to +10 [*Cohen and O'Nions*, 1982; *Hemming*, 2004]) would lead to significantly more positive signatures in the leachates. This contamination is also supported by the close correspondence of the Nd isotopic composition of the leach fraction and of the detrital fraction of Site 984. In contrast, Site 907 sediments have less radiogenic ε_{Nd} values of the detrital fraction (ε_{Nd} ~ -8) than in the leachates. This isotope signature is most probably a consequence of the highly unradiogenic sediment input from Greenland and the radiogenic input from Iceland or from a basaltic rock formation in the southeast of Greenland with an ε_{Nd} of +8 [*Bernstein et al.*, 1998]. *Elmore et al.* [2011] found similarly radiogenic Nd isotopic compositions in sediments and foraminifera near Iceland, supposedly accurately reflecting past seawater in the North Atlantic Ocean. They also describe values between an ε_{Nd} of -2.6 and +3.1 in core top leachates, which were also inferred to be caused by contamination with volcanic material from Iceland. In addition, the Nd isotopic compositions of the calcitic shells of planktonic and benthic foraminifera yielded much

more negative and in the case of Site 907 reliable seawater signatures. Compared to the seawater Nd isotope signature of station 21 [*Lacan and Jeandel*, 2004b] southeast of Site. Here, the cleaned planktonic foraminifera reflect the surface waters in 100 m water depth within error ($\varepsilon_{Nd\ planktonic\ foraminifera}$ = - 9.75; $\varepsilon_{Nd\ seawater}$ = - 9.2) and the benthic foraminifera are similar the bottom water Nd signature ($\varepsilon_{Nd\ benthic\ foraminifera}$ = -8.8; $\varepsilon_{Nd\ seawater}$ = - 7.9). Whereas, for Site 984 the signatures still appear too positive, which also corroborates the findings of *Elmore et al.* [2011] (ε_{Nd} = -6.8 to -2.3).

Furthermore we observed no significant difference between cleaned and uncleaned planktonic foraminiferal shells, suggesting that the cleaned foraminifera were not fully cleaned from the ferromanganese coatings and reflect bottom water signatures. This finding is consistent with the results of *Roberts et al.* [2010], who postulated that 90 – 98% of all coatings must be removed in order to achieve a realistic surface seawater signal. Nevertheless, the extraction of the Nd isotope compositions from the foraminiferal shells clearly reduces the Icelandic contamination, and therefore ε_{Nd} signatures extracted from foraminifera are considered more reliable than the leached bulk sediment coatings, at least in areas proximal to volcanic sources. Similar to the leachates, the offset between the seawater signal and radiogenic values of the foraminifera shells next to Iceland can be explained by small amounts of glass shards that were not completely removed during the cleaning procedure of the foraminiferal shells e.g. due to closed chambers, which may not all have been cracked open due to the small size fraction (>63 µm) and which were thus subsequently partially dissolved during the cleaning procedure.

While contamination of the leachates by volcanic material is most probable, it is also possible that the seawater above Site 984 is more radiogenic than we expect through comparison with "nearby" water column data [*Lacan and Jeandel*, 2004b; 2005b]. In this instance, the extracted seawater signal would reflect the local bottom water more closely. This supposition is supported by the Sr isotope compositions of Site 984 and 907, which largely reflect the seawater Sr isotope signature independent from the applied leaching method. Such a shift to more radiogenic values of the bottom waters near the Mid Atlantic Ridge south of Iceland may be caused by boundary exchange with basaltic rocks, which has been shown to be significant along the continental margins of the Nordic Seas and northernmost Atlantic [*Lacan and Jeandel*,

2004a, 2005a]. *Lacan and Jeandel* [2004a] describe a change of the Nd isotope composition of the East Greenland Current in the northernmost Atlantic and Nordic Seas by 3 ε_{Nd} units to more radiogenic values after passing the volcanic rocks that outcrop in the Denmark Strait. Similar changes have been observed for the Iceland Scotland Overflow Water (ε_{Nd} = -8.2), which are influenced by the radiogenic signature of the Norwegian basin basaltic margin characterized by ε_{Nd} signatures between -2.5 and +0.8 near the Iceland Faroer Ridge [*Lacan and Jeandel*, 2004b]. Due to the absence of dissolved Nd isotope compositions of the water column at the location of Sites 984 and 907 it is not possible to make unambiguous conclusions on this possibility, which should be subject of future investigations of the water column. As such, the only method that confidently reproduced a reliable Nd isotopic composition of bottom water are the core top foraminifera data of Site 907; but unfortunately this site is barren in foraminifera down core. The Nd isotope composition of core top sample of Site 907 extracted by *leaching method B* show almost seawater composition, but differs down core significantly from seawater signature and is not used for further analysis.

The Sr isotope composition of Site 984 and 907 extracted by the different leaching methods largely reflect the present seawater Sr isotope signature, although the different leaching methods do not provide a reliable Nd isotope composition. A possible reason could be that the Sr isotope composition, in contrast to the Nd isotope composition, released from basaltic particles does not influence the seawater Sr isotope signal significantly. This is most likely caused by a much higher Sr concentration in seawater than released from the basaltic material, which implicates an overprinting of the volcanic signature by the seawater Sr signal. Based on these observations Sites 984 and 907 were not considered further for detailed paleoreconstructions based on Nd isotopes.

2.4.2. Application of different leaching methods in the area of the Atlantic water inflow

Leachates from the sites influenced by the modified Atlantic waters in the Nordic Seas reflect the seawater Sr and Nd isotope signal of the water masses in the corresponding water depth and are not influenced by exchange with volcanic material.

However, there are differences between the results of the two leaching methods applied. The analysis of the Nd isotope compositions indicated that the carbonate fraction yielded within error the same ε_{Nd} values as the results of *leaching method B*, which represents a mixed signal of the carbonate fraction and the ferromanganese coating ("leach") fraction, when the carbonate is not removed before the hydroxylamine leaching step. In this case, the Nd isotope composition of the carbonate fraction dominates the Nd isotope results due to the high Nd concentration in the carbonate, which we measured for selected samples (from Site 911 and 907). Concentration measurements of the carbonate and leach fractions show that the Nd concentration in the carbonate fraction are one order of magnitude higher (~7 – 10 ppm Nd), than in the leach fraction (500 – 700 ppb Nd), contrary to previous studies observing a very low Nd concentration in the foraminiferal calcitic tests [*Palmer*, 1985; *Pomiès et al.*, 2002; *Tachikawa et al.*, 2013]. Hence the high Nd concentration is caused by a different Nd carrier, for example framboidal aggregates inside test pores and inner chambers of the foraminifera, described by *Tachikawa et al.* [2013]. These framboidal particles consists of Fe-Mn oxides and oxidized Fe sulphides as pyrite, greigite, hematite and magnetite and contain high amounts of Nd, which were absorbed on the sediment particles, not directly incorporated due to the high affinity of Nd to Mn and Fe oxides [*Koeppenkastrop and De Carlo*, 1992]. Another explanation for the high Nd on the foraminiferal test is described by *Martínez-Botí et al.* [2009], who indicate that the organic material within the foraminiferal tests contains high amounts of Rare Earth Elements (REE). So even if the Nd concentration in the foraminiferal test calcite is low, it increases in the whole shell through incorporation of framboidal aggregates or organic material. Hence, if just a minor amount of carbonate is not dissolved during the carbonate removal step, it will dominate the Nd isotope signal of the leach fraction.

2.4.2.1. Offset between leaching methods applied at sites under the influence of the Atlantic inflow

The offset between the different leaching methods (Fig. 2.5) most probably originates from a less radiogenic phase being removed while dissolving the carbonate. Furthermore, the carbonate fraction extracted by leaching with the buffered acetic acid

solution is significantly different from the cleaned and uncleaned foraminifera test (Fig. 2.4). This points to the fact that not only foraminiferal carbonate is dissolved in the buffered solution but also other biogenic carbonates or a completely different phase, e.g. less stable Fe oxides. Contamination during application of *leaching method A* by partial dissolution of the detrital phase can be excluded, because the leach fraction obtained by *method B* is even less radiogenic than by *leaching method A* and resembles more the Nd isotopic composition of the detrital fraction. The offset between the different leaching methods appears to increase with latitude and with the corresponding carbonate content of the cores (Fig. 2.9):

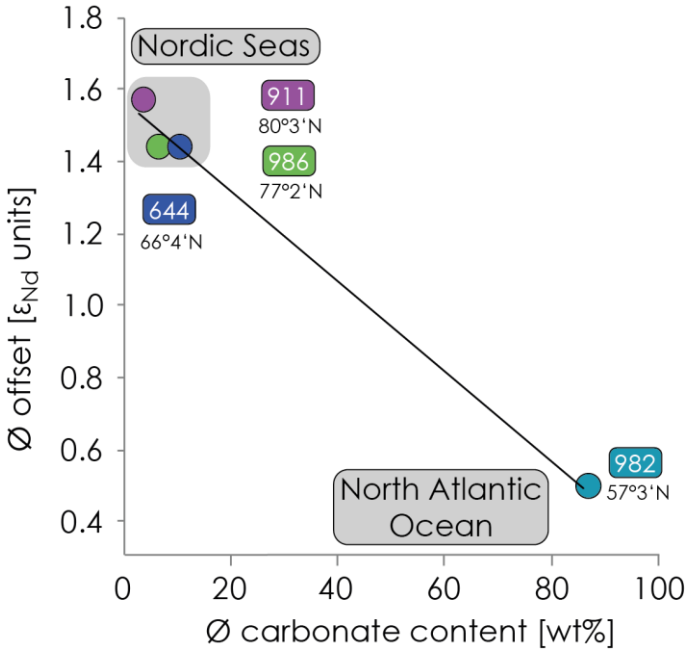

Figure 2.9: *The average offset between leach method A (with carbonate removal) and leach method B (only hydroxylamine solution) compared with the average carbonate content of the sites in the Nordic Seas (911, 986, 644) and in the North Atlantic Ocean (982).*

Site 982, the southernmost Site, with the highest carbonate content (86% [*Jansen et al.*, 1996]) yields the smallest offset (0.5 ε_{Nd} units), Site 911 on the Yermak Plateau with the lowest carbonate content of ~1 – 6% [*Myhre et al.*, 1995] has the most significant offset of 1.6 ε_{Nd} units. One explanation for the small offset at Site 982 may be an incomplete removal of the carbonate during the decarbonation step. This is supported by investigations of *Martin et al.* [2010], who measured, besides biogenic silica and clay, biogenic carbonate in the samples after the decarbonation step of the

leaching procedure. They also found a similar correlation between the offset and carbonate content in a core top sample of one location on the Gloria Drift in the North Atlantic Ocean, which is characterized by low carbonate content and an offset between the two fractions of about 1.2 ε_{Nd} units.

2.4.3. Strontium and lead isotope composition

In the southern Sites (Site 907, 984, 982, 644), the Sr isotopic compositions obtained with both leaching methods reveals the expected bottom water signature, indicating no significant contamination by detrital material. However, if the carbonate fraction is not fully dissolved and removed, this seawater signal can completely overprint that of any potential contamination from partial dissolution of the detrital fraction, as described by *Bayon et al.* [2002]. The offset of the Sr isotopic compositions to more radiogenic values away from the seawater signal is highest in the northernmost Sites on the shelf of Svalbard (Site 911 and 986) and is most likely cause by detrital contamination. The mass balance calculations made by *Gutjahr et al.* [2007] imply that the $^{87}Sr/^{86}Sr$ ratio is susceptible to detrital contamination compared to the Nd and Pb isotope composition of the leach fraction, which is less sensitive. Therefore, it is possible that carbonate-free sedimentary leach Sr isotopic signatures can reflect potential detrital contamination that is not apparent in the Nd isotope signature.

Considering their Nd isotope compositions, which reliably reflect the expected seawater values, Sites 911 and 986 as well as 982 and 644 can be used further for paleoreconstructions. Our results show clearly that every Site needs to be checked in terms of the reliability of the applied leaching method. In the case of Site 911 on the Yermak Plateau it was decided to use *leaching method B*, because the core top ε_{Nd} value of -11 reflects the most plausible seawater value at a location slightly south of Svalbard [*Lacan and Jeandel*, 2004b] (see Chapter 3). For the Sites (986, 644, 982) located further south we show that *leaching method A* (after *Gutjahr et al.* [2007]) yields more reliable results when compared with present seawater values determined by *Andersson et al.* [2008] and *Lacan and Jeandel* [2004b] for the Sites on the Vøring Plateau (644) and on the western shelf of Svalbard (986). For Site 982 on the Rockall Plateau with a high carbonate content of 86% [*Jansen et al.*, 1996] there seems to be no difference

between the *leaching method A* and *B*, supported by the small offset of both methods and a good agreement with the present seawater signal [*Lacan and Jeandel*, 2004b, 2005b]. The results of the application of the preferred leaching methods of Sites 986, 644 and 982 and their paleoceanographic implications will be described in Chapter 4.

For the Pb isotope composition extracted from the ferromanganese coatings the leaching method seems to be not substantial, supported by the high similarity of the $^{206}Pb/^{204}Pb$ ratios. The reason therefore can be the low concentration of Pb in the carbonate fraction of the sample. Hence, the Nd isotope composition extracted by the different leaching methods is the basis for the decision which method will be applied for the particular site.

2.5. CONCLUSION

In this study we tested the application of different leaching methods on different sites in the Nordic Seas and northernmost Atlantic Ocean, influenced by different water masses from the Arctic and Atlantic Ocean and by volcanic input from Iceland. The leaching methods to extract the seawater derived radiogenic Nd isotope signatures from the early diagenetic ferromanganese coatings of the sediments [*Gutjahr et al.*, 2007] was extensively tested and, where necessary, modified for the different core locations by comparison of core top data to the present bottom water Nd isotope signatures in the same areas [*Lacan and Jeandel*, 2004b; *Andersson et al.*, 2008].

Our study shows that no reliable results can be obtained that reflect bottom water at site locations near Iceland (Sites 984, 907) due to the contamination with volcanic material from Icelandic basalts and/or ash particles. This volcanic material is either partially dissolved during the leaching procedure in the lab or already in the pore waters during the formation of the ferromanganese coatings [*Elmore et al.*, 2011], which shifts the leached Nd isotope composition to significantly more radiogenic values than expected from the present day seawater signal of the AIW and its mixtures. We furthermore analyzed the Nd isotope composition of foraminiferal tests for the near Icelandic sites and still observe values too radiogenic in reductively cleaned and "uncleaned" (clays removed) foraminifera of Site 984, most likely caused by the contamination of small ash particles within the chambers of the foraminifera or by

framboidal ferromanganese oxyhydroxide precipitates within the shells. It is also possible that the foraminiferal Nd isotope results of Site 984 correctly reflect a more radiogenic seawater signal that could originate from boundary exchange with the Bjørn Drift and the Mid Atlantic Ridge, but this needs to be confirmed by seawater data from this area. The core top foraminiferal calcite data of Site 907 reflects the present seawater signal, but unfortunately this site is barren in foraminifera down core and could not be used for further paleoreconstructions.

The comparison of the bottom water data and core top leach data of four Sites (982, 644, 986 and 911) located in the modified Atlantic waters reveals reliable agreement between seawater signatures [*Lacan and Jeandel*, 2004b, 2005b] and those obtained by the different leaching methods. The down core data of the different leaching methods and sites show an offset, whereby *leaching method A* (with prior carbonate removal) always produces more radiogenic values than *leaching method B*, which are indistinguishable from the Nd isotope composition of the carbonate fraction measured for selected samples. In addition, there is an indication for a correlation between this offset in Nd isotopic composition and the carbonate content of the sites, wherein the core sites with the highest carbonate content have the lowest offset in ε_{Nd}. Based on our core top and down core results we suggest using *leaching method B* for the northernmost Site 911 and *leaching method A* for the three sites on Svalbard shelf (986), Vøring Plateau (644) and Rockall Plateau (982). The Pb isotope composition extracted from the Fe-Mn coatings of all sites show similar results between the different leaching methods and play therefore no role for the decision, which leaching method will be used for further approach of each particular site.

CHAPTER 3

Plio–Pleistocene evolution of water mass exchange and erosional input at the Atlantic–Arctic gateway

Abstract

Water mass exchange between the Arctic Ocean and the Nordic Seas has played an important role for the strength of the Atlantic thermohaline circulation and for Northern Hemisphere climate. We reconstruct past water mass mixing and erosional inputs from the radiogenic isotope composition of neodymium (Nd), lead (Pb) and strontium (Sr) at ODP site 911 (leg 151) from 900 m water depth on Yermak Plateau in the Fram Strait over the past 5.2 Myr. The isotopic composition of past bottom waters was extracted from authigenic oxyhydroxide coatings of the bulk sediments. Neodymium isotope compositions extracted from surface sediments agree well with the present day deep water ε_{Nd} signature of -11.0 ± 0.2. Prior to 2.7 Ma the Nd and Pb isotope compositions of the bottom waters only show small variations mainly due to the continuous inflow of Atlantic waters to the Yermak Plateau. Since the major Intensification of the Northern Hemisphere Glaciation (INHG) at 2.7 Ma the Nd isotopic composition has varied pronouncedly on glacial-interglacial time scales due to the waxing and waning of the icesheets on Svalbard, the Barents Sea, and the Eurasian shelf, changes in water mass exchange, and the increasing deposition of IRD from the Arctic Ocean. The Pb isotope record shows a trend to more radiogenic values as a consequence of increasing glacial weathering inputs from old continental landmasses after 2 Ma.

This chapter is going to be submitted to Paleoceanography as:

Teschner, C., M. Frank, B.A. Haley, and J. Knies. Plio–Pleistocene evolution of water mass exchange and erosional input at the Atlantic–Arctic gateway.

3.1. INTRODUCTION

The Arctic Ocean and the Nordic Seas have played an important role in determining the strength of thermohaline circulation, as well as in controlling Northern Hemisphere climate evolution. Besides the Labrador Sea, the Nordic Seas are the most important areas for the formation of cold and saline deep waters contributing to the export of North Atlantic Deep Water (NADW), which is responsible for the ventilation of the present day deep Atlantic Ocean as part of the Atlantic Meridional Overturning Circulation (AMOC). Many studies have shown that the AMOC underwent drastic changes in the past. Severe reductions or even shut downs during cold periods in the past were inferred as a consequence of diminished surface water salinity in the Nordic Seas induced by freshwater input originating from glacial melt waters [*Ganopolski & Rahmstorf*, 2001; *Clark et al.*, 2002]. Similar freshwater-triggered "slowdowns" of the AMOC may occur in the near future due to accelerated melting of the ice sheets in response to anthropogenic forcing [*Peterson et al.*, 2006].

3.1.1. Hydrographic setting

At present the Fram Strait is the only deep water (~2,600 m mean water depth) connection between the Arctic and Atlantic Ocean. The water masses in the Fram Strait and on Yermak Plateau are dominated by inflowing Atlantic Water [*Rudels et al.*, 2000, 2005]. This relatively warm and saline near-surface North Atlantic Current (NAC) enters the Norwegian Sea by crossing the Iceland-Faroe Ridge and Faroe-Shetland channel to flow northwards, where it encounters the colder, less saline waters of the East Iceland Current (EIC). The warm Atlantic sourced water remains traceable as the Norwegian Atlantic Current (NWAC) at the western shelf of Norway [*Hansen & Østerhus*, 2000] (Fig. 3.1). The NWAC inflow into the Arctic Ocean occurs via the main branch through Fram Strait [*Rudels et al.*, 2000; *Karcher & Oberhuber*, 2002], which cools and continues northwards into the Arctic Ocean as the subsurface West Spitsbergen Current (WSC). The water masses forming the Arctic Ocean outflow pass through the western Fram Strait and flow south into Denmark Strait as the East Greenland Current (EGC) (Fig. 3.1), which transports sea ice and cold, low salinity

Arctic surface waters, as well as denser water masses from the Arctic basin into the North Atlantic Ocean [*Rudels et al.*, 2005].

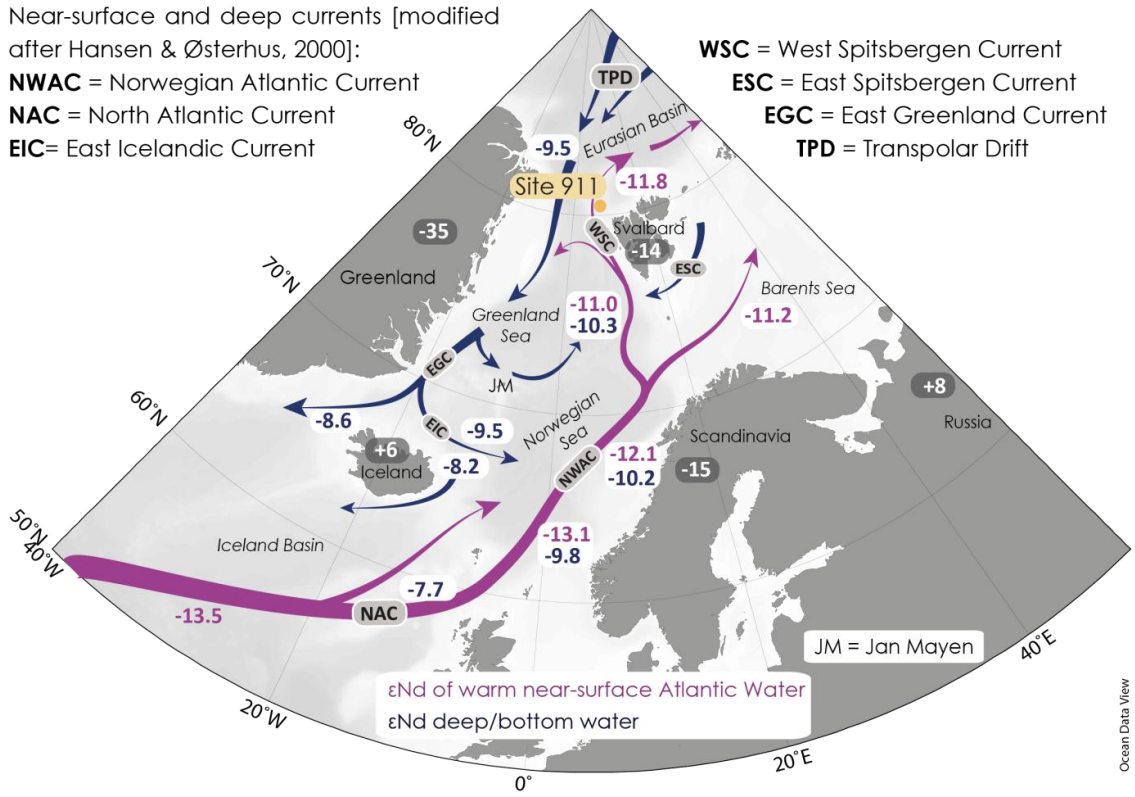

Figure 3.1: Map of the North Atlantic Ocean and Nordic Seas and study Site 911 together with schematic flow paths of the main water masses [Hansen & Østerhus, 2000] and their ε_{Nd} signatures. *Purple arrows and numbers mark the warm inflowing Atlantic water, dark blue arrows and numbers represent the cold deep and surface water masses flowing out of the Arctic Ocean, as well as the deep waters in the Norwegian-Greenland [Lacan & Jeandel, 2004a, 2004b; Anderson et al., 2008]. White numbers mark average ε_{Nd} values of the bedrocks of Svalbard [Tütken et al., 2002], Norwegian Caledonian Margin and Iceland [Lacan & Jeandel, 2004b and references therein], Putorana basalts in Russia [Sharma et al., 1992] and Greenland [Lacan & Jeandel, 2004a and references therein].*

ODP Site 911 on Yermak Plateau [ODP leg 151; *Myhre et al.*, 1995] is located within the influence of the warm modified Atlantic waters from the south. While the deep and intermediate waters are dominated by the Atlantic export into the Arctic Ocean, the Transpolar Drift (TPD) strongly influences the surface waters at the location

of Site 911 today. The TPD exports icebergs and sea ice with incorporated sediments from the Siberian shelf (Kara/Laptev Sea) towards the Fram Strait, which melt when the TPD encounters the warmer Atlantic Water and release entrained IRD. The Barents Sea, Svalbard shelf and the eastern Fram Strait are mainly influenced by sediment-laden ice transported southwards from the Kara Sea/Laptev Sea [*Pfirman et al.*, 1997], which likely had a stronger influence on the dissolved radiogenic isotopic composition during glacial periods due to enhanced erosional input and IRD release, which potentially also modified the composition of bottom waters.

3.1.2. Plio–Pleistocene evolution of high northern latitude climate

The major intensification of the NHG marked a point of significant change in earth's climate. First evidence of a glaciation of the Northern Hemisphere data were found on the basis of sedimentological and IRD during the late Miocene [*Wolf and Thiede*, 1991, *Jansen and Sjoholm*, 1991, *Fronval and Jansen*, 1996], when the first ice sheets on Greenland formed. At 3.3 Ma, after an insignificant phase, *Jansen et al.* [2000] described a pronounced increase of the Greenland ice sheet size. *Sarnthein et al.* [2009] defined 2.82 Ma as the onset of the NHG on the basis of a pronounced increase of perennial Arctic sea ice cover as a consequence of the full closure of the Panama gateway [e.g. *Driscoll & Haug*, 1998; *Frank et al.*, 1999; *Bartoli et al.*, 2005] and enhanced transport of heat to the high northern latitudes. At this time, the Atlantic circulation experienced a reorganization including the intensification of the Gulf Stream and consequently an enhanced atmospheric moisture transport to the continental polar latitudes of Siberia. This resulted in increased freshwater supply to the Arctic Ocean via rivers, which then enabled enhanced large scale formation of sea ice [*Driscoll & Haug*, 1998]. The onset of the NHG was marked by a rapid increase of benthic $\delta^{18}O$ by 0.4 ‰ between 2.93 – 2.82 Ma reflecting major ice-sheet build-up and a decrease of the global sea level on the order of 43 m [*Mudelsee and Raymo*, 2005]. Furthermore, at this transition a major change of the climatic conditions prevailing in the Norwegian Sea has been observed from a marked increase in the supply and deposition of IRD on the Vøring Plateau beginning at isotope stage G6 (2.72 Ma) [e.g., *Jansen et al.*, 2000; *Kleiven et al.*, 2002]. However, while the changes in circulation between the two basins

were clearly critical for the climate system, they have so far remained largely unconstrained, which is partly a consequence of the almost complete absence of foraminifera in Arctic Ocean sediments. We thus apply radiogenic Nd and Pb isotopes extracted from Yermak Plateau sediments as proxies for past water mass composition and water mass exchange between the Arctic and Atlantic Ocean, as well as of changes in erosional inputs and continental weathering regime.

3.1.3. Tracing water masses with radiogenic Nd and Pb isotopes

The radiogenic isotope composition of Nd in seawater reveals changes in water mass mixing and circulation patterns, due to its quasi-conservative behavior and average oceanic residence time of 360 - 2000 years [*Tachikawa et al.*, 2003; *Arsouze et al.*, 2009; *Rempfer et al.*, 2011] compared to the global ocean mixing time of about 1500 yr [*Broecker and Peng*, 1982]. The radiogenic neodymium isotopic composition is expressed as $\varepsilon_{Nd} = [(^{143}Nd/^{144}Nd)_{Sample}/(^{143}Nd/^{144}Nd)_{CHUR} -1] * 10{,}000$, whereby a $^{143}Nd/^{144}Nd = 0.512638$ for present day *CHUR = Chondritic Uniform Reservoir* is applied [*Jacobsen and Wasserburg*, 1980]. Unlike stable isotopic systems, such as those of oxygen or carbon, radiogenic Nd isotope ratios are not influenced by isotope fractionation caused by biological and low-temperature processes.

Pb has a much shorter residence time of only about 50 yrs in the Atlantic Ocean [*Schaule and Patterson*, 1981; *Erel et al.*, 1994; *Frank et al.*, 2002] and therefore provides a more localized dissolved seawater signal mainly reflecting the erosional input from nearby continental rocks. In addition, Pb experiences pronounced incongruent weathering as a consequence of the α-recoil effect causing fractionation of the Pb isotopes prior to release to the oceans. The radioactive decay of the U-series isotopes causes damages of the crystal structure of the minerals, which leads to preferential mobilization of the radiogenic Pb isotopes (^{206}Pb, ^{207}Pb, ^{208}Pb) over primordial ^{204}Pb, in particular from freshly exposed granitic rocks [*Erel et al.*, 1994; *von Blanckenburg and Nägler*, 2001]. The Pb isotope composition extracted from ferromanganese crusts and marine sediments to reconstruct changes in local circulation and continental input had been used in several studies [*Frank et al.*, 1999, *Reynolds et al.*, 2009; *Frank et al.*, 2002; *Haley et al.*, 2008b, *Gutjahr et al.*, 2009].

Important sources for both dissolved Nd and Pb in seawater are eolian and riverine inputs but, in the case of Nd, boundary exchange with the continental shelf sediments also plays a significant, if not a dominating role for its oceanic budget. The effects of boundary exchange have been clearly observed along different continental margins in the subpolar regions including the Nordic Seas [*Lacan and Jeandel*, 2004a, 2005a] and modeling results confirmed the importance of this input mechanism [*Arsouze et al.*, 2009; *Rempfer et al.*, 2011]. In the case of the Mediterranean Arctic Ocean basin, both the riverine Nd input in particulate [*Eisenhauer et al.*, 1999; *Haley et al.*, 2008a] and in dissolved form [*Andersson et al.*, 2008; *Porcelli et al.*, 2009] are important contributors. Due to the large percentage of shelf areas of the modern Arctic Ocean boundary exchange is also expected to play a role although the water column data available so far do not give clear evidence for this process [*Andersson et al.*, 2008; *Porcelli et al.*, 2009]. In addition, ice sheet and sea ice transport of particulates have also played a relevant role for the supply of dissolved Nd into the Arctic Ocean.

These input and exchange mechanisms control the isotope composition of the water masses in the Nordic Seas and the Fram Strait, leading to distinct ε_{Nd} values. The warm NAC is characterized by ε_{Nd} values of -13.2 to -13.0 at its areas of origin in the North Atlantic Ocean (T > 5°C; S > 35.0) [*Piepgras and Wasserburg*, 1987; *Lacan and Jeandel*, 2004b, 2005b]. Southwest of Svalbard at 600 m water depth the inflowing Atlantic water has an ε_{Nd} value of -11.0 ± 0.2, which is significantly more radiogenic than the core of the inflowing Atlantic water detected further south at 60°N at water depths between 200 to 400 m, which has an ε_{Nd} value of -13.0 [*Lacan & Jeandel*, 2004b]. The more radiogenic values found off Svalbard are caused by mixing with Norwegian Sea Deep Water (NSDW) (ε_{Nd} = -10.2 ± 0.2) [*Lacan & Jeandel*, 2004b]. On the Yermak Plateau the warmer subsurface Atlantic-sourced water [*Rudels et al*., 2000, 2005] is the dominant water mass occupying depths between 250 and 1000 m [*Karcher & Oberhuber*, 2002]. It is characterized by an ε_{Nd} signal of -11.2 ± 0.7 at 300 m water depth north of Svalbard [*Andersson et al*., 2008]. In contrast, the deep waters and the Polar Mixed Layer (PML) flowing out the Arctic Ocean measured so far have a significantly more radiogenic Nd isotope composition in the western part of the Fram Strait (between -9.5 and -9.8 ± 0.4) compared to the eastern inflow branches [*Andersson et al.*, 2008]. Further south in the Denmark Strait the Nd isotopic compositions range

from -10.8 ± 0.2 for the surface waters to -7.9 ± 0.6 for the intermediate water at ~ 500 m [*Lacan & Jeandel*, 2004a; 2004b].

Today, there are only few studies reconstructing past water mass mixing and sediment transport in the Arctic Ocean and the Fram Strait on the basis of radiogenic Nd and Pb isotopes. *Winter et al.* [1997] reconstructed changes of sediment sources, weathering inputs and deep water masses using radiogenic isotope compositions of diagenetic micronodules, foraminifera and bulk sediment in deep-sea sediments in the Central Arctic Ocean (Alpha ridge) covering the past approximately 6 Myr. In the study of Winter et al. [1997] a significant increase in $^{87}Sr/^{86}Sr$ and $^{206}Pb/^{204}Pb$ ratios and a decrease in ε_{Nd} signatures of the silicate fraction were observed since ~1.7 Ma. This was interpreted in terms of a change in the main sediment transport mechanism from deposition by sea ice to glacial ice-rafted detritus (IRD), as well as in sediment provenance to source areas in northern Canada and Queen Elizabeth Island.

Haley et al. [2008a, 2008b] reconstructed the dissolved Nd and Pb isotope evolution of Arctic Intermediate Water (AIW) leached from metal-oxide coatings on bulk sediments from the Lomonosov Ridge following the methods of *Bayon et al.* [2002] and *Gutjahr et al.* [2007] over the past 15 Myrs and inferred a major switch to a pronounced variability of Atlantic inflow, as well as of brine formation on the Siberian shelf on glacial/interglacial time scales after the onset of NHG. A more recent study focused on the evolution of water mass exchange and sediment transport on the western slope of Svalbard in the Fram Strait from the Last Glacial Maximum (LGM) to the present [*Maccali et al.*, 2012] based on variations of Pb isotope signatures of the leached and detrital fractions of sediment core tops, as well as of down core samples covering a section across the Fram Strait at 79°N from the LGM to the present. In this study the Canadian and Siberian shelves as well as Greenland were found to have been the main sources of detrital material exported through Fram Strait via sea ice and icebergs, which also influenced the leached Pb isotope composition of past bottom waters. Our study presents the first reconstruction of water mass exchange and erosional input/sediment transport across the Yermak Plateau in the Fram Strait applying radiogenic isotope signatures of past seawater extracted from early diagentic metal-oxide coatings, as well as of the detrital fraction itself over the past 5.2 Myr, which includes the major intensification of Northern Hemisphere Glaciation (2.7 Ma).

3.2. MATERIAL AND METHODS

Sediments of ODP site 911 (leg 151) from a water depth of 900 m have been analyzed in this study. The stratigraphy and composition of the sediments of this core have been subject to several previous studies [*Knies et al.*, 2002, 2009]. We apply the age model of *Knies et al.* [2009] for the interval <2.7 Ma, which is based on magnetostratigraphy and calcareous nanofossils. Prior to 2.7 Ma, a new stratigraphic framework established by *Mattingsdal et al.* [in review] based on seismo-, magneto-, and biostratigraphic correlations is adopted. Radiogenic isotopes of Nd and Pb are used for paleoenvironmental reconstruction. We apply the method of *Gutjahr et al*. [2007] to extract the Nd, Pb, and Sr isotope composition of past bottom water incorporated into authigenic ferromanganese oxyhydroxide coatings on the sediment particles. Similar to a previous study of central Arctic sediments [*Haley et al.*, 2008a, 2008b] and given the carbonate content of the sediments at Site 911 only reaching between 1% and 6% [*Myhre et al.*, 1995] a carbonate removal step was not included in the leach procedure (see chapter 2). The procedure thus directly started with extracting the past seawater signal contained in the diagenetic coatings with a 0.05 M hydroxylamine hydrochloride/15% acetic acid solution, buffered to a pH of ~ 3.5 to 4.0. Furthermore the $MgCl_2$ step to remove metals adsorbed to the particle surfaces [*Gutjahr et al.*, 2007] was also omitted because *Haley et al.* [2008a, 2008b] found that there was no measureable difference in the isotope compositions of Nd, Pb and Sr extracted from Arctic Ocean sediments with or without this step. The radiogenic $^{87}Sr/^{86}Sr$ ratio in the solutions containing the sea-water derived extracted metals was monitored to identify detrital contamination by major deviations from the expected and well-known seawater signature of the past 5.2 Myr despite that this method does provide an unambiguous measure of such contamination for the Nd and Pb isotope data [*Gutjahr et al.*, 2007].

After removal of the leach solution by centrifugation, the remaining sediment was allowed to react with an additional batch of hydroxylamine solution for at least 12 more hours to guarantee complete removal of any authigenic coatings left on the particles and was then totally dissolved following *Haley et al.* [2008b]. Afterwards the detrital fraction was rinsed with deionized water three times, dried, and ground to prepare for the total dissolution of the detrital fraction. 50 mg of the ground sediment were weighed and dissolved in a mixture of concentrated HNO_3 + HF at 180°C over

three days. The samples were evaporated to dryness and treated with a mixture of HNO_3 + $HClO_4$ at 190°C to destroy remaining organic material prior to the ion chromatographic separation and purification steps.

In a first step Pb was separated from the solution on anion exchange columns containing 50 µl of AG1-X8 resin (mesh 100-200) following the method of *Lugmair and Galer* [1992]. The Rare Earth Elements (REEs) and the Sr in the remaining solution were separated using cation exchange columns filled with 0.8 ml AG50W-X12 resin (mesh 200-400). The Sr cut was further purified on columns with 50µl Sr-Spec resin (mesh 50-100) following the method of *Horwitz et al.* [1992] and *Bayon et al.* [2002]. Using columns with 2ml Ln Spec resin (50-100 mesh) the Nd was separated from the other REEs [*Le Fèvre and Pin*, 2005].

All measurements were carried out on a *Nu Plasma* Multicollector ICP-MS at GEOMAR, Kiel. Mass bias corrections were carried out using a value of 0.7219 for the $^{146}Nd/^{144}Nd$ and all $^{144}Nd/^{143}Nd$ data were normalized to the accepted value of the JNdi-1 standard of 0.512115 [*Tanaka et al.*, 2000]. Repeated measurements of this standard gave a long term reproducibility for the JNdi-1 standard solution of ±0.3 ε_{Nd} (2σ) over a period of 16 months. The procedural blanks for Nd were ≤ 80 pg. Similarly, Sr mass bias correction used a $^{86}Sr/^{88}Sr = 0.1194$ [*Steiger & Jäger*, 1977] while also correcting for interferences of ^{86}Kr and ^{87}Rb. These Sr measurements were normalized to $^{87}Sr/^{86}Sr = 0.710245$ of the NIST NBS987 standard, which was also used to derive the long term reproducibility of the radiogenic Sr isotope measurements of ±0.000032 (2σ) over one year. The procedural blanks for Sr were below 2 ng. The Pb isotope ratios were analyzed with the standard bracketing method of *Albarède et al.* [2004] and all measured data were normalized to the Pb standard NIST NBS981 applying values of $^{206}Pb/^{204}Pb = 16.9405$, $^{207}Pb/^{204}Pb = 15.4963$, $^{208}Pb/^{204}Pb = 36.7219$ [*Abouchami et al.*, 1999]. The long term reproducibility (2σ) over one year for this standard was ±0.008 for $^{206}Pb/^{204}Pb$, ±0.009 for $^{207}Pb/^{204}Pb$, ±0.033 for $^{208}Pb/^{204}Pb$, ±0.0009 for $^{208}Pb/^{206}Pb$, and ±0.0002 for $^{207}Pb/^{206}Pb$. The procedural blanks for all Pb isotope measurements were ≤ 1.45 ng.

3.3. RESULTS

3.3.1. Strontium and Neodymium isotopic signatures of past seawater and the detrital sediment fraction

The $^{87}Sr/^{86}Sr$ signatures of the leached ferromanganese coatings of Site 911 sediments range from 0.70891 to 0.71249 with an average value of 0.70965 and are thus close to the present $^{87}Sr/^{86}Sr$ seawater value of 0.70916 [*McArthur et al.*, 2001]. The $^{87}Sr/^{86}Sr$ composition of the detrital fraction ranges from 0.71608 to 0.72432 with an average value of 0.71922 and is thus significantly more radiogenic than the leach data (Fig. 3.2) supporting a pure seawater origin of the Nd and the Pb isotope signature in the leachates of this core.

The down core Nd isotope composition of the leached coatings varies between -6.9 and -12.1 (Fig. 3.2, Tab. A.4). The core top value (0 – 3cm) of -11.0 is indistinguishable from present day deep water values observed at this site [*Lacan & Jeandel*, 2004b; *Andersson et al.*, 2008] thus also supporting the reliable extraction of the deep water signature without contamination by the detrital sediment. Prior to the INHG at 2.7 Ma the ε_{Nd} values of the bottom water on the Yermak Plateau ranged from -8.5 to -11.5 (with a mean ε_{Nd} of -10.4), whereas after 2.7 Ma the variability in the ε_{Nd} record increased and shows values between -6.9 to -12.1. In contrast to the less radiogenic interglacials (with a mean ε_{Nd} value of -10.3), the glacial deep water signatures have generally been more radiogenic (with mean ε_{Nd} values of -9.5) after the INHG (Fig. 3.3). There is no significant long-term trend in the Nd isotopic data over the past 5.2 Myr at Site 911.

The detrital fraction deposited in the Fram Strait sediments has generally had less radiogenic ε_{Nd} values than the corresponding leach data ranging between -8.4 and -12.9 (Fig. 3.2, Tab. A.4). A more pronounced glacial/interglacial variability observed in the Nd isotope composition of the leachates after the onset of the NHG is also obvious for the detrital fraction over the same period of time. Prior to 2.7 Ma the range was between -12.9 and -11.5, while after the onset of the NHG the range has been between -12.2 and -8.4, whereby the glacial periods have shown systematically more radiogenic values. The isotopic compositions of Nd and Sr of the detrital sediment cluster around an average ε_{Nd} value of -11.5 and an average $^{87}Sr/^{86}Sr$ of 0.71867, consistent with

previous analyses of Late Quaternary sediments from the Yermak Plateau [*Tütken et al.*, 2002].

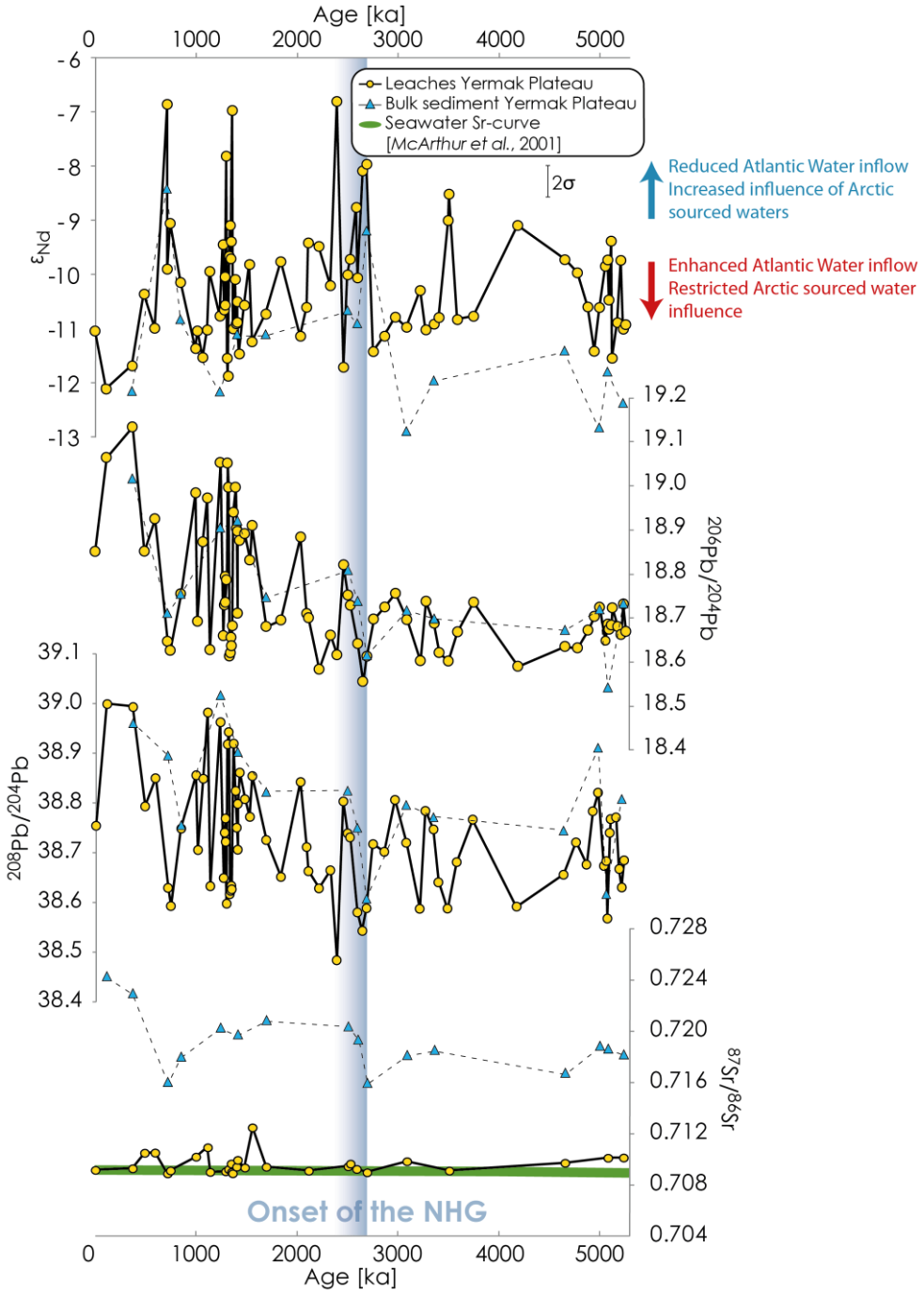

Figure 3.2: Down core Nd, Pb, and Sr isotope records. *The evolution of the radiogenic Nd, Pb and Sr isotope composition of the weak leachates (yellow dots) supposed to reflect dissolved seawater signatures and of bulk sediment (blue triangles) of Site 911 for the past 5.2 Myr. The green line denotes the Sr isotope evolution of global seawater [McArthur et al., 2001] over the past 5.2 Myr. (2σ of the Pb isotope composition is smaller than dot size)*

3.3.2. Lead isotope signatures of past seawater and the detrital sediment fraction

The Pb isotope evolution and variability at Site 911 has been closely coupled to that of the Nd isotopes, but in contrast to Nd there has been a clear trend towards more radiogenic values after the onset of the NHG. The $^{206}Pb/^{204}Pb$ signatures of past seawater leached from the Fe-Mn coating of the Fram Strait sediment show an increase from around 18.6 to values near 19.15 at 0.37 Ma with enhanced millennial scale amplitude of the variations over the last 2 Myrs (Fig. 3.2, Tab. A.4). This is also the case for $^{207}Pb/^{204}Pb$ and $^{208}Pb/^{204}Pb$ of the leached fraction. The coarse resolution data of the detrital fraction follow the trend of the seawater data. The core top (0 – 3cm ≈ last 350 yrs) Pb isotope signal shows a marked less radiogenic value of 18.85 due to contamination with anthropogenic lead (the $^{206}Pb/^{204}Pb$ ratio for anthropogenic Pb in the Greenland Sea and Eurasian basin ranging between 17.75 and 18.38 [*Gobeil et al.*, 2001]) during the last ~100 yrs and will not be considered for paleoceanographic interpretation. Comparison of the leached data with the IRD/sand content data of this core shows that unradiogenic peaks of the $^{206}Pb/^{204}Pb$ ratios systematically occurred during glaciations.

3.4. DISCUSSION

3.4.1. Deep water mass mixing on Yermak Plateau over the past 5.2 Myrs

The Fram Strait is a hydrographically complex area, which has undergone large changes in water mass exchange and sediment transport processes during the past 5.2 Myrs [*Knies et al.*, 2002, 2009*; Maccali et al.*, 2012]. At present, Site 911 is dominated by warm Atlantic Water inflow from the Nordic Seas and the measured core top Nd isotope signature of deep water on Yermak Plateau ($\varepsilon_{Nd} = -11.0 \pm 0.3$) is consistent with the present day seawater Nd isotope composition at a location proximal to the Atlantic inflow branch at 600 m water depth [*Lacan & Jeandel*, 2004b]. The past marine environment on Yermak Plateau has also been influenced by variable glacial/interglacial sea ice extent and calving icebergs transported through Fram Strait via the Transpolar Drift [*Pfirman et al.*, 1997].

The Nd isotope record of past seawater at Site 911 implies that similar forcing mechanisms have prevailed over the entire past 5.2 Myrs. The most pronounced change occurred at the onset of major NHG at 2.7 Ma. Thus we separate the discussion of the record into two time intervals: 1) the Pliocene period prior to the onset of the NHG, which was characterized by lower amplitude of Nd and Pb isotope variability and 2) the mostly Quaternary period after 2.7 Ma characterized by a higher amplitude of Nd and Pb isotope variability which generally covaried with the overall trends in ice volume reflected by the global deep water $\delta^{18}O$ record [*Lisiecki & Raymo*, 2005].

3.4.1.1. The Pliocene record (5.2 to 2.7Ma)

The early part of the record reflects the more stable and warmer climate of the Mid to Early Pliocene, which was characterized by smaller polar ice sheets and higher deep sea temperatures [*Sarnthein et al.*, 2009]. The Nd isotope composition at the Yermak Plateau during the Zanclean/Early Pliocene (5 – 3.6 Ma) varied only moderately, often recording values similar to contemporaneous NADW. This similarity in ε_{Nd} between the Yermak Plateau and North Atlantic Ocean, seen only in the earliest part of our record, suggests an efficient exchange of water masses between the two basins. The highest inflow intensity of Atlantic water occurred between 4.8 and 3.0 Ma, as deduced from enhanced carbonate accumulation and conservation caused by intensified productivity in warm Atlantic surface waters and/or decreased dissolution of planktonic foraminiferal shells [*Henrich et al.*, 2002]. During the period between 4.2 to 4.0 Ma an increase of 0.2 – 0.3‰ in the benthic $\delta^{18}O$ record [*Lisiecki & Raymo*, 2005] indicates colder conditions and the incipient growth of ice sheets, which is also reflected by a step to more radiogenic ε_{Nd} signatures at Site 911. The radiogenic Nd isotope peaks at 4.2 and 3.5 Ma may also point to an early onset of enhanced brine formation and increased ice sheet growth. Relatively stable climatic and oceanographic conditions are implied by the low amplitude variability in the global benthic $\delta^{18}O$ record, as well as in the ε_{Nd} and Pb isotope records, in particular during the Piacenzian/Mid Pliocene period (3.6 - 2.7 Ma). At 3.3 Ma, Jansen et al. [2000] showed evidence for a pronounced increase of the Greenland ice sheet size, which is supported by a peak to more radiogenic values in the ε_{Nd} record. It is followed by the Pliocene climate optimum from

3.3 – 3.0 Ma, a pronounced deglaciation characterized by significantly warmer temperatures than observed for modern surface water in the Subarctic Ocean [*Robinson*, 2009]. A strongly reduced continental ice volume in the Northern Hemisphere resulted, which was accompanied by ice-free conditions in the marginal Arctic Ocean [*Knies et al.*, 2002] and accordingly an increase of the sea level by about 25m [*Mudelsee & Raymo*, 2005]. At this time the highest abundance of dinoflagellate cysts occurred at Site 911 pointing to an enhanced inflow of Atlantic waters into the Arctic Ocean [*Knies et al.*, 2002]. In the ε_{Nd} record this period is characterized by relatively unradiogenic values and a low variability compared to after 2.7 Ma consistent with the predominantly strong Atlantic inflow and the low influence of water masses from the Arctic Ocean, which is supported by comparison to the ε_{Nd} signatures of NADW or a precursor of it extracted from North Atlantic ferromanganese crusts being similar to those at the Yermak Plateau, in particular in the oldest part of the record near 5 Ma.

3.4.1.2. The Pleistocene – Holocene record (2.7 Ma to present)

After 2.7 Ma ocean circulation, as well as erosional input in the Nordic Seas changed significantly resulting in enhanced glacial/interglacial variability and pronounced waxing and waning of the ice sheets and sea ice extent. Unlike the North Atlantic [e.g. *Reynolds et al.*, 1999] and the Central Arctic Ocean [*Winter et al.*, 1997; *Haley et al.*, 2008a] a general trend to less radiogenic ε_{Nd} values of deep waters since the onset of the NHG did not occur in the Fram Strait. Northwestern Atlantic ferromanganese crusts located in the present North Atlantic Deep Water (NADW) recorded a long-term trend from an ε_{Nd} signature of -11.0 at 4 Ma to Holocene values of -13.5 [*Burton et al.*, 1999] (Fig. 3.3). Deep water compositions recorded at IODP Leg 302 ("ACEX") from 1100 m water depth on the Lomonosov Ridge in the central Arctic Ocean showed a similar post-NHG trend towards less radiogenic ε_{Nd} signatures [*Haley et al.*, 2008a], though not as pronounced as in the smoothed North Atlantic ferromanganese crust records. The main reason for the absence of the trend in the Yermak Plateau record is most likely that the mechanisms causing these trends in North Atlantic Fe-Mn crusts and Arctic leaches played no or only a subordinate role on the Yermak Plateau. *Haley et al.* [2008a] ascribed an overall trend towards less radiogenic

values in the Central Arctic Ocean since the intensification of the NHG to a major weakening of the oceanographic stability in the Arctic Ocean. *Winter et al.* [1997] explained the shift to less radiogenic values as changes in the continental sources of IRD, influencing the Nd isotope composition of Arctic seawater. The influence of these Arctic signatures on Yermak Plateau has, however, been outcompeted by the prevailing admixture of warm Atlantic water from the Nordic Seas which must have experienced a different Nd isotope evolution. The trends to less radiogenic Nd and more radiogenic Pb isotope values recorded in ferromanganese crusts from the NW Atlantic were caused by either a change in the provenance of sediment supply or an increase in the weathering contributions of older continental rocks in the Baffin Bay/Labrador Sea region [*Reynolds et al.*, 1999]. This mechanism did not significantly influence the Nd and Pb isotope signatures on Yermak Plateau either because waters originating in the Labrador Sea were most likely mainly flowing west- and southwards and only constituted a minor fraction of the northward flowing branch of Labrador Sea water [*Lacan & Jeandel*, 2004c].

Generally Site 911 has been strongly influenced by water mass mixing between the Nordic Seas fed by the North Atlantic Current crossing the Iceland – Faroe – Ridge and the Arctic Ocean outflow water. The evolution of the mixing proportions of the different endmember water masses have been recorded by the Nd isotope signatures of past seawater on Yermak Plateau over the past 5.2 Myrs. Less radiogenic values indicate a stronger influence of the North Atlantic Current (NAC) flowing into the Nordic Seas (present day ε_{Nd} = -15.0 to -13.0) [*Lacan & Jeandel*, 2004c, 2005b]. More radiogenic values point to a stronger influence of the Arctic Ocean outflow branch through the Fram Strait which at present is characterized by an ε_{Nd} value of = -9.5 between 100 m and 1300 m water depth [*Andersson et al.*, 2008]. The influence of Arctic sourced waters was stronger during glacial times whereas the Atlantic sourced water dominated during interglacial periods. During glacials the sea ice extent and freshwater supply through the Fram Strait from the Arctic Ocean was enhanced, which contributed to diminished formation of deep water in the Nordic Seas [e.g. *Henrich et al.*, 2002]. This inference is consistent with observations by *Ganopolski & Rahmstorf* [2001] and *Clark et al.* [2002], who suggested a reduction of the thermohaline circulation during glaciations, when the amount of Atlantic Water advected to the

Nordic seas is thought to have been lower than at present. Further support for these glacial-interglacial changes in hydrography has been provided by *Crocket et al.* [2011], who found more radiogenic ε_{Nd} values during Heinrich events, reflecting decreased entrainment and advection of north Atlantic waters into the Nordic Seas [*Sarnthein et al.*, 1995; *McManus et al.*, 2004].

In addition to the dominant impact of variations in Arctic and Atlantic Ocean water mass exchange, Site 911 has been covered by ice derived from the waxing and waning of the ice sheets from Svalbard/Barents Sea as well as by the sea ice extent in the Nordic Seas [*Bischof*, 1994; *Bauch et al.*, 2001]. *Knies et al.* [2009] highlighted three different growth phases of the Svalbard/Barents ice sheet between 3.5 and 2.4 Ma, between 2.4 and 1.0 Ma, and between 1.0 Ma and present on the basis of IRD deposition on the Yermak Plateau. Peaks of IRD abundance and deposition were inferred to be a consequence of enhanced inflow of the warm Atlantic water masses affecting ice extent through melting from below [*Knies et al.*, 2009].

The Nd isotope record at Site 911 shows a significant transient peak of 3.5 ε_{Nd} units to more radiogenic values in the leachated deep water values, as well as in the bulk sediment exactly at 2.7 Ma (MIS G6/4) (Fig. 3.2), indicating changes of both water mass exchange and contributing sediment sources, which lasted for at least 100 kyrs. At the beginning of the NHG, enhanced moisture supply to the northern high latitudes as a consequence of the closure of the Isthmus of Panama has been suggested to cause increased freshwater export from the Arctic Ocean into the Nordic Seas [*Driscoll & Haug*, 1998], which was characterized by a more radiogenic Nd isotope signature due to weathering of basaltic areas in Siberia transferred to intermediate waters in the central Arctic Ocean [*Haley et al.*, 2008a; *Chen et al.*, 2012]. This signal may have been introduced as a consequence of the occurrence of the first ice sheets on Svalbard, Franz Josef Land and Novaya Zemlya, which were established between 3.5 and 2.4 [*Knies et al.*, 2009], and was suggested to have been the result of enhanced brine formation near the edges of these ice sheets, in particular in the Kara Sea area [*Haley et al.*, 2008a], which led to more radiogenic Nd isotope compositions of the bottom waters on the Yermak Plateau.

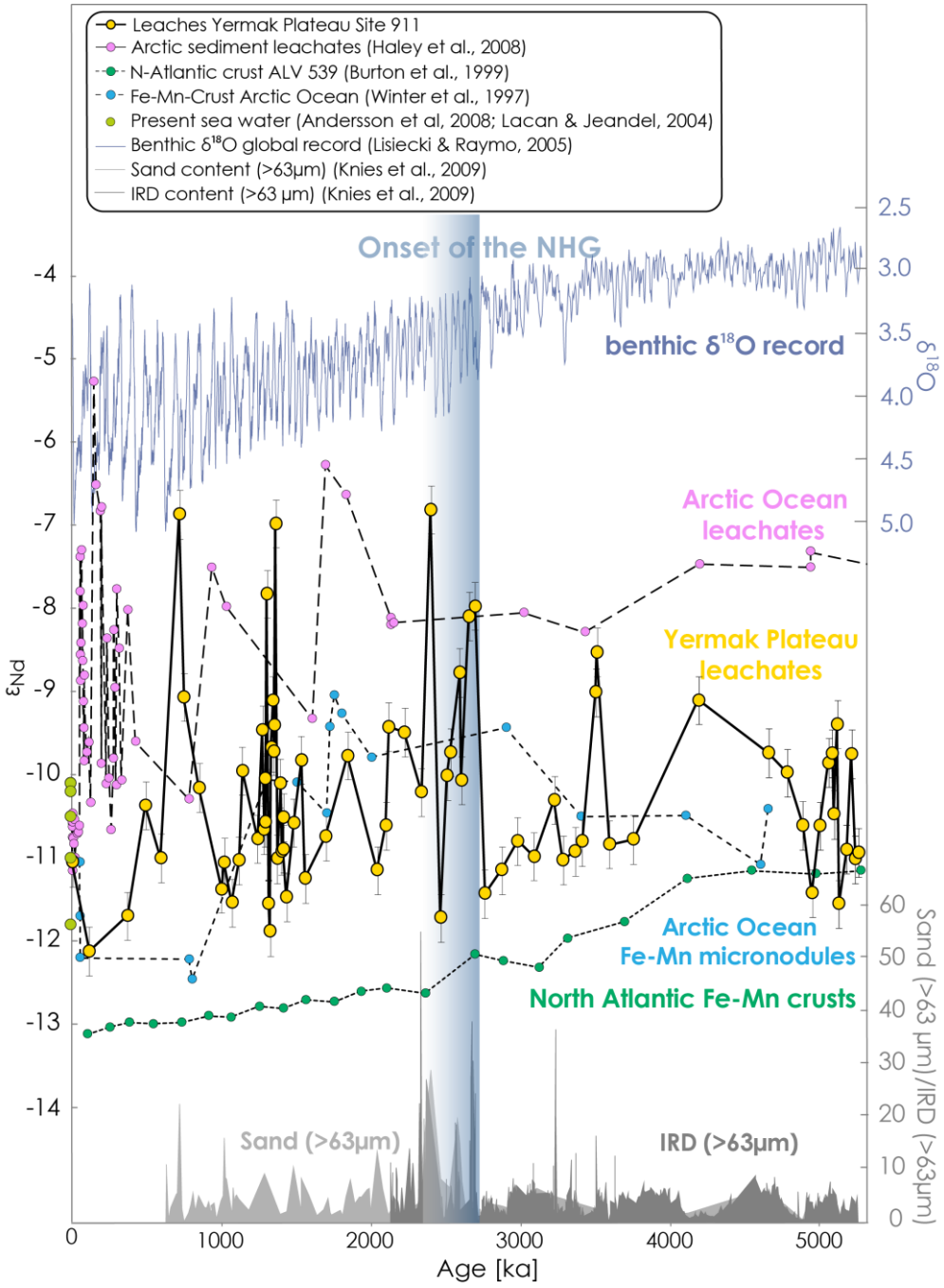

Figure 3.3: Comparison of the deep water Nd isotope data of Site 911 (yellow circles) with other paleo environmental record. *The present day dissolved deep water Nd isotope compositions near site 911 are shown as light green circles. Displayed are: the central Arctic Ocean deep water (pink circles), the Arctic Alpha Ridge micronodule (blue circles), the North Atlantic Fe-Mn-crust record of NADW (green circles), the global benthic $\delta^{18}O$ stacked record (blue line) and the variability of the amount of IRD (>63 µm) and sand (>63 µm) content of Site 911. The colored shadings mark the onset of the major Northern Hemisphere Glaciation.*

Additionally remarkable to the peak at 2.7 Ma, three further highly radiogenic Nd isotope peaks at 2.39 Ma (MIS 94), 1.365 Ma (MIS 44) and 0.715 Ma (MIS 18) were found (Fig. 3.3), all of which occurred during glacial periods. These peaks also reflect increased contributions from highly radiogenic source waters, which were 1) either supplied by brine formation near the Siberian shelf fed by weathering products of the Putorana Flood Basalts and/or 2) originated from exchange with the Icelandic basalts south of the GNS.

The most likely origin of the highly radiogenic glacial signals of the bottom water and sediment on the Yermak Plateau was the Eurasian Shelf in the Kara Sea/Laptev Sea region. The radiogenic Nd isotope signature of the bottom waters above Yermak Plateau may thus have been produced by the glacial outflow of radiogenic waters from the Arctic Ocean assuming that the inflowing Atlantic waters were at the same time strongly reduced [*Haley et al.*, 2008a]. The Nd isotopic signature on the Eurasian shelf, in particular in the Kara Sea is largely controlled by the drainage of the Ob (ε_{Nd} ~ -6) and Yenisei River (ε_{Nd} ~ -5) [*Porcelli et al*., 2009; *Chen et al.*, 2012]). The ε_{Nd} values on the Eurasian shelf in the Kara Sea region thus reflect a mixture of contributions from 1) the Yenisei river which obtains its Nd isotope signature dominantly from weathering of the rocks of the Siberian flood basalt province (ε_{Nd}= 0 to +2.9) [*Sharma et al.*, 1992], the Sayan mountains (ε_{Nd}= -5 to +3) [*Vorontsov et al.*, 2010], and rocks of Precambrian age in the lower part of the rivers and 2) the Ob river, which carries a mixture of the signatures of the West Siberian Lowland, the Altai Mountains, and the Ural Mountains (ranging from -6 to +8.4 ε_{Nd}) [*Chen and Jahn*, 2002]. This highly radiogenic signal was most likely transported either in dissolved form (brine formation) or within particles towards the Arctic outflow, where it significantly influenced the isotopic signatures of both deep waters and of detrital sediments on Yermak Plateau during glacial periods.

The changes in the Nd isotopic composition of the deep waters to more radiogenic values were in most cases coincident with peaks in IRD abundance. Hence the radiogenic peaks of the bottom water signal extracted from the Site 911 sediments may at least partly have been caused by “preformed” coatings, which originated from precipitation of Fe in the transition zones of the rivers between freshwater and salt water [*Bayon et al.*, 2004]. These coatings contained the highly radiogenic Nd isotope signal

from the Siberian rivers and shelves and were transported to the Yermak Plateau as IRD incorporated in icebergs and sea ice via the Transpolar Drift (TPD) [*Tütken et al.*, 2002; *Pfirman et al.*, 1997]. Under modern interglacial conditions, sea ice and iceberg rafting [*Dethleff & Kuhlmann*, 2010], as well as melt water events [*Darby et al.*, 2006] are known to be effective mechanisms to transport IRD from the Kara Sea to the Fram Strait. Sea ice formed on the shelves incorporated small lithic grains by suspension freezing [*Reimnitz et al.*, 1992; *Nürnberg et al.*, 1994], which assimilated the signal from the water masses on the Eurasian shelf. This sediment was then transported via the Siberian branch of the Transpolar Drift to the Fram Strait, where the sea ice melted due to the mixing with the relatively warm Atlantic water and released the IRD containing the "preformed coatings". This was suggested to have been the dominating sediment supply mechanism to the Arctic Ocean over the past 15 Ma [*Bischof & Darby*, 1997, *Winter et al.*, 1997]. The "preformed" coatings on the IRD may release their more radiogenic signal during the leaching procedure in the laboratory causing a contamination of the local bottom water signal with the transported signal from the Kara Sea. The ε_{Nd} and $^{87}Sr/^{86}Sr$ signatures of the detrital sediment fraction, as well as the fact that the IRD peaks coincide with the peaks in the Nd isotope record support this hypothesis.

A second hypothesis to explain the radiogenic Nd isotope peaks is boundary exchange with Icelandic basalts, a process that has been shown to play an important role for the signature of the modern East Greenland Current [*Lacan and Jeandel*, 2004b] and may also explain the radiogenic peaks of the Site 911 record. For glacial periods severe reductions of the Atlantic Meridional Overturning Circulation [*Ganopolski & Rahmstorf*, 2001; *Clark et al.*, 2002] or even shutdowns due to the enhanced freshwater input from the Arctic Ocean have been reported [*Peterson et al.*, 2006]. During those times the Nordic Sea waters may have become more radiogenic caused by boundary exchange with the basaltic margin of the Norwegian Sea basin including Iceland, Jan Mayen, and the Faroe Islands. This boundary exchange may have led to much more radiogenic glacial deep waters in the Norwegian basin, if the radiogenic Norwegian Sea deep water indeed flowed northwards [*Lacan and Jeandel*, 2004b and references therein] across Yermak Plateau into the Arctic Ocean. During interglacials (i.e. analogous to the present day situation) such a radiogenic "Icelandic" signature will not

be detectable due to the volumetrically overwhelming Atlantic waters transported to the Yermak Plateau via the West Spitsbergen Current. During glacial periods, however, the radiogenic signal acquired through boundary exchange with the Icelandic basalts will have been more important as a consequence of the reduced circulation and both the Norwegian Sea and the Fram Strait signatures may have become more radiogenic. We consider this second hypothesis rather unlikely, because the radiogenic Nd isotope signal needs to be transported over a very long distance from Iceland to the Yermak Plateau, wherefore there is no evidence or records so far. In contrast, there are many studies documenting the transport of waters and sediment from the Arctic Ocean to the Yermak Plateau, e.g. via the Transpolar Drift [*Pfirman et al.*, 1997; *Tütken et al.*, 2002; *Knies et al.*, 2002, 2009; *Maccali et al.*, 2012].

Another possibility to transfer the radiogenic signal of Icelandic origin to the Yermak Plateau may have been volcanic ash, which is very labile and dissolves readily in contact with seawater [*Gislason and Oelkers*, 2003]. This scenario, however, also appears unlikely because there are no documented major ash layers at Site 911 coinciding with the peak radiogenic Nd isotope signatures.

3.4.2. Sediment transport on the Yermak Plateau based on Nd and Pb isotopes

The bulk sediment signatures on the Yermak Plateau (ε_{Nd} = -8.4 to -12.9) have been dominated by contributions from Svalbard (ε_{Nd} values ranging between -3.3 in the western part [*Peucat et al.*, 1989] and -21 in the northern part [*Johansson et al.*, 1999]), as well as sediments from Bear Island and the Norwegian shelf from the south (ε_{Nd} values = -15.1 to -10.1 [*Farmer et al.*, 2003]). This is supported by seismic profiles [*Geissler et al.*, 2011] showing the predominant deposition of contourites (from a southern source) on the Yermak Plateau prior to 2.7 Ma. Our data nevertheless suggest that Svalbard was the dominant sediment source area prior to 2.7 Ma, which switched to increasing contributions from the Arctic Ocean thereafter, in particular from the Eurasian shelf (Kara/Laptev sea), as well as Novaya Zemlya (average ε_{Nd} = -6.4) and Franz Josef Land (ε_{Nd} = -9.5) [*Tütken et al.*, 2002]. This is documented by the shift from less radiogenic values (ε_{Nd} = -12.9 to -11.4, mean = -12.2) prior to the INHG to more radiogenic (ε_{Nd} = -12.2 to -8.4, mean = -10.7) afterwards clearly indicating a change of

the sediment sources (Fig. 3.4). The Norwegian shelf signatures are overall not radiogenic enough in their Nd isotope compositions to cause the radiogenic peaks of the detrital fraction on Yermak Plateau. In support of this, there are two pronounced depth layers deposited during glacial periods (at 0.715 and 2.69 Ma), which show the most radiogenic ε_{Nd} signatures of the detrital fraction and reveal the closest correspondence and thus highest contributions of the sediments originating from the Kara Sea. This is similar to the scenarios described by *Tütken et al.* [2002] who showed variations in the ε_{Nd} signature of the detrital fraction between -9.3 during glacial periods and -14.9 during interglacials recorded in Late Quaternary sediments from the Yermak Plateau.

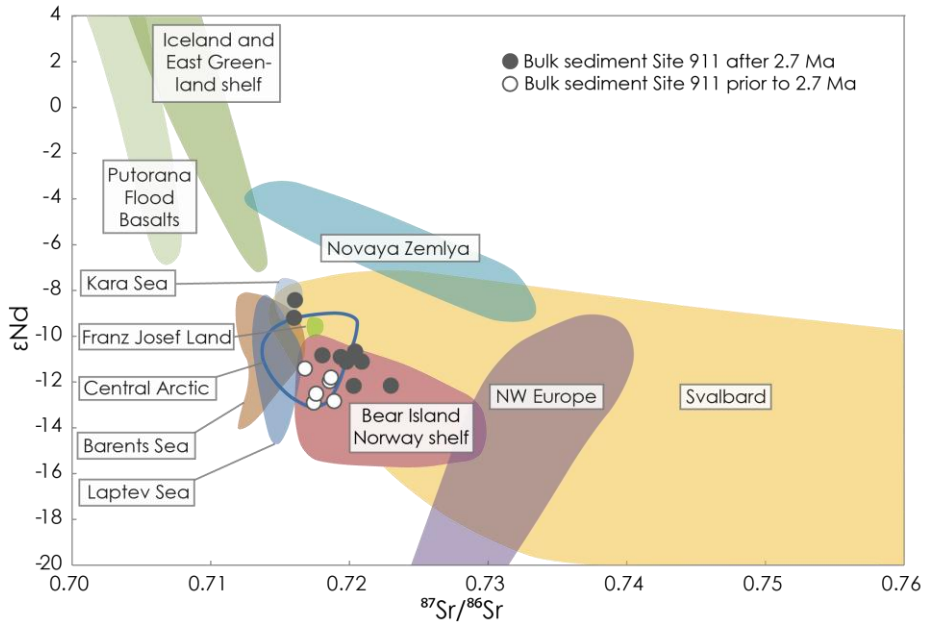

Figure 3.4: Comparison of the Nd and Sr isotopic composition of the detrital sediment fraction of Site 911 (black dots = younger than 2.7 Ma; open dots = prior to 2.7 Ma) with possible sediment sources. *Colored arrays display areas as follows: light green = Norilsk/Putorana Flood Basalts [Sharma et al., 1992], blue = Kara and Laptev Sea sources [Eisenhauer et al., 1999], turquoise = Novaya Zemlya [Tütken et al., 2002], brown = Barents Sea, bright green = Franz Josef Land [Tütken et al., 2002], yellow = Svalbard bedrocks [Peucat et al., 1989; Johansson & Gee, 1999], dark green = Iceland and the East Greenland Shelf (basaltic), red = sediments from Bear Island and Norwegian shelf [Farmer et al., 2003] and lavender = NW Europe including British Isles, Scandinavia and the Norwegian Sea [Farmer et al., 2003]. The blue framed array presents the bulk sediment from the Lomonosov ridge (Central Arctic Ocean) [Haley et al., 2008b].*

As discussed above, the glacial deep water signature extracted from these samples also shows highly radiogenic peaks. The sediments from the Kara and Laptev Sea were most likely transported by ice via the Siberian branch of the Transpolar Drift similar to the situation of the last glacial [*Tütken et al.*, 2002; *Pfirman et al.*, 1997]. Moreover, our data indicate that the influence of the more radiogenic Kara Sea sediments dominated over those from the Laptev Sea during glacial periods.

The Pb isotope signatures of the detrital material are supposed to reflect the same source areas of the sediments supplied to Yermak Plateau as the Nd isotope signatures. The bulk sediment signatures of Site 911 are similar to those seen in the Central Arctic Ocean [*Haley et al.*, 2008b], which have mainly been derived from the Siberian shelves. The sediments on Yermak Plateau have been slightly more radiogenic than the bulk sediment from the Siberian Flood basalts [*Sharma et al.*, 1992] and Svalbard bedrocks [*Ionov et al.*, 2002]. Prior to 2 Ma the Pb isotope compositions of Site 911 sediments were more similar to those of the bulk rocks of Svalbard [*Ionov et al.*, 2002] also supporting that Svalbard was the dominant sediment source (Fig. 3.5). Afterwards the Pb isotope compositions of the sediments became more radiogenic, consistent with enhanced contributions of Siberian material from the Eurasian shelf. Similar to the Nd isotopic composition, the Pb isotopic signal indicates that Franz Josef Land [*Levskii et al.*, 2006] may also have been an important source of sediment. The Pb isotopic compositions of two North Atlantic crusts (ALV 539 and BM 1969.05 [*Reynolds et al.*, 1999]) show a different trend, which documents the different source areas of the leachates and sediments on the Yermak Plateau and those that contributed Pb to the North Atlantic (Fig. 3.5). The elevated smectite content found at Site 911 [*Knies et al.*, 2009, *Wahsner et al.*, 1999] supports the idea that the isotopic composition of Pb and Nd at Site 911 has been strongly affected by sediments supplied from Svalbard and in particular the Kara Sea sediments, which are to large extent weathering products of the Siberian Flood basalts, and transported via the TPD.

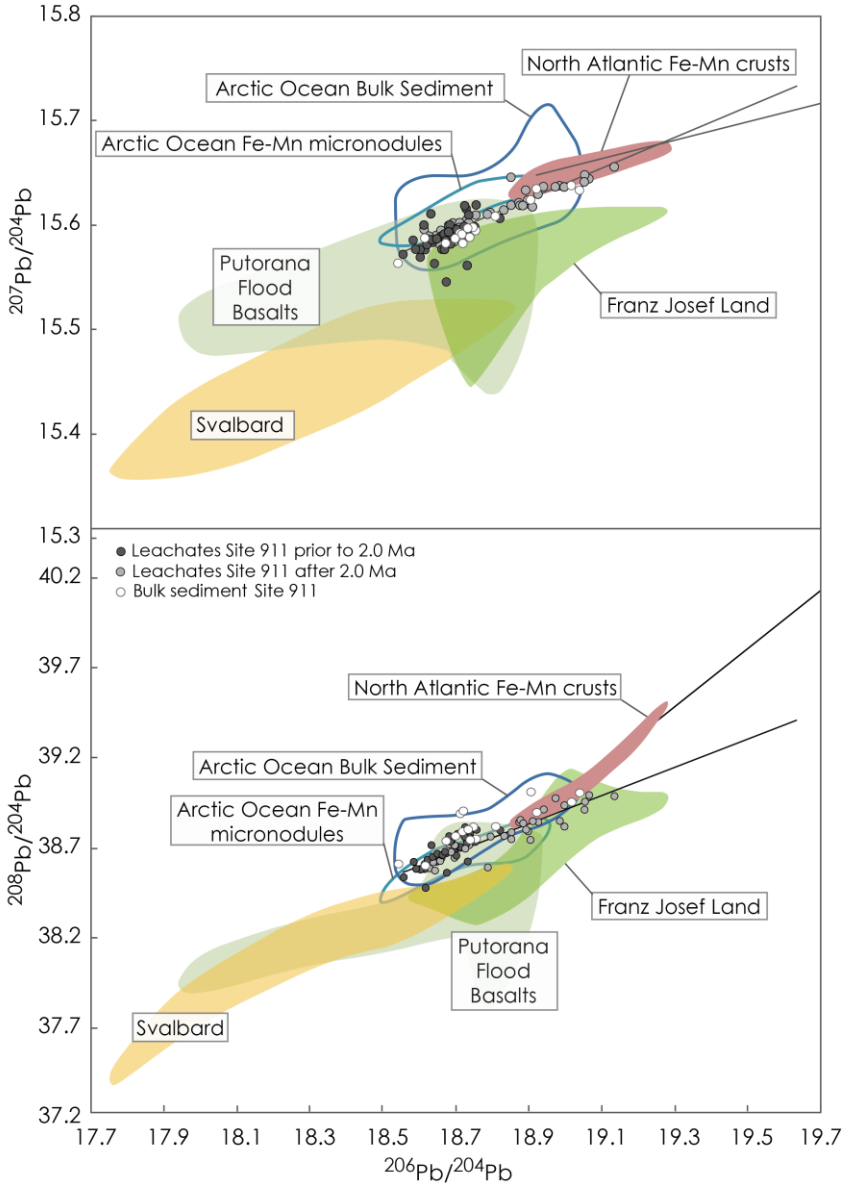

Figure 3.5: Radiogenic Pb isotope comparison of leachates (black dots = prior to 2.7 Ma; light grey dots = after 2.0 Ma) and detrital sediments (open dots) of Site 911 with possible sources. *The blue framed arrays are bulk sediment and Fe-Mn micronodules from the Arctic Ocean [Winter et al., 1997] as well as leachates from the central Arctic Ocean [Haley et al., 2008b]. The North Atlantic ferromanganese crust array in red includes crusts BM1959.05 and ALV539, both recovered from present day NADW [Reynolds et al., 1999]. For comparison, the isotopic compositions of the rocks of the volcanic Franz Josef Archipelago [Levskii et al., 2006], the Putorana flood basalts [Sharma et al., 1992], and Svalbard rocks [Ionov et al., 2002] are shown. The two black lines mark distinct mixing lines of the North Atlantic Fe-Mn-crust data representing dissolved seawater Pb and of our data supporting that the two areas have been dominated by sources with different provenances.*

3.4.3. Changes in weathering regime and sediment sources over the past 5.2 Ma: Pb isotope evidence

Due to its short oceanic residence time, the Pb isotope record of deep waters reflects a predominantly local signal, mainly controlled by weathering inputs, which explains the similarity of the isotopic composition of the leachates and the detrital sediment fraction on the Yermak Plateau similar to the records from Lomonosov Ridge [*Haley et al.*, 2008b]. If sediment incorporated in sea ice or transported as IRD is released to the water column, it imparts some of its sedimentary Pb isotope signature to the water column. Thus the seawater Pb isotope composition will largely reflect changes in the Pb isotopic composition of sediment transported by sea ice or icebergs.

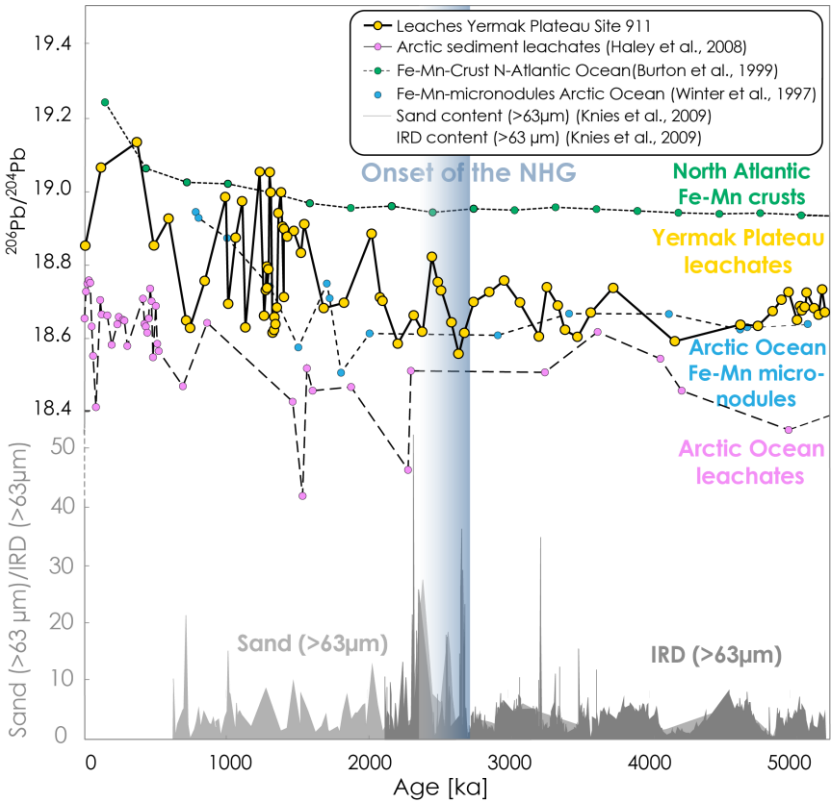

Figure 3.6. Comparison of the deep water Pb isotope data of Site 911 (yellow circles) with other paleo environmental records. *Also presented are: the Arctic Ocean leaches from the Lomonosov Ridge (pink circles), the North Atlantic Fe-Mn crust record (green circles), an Arctic diagenetic micronodules record (blue circles) and the abundance of IRD (>63 µm) and Sand (>63 µm). The colored shadings mark the onset of the major Northern Hemisphere Glaciation.*

Prior to the onset of Northern Hemisphere Glaciation the Pb isotope composition on the Yermak Plateau was characterized by low variability (Fig. 3.2) due to the limited extent of ice sheets, resulting in no pronounced incongruent weathering of Pb isotopes and thus no preferential mobilization of radiogenic ^{206,207,208}Pb relative to ^{204}Pb [*von Blanckenburg & Nägler*, 2001]. This Pb isotope stability is similar to records from the Arctic [*Winter et al.*, 1997; *Haley et al.*, 2008b] and Atlantic Oceans [*Reynolds et al.*, 1999] and was caused by largely invariant weathering conditions on glacial/interglacial time scales. The low extent of the ice cover on the Northern Hemisphere prior to 2.7 Ma implies that the Pb was mainly released by chemical weathering of older and deeply weathered soils due to the warm temperatures during the Pliocene. The relatively unradiogenic Pb isotope record prior to 2.0 Ma thus indicates essentially constant erosional supply of material, most likely mainly from Svalbard to the Yermak Plateau.

After the onset of the NHG major glacial buildup of the Northern Hemisphere ice sheets occurred and the weathering conditions changed significantly resulting in a two- to threefold decrease in chemical weathering rates during glacial periods [*Foster & Vance*, 2006]. In contrast, glacial mechanical erosion intensity increased leading to enhanced exposure of fresh mineral surfaces, which led to the predominant release of radiogenic ^{206,207,208}Pb during deglacial periods (incongruent weathering) [*von Blanckenburg & Nägler*, 2001; *Foster & Vance*, 2006]. Unlike the Nd isotope evolution, the increase to more radiogenic values and a higher variability in the Pb isotopic record on the Yermak Plateau did not begin contemporaneously with the major intensification of the NHG, but rather occurred about 0.7 to 1.0 million years later at about 2 Ma. The enhanced amplitude of the radiogenic Pb isotope ratios of past deep waters on Yermak Plateau after 2 Ma is consistent with that of seawater Pb isotope compositions leached from central Arctic Ocean sediments on the Lomonosov Ridge [*Haley et al.*, 2008b], as well as with the record extracted from diagenetic ferromanganese micronodules in sediments from the Alpha ridge of the Arctic Ocean [*Winter et al.*, 1997]. The low resolution Pb isotope records obtained from North Atlantic Ocean ferromanganese crusts [*Reynolds et al.*, 1999] indicate comparably little variability prior to 2 Ma (Fig. 3.6).

The Pb isotope variations are correlated with changes in IRD inputs and thus larger ice sheet extents during glacial periods inducing increased IRD inputs at the

Yermak Plateau. The overall gradual shift of the $^{206,207,208}Pb/^{204}Pb$ record to more radiogenic values on Yermak Plateau after 2.0 Ma resembles the Pb isotope evolution of the deep Arctic Ocean recorded by sedimentary ferromanganese micronodules [*Winter et al.*, 1997] and the Pb isotope evolution of North Atlantic Deep water in the North Atlantic recorded by ferromanganese crusts [*Burton et al.*, 1999; *Reynolds et al.*, 1999]. Other studies in the Arctic and Atlantic Ocean have shown the occurrence of this shift to more radiogenic values at different times varying between 1.7 Ma [*Winter et al.*, 1997] and after 1 Ma [*Haley et al.*, 2008b; *Reynolds et al.*, 1999] (Fig. 3.6), which may be related to sediment supply pathways and to differences in exposed lithologies, i.e. freshly exposed old granitic rocks will supply the most radiogenic Pb during incipient deglacial chemical weathering.

3.5. CONCLUSION

This study reconstructs the evolution water mass mixing and erosional input on the Yermak Plateau over the past 5.2 Ma on the basis of Nd and Pb isotope compositions leached from authigenic ferromanganese oxyhydroxide coatings, as well as of the detrital fraction of ODP Site 911 sediments. The leached Nd isotope record of past seawater did not undergo a significant trend on the Yermak Plateau suggesting that this location has been dominantly influenced by modified Atlantic Water advected from the Nordic Seas over the past 5.2 Ma. Two periods with distinctly different conditions are evident in the Nd isotope record. An early period, prior to the onset of the NHG was characterized by stable water mass compositions on glacial/interglacial time scales, as well as essentially invariable sediment supplies from Svalbard and the Arctic Ocean. After 2.7 Ma the environmental conditions have been characterized by higher amplitude ε_{Nd} variability of both deep waters and detrital sediments as a result of enhanced glacial/interglacial contrasts. This was a consequence of the climatic variability reflected by the waxing and waning of ice sheets located on the Eurasian shelf and the consequent supply of sediment laden sea ice. Glacial periods have been characterized by generally more radiogenic ε_{Nd} signatures of deep waters on Yermak Plateau, driven by either a stronger influence of Arctic water due to the reduction of the Atlantic water inflow or the release of a radiogenic signal from IRD or sediments transported by sea

ice from the Arctic Ocean via the Transpolar Drift. The detrital Nd isotope composition of the sediments from Site 911 supports the hypothesis of dominant sediment supply from Svalbard prior to 2.7 Ma, whereas after the INHG the dominant source has still been Svalbard during interglacial periods, but experienced significantly increased contributions from the Kara Sea during glacial periods.

Similar to the Nd isotopes, the seawater Pb isotope record shows low variability and supports a constant sediment supply prior to 2.0 Ma, dominantly from Svalbard. After 2.0 Ma the increasing amplitudes of glacial/interglacial cyclicity led to a stronger variability in the isotopic signal of Pb of leaches and bulk sediment on the Yermak Plateau due to increasing glacial weathering and the waxing and waning of ice sheets, as well as changes in sea ice transport. Contrary to Nd, the seawater Pb isotope record shows a pronounced trend towards more radiogenic values after 2.0 Ma, reflecting the general increase of glacial weathering of old continental rocks of Greenland and parts of Svalbard. Despite this general trend, less radiogenic Pb isotope signatures were maintained during glacial periods, which is indicative of enhanced supply of less radiogenic sediments of most likely basaltic origin from Siberia. This is supported by the similarity of the glacial sedimentary Pb isotope signatures at Site 911 to those of central Arctic sediments and the Putorana basalts.

Acknowledgements

The German Research Foundation (DFG) provided financial support of C. Teschner within the Priority Program 527 (Ocean Drilling Program/Deep Sea Drilling Project HA 5938/1-1, AOBJ: 569543). We thank Kirstin Werner for valuable comments and discussions.

CHAPTER 4

Reconstruction of the Atlantic inflow and the erosional input into the Nordic Seas and North Atlantic Ocean during the late Plio- and Pleistocene

Abstract

Deep and intermediate waters formed in the Labrador Sea, Nordic Seas and North Atlantic Ocean have strongly affected the Atlantic Meridional Overturning Circulation (AMOC), which is responsible for the ventilation of the entire Atlantic Ocean and has had a large impact on the global climate.

The aim of this study is to reconstruct past intermediate and deep water mass mixing and erosional inputs in the Nordic Seas and North Atlantic Ocean based on neodymium (Nd), lead (Pb) and strontium (Sr) isotope compositions of seawater-derived ferromanganese coatings on sediment particles of the bulk sediments, as well as on the detrital fraction serving as an indicator for changes in sediment sources over the past 3 million years. Data were obtained from ODP sites in the Nordic Seas, in particular on the Svalbard shelf (Site 986, Leg 162) and on the Vøring Plateau (Site 644, Leg 104), and in the North Atlantic Ocean on the Rockall Plateau (Site 982, Leg 162). At the sites in the Nordic Seas (Site 986 and 644) we observed a very strong local influence on the different water masses and erosional inputs, which were significantly affected by the onset of Northern Hemisphere Glaciation (NHG). These sites have most of the time been influenced by Norwegian Sea Deep Water (NSDW) and Arctic Intermediate Water (AIW), whereas Site 982 has been dominated by overflow waters from the Nordic Seas and Labrador Sea Water (LSW). Despite problems in the comparison of the records due to chronostratigraphic uncertainties, we were able to identify periods of distinct changes of the Atlantic inflow into the Nordic Seas between

---

This chapter is going to be submitted as:

Teschner, C., M. Frank, and B.A. Haley. Reconstruction of the Atlantic inflow and the erosional input into the Nordic Seas and North Atlantic Ocean during the late Plio- and Pleistocene.

2.2 and 1.5 Ma and between 1.5 and 1.2 Ma. The period between 2.2 and 1.5 Ma was characterized by a warmer climate and moderate glacial conditions, which is supported by the similarity of the Nd isotope composition in all sites, indicating an enhanced inflow of warm Atlantic water. In contrast with the beginning of the MPT at 1.5 – 1.2 Ma, the Atlantic inflow was significantly reduced, expressed in strong distinctions between the different Nd isotope records in the Nordic Seas and North Atlantic Ocean.

4.1. INTRODUCTION

The Nordic Seas, the northernmost Atlantic Ocean, and the Labrador Sea are the most important locations for the formation of North Atlantic Deep Water (NADW), which ventilates the entire North Atlantic Ocean. Warm and salty water moves northwards, cools, sinks and forms the North Atlantic Deep Water, which is a main feature of the Atlantic Meridional Overturning Circulation (AMOC). Large climatic changes are thought to have influenced the AMOC significantly, for example through freshwater inputs from the melting Greenland and Laurentide ice sheets [e.g., *Ganopolski and Rahmstorf,* 2001; *Clark et al.,* 2002; *Peltier et al.,* 2006]. A reduction of the deepwater formation occurred during the Last Glacial Maximum (LGM) due to a freshening of the surface waters in the Nordic Seas, causing a decline of the import of warmer waters from the south [*Raymo et al.,* 1992] and a shift of the iceberg extent farther south. Another consequence of the suppression of the NADW is a reduction in atmospheric CO_2 contributed to cooling of the climate [*Boyle,* 1988, *Broecker and Peng*, 1989]. *Raymo et al.* [1990] as well described a pronounced suppression of glacial NADW and a development of larger ice sheets after the onset of major Northern Hemisphere Glaciation. Prior to this period, in the late Pliocene the thermohaline circulation was more powerful and NADW formation was strong [*Raymo et al.*, 1992].

This study aims to reconstruct the strength and intensity of the Atlantic water masses flowing into the Nordic Seas in order to achieve a better understanding of the factors controlling the formation of NADW and changes in the overflow water mainly influenced by the circulation of Atlantic waters in the Nordic Seas [*Eldevik et al.,* 2009]. To understand the nature of changes in paleocirculation and weathering conditions in this region during the periods of marked climatic changes in the Plio- and Pleistocene,

the long-term evolution of the deep and intermediate water masses in the northernmost Atlantic Ocean and Nordic Seas were monitored at three different sites.

4.1.1. Plio–Pleistocene evolution of high northern latitude climate

Climate and the Atlantic Meridional Overturning Circulation (AMOC) of the past 3 Myr in the northern high latitudes were characterized by two drastic changes, the major Intensification of Northern Hemisphere Glaciation (INHG) starting at 2.82 Ma [*Sarnthein et al.*, 2009] and the Mid Pleistocene Transition (MPT) from ~1.5 Ma to ~0.5 Ma [*Lisiecki and Raymo*, 2005]. The INHG marks a significant change in earth climate and is thought to have been caused by several processes, such as orbital forcing [*Huybers and Molnar*, 2007] and occurs contemporaneously with the closure of the Indonesian Gateway Systems [*Cane and Molnar*, 2001; *Karas et al.*, 2009]. Most likely the INHG was linked to the final closure of the Isthmus of Panama and the associated intensification of heat and moisture transport towards the high northern latitudes. This resulted in an increase in freshwater supply and sea ice formation in the Arctic Ocean and an increase in Arctic albedo, ultimately promoting growth of the Northern Hemisphere ice sheets [*Driscoll and Haug*, 1998; *Bartoli et al.*, 2005; *Sarnthein et al.*, 2009]. The INHG was accompanied by a decrease of the global sea level on the order of 43 m, as well as a rapid increase of benthic $\delta^{18}O$ by 0.4 ‰ between 2.93 and 2.82 Ma reflecting major ice-sheet build-up [*Mudelsee and Raymo*, 2005]. In addition, these changed climatic conditions have been accompanied by enhanced supply of IRD on the Vøring Plateau since 2.72 Ma [e.g., *Kleiven et al*., 2002; *Jansen et al.*, 2000].

Between ~1.5 and 0.5 Ma [*Lisiecki & Raymo*, 2005] a similar increase in IRD deposition occurred during the Mid Pleistocene Transition (MPT) [e.g. *Jansen and Sjøholm*, 1991; *Helmke et al.*, 2003, 2005; *Knies et al.*, 2009] indicating another major rearrangement of the Northern Hemisphere climate system. The MPT was characterized by a shift in glacial/interglacial cyclicity from the 41 kyrs to the 100 kyrs Milanković frequency [*Hays et al.*, 1976; *Pisias & Moore*, 1981; *Raymo & Huybers*, 2008]. On the basis of benthic $\delta^{13}C$ data *Raymo et al*. [2004] suggested that the water mass structure in the northernmost Atlantic changed significantly during the MPT, which may also have

initiated the present day mode of water mass exchange between the Nordic Seas and Arctic Ocean and ultimately the Late Quaternary mode of the AMOC.

4.1.2. Tracing water masses and the erosional input from Nd and Pb isotopes

This study aims to reconstruct changes in water mass exchange and climate on the basis of the radiogenic isotope systems of Nd and Pb, because the restricted abundance of foraminiferal carbonate in the northern Nordic Seas complicates the application of classical parameters such as stable carbon and oxygen isotopes. Radiogenic Nd and Pb isotopes have been widely used as proxies for paleoceanographic and paleoclimate reconstructions [*Frank et al.*, 2002; *Martin et al.,* 2010; *Roberts et al.*, 2010; *Crocket et al*., 2011]. The Nd isotope composition of the ferromanganese coatings covering the sediment particles has been used to reconstruct past water mass exchange processes, while the Nd isotope composition of the detrital fraction provides important information on changes in sediment transport mechanisms and source provenance. One major advantage of these radiogenic isotope systems is their independence from mass fractionation by biological and low temperature processes [e.g. *Piotrowski et al.,* 2005].

The dissolved Pb isotope composition of past seawater is commonly used to obtain information about local erosional inputs into ocean basins due to its low average residence time of only 50 years in the Atlantic Ocean [*Schaule and Patterson*, 1981; *Erel et al.*, 1994], which leads to a very local Pb isotopic signal directly reflecting the erosional input from the surrounding rocks. In addition, the Pb isotopic composition does not mirror the exact isotope signature of the nearby rocks, because of incongruent weathering, which modifies the radiogenic isotope composition of Pb released to the oceans. During incongruent weathering the Pb isotopes are fractionated by the so called α-recoil effect that leads to a preferential mobilization of the radiogenic Pb isotopes (^{206}Pb, ^{207}Pb, ^{208}Pb) over primordial ^{204}Pb, in particular from freshly exposed granitic rocks [*Erel et al.*, 1994; *von Blanckenburg and Nägler*, 2001].

Globally, the most important sources of Nd and Pb in the oceans are eolian and riverine input. In addition, hydrothermal input plays a role for Pb and in the case of Nd boundary exchange as described by *Lacan and Jeandel* [2004a, 2005a] is a significant, if not the most important source. During this process the continental shelves exchange

and release significant amounts of the particulate Nd isotope signature into the water column.

In the Nordic Seas, the glacial and riverine inputs, as well as boundary exchange have been of particular importance due to the continuous waxing and waning of the ice sheets and sea ice combined with the large reactive shelf areas in the Nordic Seas, Arctic Ocean and northern Atlantic Ocean, whereas eolian or hydrothermal inputs have only been of minor importance. The input of radiogenic isotopes into the Nordic Seas, Arctic Ocean and North Atlantic Ocean is dominantly controlled by old continental rocks, such as those in Greenland and northern Canada with highly unradiogenic Nd isotopic signals (ε_{Nd} = -40 [*Taylor et al.,* 1992]). There are, however, also young basaltic rocks, such as on Iceland, which are characterized by highly radiogenic signatures (ε_{Nd} = +5 to +10) [*O`Nions and Grönvold*, 1973]. In contrast to other ocean basins, such as the Southern Ocean [*Piotrowski et al*., 2008], the Pacific Ocean [*Martin et al.,* 2010], or the Central Arctic Ocean [*Haley et al*., 2008a], where the extracting of past bottom water Nd isotope signature from sediments via bulk sediment has been demonstrated to work very well and yields reliable results, this method is connected to some difficulties in the Nordic Seas and North Atlantic Ocean, most likely originating from volcanic input from Iceland [*Elmore et al*., 2011] or preformed coatings delivered by sea ice or ice bergs [*Bayon et al.*, 2004; *Chen et al.*, 2012]. Therefore, different leach methods were tested for their reliability at every single site (see Chapter 2).

4.1.3. Hydrographic setting

The Nordic Seas, where North Atlantic Deep Water is formed by at least three individual processes: open ocean convection [*Swift and Aagaard*, 1981], shelf convection [*Rudels*, 1986, *Rudels et al.*, 1994] and brine formation [*Aagaard et al.*, 1985], combines three ocean basins, separated from each other by submarine ridges: the Norwegian Sea in the southeast, the Greenland Sea in the north and the Iceland Sea in the southwest (Fig. 4.1).

The present day circulation pattern in the Nordic Seas is dominated by two flow directions with markedly different Nd isotope compositions of the different currents. On the one hand the inflowing warm and saline Atlantic water enters the Nordic Seas,

where it cools and sinks. The Atlantic water is modified by mixing and leaves the Nordic Seas via the Denmark Strait, the Faroer Shetland Channel and over the Faroer Iceland Ridge as Nordic Seas Overflow water. The inflowing Atlantic water ($T \leq 6°C$, $S \leq 35.2$; [*Hansen and Østerhus*, 2000; *Spielhagen et al.*, 2011]) is the main heat source of the Nordic Seas and the Arctic Ocean and enters via several branches. One branch passes the ridge west of Iceland as North Icelandic Irminger Current (NIIC); a second branch flows southeast of Iceland across the Rockall-Hatton Plateau towards the Faroe Islands (North Atlantic Current) (Fig. 4.1), than splits and enters the Nordic Seas east (ε_{Nd} = -12.8 in ~200 m water depth) and west (ε_{Nd} = -13.2 at the surface) of the Faroe Islands [*Lacan and Jeandel*, 2004b]. The branch entering the Nordic Seas west of Iceland flows as Faroe branch into the Norwegian Sea. The other branch (Shetland branch) of the Atlantic water encounters the Norwegian Atlantic current (NWAC) and continues northward on the Norwegian shelf and further north at subsurface/intermediate depth as West Spitsbergen Current (WSC) into the Arctic Ocean. The inflowing AW on the eastern side of the Fram Strait can reach a thickness of up to 700 m at the Svalbard margin [*Schlichtholz and Goszszko*, 2006] with ε_{Nd} = -11.0 at ~600 m water depth and 77 °N [*Lacan and Jeandel*, 2004b]. Before entering the Arctic Ocean, the Atlantic water continues to flow between the overlying cold and less saline Polar Surface Water (ε_{Nd} = -10.2 to -9.8 [*Andersson et al.*, 2008]) and the Norwegian Sea Deep Water (NSDW), which prevails at depths below 1000 m [*Hansen and Østerhus*, 2000]. Due to the inflowing warm Atlantic water the eastern part of the Fram Strait remains ice free even in winter [*Vinje*, 2001].

The Nordic Seas are also strongly influenced by the outflow water from the Arctic Ocean and the subducted intermediate water, which forms the Arctic Intermediate Water (AIW: $\sim 0.5°C < T < 3°C$; $34.87 < S < 34.90$; ε_{Nd} = -8.0 to -9.0 in 500 to 1500 m water depth [*Lacan and Jeandel*, 2004b]) which is also called 'Norwegian Sea Intermediate Water' (NSAIW) and either flows through Denmark Strait or is advected east of Iceland as Modified East Icelandic Water (MEIW: $2°C < T < 3°C$, $34.85 < S < 34.90$; ε_{Nd} = -7.3 to -9.1 at 1000 m water depth [*Lacan and Jeandel*, 2004b]) over the Iceland-Faroer ridge and through the Faroer-Shetland Channel [*Hansen and Østerhus*, 2000] into the North Atlantic Ocean.

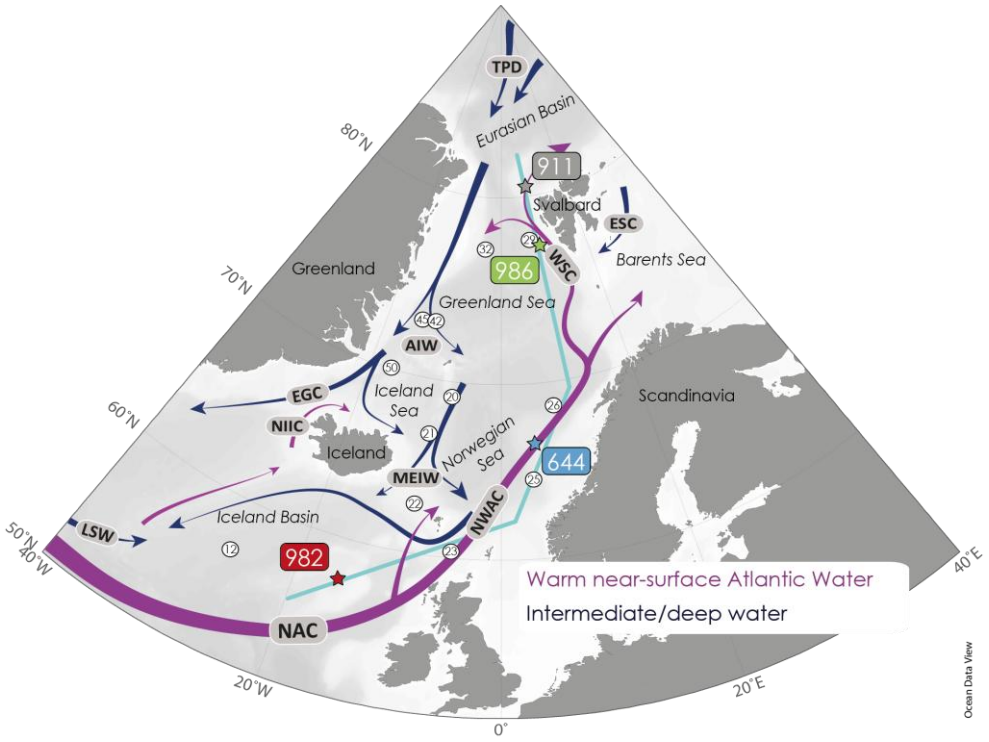

***Figure 4.1**: **Study area and locations of the different ODP sites (982, 644, 986) in the North Atlantic Ocean and the Nordic Seas.** The dominant near surface, intermediate and deep water currents are schematically illustrated, as well as locations of available water column Nd isotope measurements, analyzed by Lacan and Jeandel [2004b] (Station numbers in white circles). Near surface currents: NAC: North Atlantic Current; NWAC: Norwegian Atlantic Current; NIIC: North Icelandic Irminger Current; WSC: West Spitsbergen Current; ESC: East Spitsbergen Current; TPD: Transpolar Drift. Intermediate and deep currents: AIW: Arctic Intermediate Water; MEIW: Modified East Icelandic Water; EGC: East Greenland Current; LSW: Labrador Sea Water [Hansen and Østerhus, 2000, Lacan and Jeandel, 2005b]. The light blue line marks the position of the composite N-S profile from North Atlantic Ocean and Nordic Seas from 56°N to 82°N shown in Fig. 4.2.*

The deep Norwegian basin is filled with 'Norwegian Sea Deep Water' (NSDW), which is characterized by a salinity close to 34.91 below 2000 m and ε_{Nd} signatures of -10.1 at ~1500 m and -10.2 at 2400 m water depth [*Lacan and Jeandel*, 2004b]. The boundary between NSDW and NSAIW is placed close to 1000 m depth. Additionally, Eurasian Basin Deep Water (EBDW) and Canadian Basin Deep Water (CBDW) originating from the Arctic Ocean, which show ε_{Nd} values of -9.5 [*Andersson et al.*, 2008], may contribute to the formation of Norwegian Sea Deep Water (NSDW).

Site 644 in 1220 m water depth on the Vøring Plateau is a suitable site to reconstruct the evolution of the water mass exchange and environmental conditions, because it is located close to the boundary between the NSAIW and NSDW, which have had a significant impact on the circulation and climate in the Nordic Seas and northernmost Atlantic Ocean. Northernmost Site 986 on the Svalbard shelf is located in 2050 m water depth and is today mainly bathed in NSDW.

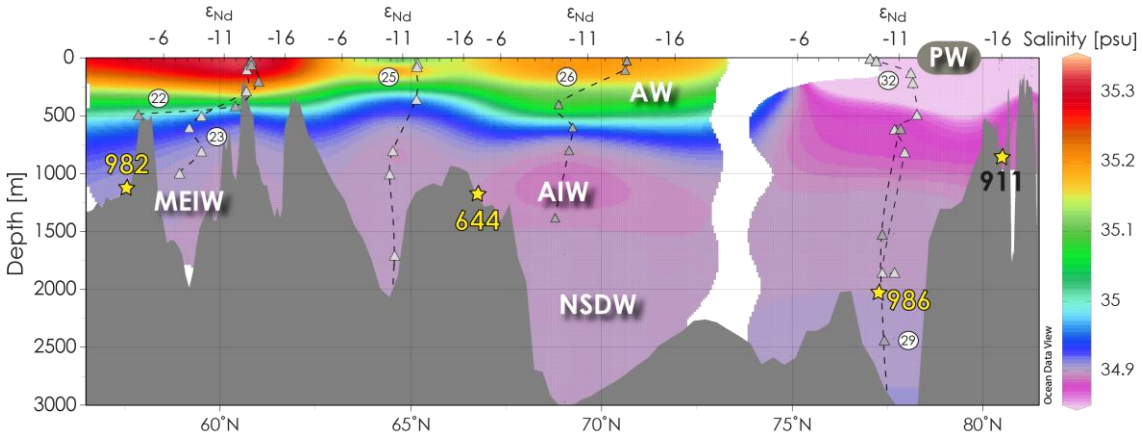

***Figure 4.2**: S-N profile of the present salinity distribution [Lacan and Jeandel, 2004b] across the Nordic Seas. The dissolved Nd isotopic composition of the water column at different stations (numbers in white circles) as measured by Lacan and Jeandel [2004b] and the location of the different ODP sites (982, 644, 986 and for comparison 911) in the North Atlantic Ocean and Nordic Seas are provided together with the different water masses prevailing in the Nordic Seas. MEIW: Modified East Icelandic Water; AW: Atlantic Water; AIW: Arctic Intermediate Water; NSDW: Norwegian Sea Deep Water; PW: Polar Surface Water [Rudels et al., 1989; Hansen and Østerhus, 2000; Schlichtholz and Goszszko, 2006].*

Overflow waters leaving the Nordic Seas over the Iceland Faroer ridge (MEIW and AIW; ε_{Nd} = -9 to -7 [*Lacan and Jeandel*, 2004b]) flow across the Rockall Plateau and are one endmember influencing Site 982 at a water depth of 1136 m. The dominant endmember is the Labrador Sea Water (LSW) flowing from the Labrador Sea northwards at intermediate water depth. The LSW carries an ε_{Nd} signal of -14.3 in 1100 m water depth in the Iceland basin (station 12; 56.37°N, 27.82°W [*Lacan and Jeandel*, 2005b]). A further water mass influencing the Rockall Plateau over the Plio- and

Pleistocene is the Mediterranean Overflow Water (MOW) coming from the south with an endmember ε_{Nd} of -9.4 at the Strait of Gibraltar [*Tachikawa et al*., 2004] and which flows northwards at water depths between 800 – 1000 m [*Kawase and Sarmiento*, 1986]. The dominant water masses in the Nordic Seas and northernmost Atlantic Ocean (characterized by salinity) are illustrated together with the locations of the investigated ODP sites on Rockall Plateau (982), Vøring Plateau (644) and the Svalbard margin (986) on a composite north to south profile from 57°N to 82°N (Fig. 4.2). The profile includes the dissolved Nd isotope composition of seawater [*Lacan and Jeandel*, 2004b] at locations close to the sites examined in this study.

In this study we applied radiogenic Nd and Pb isotopes extracted from different sites in the North Atlantic Ocean and Nordic Seas to reconstruct changes of water mass exchange and mixing, as well as changes of the erosional input and of the weathering regime. The North Atlantic Ocean and Nordic Seas have played a crucial role for the climate system and have undergone drastic changes over the past 3 Ma.

4.2. MATERIAL AND METHODS

4.2.1. Site locations and age models

For the reconstruction of water mass exchange and weathering inputs in the North Atlantic Ocean and Nordic Seas, we choose three sediment cores recovered from different sites occupied by intermediate and deep waters. The northernmost ODP Site 986 of this study (77°20.431’N, 09°04.664’E) located on the western Svalbard margin between Bellsund and Isfjorden fans (Fig. 4.1) at 2050 m water depth [*Jansen et al.*, 1996] was drilled during Leg 162 and is the deepest core of this study. The stratigraphic framework of Site 986 was subject of numerous previous studies [*Channell et al.*, 1999; *Eidvin and Nagy*, 1999; *Forsberg et al.*, 1999; *Butt et al.*, 2000; *Knies et al.*, 2009]. We adopted the age model of *Knies et al.* [2009] with an age at the base of the core of less than 3.2 Ma based on magnetostratigraphic and micropaleontological evidence [*Channell et al.*, 1999; *Eidvin and Nagy*, 1999; *Smelror et al.*, 1999]. In this core the seismic reflector R7 appears to reflect the onset of the Northern Hemisphere Glaciation [*Knies et al.*, 2009] and the glacial deposits of seismic reflector R5 reflects the

beginning of the MPT at ~1.5 Ma [*Forsberg et al.,* 1999]. Samples were chosen on the basis of IRD abundance provided by *Knies et al.* [2009] given that foraminiferal carbonate is barren in this record, especially in the part older ~1 Myr [*Jansen et al.*, 1996].

ODP Site 644 (66°40.700'N, 04°34.600'E) was drilled during Leg 104 on the Vøring Plateau (Fig. 4.1), which is part of the Norwegian shelf at a water depth of 1227 m. It is located close to the inner continental slope and overlies subsided continental crust [*Eldholm et al*., 1987] in a hemipelagic environment. The age model of Site 644 is based on magnetostratigraphy [*Bleil,* 1989] recalculated by *Cande and Kent* [1995] with a base of the core at ~ 3 Ma. Sampling intervals were chosen based on oxygen isotope stratigraphy of the benthic species *Cassidulina teretis* and *Melonis barleeanum* analyzed by *Jansen et al.* [1989].

ODP Site 982 (57°30,992'N, 15°52,001'W) is located at an intermediate water depth of 1145 m [*Jansen et al.,* 1996] on Rockall Bank (Fig. 4.1), which is a shallow platform between Iceland and Ireland. More precisely, Site 982 was drilled in the Hatton – Rockall Basin, which is a central depression of the plateau. The age model of *Venz et al.* [1999] and *Venz and Hodell* [2002], based on benthic and planktic foraminiferal oxygen isotope records was applied. Glacial and interglacial samples were chosen based on the benthic oxygen record of the foraminifera *Cibicidoides wuellerstorfi* and *Cibicidoides kullenbergi* [*Venz et al.,* 1999] for the record after 1 Ma and on the benthic oxygen record of the foraminifera *Cibicidoides wuellerstorfi* prior to 1 Ma [*Venz and Hodell*, 2002].

4.2.2. Sample and element preparation

The samples were mainly prepared as described in Chapter 2, in which different leach methods to extract the Nd, Sr and Pb isotopic composition of the ferromanganese coating on the sediment particles were tested and described in detail. For all three sites, the modified leach method established by *Gutjahr et al.* [2007] was applied, because it closely reflected the present seawater signature of surface sediments. The procedure started with a double rinsing with *MilliQ*© water for 20 minutes to dissolve all remaining seawater salts. This was followed by the removal of the carbonate fraction

with a buffered acetic acid solution (15% acetic acid/1M Na-acetate) for 2½ h and a second step with a 1:1 dilution of the acetic acid solution over night. On the following day the samples were rinsed again with *MilliQ*© water to remove the remaining acetic acid and then the leaching was performed applying a 0.05 M Hydroxylamine HCl and 15% acetic acid mixture, buffered to pH ~ 3.5 to 4.0 for 1 hour. The supernatant containing the dissolved seawater fraction was dried down in Teflon vials at ~ 90 to 95 °C. To prepare the samples for further element separation and purification they were dissolved in 1 ml HNO_3 twice and evaporated to dryness each time in order to destroy the matrix of the hydroxylamine solution. To evaluate potential detrital contamination in the leach solution containing the seawater signal, the radiogenic $^{87}Sr/^{86}Sr$ ratio was analyzed in this solution and was compared to the established seawater Sr isotope curve of *McArthur* [2001].

To prepare the sample for analyses of the detrital fraction the sediment remaining after initial leaching was allowed to react with a new batch of leach solution for a minimum of another 12 hours to guarantee complete removal of any authigenic coating. Afterwards, the triple rinsed and dried sediment was ground and 50 mg of the sediment was weighed into Teflon vials. For dissolution of the sediment a mixture of concentrated HNO_3 + HF was added and left to react at 180°C for three days. Due to particles remaining after this treatment the sample was, after evaporation to dryness, again treated with a mixture of HNO_3 + $HClO_4$ at 190°C to destroy remaining clay and organic material for final dissolution and the ion chromatographic separation and purification steps.

The separation and purification of the different elements Nd, Pb and Sr followed four steps. First, the Pb was separated from the other elements and purified on anion exchange columns filled with 50 µl of AG1-X8 resin (mesh 100-200) following the method of *Lugmair and Galer* [1992]. In a second step cation exchange columns filled with 0.8 ml AG50W-X12 resin (mesh 200-400) were used to separate the Rare Earth Elements (REEs) and the Sr. The columns to purify the Sr were filled with 50µl Sr-Spec resin (mesh 50-100) following the method of *Horwitz et al.* [1992] and *Bayon et al.* [2002]. In a final step the Nd was separated from the other REEs using columns with 2ml Ln Spec resin (50-100 mesh) [*Le Fèvre and Pin*, 2005].

4.2.3. Isotope analysis

The measurements of the Nd, Sr and Pb isotope compositions were all performed on a Nu Plasma Multicollector-ICPMS at Helmholtz Centre for Ocean Research GEOMAR, Kiel. To analyze the Pb isotope ratios the standard bracketing method of *Albarède et al.* [2004] was applied. The measured data were normalized to the Pb standard NIST NBS981 applying values of $^{206}Pb/^{204}Pb = 16.9405$, $^{207}Pb/^{204}Pb = 15.4963$, $^{208}Pb/^{204}Pb = 36.7219$ [*Abouchami et al.*, 1999]. The long term external reproducibility (2σ) for this standard was ±0.006 for $^{206}Pb/^{204}Pb$, ±0.0069 for $^{207}Pb/^{204}Pb$, ±0.020 for $^{208}Pb/^{204}Pb$, ±0.0005 for $^{208}Pb/^{206}Pb$, and ±0.0001 for $^{207}Pb/^{206}Pb$ over a period of seven months. The procedural blanks for all Pb isotope measurements were ≤ 1.2 ng. All $^{143}Nd/^{144}Nd$ data were normalized to the accepted value of the JNdi-1 standard of 0.512115 [*Tanaka et al.*, 2000] and for the mass bias correction a value of 0.7219 for the $^{146}Nd/^{144}Nd$ was used. The long term external reproducibility of repeated measurements for the JNdi-1 standard solution was ±0.25 ε_{Nd} (2σ) over a period of eight months. The procedural Nd blanks were ≤ 90 pg for the leach fractions and ≤ 130 pg for the detrital fractions of the sediment. The procedural blanks for Sr were below 2 ng. Mass bias correction of the Sr isotope applied an exponential fractionation law ($^{86}Sr/^{88}Sr = 0.1194$ [*Steiger & Jäger*, 1977]) after correcting for interferences on ^{86}Kr and ^{87}Rb. The measured Sr isotope data were normalized to $^{87}Sr/^{86}Sr = 0.710245$, which is the accepted value of the NIST NBS987 standard. The long term external reproducibility of the Sr isotope measurements was ±0.000025 (2σ) over a period of eight months.

4.3. RESULTS

4.3.1. Svalbard margin – Site 986

The $^{87}Sr/^{86}Sr$ signatures of the leached ferromanganese coatings of sediments from Site 986 range from 0.70891 to 0.71415 with an average value of 0.71100 and are thus overall somewhat more radiogenic than the present $^{87}Sr/^{86}Sr$ seawater value of 0.70916 [*McArthur et al.*, 2001]. The $^{87}Sr/^{86}Sr$ ratio of the detrital fraction is significantly more radiogenic than the leach data with values ranging from 0.71943 to

0.72975 and an average value of 0.72446 (Fig. 4.3, Tab. A.5). This supports a pure seawater origin of the Nd and the Pb isotope signature in the leachates of this core.

The Nd isotope composition of the core top sample (0 – 2cm) of -10.2 is indistinguishable from present day deep water values of NSDW observed at this site [*Lacan & Jeandel*, 2004b] thus also supporting the reliable extraction of the seawater signature without contamination by the detrital sediment (see Chapter 2). Prior to the INHG the ε_{Nd} values of the bottom water on the Svalbard margin ranged from -8.9 to -9.5 (with a mean ε_{Nd} of -9.2). Compared to Site 911 (Chapter 3) the shift at 2.71 to less radiogenic ε_{Nd} values (-10.8) is less pronounced, but still significant (1.3 ε_{Nd} units). After 2.71 Ma the amplitude of the variability in the ε_{Nd} record increased significantly to values between -8.5 to -11.8 (3.3 ε_{Nd} units) with an average of -10.1.

The period of time after the onset of the Northern Hemisphere Glaciation from 2.7 Ma to 2 Ma was characterized by less radiogenic ε_{Nd} values near -11, in particular during glacial periods as derived from the IRD record. Prior to 2 Ma the Nd isotope record reveals a clear variability between glacial and interglacial periods, characterized by more radiogenic ε_{Nd} values during interglacial and less radiogenic ε_{Nd} values during glacial times. From 2 Ma to present this correlation cannot further be monitored at this Site. During the period between 2 and 1 Ma, the record reveals an overall increase of about 3 ε_{Nd} units to -8.5 and at the same time displays a decreasing amplitude of the variability until the middle Mid Pleistocene Transition (MPT). From 1 Ma to present the Nd isotope signature of the deep waters has been highly variable and ranged from less radiogenic values of -11.8 at 0.71 Ma to radiogenic values of -8.7 at 0.32 Ma. The Nd isotope composition of the detrital fraction varied between -15.2 and -11.3 with an average value of -13.2 and was thus significantly less radiogenic than the leached seawater Nd isotope signatures. There is no obvious correlation between the detrital and leached signatures.

The Pb isotope composition of Site 986 reveals no significant trends over the past 3 Myrs. The $^{206}Pb/^{204}Pb$ ratios varied between 18.42 and 19.43 (average $^{206}Pb/^{204}Pb$ = 18.86) if the highly radiogenic peak at 0.7 Ma, despite being confirmed by a duplicate measurement, is considered an outlier ($^{206}Pb/^{204}Pb$ = 20.13) most likely originating from contamination during coring or in the laboratory.

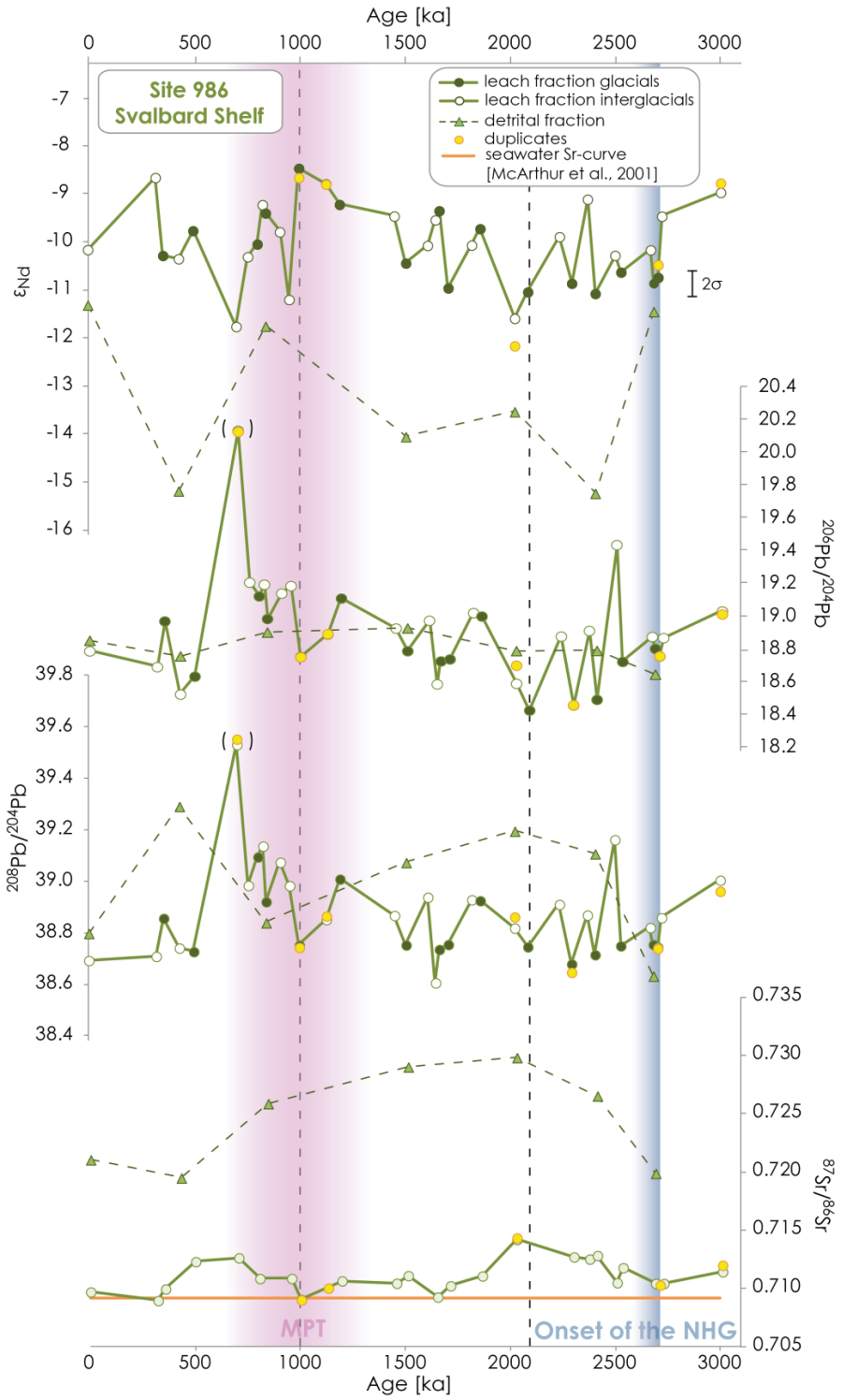

Figure 4.3: Down core Nd, Pb, and Sr isotope records of Site 986 on the Svalbard margin. *The evolution of the radiogenic Nd, Pb and Sr isotope composition of the weak leachates (open dots = interglacials; dark green dots = glacials) reflecting dissolved seawater signatures is compared to that of bulk sediment (green triangles) for the past 3 Myrs. The yellow dots indicate duplicate measurements. The orange line represents the Sr isotope evolution of global seawater [McArthur et al., 2001] over the past 3 Myrs.*

We observe a slightly higher amplitude in the glacial/interglacial variability for the periods of time prior to 2.1 Ma and after 1 Ma. The detrital fraction of $^{206}Pb/^{204}Pb$ reveals a comparably very low variability ranging only between 18.64 and 18.92 with an average value of 18.80. The $^{208}Pb/^{204}Pb$ record shows a very similar pattern without any major trend but compared to $^{206}Pb/^{204}Pb$, the $^{208}Pb/^{204}Pb$ signatures of the detrital fraction show a higher amplitude variability between 38.63 and 39.29 (Fig. 4.3, Tab. A.5).

4.3.2. Vøring Plateau – Site 644

The Sr isotope signature of Site 644 on the Vøring Plateau located on the Norwegian shelf varied between 0.70906 and 0.71065 with an average value of 0.70952 and thus closely reflects the present day Sr seawater signature of 0.70916 [*McArthur et al.*, 2001]. In addition, the Sr isotope composition of the detrital fraction differs significantly from the leach fraction. It ranged between 0.71847 (prior to 2.7 Ma) and 0.73308 with an average value of 0.72463 (Fig. 4.4, Tab. A.5), pointing as well to a seawater origin of the leach fraction extracted from the Fe – Mn coating of the sediments at this site.

Similar to Site 986, the Nd isotope record of Site 644 shows no clear trends but a very high variability between -11.2 and -6.1 (5.1 ε_{Nd} units) over the past 3 Ma. Furthermore contrary to Site 986, The Nd record shows no correlation between more radiogenic values during interglacial periods or less radiogenic values during glacials. The core top Nd isotope composition (-9.6) reflects the present seawater Nd signature of the NSDW determined by *Lacan and Jeandel* [2004b] at two stations slightly south and north of Site 644 on the Vøring Plateau (see chapter 2). Prior to 2.7 Ma the Nd isotopic composition ranged between -10.1 and -8.2 (average ε_{Nd} = -9.4), whereas between 2.7 Ma and 2.3 Ma the record reveals a significant shift of almost 4 ε_{Nd} units to more radiogenic values between -6.3 and -7.2. In the period from 2.3 Ma until the beginning of the MPT at ~1.2 Ma the amplitude of the variability in the record strongly increased (3.6 ε_{Nd} units) and the ε_{Nd} values vary between -6.8 and -10.4, with pronounced radiogenic peaks at 1.89 Ma, 1.47 Ma and 1.23 Ma and unradiogenic peaks at 2.15 Ma, 1.74 Ma and 1.42 Ma. During the MPT the record was characterized by increase to on

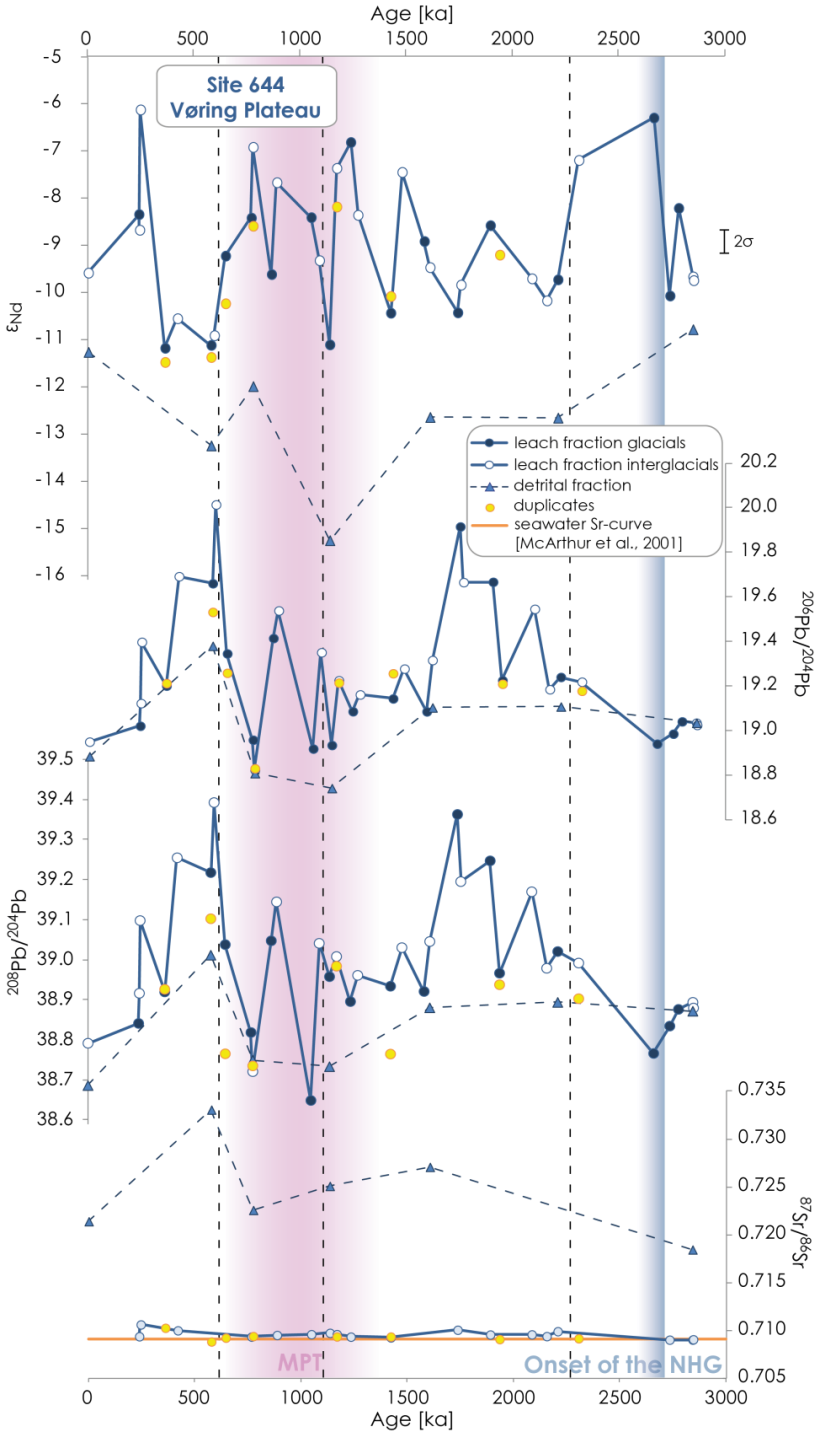

***Figure 4.4**: **Down core Nd, Pb, and Sr isotope records of Site 644 on the Vøring Plateau**. The weak leachates reflecting dissolved seawater signatures are represented by white (interglacials) and dark blue dots (glacials); the blue triangles illustrate the signatures of the detrital fraction for the past 3 Myrs. The yellow dots indicate duplicate measurements. The orange line represents the Sr isotope evolution of global seawater [McArthur et al., 2001] over the past 3 Myr.*

average more radiogenic ε_{Nd} values of -8.4. The youngest period from 0.6 Ma to present is characterized by a strong variability (5 ε_{Nd} units) with one highly radiogenic peak at 0.24 Ma. The Nd isotope composition of the detrital fraction was always less radiogenic than the Nd isotope composition of the leach fraction and ranged between -15.3 and -10.8 with an average value of -12.6 (Fig. 4.4, Tab. A.5) and revealing no obvious relationship to the leached signatures.

The seawater $^{206}Pb/^{204}Pb$ ranged between 18.82 and 20.01 at an average of 19.25 (and between 38.65 and 39.39 with an average value of 38.98 for the $^{208}Pb/^{204}Pb$ ratio) and showed a high amplitude variability. Superimposed, two pronounced radiogenic peaks at 0.6 Ma and 1.74 Ma are observed. The $^{206}Pb/^{204}Pb$ and $^{208}Pb/^{204}Pb$ ratios of the detrital fraction of the sediments of Site 644 show patterns similar to seawater albeit at a lower amplitude at values between 18.74 (38.69) and 19.38 (39.01) (Fig. 4.4, Tab. A.5).

4.3.3. Rockall Plateau – Site 982

The $^{87}Sr/^{86}Sr$ signature of Site 982, located on the Rockall Plateau in the northernmost Atlantic Ocean, essentially reflects the expected seawater evolution established by *McArthur et al.* [2001]. The down core values range between 0.70900 and 0.71042 with an average value of 0.70922, while the Sr isotopic composition of the detrital fraction is more radiogenic with values between 0.70952 and 0.71743 (average $^{87}Sr/^{86}Sr = 0.71351$) (Fig. 4.5, Tab. A.5).

The Nd isotope composition of the core top sample is -11.0 which is intermediate between the more radiogenic isotopic signal MEIW (Modified East Icelandic Water = -7.3 [*Lacan and Jeandel*, 2004b]) overflowing the Faroer – Iceland Ridge from the Nordic Seas in a water depth of ~1000 m and that of unradiogenic LSW (Labrador Sea Water) (see chapter 2) carrying a Nd isotopic signature of -14.3 in a water depth of 1100 m [*Lacan and Jeandel*, 2005b]. The down core ε_{Nd} values of Site 982 ranged between -10.4 and -9.4 (average ε_{Nd} = -10.1) prior to the onset of the Northern Hemisphere Glaciation at 2.7 Ma followed by a drop to a somewhat less radiogenic value of -10.8 about 1.4 ε_{Nd} units. The amplitude of the variability of the Nd isotope record of Site 982 is 7 ε_{Nd} units over the past 3 Ma.

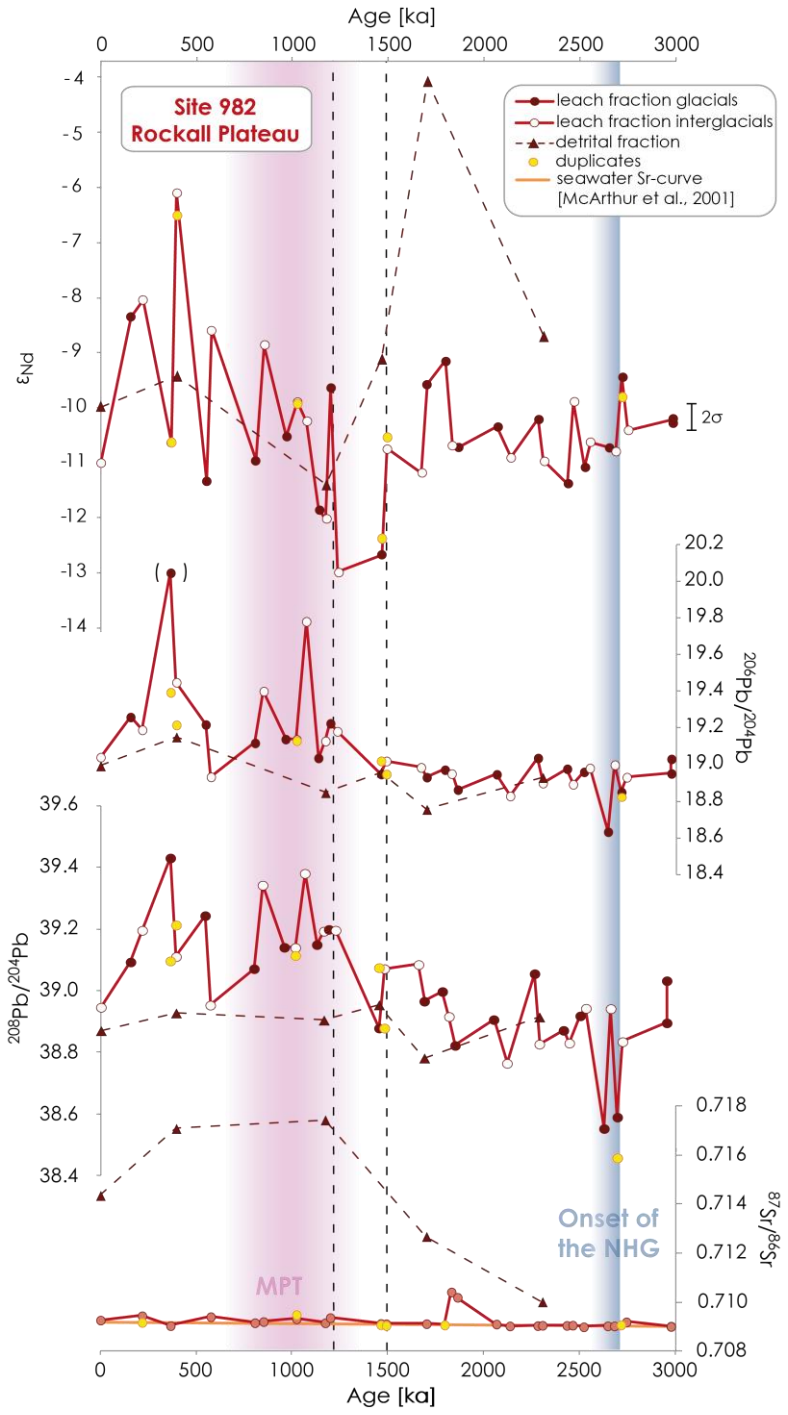

Figure 4.5: Down core Nd, Pb, and Sr isotope records of Site 982 on the Rockall Plateau in the North Atlantic Ocean. *The weak leachates are represented by white (interglacials) and dark red dots (glacials), reflecting dissolved seawater signatures; the red triangles illustrate the signatures of the detrital fraction for the past 3 Myrs. The yellow dots indicate duplicate measurements. The orange line represents the Sr isotope evolution of global seawater [McArthur et al., 2001] over the past 3 Myrs.*

The period between 2.7 Ma and 1.5 Ma reveals a relatively low variability of only 2.2 ε_{Nd} units between -11.4 and -9.1 with an average of -10.5. After a short interval (1.5 to 1.2 Ma) of highly unradiogenic values between -13 and -12.7, the period of time between the beginning of the MPT at 1.2 Ma and present has been characterized by an enhanced ε_{Nd} variability between -12 and -6.1 and an overall trend to more radiogenic ε_{Nd} values (in average -9.6) with a pronounced shift to -6.1 at 0.4 Ma. In contrast to Site 986, the Nd isotope record of Site 982 reveals no glacial/interglacial variability prior to 1.2 Ma, whereas after the beginning of the MPT a correlation of more radiogenic ε_{Nd} values during interglacial phases and less radiogenic values during glacials can be observed, accompanied with the increasing variability. The ε_{Nd} composition of the detrital fraction (ε_{Nd} = -4.1 and -11.4) shows more radiogenic values of up to -4.1 prior to 1.2 Ma and a range similar to that of the leach fraction after 1.2 Ma (Fig. 4.5, Tab. A.5).

The Pb isotope composition ($^{206}Pb/^{204}Pb$ as well as $^{208}Pb/^{204}Pb$) reveals a slight trend to more radiogenic values over the past 3 Ma with an increased amplitude of the variability after 1.2 Ma, similar to the Nd isotopic record. The $^{206}Pb/^{204}Pb$ values vary between 18.64 and 19.78 (average = 19.08) with a possible outlier at 0.37 Ma ($^{206}Pb/^{204}Pb$ = 20.05) and the $^{208}Pb/^{204}Pb$ ratios range between 38.55 and 39.43 with an average value of 39.01. The $^{206}Pb/^{204}Pb$ and $^{208}Pb/^{204}Pb$ ratios of the detrital fraction of the sediments of Site 986 show a similar evolution at a lower amplitude of the variability between 18.75 (38.78) and 19.15 (38.95) (Fig. 4.5, Tab. A.5).

4.4. DISCUSSION

Comparison of the isotope records of all sites is complicated by the low resolution combined with the high variability of the single records, as well as by uncertainties of the age models. An additional problem, in particular for the conclusions drawn from the Nd isotope compositions is the strong influence of the erosional inputs at the sites located near a shelf (Site 986 and 644), because the seawater Nd isotope signal has most likely been modified by exchange with the shelves and the erosional inputs. Hence, it is difficult to draw conclusions about the water mass exchange in and

between the entire Nordic Seas and North Atlantic Ocean based on these data. Consequently each record is discussed separately below.

Comparing the sites from the Nordic Seas and North Atlantic Ocean, the $^{87}Sr/^{86}Sr$ signatures of the leached ferromanganese coatings show a good agreement with the expected seawater signature of 0.70916 [*McArthur et al.*, 2001]. We can observe that the Sr isotope composition is closest to the seawater Sr signature at the southern Site (982) on the Rockall Plateau (Fig. 4.5), but deviates to somewhat more radiogenic values at the northernmost Site (986) on the Svalbard margin (Fig. 4.3). This is most likely caused by partial dissolution of the detrital fraction, which, however, had no significant consequences for the extracted seawater Nd and Pb isotope compositions due to the higher susceptibility of the $^{87}Sr/^{86}Sr$ ratio to detrital contamination [*Gutjahr et al.*, 2007] (see Chapter 2). A further confirmation of the seawater origin of the leached Nd and Pb isotopic signatures is the conformity of the extracted ε_{Nd} values of the core top samples and the respective measured ε_{Nd} value of seawater at locations [*Lacan and Jeandel*, 2004b, 2005b] close to the different sites (see Chapter 2). In the following, both the Nd and Pb isotope compositions of the leachates will consequently be discussed as past seawater compositions.

In general, we assume for all sites in the Nordic Seas and North Atlantic Ocean that a low variability in the Nd and Pb isotope records of the sea water derived leachates indicate general warmer climate conditions with less pronounced glacial/interglacial cycles and more stable warmer periods. Vise versa a higher variability in the isotope records point to more pronounced changes between glacial and interglacial periods due to an increased exchange between different water masses or the increased erosional input at the different sites.

4.4.1. Evolution of water masses exchange and erosional input on the Svalbard margin

The variability of the Nd isotope compositions extracted from the ferromanganese coatings on the sediment particles of Site 986 reflect differences in water mass mixing and composition, as well as exchange with the sediments of the western shelf of Svalbard. The ε_{Nd} values of the record vary around an average value of

-10.1 close to the present Norwegian Sea Deep Water (NSDW), which has most likely been the dominant water mass over the past 3 Myrs. A more radiogenic Nd isotope composition of NSDW may have been caused by reduction of the Atlantic inflow, which would have resulted in more radiogenic ε_{Nd} values in the deep and intermediate waters of the Nordic Seas. Another possibility to change the Nd isotope composition of past seawater at the study site to more radiogenic values is the advection of a different water mass, i.e. more radiogenic deep water from the Eurasian basin of the Arctic Ocean (EBDW: ε_{Nd} = -9.5 [*Andersson et al.*, 2008]) or Arctic Intermediate Water, which changed its properties or the volume of its outflow and thus prevailed at greater water depth.

In addition, the erosional input, which isotopic signal can be transported to greater depths through brine formation on the shelf [*Aagaard et al.*, 1985], may have played a role. This process is thought to play a dominant role for deep water production in the Arctic Ocean and the entire Nordic Seas [*Henrich and Baumann*, 1994]. Sources of more radiogenic Nd isotope signatures can be sediments from the Barents Sea (ε_{Nd} = -9.4 to -8.3 [*Tütken et al.*, 2002]) or basaltic material like the Putorana basalts from Siberia (ε_{Nd} = -5 to +3 [*Sharma et al.*, 1992]) transported as ice rafted debris (IRD) to the Svalbard margin. The most effective transport mechanism of IRD to the Svalbard shelf – besides melt water events that are common for present interglacial conditions [*Darby et al.*, 2006] – is incorporation in sea ice or ice sheets and transport from the Svalbard/Barents Sea ice sheet [*Tütken et al.*, 2002]. Weathering contributions from the Icelandic basalts (ε_{Nd} = +6 [*Farmer et al.*, 2003]) most likely only play a subordinate role for this location due to the large distance to Iceland. Besides Greenland (ε_{Nd} up to -35 [*Lacan and Jeandel*, 2004a]), which is most likely of minor importance, potential unradiogenic sources of the erosional input are the continental rocks of Svalbard which range from ε_{Nd} = -10 to -21 [*Johansson and Gee*, 1999; *Johansson et al.*, 2002; *Tütken et al.*, 2002; *Andersson et al.*, 2008]. This is supported by several studies showing that Svalbard is the dominant sediment supplier of the Svalbard shelf [*Geissler and Jokat*, 2004; *Knies et al.*, 2009, *Geissler et al.*, 2011].

No systematic trend to less radiogenic values can be observed over the past 3 Myrs (Fig. 4.6). In detail, our Svalbard margin record can be divided into three distinct

phases, which resemble with some small differences the phases of the ice growth of the Barents Sea ice sheet described by *Knies et al.* [2009].

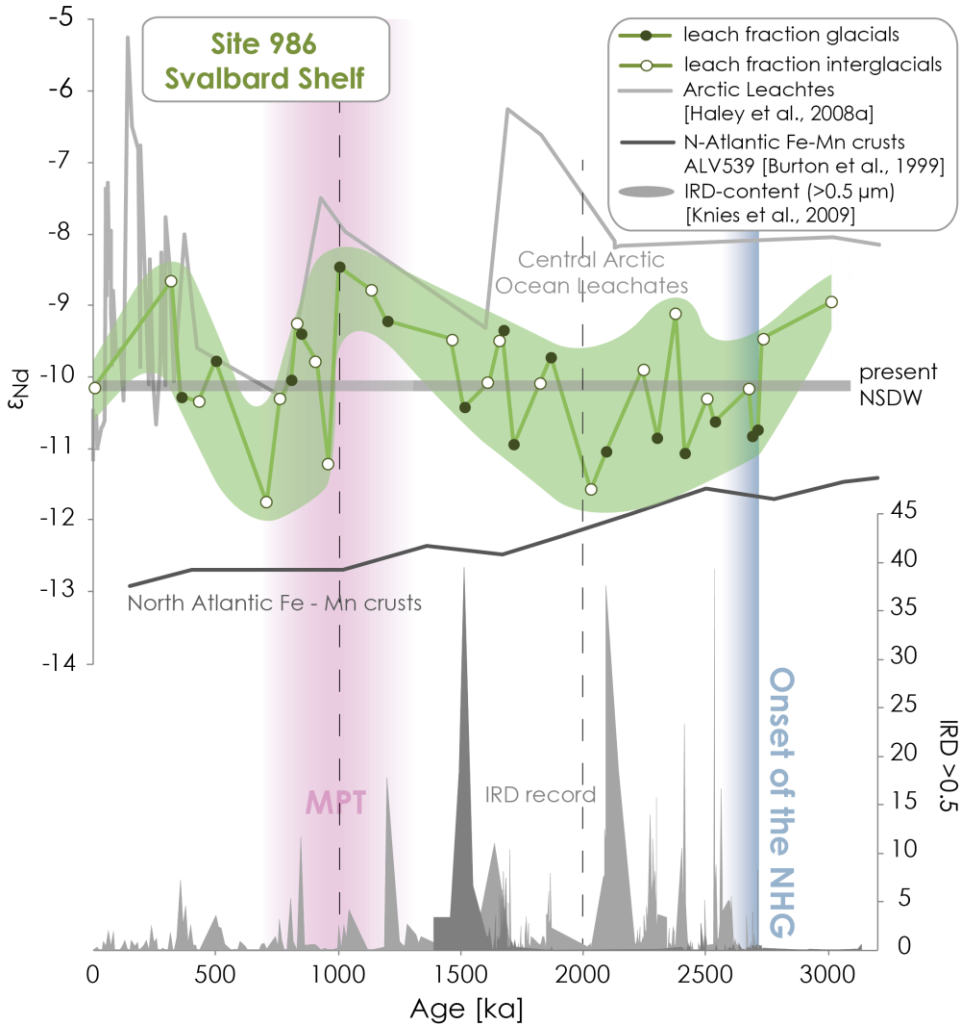

***Figure 4.6**: **Comparison of the Nd isotope record of Site 986** (open dots = interglacial periods, filled dots = glacial periods) extracted from the ferromanganese coatings with leaching results from the Central Arctic Ocean (light grey line) [Haley et al., 2008a] and the western North Atlantic Fe-Mn crust record of NADW (dark grey line) [Burton et al., 1999]. The green shaded area mark the general evolution of the record with the different variability in the different parts of the record. Furthermore the IRD (>0.5 µm) content of this site is displayed as grey shaded areas [Knies et al., 2009]. The dashed lines divide the record in the different periods and the colored shadings mark the onset of the Northern Hemisphere Glaciation (2.7 Ma) and the Mid Pleistocene Transition.*

For the period of time between 3 Ma and 2 Ma, we observe a systematic correlation between more radiogenic values during interglacial periods and less radiogenic Nd isotope compositions during glacials as inferred from variations in IRD abundance. The more radiogenic ε_{Nd} values of the interglacial periods (-10.3 to -9.0) are consistent with NSDW. The less radiogenic glacial ε_{Nd} values (-11.1 to -10.6) may be the result of an increasing glacial input from Svalbard and/or the presence of a less radiogenic water mass such as Atlantic water. The increasing erosional input caused by the intensification of the Northern Hemisphere Glaciation is consistent with the drop to less radiogenic Nd isotope compositions at 2.71 Ma. This is also supported by an increasing IRD input (Fig. 4.6) as a consequence of enhanced glacial erosion accompanied by a short term glacial expansion on the northwestern Barents Sea described on the Svalbard shelf [*Knies et al.,* 2009] during the *Initial phase* between 3.5 Ma and 2.4 Ma, as defined on the basis of IRD content and the abundance of clay minerals. Increased erosional input is also supported by the slightly increased variability of the Pb isotope signatures.

After 2 Ma the clear correspondence between the interglacials/glacials and the Nd isotope variability disappeared, possibly because the IRD-peaks (Fig. 4.6) that provided the basis for assigning interglacial/glacial stages did not exactly correspond to climatic stages or do not represent the maxima of each glacial phase given that peaks in the IRD record may also originate from deglacial melt water pulses. Stable oxygen isotope data would represent a better basis to assign glacial and interglacial cycles, but due to the high latitude the sediments of this site only contain minor and discontinuous amounts of foraminiferal carbonate [*Jansen et al.,* 1996]. In the phase between 2 Ma and 1 Ma the erosional influence of unradiogenic material from Svalbard decreased as reflected by a significant shift in the Nd isotope record to more radiogenic values. This is supported by a reduced IRD input on the Svalbard shelf described for the *Transitional phase* (2.4 – 1.0 Ma) of the glacial development of the Barents Sea ice sheet [*Knies et al.,* 2009]. The pronounced trend to more radiogenic values is most likely not only explainable by the decrease of supply of unradiogenic material from Svalbard, but points more to a change in the prevailing sediment sources towards a Barents Sea origin. Another feature of this period of time supporting this assumption is the drastic decline in smectite content and a persistent growth of glaciogenic wedges, which

implies a gradual increase in the supply of glacially eroded material from Barents Sea as a consequence of the expanding ice sheet. This may have led to more radiogenic Nd isotope signatures, because sea ice sediments from the Barents Sea are characterized by ε_{Nd} values of -9.4 to -8.3 [*Tütken et al.*, 2002]. The sediment transport from the Barents shelf, which was dominant during several periods over the past million years, occurs via the main drainage areas into the Bear Island and Storfjorden Troughs [*Nøttvedt et al.*, 1988] and further via the WSC [*Smelror et al.*, 1999; *Butt et al.*, 2000]. A further source of radiogenic Nd isotope signatures is basaltic material from the Knipovich Ridge spreading axis (west) and Vestbakken Volcanic province (southeast), which has been attributed to an enhanced smectite content at Site 986 as a consequence of a further glacial expansion between 1.5 and 1.3 Ma [*Butt et al.*, 2000]. Increased glacial erosion is supported by more radiogenic $^{206}Pb/^{204}Pb$ signatures as a consequence of the enhanced mobilization of ^{206}Pb during enhanced glacial incongruent weathering (Fig. 4.3). This is consistent with increased erosion caused by the glacial extension of the continental ice sheet on Svalbard and the increased erosional input due to a fluctuating ice margin [*Forsberg et al.*, 1999].

During the last phase from 1.0 Ma to present, equivalent to the *Final growth phase* [*Knies et al.*, 2009], the increasing variability of the Nd isotope record was the result of the increased glacial/interglacial cyclicity influencing the water mass exchange and erosional input, supported by a large intensification of the glaciation [*Knies et al.*, 2009]. Two unradiogenic peaks at 0.71 Ma (ε_{Nd} = -11.8) and 0.95 Ma (ε_{Nd} = -11.2) both correlated to interglacial periods pointing to either an enhanced inflow of Atlantic water, which led to generally less radiogenic values in the Nordic Seas and thus also of the NSDW or a strongly increased IRD input from Svalbard. *Knies et al.* [2009] ascribed this phase to a large scale intensification of the Svalbard-Barents Sea glaciation supporting the strong variability in the Nd isotopic record, most likely linked to the waxing and waning of the Barents Sea ice sheet, which was deduced from the inputs of erosional products such as kaolinite and IRD pointing to a dominance of a circum Arctic ice sheet [*Knies et al.*, 2009].

The mixing between the Arctic and Atlantic influence at Site 986 is clearly recognizable in the comparison of its Nd isotope record with other paleo seawater records from the Central Arctic Ocean [*Haley et al.*, 2008a] and with ferromanganese

crusts from the North Atlantic Ocean [*Burton et al.*, 1999] (Fig. 4.6). Prior to 1.7 Ma the Nd isotope record of Site 986 indicates a stronger influence of Atlantic waters, especially during glacial periods. After 1.7 Ma the influence of the Atlantic water decreases and the Arctic influence increased significantly until present given that the Nd isotopic signatures of both records were very similar in their Nd isotope variability and compositions supporting the dominant influence of water masses and erosional input from the Arctic Ocean, most likely promoted by the enhanced glaciation around the Arctic Ocean and Nordic Seas. This supports the previously made assumptions for the driving factors of the different phases of the Nd isotope evolution of Site 986 during the past 3 Myrs.

4.4.2. The Vøring Plateau - Water mass exchange and erosional input in the eastern Norwegian Sea over the past 3 Myrs

The pronounced variability in the Nd isotope record of Site 644 has been a consequence of the waxing and waning of the continental ice sheets, as well as changes of the circulation leading to the variable influence of different water masses. In general, the seawater Nd isotope composition extracted from the coatings of the sediments particles has on average been close the Nd isotope signal of the present NSDW in that area (ε_{Nd} = -10.3 to -9.1 in 1000 to 1700 m water depth [*Lacan and Jeandel*, 2004b]). More radiogenic ε_{Nd} signatures of past seawater may have been caused by a more radiogenic water mass influencing Site 644, i.e. AIW or changes in the Nd isotopic composition of the NSDW itself. The dominant water mass carrying an unradiogenic signal in the Nordic Seas has been the Atlantic inflow water with a present Nd isotope signal of -13.1 at 100 m water depth and -12.1 at 350 m water depth at the Vøring Plateau [*Lacan and Jeandel*, 2004b]. Hence, enhanced inflow of Atlantic water into the Nordic Seas is required to reach the depths of Site 644 or a change of the Nd isotope composition of the entire Nordic Seas to less radiogenic signatures occurred.

The highly radiogenic signatures cannot only be explained by the influence of different water masses, which is why we suggest that erosional inputs with a radiogenic signal were released into the Nordic Seas. Major radiogenic sources for the erosional input are the Icelandic basalts and possibly basaltic material from Siberia, transported

by sea ice and ice sheets to the Vøring Plateau. Clearly, enhanced influence of Icelandic material (ε_{Nd} = +6 [*Farmer et al.*, 2003]) transported either in dissolved form by northwards directed surface currents or by volcanic ash as eolian input is more likely to have caused radiogenic shifts. The predominant source of the erosional input to the Norwegian shelf have been the old continental rocks of the Scandinavian shield exposed of Norway, which resulted in less radiogenic Nd isotope signatures (ε_{Nd} ~ -21 [*Fagel et al.*, 2002]).

The Nd isotope record of Site 644 reveals no overall trends and no systematic correlation between glacial and interglacial periods (as identified by benthic foraminiferal oxygen isotopes) and Nd isotope variability over the past 3 Ma (Fig. 4.7). In detail, the environmental changes were separated into three phases, closely related with the phases of the paleoceanographic evolution of the surface and deep waters in the Norwegian Sea [*Henrich and Baumann*, 1994] on the basis of changes in biogenic and terrigenous components and $\delta^{18}O$ variability, as well as carbonate content. Similar to Site 911 (Fig. 4.2) on the Yermak Plateau (see Chapter 3), the onset of the Northern Hemisphere Glaciation at 2.7 Ma was reflected by a pronounced shift of 3.8 ε_{Nd} units to more radiogenic ε_{Nd} values of up to -6.3 on the Vøring Plateau, which remained highly radiogenic until 2.3 Ma. At Site 911, this shift to more radiogenic signatures was explained by the enhanced glaciation, which supplied more radiogenic material from the Eurasian shelf of the Arctic Ocean via the Transpolar Drift (TPD). Increased glacial input during this period of time is supported by *Kleiven et al.* [2002], who documented that the change at 2.72 Ma was also reflected by a pronounced increase in IRD influx on Vøring Plateau. After this shift the IRD input on the Norwegian shelf was one to two orders of magnitude higher (Fig. 4.7).

Another possibility to explain the observed variability similar to Site 911 (Chapter 3) is the change of water mass circulation caused by the closure of the Isthmus of Panama followed by an enhanced moisture supply to the high northern latitudes at the beginning of the NHG. This resulted in an increased freshwater export from the Arctic Ocean into the Nordic Seas [*Driscoll and Haug*, 1998] supplying a more radiogenic Nd isotope signal, as well as inhibiting the inflow of Atlantic water, which may also have produced the observed shift of the Site 644 record to more radiogenic values. The reduction of Atlantic water inflow into the Nordic Seas, associated with the

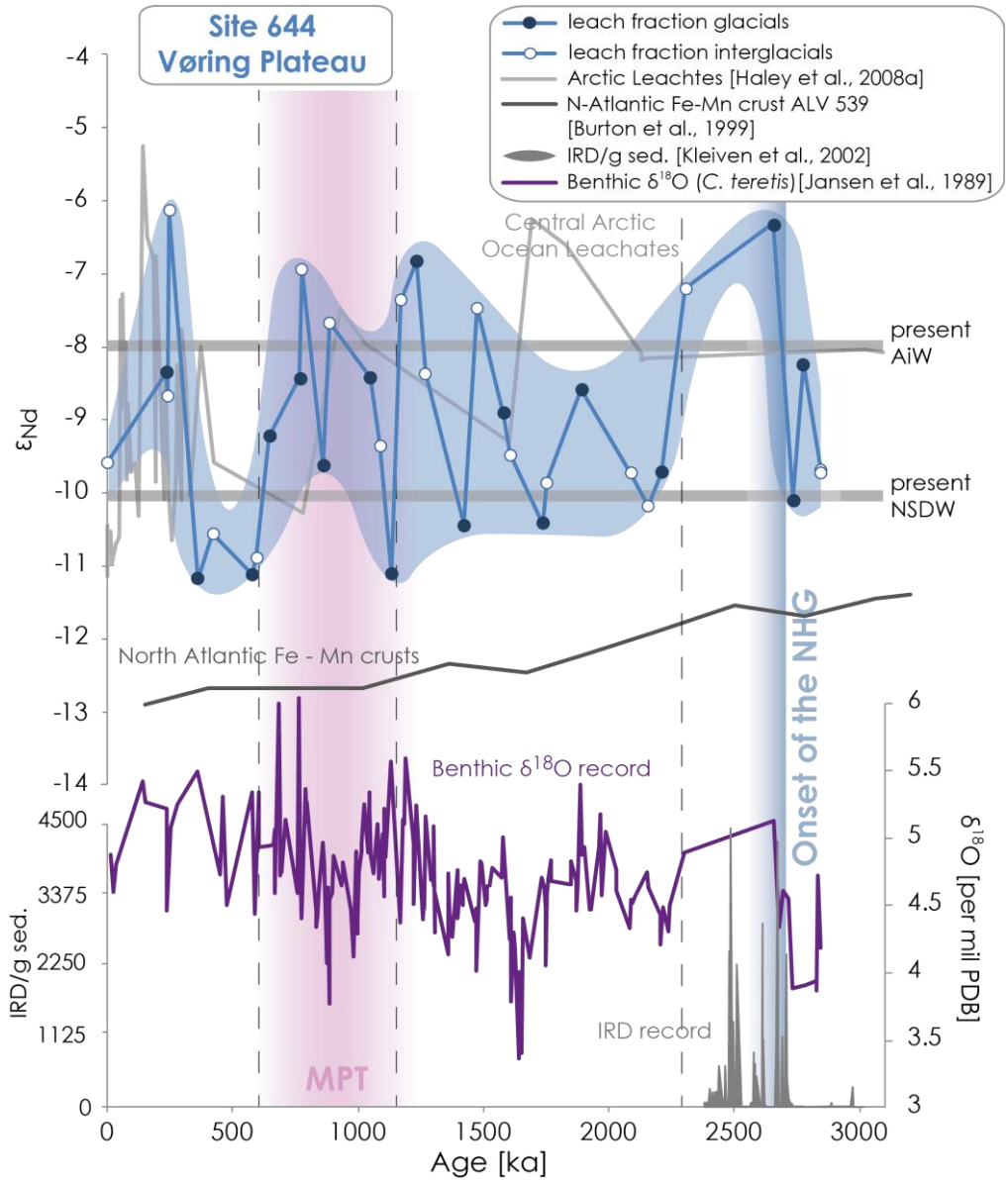

***Figure 4.7*: Leached Nd record of Site 644** *(open dots = interglacial periods, filled dots = glacial periods) compared to the leached seawater data from the Lomonosov ridge in the Central Arctic Ocean (light grey line) [Haley et al., 2008a] and the North Atlantic Fe-Mn crust record of NADW (dark grey line) [Burton et al., 1999]. The blue shaded array displays the high variability in this record over the past 3 Ma. Additionally, displayed as purple line is the $\delta^{18}O$ record of the benthic foraminiferal species Cassidulina teretis [Jansen et al., 1989] and green shaded the IRD content in the interval from 2.4 – 3.6 Ma [Kleiven et al., 2002]. Also displayed: dashed lines = separation of the record into the different periods; the colored shadings = the onset of the Northern Hemisphere Glaciation (2.7 Ma) and the Mid Pleistocene Transition.*

increasing freshwater supply from the Arctic Ocean may have caused a shift in the Nd isotope composition of the entire Nordic Seas to more radiogenic water mass composition. However, the second hypothesis is more likely, because the enhancement of the glaciation would have predominantly supplied material from Scandinavia with a much less radiogenic Nd isotope signature.

The first phase from the intensification of the NHG (2.7 Ma) to the MPT (1.0 Ma) was characterized by moderate glacial conditions and long term stability of rather small ice caps over Scandinavia [*Henrich and Baumann,* 1994] with an intermediate IRD flux most likely caused by glacial input from the Scandinavian shield. This mechanism is consistent with the high variability in the Nd isotope record and the unradiogenic peaks in the isotope record during glacial periods (2.16 Ma, 1.74 Ma and 1.42 Ma) between 2.3 to 1.2 Ma. A short period between 2.0 and 1.8 Ma shows very low IRD and light $\delta^{18}O$ pointing to warmer climate conditions [*Fronval et al.*, 1996]. Between 2.5 Ma and 1.5 Ma the Atlantic water inflow was weak and relatively minor ice sheet fluctuations occurred on the Vøring Plateau accompanied by a reduced IRD flux, pointing to less severe glaciations around the Nordic Seas [*Jansen et al.*, 1989; *Fronval et al.,* 1996]. This is reflected by relatively light $\delta^{18}O$ values (Fig. 4.7) [*Jansen et al.*, 1989] and by a moderate variability of our Nd isotope record between 2.3 and 1.5 Ma, before the variability increased again from 1.5 to 1.2 Ma.

The $^{206,208}Pb/^{204}Pb$ ratio as well as the variability of these records increased after 2.2 Ma as a consequence of enhanced glacial input, which itself significantly shifted near 0.5 Ma as also reflected in the Nd record, similar to Site 911 (Chapter 3). After 1.7 Ma the $^{206,208}Pb/^{204}Pb$ ratios and variability decreased indicating a warmer period, supported by relatively small ice sheet fluctuation (1.9 – 1.2 Ma) [*Jansen et al.*, 1989].

The period between 1.2 and 0.6 Ma is consistent with the Mid Pleistocene Transition (MPT), which is characterized by moderate to enhanced IRD input, an increased abundance of foraminifera, and an increase of the planktonic $\delta^{18}O$ during glacials. These records support a shift towards more extensive glacial periods of longer duration and short, but relatively warm interglacials with the influx of warm surface waters [*Jansen et al.,* 1989; *Fronval et al.,* 1996], as well as an intensified contrast between glacial and interglacial conditions [*Henrich and Baumann,* 1994]. Furthermore, the strength of the Norwegian current was enhanced during interglacial periods and

more severe glaciations affected the Scandinavian mainland [*Henrich and Baumann*, 1994]. These features would lead to expect a strongly enhanced variability as well as less radiogenic ε_{Nd} values in our record due to the increased erosional input of less radiogenic values from the Scandinavian hinterland. However, the Nd isotope composition of Site 644 in this period shows a significant shift to more radiogenic values and a decreasing variability was most likely caused by the enhanced influence of AIW, which carried a more radiogenic ε_{Nd} values, or a general shift of the entire Nordic Seas and consequently the NSDW to more radiogenic ε_{Nd} values as a consequence of an enhanced supply of Arctic water masses or melt water in the course of the increasing glaciation. The more radiogenic values can also be a result of a change in the sediment source. After 1 Ma the Barents Sea ice sheet extended to the Vøring Plateau [*Knies et al.*, 2009], which supplied sediments from the Barents Sea region with a more radiogenic signature (-9.4 to -8.3 [*Tütken et al.*, 2002]) or from further north to the location of Site 644. Another possibility is material from Iceland, which may have contributed basaltic particles via the northward flowing currents, which partially dissolved and released their signature to the water column.

The $^{206}Pb/^{204}Pb$ record supports the features of the MPT even better, i.e. the increasing variability starting 1.2 Ma again, caused by the intensified distinction between the glacial and interglacial periods. In addition, the more radiogenic $^{206}Pb/^{204}Pb$ values support the increased IRD input induced by stronger glaciations of longer duration affecting Scandinavia [*Henrich and Baumann*, 1994].

The period from 0.6 Ma to present has been characterized by stronger glaciations on Scandinavia, as well as a broad Atlantic water inflow far into the Arctic Ocean [*Henrich and Baumann*, 1994]. Both mechanisms can explain the less radiogenic values in the first part of this period, as well as the similarity between the glacial and interglacial times, because stronger glaciations led to increased erosional input originating from less radiogenic Scandinavian rocks, whereas the enhanced Atlantic water inflow during interglacials supplied water masses with an unradiogenic Nd isotope composition to the Nordic Seas. This period, marked by an unradiogenic Nd isotope composition, was accompanied by more radiogenic $^{206}Pb/^{204}Pb$ ratios, most likely caused by increased glacial input and incongruent weathering effects. At 0.25 Ma a highly radiogenic peak of up to an ε_{Nd} of -6.1 is observed, which can be explained

either by a direct erosional input from a basaltic origin as Iceland or a northern source like the Eurasian shelf, or by boundary exchange with the basaltic margins in the Nordic Seas around Iceland [*Lacan and Jeandel,* 2004a, 2005a].

For the Nd isotope record of Site 644 the comparison with other paleorecords shows a very agreement with the Central Arctic Ocean seawater record [*Haley et al.*, 2008a] and only a minor influence from the Atlantic Ocean [*Burton et al.,* 1999] (Fig. 4.7). Between 2.2 and 1.5 Ma and from 0.6 to 0.3 Ma the Nd isotope record from Site 644 was distinct from the Arctic Ocean record, pointing to an increased influence from the North Atlantic Ocean, possibly caused by increased Atlantic inflow. It has to be mentioned that Site 644 has been strongly influenced by erosional input and that the conclusions based only on water mass exchange remain speculative in view of potential alteration by the input of erosional products.

4.4.3. Evolution of water mass exchange on the Rockall Plateau in the North Atlantic Ocean

Compared to the locations on the Svalbard margin and the Norwegian shelf in the Nordic Seas, which are influenced by different water masses, as well as exchange with the shelves, Site 982 is located at a larger distance from land and therefore its seawater radiogenic isotope compositions have been dominantly influenced by water mass mixing. As a consequence the erosional input only plays a subordinate role. The actual prevalent mixture between the overflow waters from the Nordic Seas (AIW/MEIW) and Labrador Sea Water (LSW) from the south can also be observed during the past 3 Ma. An alternation between a stronger influence by the overflow waters revealing more radiogenic seawater ε_{Nd} signatures and a stronger influence of LSW from the south [*Venz and Hodell*, 2002] carrying a less radiogenic signature has been recorded. Another water mass that may have influenced Rockall Plateau over the past 3 Ma is Mediterranean Overflow Water (MOW) characterized by a Nd isotope composition of ~-9.4 at the Strait of Gibraltar [*Tachikawa et al.,* 2004; *Stumpf et al.*, 2010]. The erosional input on Rockall Plateau has been dominated by Iceland, supplying radiogenic values (ε_{Nd} = +6 [*Farmer et al.,* 2003]) and Greenland (ε_{Nd} ~ -35

[*Fagel et al.*, 2002]) and the Scandinavian shield (ε_{Nd} ~ -21 [*Fagel et al.*, 2002]) supplying highly unradiogenic signatures.

In the period from 3 Ma to 1.5 Ma, the comparatively low variability in the Nd isotope record points to small shifts between the different water masses and stable climatic conditions in the North Atlantic Ocean and Nordic Seas [*Henrich*, 1989; *Thiede et al*., 1998; *Jansen et al.*, 2000]. At 2.7 Ma the Nd isotope record reveals just a small and transient shift of 1.3 ε_{Nd} units to less radiogenic values (Fig. 4.8), which is in the same order of magnitude as the average variability, but could point to a greater influence by AIW during the major intensification of the NHG. Overall the Nd isotope composition of this period points to the enhanced influence of a less radiogenic water mass such as LSW, except for a small excursion between 1.8 Ma to 1.7 Ma indicating a stronger influence of the overflow waters from the Nordic Seas or MOW. In the short period of time between 1.5 Ma to 1.2 Ma characterized by highly unradiogenic values the influence of the LSW was strongly increased.

Similar to Site 986, the enhanced amplitude of variability in the period from the MPT (1.2 Ma) to the present reflects enhanced glacial/interglacial cyclicity. In this period, compared to the record prior to 1.2 Ma, a clear differentiation between interglacial periods, displaying particularly radiogenic values and the glacial periods showing less radiogenic periods is observed. During interglacial periods the NADW dominated the ventilation of the North Atlantic Ocean [*Kleiven et al.*, 2003] similar to present day conditions. The North present day and interglacial Atlantic Ocean has been dominated by the "Nordic Seas" convection, in which NSDW has passed the Faroer-Scotland-Channel and Wyville-Thomson Ridge into the North Atlantic Ocean has influenced the Rockall Plateau [*Crocket et al.*, 2011] with more radiogenic ε_{Nd} values between -7 and -9 [*Lacan and Jeandel*, 2004b].

During glacial periods the water masses were strongly stratified and less ventilated [*Venz et al.*, 1999; *Kleiven et al.*, 2003] and the production of the NADW between 1 Ma and present was reduced, most likely caused by a major deglacial iceberg melting and the consequent reduction of North Atlantic surface water salinity [*Venz et al.*, 1999]. Hence, the convection in the North Atlantic Ocean switched from deep (NADW) water influence to an intermediate mode dominated by Glacial North Atlantic Intermediate Water (GNAIW) [*Boyle and Keigwin*, 1987; *Oppo and Fairbanks*, 1987].

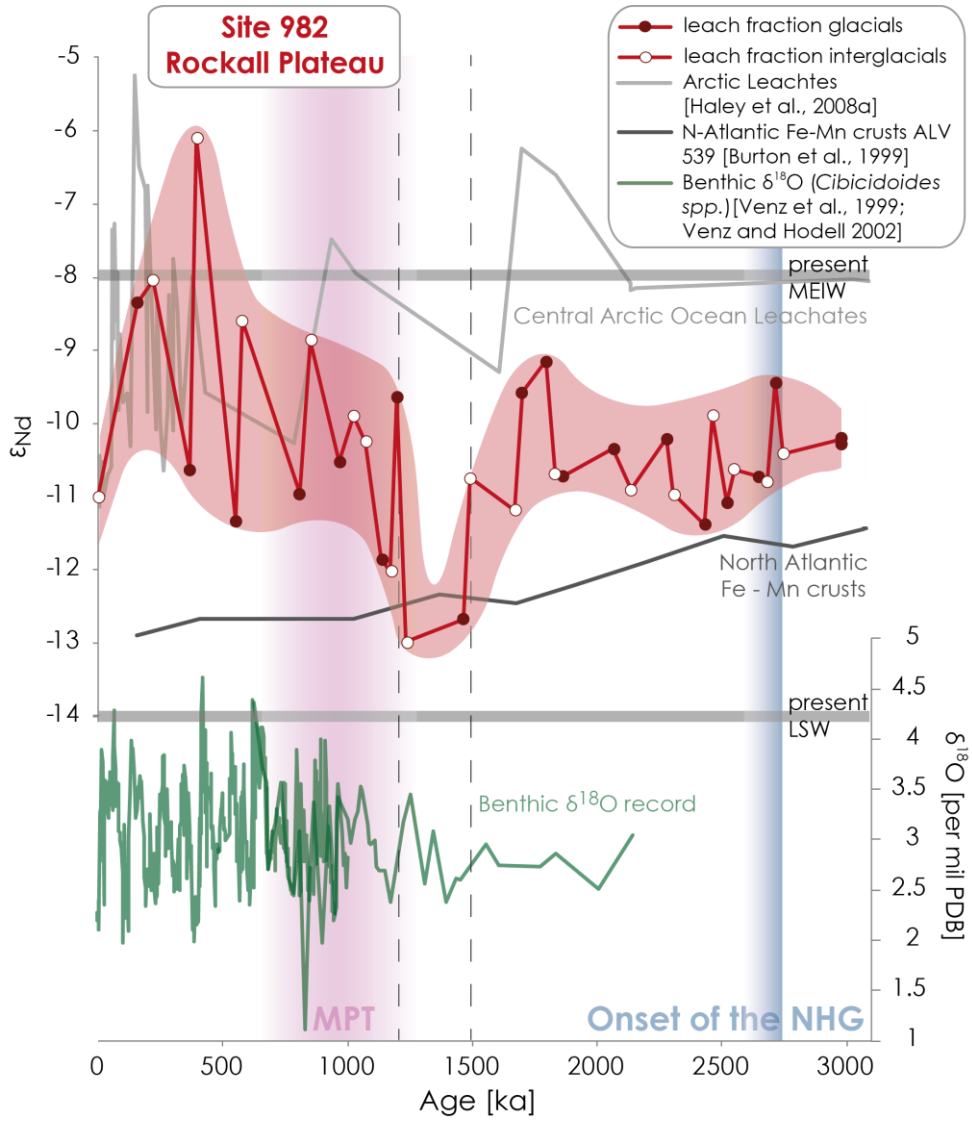

***Figure 4.8**: The Nd isotopic record (open dots = interglacial periods, filled dots = glacial periods) of Site 982 in comparison to the Arctic leach record (light grey line) [Haley et al., 2008a] and the North Atlantic Fe-Mn crust (dark grey line) [Burton et al., 1999]. The red shaded area mark the general evolution of the record with the increasing variability in the record after 1.2 Ma. The dark green line indicates the benthic $\delta^{18}O$ record of Cibicidoides wuellerstorfi and Cibicidoides kullenbergi [Venz et al., 1999, Venz and Hodell, 2002] of Site 982 over the past 2.2 Ma. Displayed as well: dashed line = separation of the record into different periods; the colored shadings = the onset of the Northern Hemisphere Glaciation (2.7 Ma) and the Mid Pleistocene Transition.*

At that time, the ice-covered and stagnant Nordic Seas produced no overflow into the North Atlantic Ocean and hence the North Atlantic Ocean was dominantly influenced by a sub-polar convection producing GNAIW from subpolar waters during glacial periods. The water masses produced were derived from North Atlantic surface waters carrying a less radiogenic Nd isotope signature around -13 [*Crocket et al.*, 2011].

The location of Site 982 has been influenced by alternations between these different water masses, but the highly radiogenic excursion at 0.4 Ma can only be explained by an additional radiogenic source, i.e. enhanced influence from Iceland or an additional basaltic source. The peak radiogenic Nd signal was most likely supplied by direct erosional input or by highly radiogenic waters originating from boundary exchange with the basaltic material of Iceland or the Mid Atlantic ridge [*Lacan and Jeandel*, 2004a, 2005a].

Similar to the Nd isotope record, the Pb isotope composition of Site 982 has shown a slight trend towards more radiogenic signatures over the past 1.5 Ma reflecting the increase in the glacial input from a continental source. Due to the large distance from land and the very local influence of the Pb isotope signal, Site 982 can only have been influenced by erosional inputs to a very small extent. This is supported by the very low variability of the $^{206}Pb/^{204}Pb$ ratio, especially prior to 1.5 Ma.

In the older part of the core prior to 1.5 Ma, the less variable Nd record indicates mixing between the Central Arctic Ocean [*Haley et al.*, 2008a] and Atlantic Nd records [*Burton et al.*, 1999] (Fig. 4.8) with a better coincidence with the Atlantic Ocean record, which increases significantly in the period between 1.5 to 1.2 Ma, pointing to a strong enhancement of the Atlantic inflow. Similar to Site 986, the Atlantic influence decreases and the influence of waters derived from the Arctic strongly increased after the beginning of the MPT. This change can be explained by the enhanced overflow from the intermediate waters from the Nordic Seas since the onset of NHG.

4.4.4. History of water mass exchange and erosional input in the Nordic Seas and North Atlantic Ocean based on Nd and Pb isotopes – A synthesis of all sites

Comparing the Nordic Seas and North Atlantic Ocean sites (Fig. 4.9) we observe that the amplitude of the variability in the Nd isotopic records decreases the more to the

north the sites are located, i.e. Site 982 on the Rockall Plateau reveals a variability of almost 7 ε_{Nd} units over the past 3 Ma, whereas Site 644 shows 5.1 ε_{Nd} units and Site 986 on the Svalbard margin shows 3.3 ε_{Nd} units. This has most likely been a the result of the increasing influence of different water masses in the North Atlantic Ocean on the one hand and the dominant erosional input from Svalbard on the Svalbard margin (Site 986) on the other. Furthermore, the predominant water mass at Site 986 over the past 3 Myr has been the NSDW, whereas the erosional input has been the dominant process suppressing major changes in the Nd isotope record. Besides erosional input from Scandinavia, Site 644 has been influenced by NSDW as well as AIW, the ε_{Nd} signatures of which have mainly ranged between -11 and -7 over the past 3 Ma [*Haley et al.*, 2008a]. In contrast, Site 982 has been influenced by LSW, the overflow water from the Nordic Seas, and MOW, which have been characterized by markedly different isotopic signatures ranging between -14 for LSW and -8 for the overflow water. In addition, erosional inputs which have been strongly influenced by Icelandic basalt carrying a very radiogenic signature, have to be taken into account from 1.5 Ma onwards due to the increased glaciation enhancing the erosional input, which is expressed in the increased variability in the Nd isotope record since this period of time (Fig. 4.8).

Despite the large variability of each record comparison between the sites provides important information on the paleoenvironmental evolution of the study area. Prior to the INHG at 2.7 Ma the Nd isotope composition of the water masses showed similar values, supporting the warmer climatic conditions at that time. The data suggest that water mass exchange was very efficient, as for example also indicated by benthic carbon isotope records [e.g. *Raymo et al.*, 1992; *Ravelo and Andreasen*, 2000]. At the same time the erosional input did not vary significantly, most likely due to the limited extent of glaciation at that time. Between 2.7 and 2.2 Ma, Site 982 and 986 show a similar isotopic range and a low variability indicating a homogenous water mass exchange and a limited glacial input at Site 982 and a relative continuous erosional input at Site 986. In contrast, Site 644 shows a significant different isotopic range, which is attributed to the enhanced erosional input from a more radiogenic source, e.g. the Eurasian shelf, which has no influence on the Rockall Plateau (Site 982) due to the larger distance or on the Svalbard margin, which is predominantly influence from Svalbard at that period.

The period between 2.2 Ma and 1.5 Ma (Fig. 4.9) was again characterized by a somewhat warmer climate supported by a reduced glacial IRD input on the Vøring Plateau [*Fronval et al.*, 1996] and light $\delta^{18}O$ values [*Jansen et al.*, 1989]. For Site 644, *Henrich and Baumann* [1994] described that period as dominated by long-term persistent moderate glacial conditions and a long-term stability of relatively small ice sheets on Scandinavia. This observation is supported by the relatively good agreement of all records in this period of time. The low to moderate intensity of the glaciation led to a decreasing influence of the erosional input and led to a more efficient water mass exchange between the Nordic Seas and the Northern Atlantic Ocean. These features indicate an enhanced influence of inflowing warm Atlantic waters.

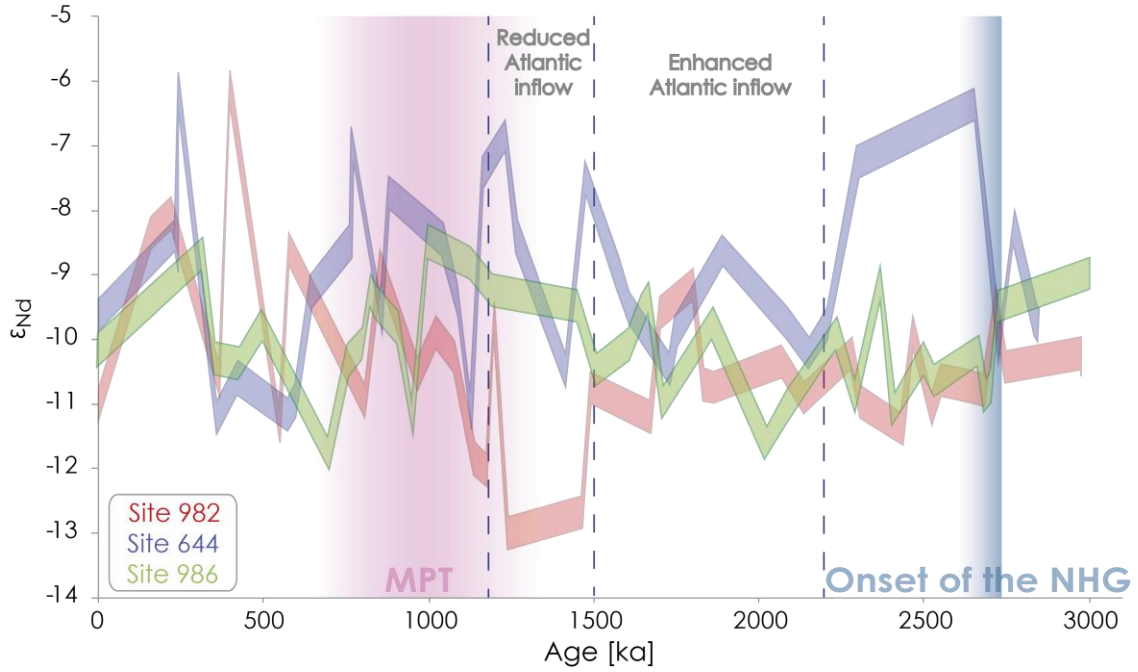

***Figure 4.9**: **The Nd isotopic record of the ODP sites in the Nordic Seas (Site 986 = green curve; Site 644 = blue curve) and in the Atlantic Ocean (Site 982 = red curve)**. The ranges show the 2σ error of each record over the past 3 Ma. The blue shaded area indicates the onset of the Northern Hemisphere Glaciation; the purple shaded area marks the Mid Pleistocene Transition. The significant area between 2.2 and 1.5 Ma is characterized by a decreased variability pointing to an enhanced Atlantic inflow, whereas the period 1.5 to 1.2 Ma was characterized by a decreased inflow.*

The phase from 1.5 to 1.2 Ma was again dominated by a reduced Atlantic inflow into the Nordic Seas [*Jansen et al.,* 1989, 1991] (Fig. 4.9), which had different consequences at each site. Site 986 was characterized by highly radiogenic values at that time, which was most likely caused by the increasing influence of the Arctic Ocean that carried a relatively radiogenic Nd isotope signature at that time [*Haley et al.,* 2008a]. The water mass signature behaved similarly at Site 644, where it was the reduced Atlantic inflow that led to a higher variability, as well as relatively radiogenic Nd isotope signatures. In contrast, at Site 982 the Nd isotope record reveals highly unradiogenic values, which were most likely caused by the absence of overflow waters from the Nordic Seas and the dominant influence of GNAIW produced in the North Atlantic [*Boyle and Keigwin*, 1987; *Oppo and Fairbanks*, 1987] as well as a decreased erosional input prior to 1.2 Ma. After 1.0 Ma we find a very strong Nd isotope variability at all three sites caused by the strongly increased glacial/interglacial contrasts of ocean circulation patterns and erosional inputs, then following the major 100 kyrs frequency of climate variability. The low resolution of our records and uncertainties of the age models preclude more detailed interpretations on changes of the prevailing water mass exchange mechanisms or intensified erosional inputs.

Compared to the Nd isotope evolution of the water masses, the $^{206}Pb/^{204}Pb$ record of the different sites shows a shift to an enhanced variability after 2.7 Ma as a consequence of the increasing intensity of glaciation in the Northern Hemisphere, similar to Site 911. The first site showing the evidence for an increasing amplitude of the variability and overall more radiogenic $^{206}Pb/^{204}Pb$ ratios as a consequence of an enhanced glacial and a deglacial incongruent weathering process is Site 986 on the Svalbard shelf. This early change occurred at 2.5 Ma, which is supported by frequent IRD pulses and maximum illite contents at 2.5 Ma reflecting increased glacial erosion [*Knies et al.,* 2009] afterwards the ratio decreased and showed a further increase since 2.1. Ma. At Site 644 the shift to an increased variability occurred at 2.2 Ma during a period of widespread and enhanced glaciations [*Schackelton et al.*, 1984], followed by a period of moderate IRD input due to relatively small glacial episodes in a somewhat warmer climate [*Fronval et al.,* 1996], which is supported by lower variability in the Pb isotope record from the Vøring Plateau after 1.7 Ma. At Site 982 we do not find evidence for an increasing influence of glaciation until 1.2 Ma, which is when

increasing variability and a first shift in the Pb isotope record to more radiogenic values due to enhanced incongruent weathering occurred. The Pb isotope record of all sites in the Nordic Seas and North Atlantic Ocean during last 1.2 Ma is characterized by a strong variability due to strong enhanced glaciations increasing the erosional input at all sites.

4.4.5. Evolution of sediment source provenance and transport pathways in the Nordic Seas and North Atlantic Ocean based on Nd and Pb isotopes of the detrital fraction of the sediments

The Nd, Sr and Pb isotope composition of the detrital fraction of the bulk sediment is commonly used to trace different sediment sources and transport mechanisms. The Nd isotope composition of the sediments deliver reliable signatures of the surrounding rocks, because it is not fractionated by weathering effects especially during glaciations and can therefore be used to trace the sediment origin. In the case of the isotope composition of Pb and Sr the conclusions concerning the sediment origin has to be drawn carefully, because the isotopic signal of Pb and Sr changes with the grain size especially during strong glaciations and deglacial periods. The reconstruction of the seawater derived signal the clay fraction is most efficient due to the slow sinking speed and longer residence time [*Frank et al.,* 2002]. In contrast to that, the reconstruction of the sediment source provenance is most reliable on the basis of a larger grain size fraction of sediments from surrounding rocks [*Innocent et al.*, 2000]. In detail, the Sr isotope composition becomes more radiogenic with decreasing grain size [*Tütken et al.*, 2002] and the Pb isotopes are fractionated during the glaciations due to the incongruent weathering, causing stronger mobilization of the radiogenic isotopes (^{206}Pb, ^{207}Pb and ^{208}Pb) than of the unradiogenic ^{204}Pb [*Erel et al.*, 1994, *von Blanckenburg and Nägler*, 2001].

The Nd isotope signature of the detrital fraction of the sediments of northernmost Site 986 plots on an apparent mixing line between Svalbard and the Eurasian shelf sediments, which are in turn predominantly influenced from weathering products of the Siberian Flood basalts and rocks from the Siberian hinterland. The dominant source has been weathering of Svalbard rocks revealing a similar Nd isotope composition between -10 and -21 [*Peucat et al.,* 1989; *Johansson and Gee,* 1999;

Tütken et al., 2002]. The other sediment sources transported to the Svalbard margin via sea ice and ice sheets have been the Barents Sea and Eurasian shelf (Fig. 4.10) sediments [*Tütken et al.*, 2002; *Knies et al.*, 2009] which mainly consist of weathered rocks mainly delivered as fluvial suspended particulate matter by the big Siberian rivers, e.g. Yenisei and Ob.

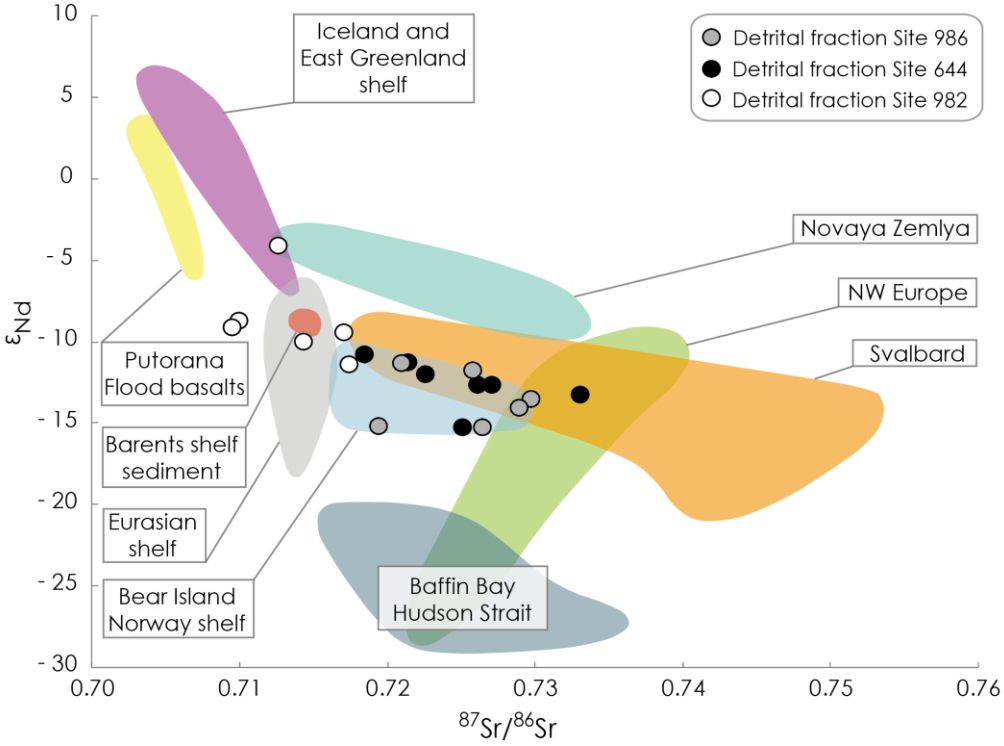

Figure 4.10: Comparison of the Nd and Sr isotopic composition of the detrital sediment fraction of Site 986 (grey dots), Site 644 (black dots) and Site 982 (open dots) with possible sediment sources*. Colored arrays display areas as follows: yellow = Norilsk/Putorana Flood Basalts [Sharma et al., 1992], turquoise = Novaya Zemlya [Tütken et al., 2002], orange = Svalbard bedrocks [Peucat et al., 1989; Johansson & Gee, 1999], purple = Iceland and the East Greenland Shelf (basaltic), light grey = Eurasian shelf [Farmer et al., 2003], red = Barents Sea shelf sediments [Tütken et al., 2002], light blue = sediments from Bear Island and Norwegian shelf [Farmer et al., 2003], grey blue = Baffin Bay/Hudson Strait [Farmer et al., 2003] and green = NW Europe including British Isles, Scandinavia and the Norwegian Sea [Farmer et al., 2003].*

The isotopic composition of the bulk sediments on the Svalbard margin at Site 986 are produced by a mixture of Barents Sea sediments carrying an ε_{Nd} value of -9.4 and -8.3 and $^{87}Sr/^{86}Sr$ ratios between 0.713129 and 0.714894 [*Tütken et al.*, 2002] and the less radiogenic ε_{Nd} values of Svalbard. This assumption is partly supported by the Pb isotope composition of the bulk sediment displayed in a $^{207,208}Pb/^{204}Pb$ vs. $^{206}Pb/^{204}Pb$ plot (Fig. 4.11a), which is in good agreement with sediments from the Norwegian shelf and Central Arctic Ocean [*Winter et al.*, 1997], as well as bulk rocks from Scandinavia and Iceland, while the bedrocks from Svalbard reveal less radiogenic Pb values. Furthermore, the Pb isotope composition of the leachates and sediments from the Svalbard margin also coincides with sediments [*Winter et al.*, 1997] and leachates [*Haley et al.*, 2008b] from the Central Arctic Ocean, which have likewise mainly been supplied by weathering of rocks from Siberia.

Compared to Site 986, Site 644 shows very similar Nd isotopic signatures, whose radiogenic endmember has most likely been the result of the supply of sediments from the Barents Sea shelf transported via icebergs and sea ice during glaciations, as well as of basaltic material from Iceland carried by the northward flowing currents or transported in the form of ash. The unradiogenic endmember for the Vøring Plateau sediments has mainly been the Norwegian shelf, dominantly influenced by the weathered of unradiogenic rocks from the Paleoproterozoic crust underlying the Fennoscandian Ice sheet or its reworked Caledonian equivalent at the western margin of the Baltic Shield [*Farmer et al.*, 2003] (Fig. 4.10), dominantly supplied by glacial erosion. In the case of this site, the Pb isotope signatures show a good agreement with the ε_{Nd} vs. $^{87}Sr/^{86}Sr$ results. The leach results as well as the bulk sediment are overlapping with signatures of sediments from the Norwegian shelf and the bulk rocks from Iceland [*Farmer et al.*, 2003] (Fig. 4.11b).

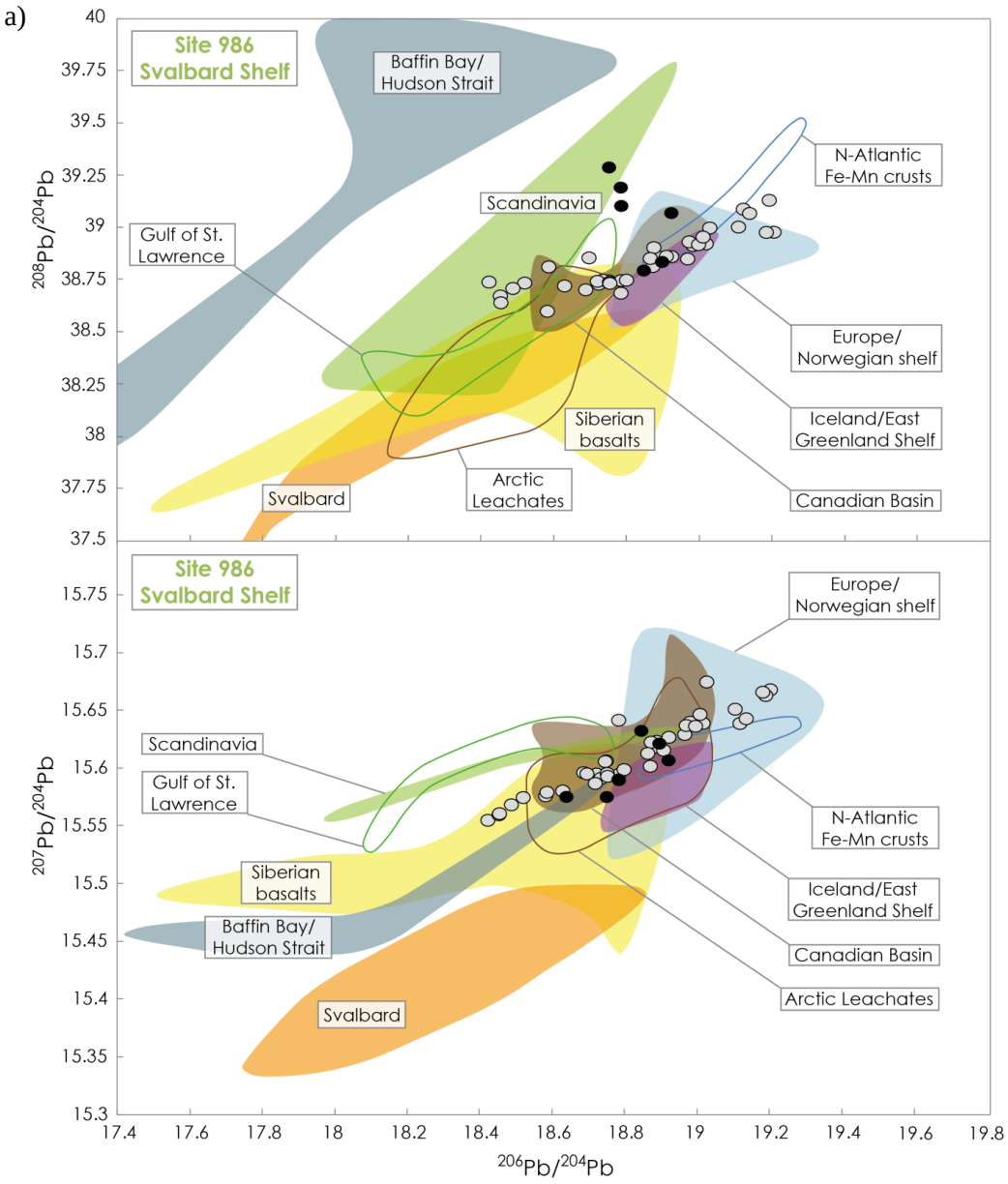

***Figure 4.11**: Radiogenic Pb isotope comparison of leachates (grey dots) and detrital sediment (black dots) of a) Site 986, b) Site 644, c) Site 982 and possible sources. The orange area presents the bedrocks of Svalbard [Ionov et al., 2002]; yellow = Siberian basalts [Sharma et al., 1992], dark blue = Baffin Bay/Hudson Strait [Farmer et al., 2003], light blue = Europe/Norwegian shelf sediments [Fagel et al., 2002], green = Scandinavian bedrocks [Farmer et al., 2003], green framed = Gulf of St. Lawrence [Farmer et al., 2003], brown = bulk sediments from Central Arctic Ocean/Canadian basin [Winter et al., 1997], brown framed = leachates from the Central Arctic Ocean [Haley et al., 2008b], purple = basaltic rocks from Iceland/East Greenland shelf [Farmer et al., 2003], blue framed = North Atlantic ferromanganese crusts (BM1959.05 and ALV539) [Reynolds et al., 1999].*

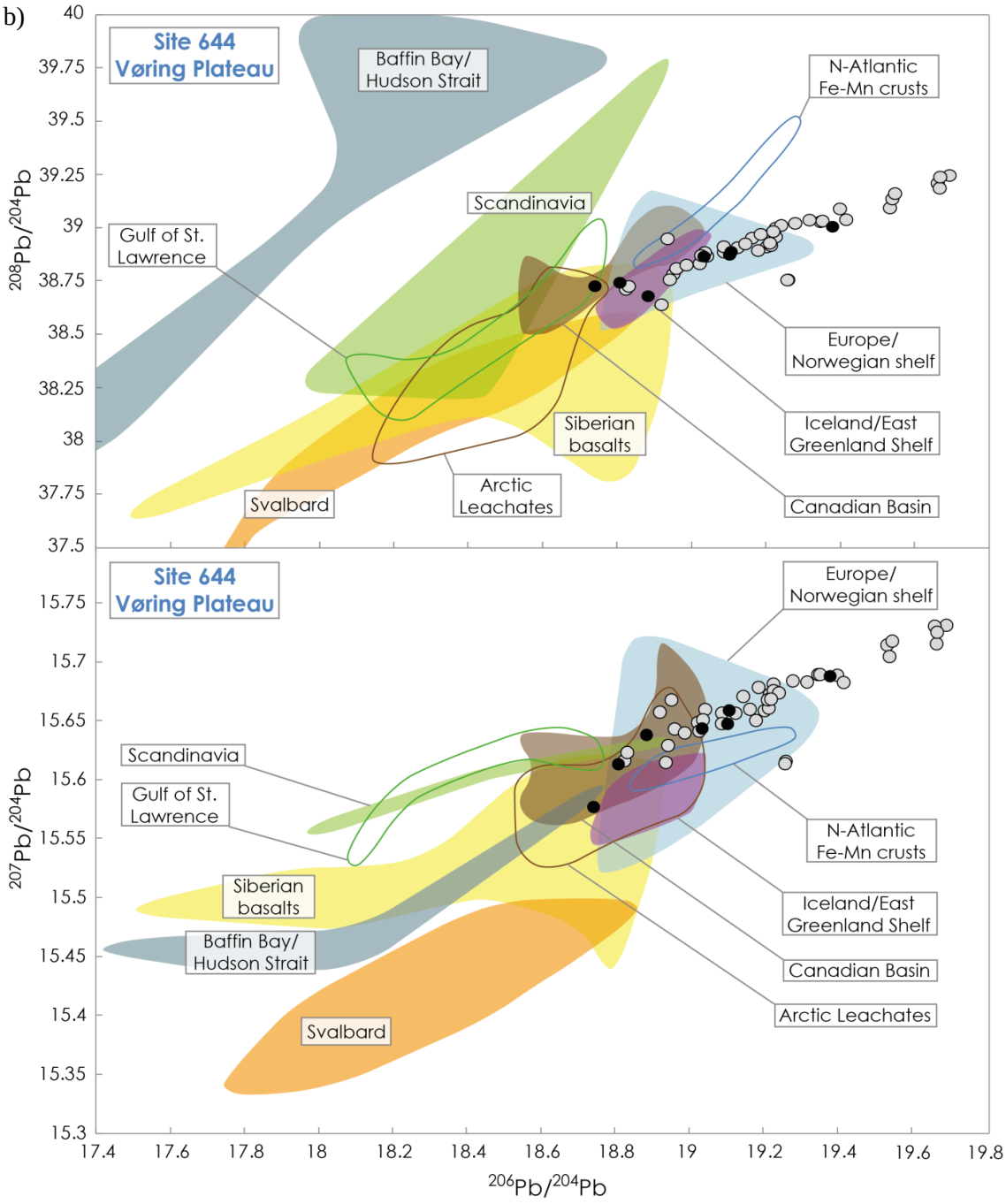
b)
Site 644
Vøring Plateau
Baffin Bay/
Hudson Strait
N-Atlantic
Fe-Mn crusts
Scandinavia
Gulf of St.
Lawrence
Europe/
Norwegian shelf
Siberian
basalts
Iceland/East
Greenland Shelf
Arctic
Leachates
Svalbard
Canadian Basin
$^{208}Pb/^{204}Pb$
$^{207}Pb/^{204}Pb$
$^{206}Pb/^{204}Pb$

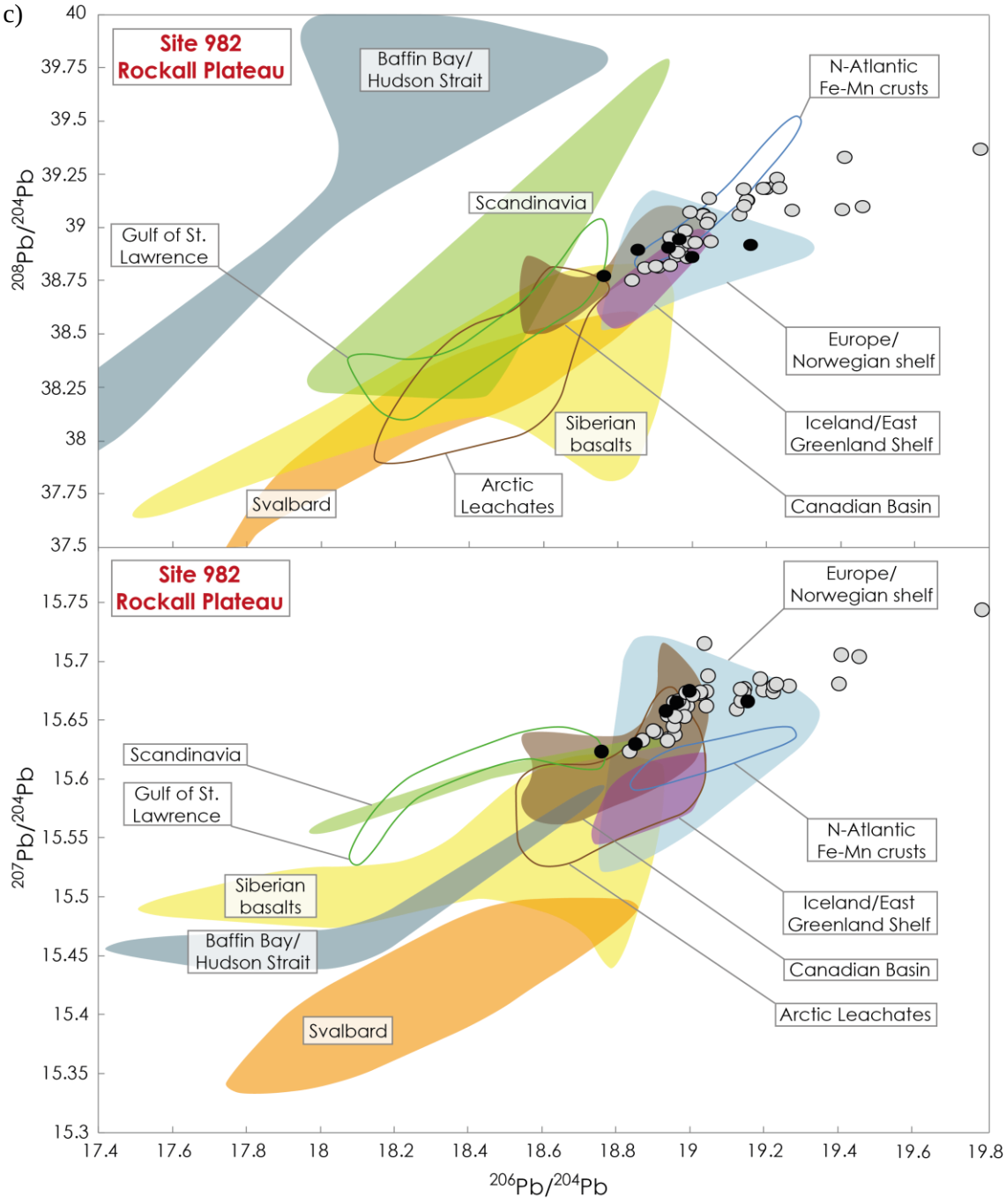

Site 982 is significantly different from the sites located in the Nordic Seas with a less radiogenic $^{87}Sr/^{86}Sr$ ratio and more radiogenic Nd isotope signatures. The erosional input of the radiogenic endmember for Site 982 was dominated by sources in Iceland and on the East Greenland shelf, which may partly have been transported by the overflow currents from the Nordic Seas. The unradiogenic endmember was most likely continental rocks from NW Europe (Fig. 4.10), which were supplied by rafting icebergs

during extensive glaciations. This supports the hypothesis of *Venz et al.* [1999], who indicated that Greenland and Iceland, besides Scandinavia and Barents/Kara Sea, have been the dominant supply areas of the IRD to the Vøring Plateau.

The $^{207,208}Pb/^{204}Pb$ vs. $^{206}Pb/^{204}Pb$ plot (Fig. 4.11c) of Site 982 leads to a similar assumption as for the other sites due to a similar agreement of its detrital signatures with sediment sources such as the Norwegian shelf and Iceland [*Farmer et al.,* 2003] and additionally the coincidence with the Central Arctic Ocean sediments [*Winter et al.*, 1997] and leachates [*Haley et al.,* 2008b]. The $^{206}Pb/^{204}Pb$ ratios of seawater extracted from the ferromanganese coatings of the sediment at the different sites apparently plot on a mixing line near the unradiogenic endmember. However, the radiogenic endmember of the seawater signatures could not be defined for all sites due to fractionation during incongruent weathering and the consequent preferential mobilization of ^{206}Pb. This strongly suggests that the apparent unradiogenic endmember was also modified by incongruent weathering.

4.5. CONCLUSION

Seawater Nd and Pb isotope signatures obtained from leached ferromanganese coatings of core top and down core bulk sediments, as well as from the corresponding detrital fractions of samples from the Nordic Seas and North Atlantic Ocean were analyzed in this study. The main goal was to reconstruct the long term evolution of water mass mixing and erosional input over the past 3 Ma with a focus on the NHG and MPT. The investigated sites on the Svalbard margin (Site 986), Vøring Plateau (Site 644) and Rockall Plateau (Site 982) reveal a strong local influence of the different water masses as well as of erosional inputs, which has the consequence that every site had to be considered separately at first. The northern sites 986 and 644 have been predominantly influenced by NSDW during the last 3 Myrs, whereas Site 982 in the North Atlantic Ocean has been influenced by the overflow water from the Nordic Seas (MEIW, AIW) and by LSW from the south.

The strong influence of the erosional input on the sites in the Nordic Seas complicates clear statements about the evolution of the Atlantic inflow into the Nordic Seas. But to some extent comparison of the Nd isotope records of all three sites make

some periods identifiable with an enhanced influence of the Atlantic inflow, i.e. between 2.2 and 1.5 Ma, where the variability of the records is relatively low and the Nd isotope compositions in the study area were relatively homogenous, similar to the present day conditions. A period with a reduced Atlantic inflow is recognizable at the early MPT between 1.5 and 1.2 Ma, which had different consequences on each site. Sites 986 and 644 showed more radiogenic ε_{Nd} values due to the increased influence from the Arctic Ocean and the Barents Sea ice sheet, whereas Site 982 was dominated by GNAIW, due to the absence of overflow waters from the Nordic Seas. Similar to Site 911, the Pb isotope composition of the leachates showed a shifted onset of the erosional input by the increased radiogenic values at the different sites. First the northernmost site on the Svalbard margin shows evidence for the increasing intensity of glaciation, then the Vøring Plateau site followed at 2.2 Ma and at last Site 982 on the Rockall Plateau shows the influence of enhanced glaciation at 1.2 Ma.

During the increasing intensity of glaciation of the Northern Hemisphere since 2.7 Ma the importance of the glacial erosional input for the detrital sediment composition has increased. The dominant sediment supply area on the Svalbard shelf at Site 986, besides Svalbard, has been the Barents Sea and Kara shelves releasing more radiogenic material. The detrital fraction of Site 644 points to Scandinavia as the dominant sediment source but sediments from the Barents Sea transported via icebergs and sea ice during glaciations and/or basaltic material from Iceland carried by the northward flowing currents or via ash also played a role. Site 982 in the North Atlantic has been influenced least by changes of the erosional inputs due to the larger distance to land, but from 1.2 Ma onwards the erosional input has been dominated by sediments from Greenland and Iceland. This study shows that the water mass exchange as well as sediment transport processes in the Nordic Seas and North Atlantic Ocean are strongly influenced by local sedimentary processes and exchange with these sediments, which makes it difficult to reconstruct changes of the inflowing Atlantic water masses and their mixing.

CHAPTER 5

Summary and outlook

5.1. General conclusions

One main goal of this study is to reconstruct the variability of water mass exchange and circulation patterns between the northernmost Atlantic Ocean, the Nordic Seas, and the Arctic Ocean and its link to northern hemisphere climate. In particular, this study aims at an improved understanding of the major climate changes during the past 5 Myrs, i.e., the Northern Hemisphere Glaciation and the Mid Pleistocene Transition. To achieve this goal, the seawater-derived Nd isotope compositions stored in authigenic ferromanganese oxyhydroxide coatings of the sediment particles, were analyzed. These data are complemented by Nd and Pb isotope compositions of bulk sediment at four sites in the Nordic Seas and in the North Atlantic Ocean in order to reconstruct changes in sediment provenance and transport mechanism. In addition, two sediment cores near Iceland served to test the reliability of different sediment leaching methods and the reliable extraction of deep water Nd isotope signatures from foraminiferal calcite.

The verification of different leaching methods to extract seawater radiogenic isotope ratios from ferromanganese oxyhydroxide coatings on sediment particles on six sediment cores in the Nordic Seas and North Atlantic Ocean is one of the main objectives of this study. A sediment leaching method established by *Gutjahr et al.* [2007] was tested extensively and, where necessary, modified for the different locations of the sediment core. Seawater-derived Nd isotope compositions extracted from core top sediments were compared to the present-day bottom water Nd isotope compositions, where available [*Lacan and Jeandel,* 2004b, *Andersson et al.*, 2008]. The ε_{Nd} data of core top samples close to Iceland (Sites 907 and 984) were significantly more radiogenic than modern ε_{Nd} signatures of the predominant intermediate waters [*Lacan and Jeandel,* 2004b], most likely due to contamination with Nd originating from partial dissolution of volcanic ashes. In addition, calcite tests of cleaned and uncleanded foraminifers were analyzed in order to obtain a more reliable seawater-derived Nd isotope composition. While ε_{Nd} signatures extracted from the foraminiferal calcite of

Site 984 south of Iceland are still more radiogenic than present day seawater, the Nd isotope composition of the foraminiferal tests in the core top sample of Site 907 agrees well with present-day seawater ε_{Nd}. However, given that the subsurface sediments of Site 907 are essentially barren of foraminifera tests this method could not be used for further paleoreconstructions. The leaching tests performed at the sites located in the area of Atlantic Water inflow (Site 982, 644, 986 and 911) reflect modern-day seawater signatures. A small offset was only observed between two different modifications of the bulk sediment leaching method. When carbonate was removed prior to the treatment of the sample with the hydroxylamine leach solution systematically more radiogenic ε_{Nd} values than for samples without a carbonate removal step were obtained. Core sites with the highest carbonate content, e.g., Site 982 on the Rockall Plateau in the North Atlantic show the smallest offset between the different leach methods. The offset between the different leach methods most probably originates from a labile less radiogenic phase being removed while dissolving the carbonate. The low offset in Site 982 between the different leach methods could also be caused by the incomplete removal of the carbonates prior to the leaching treatment.

For the reconstruction of changes of the water mass circulation and exchange between the Nordic Seas and North Atlantic Ocean four sites in the influence area of the Atlantic inflow water (Site 911, 986, 644 and 982) were chosen, based on the results of the different successful leaching tests. Due to low carbonate content, the bulk sediment of the northernmost Site 911 located on the Yermak Plateau in the Fram Strait was directly treated with the hydroxylamine leach solution without a preceding carbonate removal step as previously applied by *Haley et al.* [2008a, 2008b] for Arctic Ocean sediments. In Chapter 3 (Site 911) the Nd and Pb isotope record of past seawater and of the supply of the detrital fraction is discussed in order to elucidate both past changes in deep water exchange between the North Atlantic and the Arctic Ocean in sources of sediment input and sediment transport mechanisms over the past 5.2 Ma. The Nd isotope record of the leached sediment fraction was mainly influenced by modified Atlantic water from the Nordic Seas while a trend to less radiogenic values similar to Nd isotope records measured in the Arctic Ocean [*Haley et al.*, 2008a] or the North Atlantic Ocean [*Reynolds et al.*, 1999] could not be identified, which suggests that the

influence of Arctic waters on the Yermak Plateau have been outcompeted by the prevailing admixture of warm Atlantic water from the Nordic Seas. Furthermore, the trend in the North Atlantic ferromanganese crusts where caused by changes in the sediment provenances and supply in the Baffin Bay/Labrador Sea and is from minor importance from the Yermak Plateau, because the waters originating in the Labrador Sea only constituted a minor fraction of the northward flowing branch of Labrador Sea water [*Lacan & Jeandel*, 2004c].

Two periods of time revealing distinctly different conditions were identified in the Nd isotope record of Site 911. Prior to the onset of the Northern Hemisphere Glaciation at 2.7 Ma the Nordic Seas, in particular the Yermak Plateau was characterized by relatively stable conditions of the deep circulation dominated by constant inflow of warm Atlantic waters and invariant sediment supply, mainly originating from Svalbard and the Arctic Ocean. Similarly, the deep water Nd isotope compositions at the investigated sites on the Svalbard margin (Site 986), Vøring Plateau (Site 644), and Rockall Plateau (Site 982) showed no significant ε_{Nd} variations prior to 2.7 Ma. Influence of local water mass changes (e.g., brine formation at the Svalbard continental margin), as well as of erosional inputs complicate the interpretation of the ε_{Nd} signatures with regard to the evolution of the Atlantic inflow into the Nordic Seas. Similar to Site 911 from the Yermak Plateau, the low variability in the Nd isotope records from all three sites in the Nordic Seas and northernmost Atlantic Ocean point to warm climate conditions, an efficient water mass exchange, and low glacial weathering inputs due to the limited extent of continental glaciation prior to 2.7 Ma.

After the onset of Northern Hemisphere Glaciation higher amplitude ε_{Nd} variability of the leach record, as well as of the detrital sediment fraction at Site 911 reveal a change of the environmental conditions in the Nordic Seas and the Arctic Ocean related to the cooling and accompanying waxing and waning of the ice sheets on the Eurasian shelves. During glacial periods, the Nd isotope signatures at Site 911 were dominantly characterized by more radiogenic ε_{Nd} signatures of deep waters. This was caused by either a stronger influence of Arctic waters due to the reduction of the Atlantic Water inflow or by increased release of ice-rafted material with more radiogenic signatures transported by sea ice from the Arctic Ocean across the Fram Strait via the Transpolar Drift.

After 2.7 Ma the other sites in the Nordic Seas and North Atlantic Ocean revealed several distinct periods with different climatic conditions. Between 2.7 and 2.2 Ma the Nd isotope compositions between all sites differed significantly, in particular the record of Vøring Plateau (Site 644) reveals more radiogenic ε_{Nd} values, most likely due to increased glacial input from a radiogenic source (e.g. Iceland or the Barents shelf). A low ε_{Nd} variability of in all records points to enhanced inflow of Atlantic Water between 2.2 and 1.5 Ma, similar to present-day conditions. In contrast, the beginning of the MPT (1.5 – 1.2 Ma) was characterized by a reduced Atlantic inflow, with different consequences at each site. The sites in the Nordic Seas show more radiogenic ε_{Nd} values indicating increased influence from the Arctic Ocean and possibly the Barents Sea ice sheet. In contrast, more radiogenic ε_{Nd} values at Site 982 are interpreted to represent increased inflow of GNAIW and the absence of overflow waters from the Nordic Seas. After 1.2 Ma sites 986, 644, and 982 reveal a very strong Nd isotope variability as a consequence of the strongly enhanced glacial/interglacial differences and its consequences for ocean circulation patterns and erosional inputs.

The Pb isotope composition of sediment leachates of all sites in the Nordic Seas indicates a different timing of the onset of the erosional input at the different sites from north to south and dependent of the distance to land. Increasingly radiogenic values at the Svalbard margin indicate the onset of glacial conditions already at 2.5 Ma. This is followed by the Vøring Plateau Site at 2.2 Ma and the Yermak Plateau at 2.0 Ma, the latter showing a low variability prior to 2.0 Ma and an enhanced amplitude of glacial/interglacial cyclicity thereafter, most likely caused by the increasing glacial weathering as a consequence of the waxing and waning of the ice sheets, as well as changes in sea-ice transport. Enhanced influence of glaciations at the southernmost Site 982 on the Rockall Plateau was only detected after 1.2 Ma.

The changes in the sediment provenance and transport mechanisms in the Nordic Seas and northernmost Atlantic Ocean were reconstructed by the Nd and Pb isotope composition of the detrital fraction of the bulk sediment for Sites 911, 986, 644, and 982. All studied sites in the Nordic Seas and Northern Atlantic Ocean reveal different ε_{Nd} signatures, with more radiogenic ε_{Nd}/less radiogenic $^{87}Sr/^{86}Sr$ values in the Northern Atlantic Ocean and less radiogenic ε_{Nd} in the Nordic Seas pointing to

significantly different source areas of the sediments. The data indicate that the Svalbard margin and Yermak Plateau were dominated by inputs from Svalbard, as well as from the Barents and Kara Sea. Additionally, for the Yermak Plateau the data show that Svalbard has been the dominant sediment source during interglacial periods while it was the Eurasian shelf during glacials. The Vøring Plateau has been dominated by sediment input from Scandinavia but also received supply from the Barents Sea via icebergs and sea ice during glaciations. In contrast, due to its distant location to land, the Rockall Plateau shows the lowest erosional influence. However, a shift to more radiogenic ε_{Nd} isotope compositions points to slightly enhanced erosional inputs from Iceland since 1.2 Ma.

In general, the circulation patterns between the Northern Atlantic Ocean, Nordic Seas and Arctic Ocean prior to the Northern Hemisphere Glaciation at 2.7 Ma were characterized by stable conditions due to a constant and warm climate. Thereafter, water mass exchange became more variable as a consequence of climatic changes, e.g. an increasing glacial/interglacial variability. Besides the changes in circulation patterns of water masses, the enhanced glaciations had a huge impact on the sedimentation regime. After the onset of the NHG new sediment provenance areas, such as the Eurasian or Barents Sea shelf played an increasing role. Probably, sediment transport by sea ice and icebergs allowed sediments to reach the sites in the Nordic Seas over large distances. Sites 911 and 986 near Svalbard were dominantly impacted by sediments from the Eurasian ice sheet during glacials, while the Fennoscandian ice sheet provided sediments to Site 644 on the Vøring Plateau. Since the beginning of the Mid Pleistocene Transition (1.2 Ma) the Nd and Pb isotope records of the sites in the Nordic Seas and North Atlantic Ocean were highly variable due to changes in volume and extent of the continental ice sheets and corresponding changes in erosional inputs. However, enhanced erosional input and the low resolution of the records make it difficult to draw firm conclusions concerning the potential control or consequences of changes in ocean circulation for the climate variability at this stage.

5.2. Outlook

This study aimed at reconstructing the long-term variations of the circulation patterns of deep and intermediate waters as well as changes in sediment regime over the

past 3 Ma in the northern North Atlantic. To fully understand the changes in the Nordic Seas and North Atlantic Ocean, especially after the onset of the Northern Hemisphere Glaciation and during the Mid Pleistocene Transition the resolution and age control of the different records needs to be increased and improved, respectively, in future studies. Higher-resolution records would especially facilitate more insight into the short-term variability of water mass exchanges and sediment transport during glacial/interglacial transitions or even shorter time scales. The increased resolution of the isotope records especially of the sites from the Svalbard margin, Vøring Plateau and Rockall Plateau will improve the comparison between different sediment cores used in this and previous studies. It would further allow a better statement about the glacial/interglacial variability in the Nordic Seas and North Atlantic Ocean and a detailed picture about the changes in the ocean circulation and glacial input. Additionally, the age models, especially of the northernmost sites near Svalbard, need to be improved in order to obtain a better comparability between the sites and also to be able to look into phase relationships between the different sites. Particularly valuable would be the extraction of past surface water signatures from the foraminiferal carbonates for those sites that contain sufficient amounts of carbonate.

The results of the accomplished sediment leach tests showed more radiogenic ε_{Nd} values in core top samples of Site 907 and 984 near Iceland than expected from the surrounding seawater of the present. The reason for this disagreement needs to be addressed and removed in further studies. In particular, it needs to be clarified whether volcanic material contaminates the Nd isotope signatures extracted from the core material. Additional water column data are also required in order to better constrain if the core top samples from these sites do indeed not agree with the present-day Nd isotope signature of the ambient seawater or if the water column profiles compiled from the literature for this study were taken from too large a distance to the ODP Sites.

The leach methods applied in this study should be further improved in order to obtain more details of the differences between the two leach methods. This could provide insights about the dissolution of the various phases during the leach procedure. Furthermore it should be verified why the offset between different methods correlates with the carbonate content.

References

Aagaard, K., J.H. Swift, and E.C. Carmack (1985), Thermohaline Circulation in the Arctic Mediterranean Seas, *J. Geophys. Res., 90*, 4833-4846, doi:10.1029/JC090iC03p04833.

Aagaard, K., and E.C. Carmack (1989), The role of sea ice and other fresh water in the Arctic circulation, *J. Geophys. Res., 94*, 14485-14498, doi:10.1029/JC094iC10p14485.

Abouchami, W., S.J.G. Galer, and A. Koschinski (1999), Pb and Nd isotopes in NE Atlantic Fe-Mn crusts: Proxies for trace metal paleosources and paleocean circulation, *Geochim. Cosmochim. Acta, 63*, 1489-1505, doi:10.1016/S0016-7037(99)00068.

Albarède, F., P. Telouk, J. Blichert-Toft, M. Boyet, A. Agranier, and B. Nelson (2004), Precise and accurate isotopic measurements using multiple-collector ICPMS, *Geochim. Cosmochim. Acta, 68*, 2725-2744, doi:10.1016/j.gca.2003.11.024.

Andersson, P., D. Porcelli, M. Frank, G. Björk, R. Dahlqvist, and Ö. Gustafsson (2008), Neodymium isotopes in seawater from the Barents Sea and Fram Strait Arctic-Atlantic gateways, *Geochim. Cosmochim. Acta, 72*, 2854-2867, doi:10.1016/j.gca.2008.04.008.

Arsouze, T., J.-C. Dutay, F. Lacan, and C. Jeandel (2009), Reconstructing the Nd oceanic cycle using a coupled dynamical-biogeochemical model, *Biogeosciences, 6*, 2829–2846, doi:10.5194/bg-6-2829-2009.

Barrat, J.A., F. Keller, and J. Amossé (1996), Determination of rare earth elements in sixteen silicate reference samples by ICP-MS after Tm addition and ion exchange separation, *Geostandards Newsletters, 20*, 133-139, doi:10.1111/j.1751-908X.1996.tb00177.

Bartoli, G., M. Sarnthein, M. Weinelt, H. Erlenkeuser, D. Garbe-Schönberg, and D. Lea (2005), Final closure of Panama and the onset of northern hemisphere glaciation, *Earth Planet. Sci. Lett., 237*, 33–44, doi:10.1016/j.epsl.2005.06.020, 2005.

Bauch, H.A., H. Erlenkeuser, R.F. Spielhagen, U. Struck, J. Matthiessen, J. Thiede, and J. Heinemeier (2001), A multiproxy reconstruction of the evolution of deep and surface waters in the subarctic Nordic seas over the last 30,000 yr, *Quat. Sci. Rev., 20*, 659-678, doi:10.1016/S0277-3791(00)00098-6.

Bayon, G., C.R. German, R.M. Boella, J.A. Milton, R.N. Taylor, and R.W. Nesbitt (2002), An improved method for extract in marine sediment fractions and its application to Sr and Nd isotopic analysis, *Chem. Geol., 187*, 179-199, doi:10.1016/S0009-2541(01)00416-8.

Bayon, G., C.R. German, K.W. Burton, R.W. Nesbitt, and N. Rogers (2004), Sedimentary Fe–Mn oxyhydroxides as paleoceanographic archives and the role of aeolian flux in regulating oceanic dissolved REE, *Earth Planet. Sci. Lett., 224*, 477– 492, doi:10.1016/j.epsl.2004.05.033.

Berger, A., X.S. Li, and M.F. Loutre (1999), Modeling northern hemisphere ice volume over the last 3 Ma. *Quat. Sci. Rev., 18*, 1–11, doi:10.1016/S0277-3791(98)00033.

Bernstein, S., P.B. Kelemen, C. Tegner, M.D. Kurz, J. Blusztajn, and C.K. Brooks (1998), Post-breakup basaltic magmatism along the East Greenland Tertiary rifted margin. *Earth Planet. Sci. Lett. 160*, 845–862, doi:10.1016/S0012-821X(98)00132-0.

Bischof, J.F. (1994), The decay of the Barents ice sheet as documented in Nordic Seas ice-rafted debris, *Mar. Geol., 117*, 32-55, doi:10.1016/0025-3227(94)90005-1

Bischof, J.F., and D.A. Darby (1997), Mid- to Late Pleistocene Ice Drift in the Western Arctic Ocean: Evidence for a Different Circulation in the Past, *Science, 277*, 74 -78, doi: 10.1126/science.277.5322.74.

Bleil, U. (1989) Magnetostratigraphy of Neogene and Quaternary sediment series from the Norwegian Sea, In: O. Eldholm, J. Thiede and E. Taylor et al., *Proc. ODP, Sci. Res., 104*, 829-901, Ocean Drilling Program, College Station, TX.

Boyle, E. A. (1981), Cadmium, Zinc, Copper, and Barium in Foraminifera Tests. *Earth Planet. Sci. Lett., 53*, 11-35. doi:10.1016/0012-821x(81)90022-4.

Boyle, E.A., and L.D. Keigwin, (1985), Comparison of Atlantic and Pacific paleochemical records for the last 215,000 years: changes in deep ocean circulation and chemical inventories. *Earth Planet. Sci. Lett, 76*, 135-150, doi:10.1016/0012-821X(85)90154-2

Boyle, E. A., and L. D. Keigwin (1987), North Atlantic thermohaline circulation during the past 20,000 years linked to high-latitude surface temperature, *Nature, 330*, 35-40, doi:10.1038/330035a0.

Boyle, E. A. (1988), Vertical oceanic nutrient fractionation and glacial/interglacial CO_2 cycles *Nature, 331*, 55-56, doi:10.1038/331055a0.

Brinkhuis, H., S. Schouten, M.E. Collinson, A. Sluijs, J.S.S. Damsté, G.R. Dickens, M. Huber, T.M. Cronin, J. Onodera, K. Takahashi, J.P. Bujak, R. Stein, J. van der Burgh, J.S. Eldrett, I.C. Harding, A.F. Lotter, J. Backman, K. Moran, and the Expedition 302 Scientists (2006), Episodic fresh surface waters in the Eocene Arctic Ocean. *Nature, 441*, 606–609, doi:10.1038/nature04692.

Broecker W. S., and T.-H. Peng (1982), Tracers in the Sea, Lamont-Doherty Geol. Obs., Palisades, NY.

Broecker, W.S., C. Rooth, and T.-H. Peng (1985), Ventilation of the deep Northeast Atlantic. *J. Geophys. Res.*, 90, 6940–6944, doi:10.1029/JC090iC04p06940.

Broecker, W. S., and T. -H. Peng (1989), The cause of the glacial to interglacial atmospheric CO_2 change: A polar alkalinity hypothesis, *Global Biogeochem. Cycles, 3*, 215-239, doi:10.1029/GB003i003p00215.

Budéus, G., W. Schneider, and G. Krause (1998), Winter convective events and bottom water warming in the Greenland Sea. *J. Geophys. Res. – Oceans*, 103, 18513–18527, doi: 10.1029/98JC01563.

Burton, K.W., D.-C. Lee, J.N. Christensen, A.N. Halliday, and J.R. Hein (1999), Actual timing of neodymium isotopic variations recorded by Fe–Mn crusts in the western North Atlantic, *Earth Planet. Sci. Lett.*, *171*, 149-156, doi:10.1016/S0012-821X(99)00138-7.

Butt, F.A., A. Elverhoi, A. Solheim, and C.F. Forsberg (2000), Deciphering Late Cenozoic development of the western Svalbard Margin from ODP Site 986 results, *Mar. Geol. 169*, 373−390, doi:10.1016/S0025-3227(00)00088-8.

Cande, S.C., and D.V. Kent (1995), Revised calibration of the geomagnetic polarity timescale for the Late Cretaceous and Cenozoic, *J. Geophys. Res.*, *100*, 6093−6095, doi:10.1029/94JB03098.

Cane, M. A., and P. Molnar (2001), Closing of the Indonesian seaway as precursor to east African aridification around 3–4 million years ago, *Nature, 411*, 157–162, doi:10.1038/35075500.

Channell, J.E.T., M. Smelror, E. Jansen, S. Higgins, B. Lehman, T. Eidvin and A. Solheim (1999) Age models for glacial fan deposits off East Greenland and Svalbard (ODP Site 986 and Site 987), In: Raymo, M., E. Jansen, P. Blum, and T.D. Herbert (Eds.), *Proc. ODP, Sci. Results, 162*, 149-166, Ocean Drilling Program, College Station, TX, USA.

Chen, B., and B.-M. Jahn (2002), Geochemical and isotopic studies of the sedimentary and granitic rocks of the Altai orogen of northwest China and their tectonic implications. *Geol. Mag.*, *139*, 1-13.

Chen, T., M. Frank, B.A. Haley, M. Gutjahr, and R. Spielhagen (2012), Variations of North Atlantic inflow to the central Arctic Ocean over the last 14 million years inferred from hafnium and neodymium isotopes, *Earth Planet. Sci. Lett.*, *353–354*, 82–92, doi:10.1016/j.epsl.2012.08.012.

Clark, P.U., and D. Pollard (1998), Origin of the Middle Pleistocene transition by ice sheet erosion of regolith. *Paleoceanography, 13*, 1–9, doi:10.1029/97PA02660.

Clark, P.U., N.G. Pisias, T.F. Stocker, and A.J. Weaver (2002), The role of the thermohaline circulation in abrupt climate change. *Nature, 415*, 863-869, doi:10.1038/415863a.

Clark, P.U., D. Archer, D. Pollard, J.D. Blum, J.A. Rail, V. Brovkin, A.C. Mix, N.G. Pisias, and M. Roy (2006), The middle Pleistocene transition: characteristics, mechanisms, and implications for long-term changes in atmospheric pCO_2, *Quat. Sci. Rev.*, *25*, 3150–3184, doi:10.1016/j.quascirev.2006.07.008.

Clemens, S.C., D.W. Murray, and W.L. Prell (1996), Non-stationary phase of the Plio-Pleistocene Asian monsoon. *Science, 274*, 943–948, doi:10.1126/science.274.5289.943.

Cohen, R. S., and R. K. O'Nions (1982), The lead, neodymium and strontium isotopic structure of Ocean Ridge Basalts, J. Petrol., 23(3), 299–324, doi:10.1093/petrology/23.3.299.

Cohen, A.S., R.K. O'Nions, R. Siegenthaler, and W.L. Griffin (1988), Chronology of the pressure-temperature history recorded by a granulite terrain, *Contrib. Mineral. Petrol., 98*, 303-311, doi:10.1007/BF00375181.

Crocket, K.C., D. Vance, M. Gutjahr, G.L. Foster, and D.A. Richards (2011), Persistent Nordic deep-water overflow to the glacial North Atlantic, *Geology, 39*, 515-518. doi:10.1130/G31677.1.

Darby, D.A., L. Polynak, and H.A. Bauch (2006), Past glacial and interglacial conditions in the Arctic Ocean and marginal seas – a review, *Prog. Oceanogr., 71*, 129-144, doi:10.1016/j.pocean.2006.09.009.

Dethleff, D., and G. Kuhlmann (2010), Fram Strait sea-ice sediment provinces based on silt and clay compositions identify Siberian Kara and Laptev seas as main source regions, *Polar Research, 29*, 265-282, doi:10.1111/j.1751-8369.2010.00149.

Dickson, R.R., and J. Brown (1994), The production of North Atlantic Deep Water: sources, rathes and pathways, *J. Geophys. Res., 99*, 12319–12341, doi:10.1029/94JC00530.

Dmitrenko, I.A., I.V. Polyakov, S.A. Kirillov, L.A. Timokhov, I.E. Frolov, V.T. Sokolov, H.L. Simmons, V.V. Ivanov, and D. Walsh (2008) Towards a warmer Arctic Ocean: Spreading of the 21st century Atlantic Water warm anomaly along the Eurasian Basin margins, *J. Geophys. Res., 113*, C05023, doi:10.1029/2007JC004158.

Dmitrenko, I.A., S.A. Kirillov, L.B. Tremblay, D. Bauch, J.A. Hölemann, T. Krumpen, H. Kassens, C. Wegner, G. Heinemann, and D. Schröder (2010), Impact oft he Arctic Ocean Atlantic water layer on Siberian shelf hydrography, *J. Geophys. Res., 115*, C08010, doi:10.1029/2009JC006020.

Dmitrenko, I.A., S.A. Kirillov, V.V. Ivanov, B. Rudels, N. Serra, and N.V. Koldunov (2012), Modified halocline water over the Laptev Sea continental margin: Historical Data Analysis, *J. Clim., 25*, 5556-5565, doi:10.1175/JCLI-D-11-00336.1.

Driscoll, N.W., and G.H. Haug (1998), A short-circuit in thermohaline circulation: a cause for northern hemisphere glaciation? *Science, 282*, 436-438, doi:10.1126/science.282.5388.436.

Eidvin, T., and J. Nagy (1999), Foraminiferal biostratigraphy of Pliocene deposits at Site 986, Svalbard margin, In: Raymo, M., E. Jansen, P. Blum, and T.D. Herbert (Eds.), *Proc. ODP, Sci. Results, 162*, 3–17. Ocean Drilling Program, College Station, TX, USA.

Eisenhauer, A., H. Meyer, V. Rachold, T. Tütken, B. Wiegand, B.T. Hansen, R.F. Spielhagen, F. Lindeman, and H. Kassens (1999), Grain size separation and sediment mixing in Arctic Ocean sediments: Evidence from the strontium isotope systematic, *Chem. Geol., 158*, 173-188. 35.

Elderfield, H., P. Ferretti, M. Greaves, S. Crowhurst, I.N. McCave, D. Hodell, and A.M. Piotrowski (2012), Evolution of ocean temperature and ice volume through the Mid-Pleistocene Climate Transition, Science, 337, 704–709, doi:10.1126/science.1221294.

Eldevik, T., J.E.Ø. Nilsen, D. Iovino, K.A. Olsson, A.B. Sandø, and H. Drange (2009), Observed sources and variability of Nordic seas overflow, *Nat. Geosci., 2*, 406–410, doi:10.1038/ngeo518.

Eldholm, O., J. Thiede, E. Taylor and the Leg 104 Shipboard Scientific Party (1987) In: *Proc. ODP Initial Reports, 104*, College Station, TX, USA.

Elmore, A.C., A.M. Piotrowski, J.D. Wright, and A.E. Wright (2011), Testing the extraction of past seawater Nd isotopic composition from North Atlantic deep sea sediments and foraminifera, *Geochem. Geophys. Geosyst., 12*, Q09008, doi:10.1029/2011GC003741.

Erel, Y., Y. Harlavan, and J.D. Blum (1994), Lead isotope systematics of granitoid weathering, *Geochim. Cosmochim. Acta, 58*, 5299-5306, doi:10.1016/0016-7037(94)90313-1.

Fagel, N., C. Innocent, C. Gariepy, and C. Hillaire-Marcel (2002), Sources of Labrador Sea sediments since the last glacial maximum inferred from Nd-Pb isotopes, *Geochim. Cosmochim. Acta, 66*, 2569-2581, doi:10.1016/S0016-7037(02)00866-9.

Fagel, N., C. Hillaire-Marcel, M. Humblet, R. Brasseur, D. Weis, and R. Stevenson (2004), Nd and Pb isotope signatures of the clay-size fraction of Labrador Sea sediments during the Holocene: Implications for the inception of the modern deep circulation pattern. *Paleoceanography, 19*, PA3002, doi:10.1029/2003PA000993.

Farmer, G.L., D. Barber, and J. Andrews (2003), Provenance of Late Quaternary ice-proximal sediments in the North Atlantic: Nd, Sr and Pb isotopic evidence, *Earth Planet. Sci. Lett., 209*, 227-243, doi:10.1016/S0012-821X(03)00068-2.

Forsberg, C.F., A. Solheim, A. Elverhoi, E. Jansen, J.E.T. Channell, and E.S. Andersen (1999), The depositional environment of the western Svalbard margin during the late Pliocene and the Pleistocene: Sedimentary facies changes at Site 986. In: Raymo, M., E. Jansen, P. Blum, T.D. Herbert (Eds.), *Proc. ODP, Sci. Results, 162*, 233−246, Ocean Drilling Program, College Station, TX, USA.

Foster, G.L., and D. Vance (2006), Negligible glacial–interglacial variation in continental chemical weathering rates, *Nature, 444*, 918-921.

Frank, M., B.C. Reynolds, and R.K. O'Nions (1999), Nd and Pb isotopes in Atlantic and Pacific water masses before and after closure of the Panama gateway, *Geology, 27*, doi:1147-1150.10.1130/0091-7613(1999)027.

Frank, M. (2002), Radiogenic isotopes: tracers of past ocean circulation and erosional input, *Rev. Geophys., 40*, 1001, doi:10.1029/2000RG000094.

Fronval, T., and E. Jansen (1996), Late Neogene paleoclimates and paleoceanography in the Iceland-Norwegian Sea: evidence from the Iceland and Vøring Plateaus. In: Thiede, J., A.M. Myhre, J.V. Firth, G.L. Johnson, and W.F. Ruddiman, (Eds.), *Proc. ODP Sci. Results, 151*, 455−468, Ocean Drilling Program, College Station, TX, USA.

Ganopolski, A., and S. Rahmstorf (2001), Rapid changes of glacial climate simulated in a coupled climate model, *Nature, 409*, 153-158, doi:10.1038/35051500.

Gascard, J.-C., A.J. Watson, M.-J. Messias, K.A. Olsson, T. Johannessen, and K. Simonsen (2002), Long-lived vortices as a mode of deep ventilation in the Greenland Sea. *Nature, 416*, 525–527, doi:10.1038/416525a.

Geissler, W.H., and W. Jokat (2004), A geophysical study of the northern Svalbard continental margin, *Geophys. J. Int*., *158*, 50-66, doi:10.1111/j.1365-246X.2004.02315.

Geissler, W.H., W. Jokat, and H. Brekke (2011), The Yermak Plateau in the Arctic Ocean in the light of reflection seismic data – implication for its tectonic and sedimentary evolution, *Geophys. J. Int*., *187*, 1334-1362, doi:10.1111/j.1365-246X.2011.05197.

Gislason, S. R., and E.H. Oelkers (2003), Mechanism, rates, and consequences of basaltic glass dissolution: II. An experimental study of the dissolution rates of basaltic glass as a function of pH and temperature, *Geochim. Cosmochim. Acta*, *67*, 3817–3832, doi:10.1016/S0016-7037(00)00176-5.

Gobeil, C., R.W. Macdonald, J.N. Smith, and L. Beaudin (2001), Atlantic water flow pathways revealed by lead contamination in Arctic Basin sediments, *Science, 293*, 1301–1304, doi:10.1126/science.1062167.

Goldstein, S.L., R.K. O'Nions, and P.J. Hamilton (1984), A Sm-Nd isotopic study of atmospheric dusts and particulates from major river systems. *Earth Planet. Sci. Lett*., *70*, 221-236, doi:10.1016/0012-821X(84)90007-4.

Goldstein, S. L., and S.R. Hemming (2003), Long-lived Isotopic Tracers in Oceanography, Paleoceanography and Ice Sheet Dynamics. *Treatise on Geochemistry, 6*, 453-489, doi:10.1016/B0-08-043751-6/06179-X.

Grousset, F.E., P.E. Biscaye, A. Zindler, J. Prospero, and R. Chester (1988), Neodymium isotopes as tracers in marine sediments and aerosols: North Atlantic, *Earth Planet. Sc. Lett.*, 87, 367–378, doi:10.1016/0012-821X(88)90001-5.

Grousset, F.E., and P.E. Biscaye (2005), Tracing dust sources and transport patterns using Sr, Nd and Pb isotopes, *Chem. Geol., 222*, 149-167, doi:10.1016/j.chemgeo.2005.05.006.

Gutjahr, M., M. Frank, C.H. Stirling, V. Klemm, T. van de Flierdt, and A.N. Halliday (2007), Reliable extraction of a deepwater trace metal isotope signal from Fe-Mn oxyhydroxide coatings of marine sediments, *Chem. Geol., 242*, 351– 370, doi:10.1016/j.chemgeo.2007.03.021.

Gutjahr, M., M. Frank, C.H. Stirling, L.D. Keigwin, and A.N. Halliday (2008), Tracing the Nd isotope evolution of North Atlantic Deep and Intermediate Waters in the western North Atlantic since the Last Glacial Maximum from Blake Ridge sediments. *Earth Planet. Sci. Lett., 266*, 61-77, doi:10.1016/j.epsl.2007.10.037.

Gutjahr, M., M. Frank, A.N. Halliday, and L.D. Keigwin (2009), Retreat of Laurentide ice sheet tracked by the isotopic composition of Pb in western North Atlantic seawater during termination 1, *Earth Planet. Sci. Lett., 286*, 546-555, doi:10.1016/j.epsl.2009.07.020.

Haley, B. A., G.P. Klinkhammer, and J. McManus (2004), Rare Earth Elements in Pore Waters of Marine Sediments. *Geochim. Cosmochim. Acta 68*, 1265-1279. doi:10.1016/j.gca.2003.09.012.

Haley, B. A., M. Frank, R.F. Spielhagen, and A. Eisenhauer (2008a), Influence of brine formation on Arctic Ocean circulation over the past 15 million years, *Nat. Geosci., 1*, 68–72, doi:10.1038/ngeo.2007.5.

Haley, B.A., M. Frank, R.F. Spielhagen, and J. Fietzke (2008b), Radiogenic isotope record of Arctic Ocean circulation and weathering inputs of the past 15 million years, *Paleoceanography, 23*, PA1S13, doi:10.1029/2007PA001486.

Hansen, B., and S. Østerhus (2000), North Atlantic-Nordic Seas Exchanges, *Prog. Oceanogr., 45*, 109-208, doi:10.1016/S0079-6611(99)00052-X.

Hays, J.D., J. Imbrie, and N.J. Shackleton (1976), Variations in the Earth's orbit: pacemaker of the ice ages. *Science, 194*, 1121-1132, doi:10.1126/science.194.4270.1121.

Haug, G.H. and R. Tiedemann, (1998) Effect of the formation of the Isthmus of Panama on Atlantic Ocean thermohaline circulation, *Nature, 393*, 673-676, doi:10.1038/31447.

Helmke, J. P., H.A. Bauch, and A. Mazaud (2003), Evidence for a mid-Pleistocene shift of ice-drift pattern in the Nordic seas, *J. Quat. Sci., 18*, 183–191, doi:10.1002/jqs.735.

Helmke, J. P., H.A. Bauch, U. Röhl, and A. Mazaud (2005), Changes in sedimentation patterns of the Nordic seas region across the mid-Pleistocene, *Mar. Geol., 215*, 107–122, doi:10.1016/j.margeo.2004.12.006.

Hemming, S. R. (2004), Heinrich events: Massive Late Pleistocene detritus layers of the North Atlantic and their global climate imprint, *Rev. Geophys., 42*, RG1005, doi:10.1029/2003RG000128.

Henderson, G.M., and E. Maier-Reimer (2002) Advection and removal of ^{210}Pb and stable Pb isotopes in the oceans: a general circulation model study, *Geochim. Cosmochim. Acta, 66*, 257–272, doi:10.1016/S0016-7037(01)00779-7.

Henrich, R., (1989) Glacial/interglacial cycles in the Norwegian Sea: Sedimentology, Paleoceanography, and evolution of Late Pliocene to Quaternary Northern Hemisphere climate, In: O. Eldholm, J. Thiede and E. Taylor et al., *Proc. ODP, Sci. Res., 104,* 189-232, Ocean Drilling Program, College Station, TX, USA.

Henrich, R., and K.-H. Baumann (1994), Evolution of the Norwegian current and the Scandinavian ice sheets during the past 2.6 my: evidence from ODP Leg 104 biogenic carbonate and terrigenous records, *Palaeogeogr. Palaeoclimatol. Palaeoecol. 108*, 75−94, doi:10.1016/0031-0182(94)90023-X.

Henrich, R., K.-H. Baumann, R. Huber, and H. Meggers (2002), Carbonate preservation records of the past 3 Myr in the Norwegian–Greenland Sea and the northern North Atlantic: implications for the history of NADW production, *Mar. Geol., 184,* 17–39, doi:10.1016/S0025-3227(01)00279-1.

Horwitz, E.P., R. Chiarizia, and M.L. Dietz (1992), A novel strontium-selective extraction chromatographic resin. *Solvent Extraction Ion Exch., 10*, 313-336, doi:10.1080/07366299208918107.

Huybers, P., and P. Molnar (2007), Tropical cooling and the onset of North American glaciation, *Clim. Past, 3*, 549–557, doi:10.5194/cp-3-549-2007.

Innocent, C., N. Fagel, and C. Hillaire-Marcel (2000), Sm-Nd isotope systematics in deep-sea sediments: Clay-size versus coarser fractions, *Mar. Geol., 168*, 79–87, doi:10.1016/S0025-3227(00)00052-9.

Ionov, D.A., S.B. Mukasa, and J.-L. Bodinier (2002), Sr-Nd-Pb isotopic compositions of peridotite xenoliths from Spitsbergen: Numerical modeling indicates Sr-Nd decoupling in the mantle by melt percolation metasomatism, *J. Petrol., 43*, 2261–2278, doi:10.1093/petrology/43.12.2261.

Jacobsen, S.B., and G.J. Wasserburg (1980), Sm-Nd isotopic evolution of chondrites, *Earth Planet. Sci. Lett., 50*, 139-155, doi:10.1016/0012-821X(80)90125-9.

Jansen, E., B. Slettemark, U. Bleil, R. Henrich, L. Kringstad, and S. Rolfsen (1989), Oxygen and carbon isotope stratigraphy and magnetostratigraphy of the last 2.8 Ma: paleoclimatic comparisons between the Norwegian Sea and the North Atlantic. In:

Eldholm, O., Thiede, J., Taylor, E., et al., *Proc. ODP Sci. Results, 104*, 255-269, Ocean Drilling Program, College Station, TX, USA.

Jansen, E., and J. Sjøholm (1991), Reconstruction of glaciation over the past 6 Myr from ice-borne deposits in the Norwegian Sea, *Nature, 349*, 600-603, doi:10.1038/349600a0.

Jansen, E, M.E. Raymo, P. Blum , E.S. Andersen, W.E.N. Austin, K.-H. Baumann, V. Bout-Roumazeilles, S.J. Carter, J. E.T. Channell, J.L. Cullen, B. Flower, S. Higgins, D.A. Hodell, J.A. Hood, S.M. Hyun, M. Ikehara, T. King, R. Larter, B. Lehman, S. Locker, K. Mclntyre, J. McManus, L.B. Meng, S. O'Connell, J.D. Ortiz, F.R. Rack, A. Solheim, and W. Wei (1996), *Proc. ODP, Init. Repts, vol. 162*, Ocean Drilling Program, College Station, TX, USA.

Jansen, E., T. Fronval, F. Rack, and J.E.T. Channell (2000), Pliocene-Pleistocene ice rafting history and cyclicity in the Nordic Seas during the last 3.5 Myr, *Paleoceanography, 15*, 709-721, doi:10.1029/1999PA000435.

Jeandel, C., T. Arsouze, F. Lacan, P. Techine, and J.C. Dutay (2007), Isotopic Nd compositions and concentrations of the lithogenic inputs into the ocean: A compilation, with an emphasis on the margins, *Chem. Geol., 239*, 156–164 doi:10.1016/j.chemgeo.2006.11.013.

Johansson, Å., and D.G. Gee (1999), The late Palaeproterozoic Eskolabreen granitoids of southern Ny Friesland, Svalbard Caledonides – geochemistry, age, and origin, *GFF, 121*, 113–126.

Johansson, Å., Larionov, A.N., Tebenkov, A.M., Ohta, Y., Gee, D.G. (2002) Caledonian granites of western and central Nordaustlandet, northeast Svalbard. *GFF 124*, 135-148.

Karas, C., D. Nürnberg, A. Gupta, R. Tiedemann, K. Mohan, and T. Bickert (2009), Mid-Pliocene climate change amplified by a switch in Indonesian subsurface throughflow, *Nat. Geosci., 2*, 434–438, doi:10.1038/ngeo520.

Karcher, M.J., and J.M. Oberhuber (2002), Pathways and modification of the upper and intermediate waters of the Arctic Ocean, J. *Geophys. Res., 107*, C6, 3049, doi:10.1029/2000JC000530.

Kawase, M., and J.L. Sarmiento (1986), Circulation and nutrients in middepth Atlantic waters, *J. Geophys. Res., 91*, 9748-9770, doi:10.1029/JC091iC08p09749.

Keigwin, L. (1982), Isotopic paleoceanography of the Caribbean and East Pacific: Role of Panama uplift in late Neogene time. *Science, 217*, 350–352, doi:10.1126/science.217.4557.350.

Kleiven, H.F., and E. Jansen, T. Fronval, and T.M. Smith (2002), Intensification of Northern Hemisphere glaciations in the circum Atlantic region (3.5-2.4) – ice-rafted detritus

evidence, *Palaeogeogr., Palaeoclimatol., Palaeoecol., 184*, 213-223, doi:10.1016/S0031-0182(01)00407-2.

Kleiven, H.F., E. Jansen, W.B. Curry, D.A. Hodell, and K. Venz (2003), Atlantic Ocean thermohaline circulation changes on orbital to suborbital timescales during the mid-Pleistocene, *Paleoceanography, 18*, PA000629, doi:10.1029/2001PA000629.

Klevenz, V., D., Vance, D. N. Schmidt, and K. Mezger (2008), Neodymium Isotopes in Benthic Foraminifera: Core-Top Systematics and a Down-Core Record from the Neogene South Atlantic, *Earth Planet. Sci. Lett., 265*, 571-587. doi: 10.1016/j.epsl.2007.10.053.

Knies, J., J. Matthiessen, C. Vogt, and R. Stein (2002), Evidence of 'Mid-Pliocene (~3 Ma) global warmth' in the eastern Arctic Ocean and Implications for the Svalbard/Barents Sea ice sheet during the late Pliocene and early Pleistocene (~3 – 1.7 Ma), *Boreas, 31*, 82-93, doi:10.1111/j.1502-3885.2002.tb01058.

Knies, J., J. Matthiessen, A. Mackensen, R. Stein, C. Vogt, T. Frederichs, and S.-I. Nam (2007), Effects of Arctic freshwater forcing on thermohaline circulation during the Pleistocene. *Geology, 35*, 1075–1078, doi:10.1130/G23966A.1.

Knies, J., J. Matthiessen, C. Vogt, J.S. Laberg, B.O. Hjelstuen, M. Smelror, E. Larsen, K. Andreassen, T. Eidvin, and T.O. Vorren (2009), The Plio-Pleistocene glaciation of the Barent Sea-Svalbard region: a new model based on revised chronostratigraphy, *Quat. Sci. Rev., 28***,** 812-829, doi:10.1016/j.quascirev.2008.12.002.

Koeppenkastrop D., and E.H. De Carlo (1992), Sorption of rare earth elements from seawater onto synthetic mineral particles: an experimental approach. *Chem. Geol., 95*, 251-263, doi:10.1016/0009-2541(92)90015-W.

Kuhlbrodt, T., A. Griesel, M. Montoya, A. Levermann, M. Hofmann, and S. Rahmstorf (2007), On the driving processes of the Atlantic meridional overturning circulation, *Rev. Geophys., 45*, RG2001, doi:10.1029/2004RG000166.

Lacan, F., and C. Jeandel (2004a), Denmark Strait water circulation traced by heterogeneity in neodymium isotopic compositions, *Deep Sea Res., I 51*, 71–82, doi:10.1016/j.dsr.2003.09.006.

Lacan, F., and C. Jeandel (2004b), Neodymium isotopic composition and rare earth element concentrations in the deep and intermediate Nordic Seas: Constrains on the Iceland Scotland Overflow Water signature, *Geochem. Geophys. Geosys., 5***,** Q11006, doi:10.1029/2004GC000742.

Lacan, F., and C. Jeandel (2004c), Subpolar Mode Water formation traced by neodymium isotopic composition, *Geophys. Res. Lett.***,** *31*, L14306, doi:10.1029/2004GL019747.

Lacan, F., and C. Jeandel (2005a), Neodymium isotopes as a new tool for quantifying exchange fluxes at the continent-ocean interface, *Earth Planet. Sci. Lett., 232*, 245-257, doi:10.1016/j.epsl.2005.01.004.

Lacan, F., and C. Jeandel (2005b), Acquisition of the neodymium isotopic composition of the North Atlantic Deep Water, *Geochem. Geophys. Geosys.*, *6*, Q12008, doi:10.1029/2005GC000956.

Le Fèvre, B., and C. Pin (2005), A straightforward separation scheme for concomitant Lu-Hf and Sm-Nd isotope ratio and isotope dilution analysis, *Analyt. Chim. Acta*, *543*, 209-221, doi:10.1016/j.aca.2005.04.044.

Levskii, L.K., N.M. Stolbov, E.S. Bogomolov, J.M. Vasil'eva, and E.M. Makar'eva (2006), Sr-Nd-Pb isotopic systems in basalts of the Franz Josef Land Archipelago, *Geochem. Int.*, *44*, 327-337, doi:10.1134/S0016702906040021.

Lisiecki, L.E., and M.E. Raymo (2005), A Pliocene-Pleistocene stack of 57 globally distributed benthic $\delta^{18}O$ records, *Paleoceanography*, *20*, PA1003, doi:10.1029/2004PA001071.

Loeng, H., K. Brander, E. Carmack, S. Denisenko, K. Drinkwater, B. Hansen, K. Kovacs, P. Livingston, F. McLaughlin, and E. Sakshaug (2005), Marine Systems, In: *Arctic Climate Impact Assessment*, C. Symon, L. Arris, and B. Heal (eds.), vol. 2 (pp. 454–538), New York: Cambridge University Press.

Lugmair, G.W., and S.J.G. Galer (1992), Age and isotopic relationships among the angrites Lewis Cliff 86010 and Angra dos Reis, *Geochim. Cosmochim. Acta*, *56*, 1673-1694, doi:10.1016/0016-7037(92)90234-A.

Maccali, J., C. Hillarie-Marcel, J. Carignan, and L.C. Reisberg (2012), Pb isotopes and geochemical monitoring of Arctic sedimentary supplies and water mass export through Fram Strait since the Last Glacial Maximum, *Paleoceanography*, *27*, PA1201, doi:10.1029/2011PA002152.

Martin, E.E., and B.A. Haley (2000), Fossil fish teeth as proxies for seawater Sr and Nd isotopes, *Geochim. Cosmochim. Acta*, *64*, 835-847, doi:10.1016/S0016-7037(99)00376-2.

Martin, E.E., S.W. Blair, G.D. Kamenov, H.D. Scher, E. Bourbon, C. Basak, and D.N. Newkirk (2010), Extraction of Nd isotopes from bulk deep sea sediments for paleoceanographic studies on Cenozoic time scales, *Chem. Geol.*, *269*, 414-431 doi:10.1016/j.chemgeo.2009.10.016.

Martin, E.E., K.G. MacLeod, A. Jiménez Berrocoso, and E. Bourbon (2012), Water mass circulation on Demara Rise during the Late Cretaceous, *Earth Planet. Sci. Lett.*, *327–328*, 111–120, doi:10.1016/j.epsl.2012.01.037.

Martínez-Botí, M.A., D. Vance, and P.G. Mortyn (2009), Nd/Ca ratios in plankton-towed and core top foraminifera: Confirmation of the water column acquisition of Nd, *Geochem. Geophys. Geosys.*, 10, Q08018, doi:10.1029/2009GC002701.

Maslin, M.A., G. Haug, M. Sarnthein, R. Tiedemann, H. Erlenkeuser, and R. Stax (1995), Northwest Pacific Site 882: The initiation of Northern Hemisphere Glaciation, In: Rea, D.K., I.A. Basov, D.W. Scholl, and J.F. Allan (eds.), *Proc. ODP, Sci. Res., 145*, 315–332, Ocean Drilling Program, College Station, TX, USA.

Maslin, M.A., G. Haug, M. Sarnthein, and R. Tiedemann (1996), The progressive intensification of Northern Hemisphere glaciation as seen from the North Pacific, *ICES-Geol. Rdsch. 85*, 452–465, doi:10.1007/BF02369002.

Mattingsdal, R., J. Knies, K. Andreassen, K. Fabian, K. Husum, K. Grøsfjeld, and S. de Schepper (2012), A new 6 Myr stratigraphic framework for the Atlantic-Arctic gateway, *Quat. Sci. Rev.*, in review.

McArthur, J.M., R.J. Howarth, and T.R. Bailey (2001), Strontium Isotope Stratigraphy: LOWESS Version 3: Best Fit to the Marine Sr-Isotope Curve for 0–509 Ma and Accompanying Look-up Table for Deriving Numerical Age, *J. Geol., 109*, 155–170, doi:10.1086/319243.

McManus, J.F., R. Francois, J.-M. Gherardi, L.D. Keigwin, and S. Brown-Leger (2004), Collapse and rapid resumption of Atlantic meridional circulation linked to deglacial climate changes, *Nature 428*, 834-837, doi:10.1038/nature02494.

Mudelsee, M., and M. Schulz (1997), The Mid-Pleistocene climate transition: onset of 100 ka cycle lags ice volume build-up by 280 ka. *Earth Planet. Sci. Lett., 151*, 117–123, doi:10.1016/S0012-821X(97)00114-3.

Mudelsee, M., and M.E. Raymo (2005), Slow dynamics of the Northern Hemisphere glaciation, *Paleoceanography, 20*, PA4022, doi:10.1029/2005PA001153.

Myhre, A., J. Thiede, J.A. Firth and the Leg 151 Shipboard Scientific Party (1995), *Proc. ODP Initial Reports, 151*, 951, Ocean Drilling Program, College Station, TX, USA.

Nøttvedt, A., L.T. Berglund, E. Rasmussen, and R.J. Steel (1988), Some aspects of the Tertiary tectonics and sedimentation along the western Barents Shelf, In: Morton, A.C., Parson, L.M. (Eds.), *Early Tertiary Volcanism and the Opening of the NE Atlantic, 39*, Geological Society of America, 421–425 (Special Publication).

Nürnberg, D., I. Wollenburg, D. Dethleff, H. Eicken, H. Kassens, T. Letzig, E. Reimnitz, and J. Thiede (1994), Sediments in Arctic sea ice: Implications for entrainment, transport and release, *Mar. Geol., 119*, 185-214, doi:10.1016/0025-3227(94)90181-3.

O`Nions, R.K., and K. Grönvold (1973), Petrogenetic relationships of acid and basic rocks in iceland: Sr-isotopes and rare-earth elements in late and postglacial volcanic, *Earth Planet. Sci. Lett.*, 19, 397-409, doi:10.1016/0012-821X(73)90182-9.

Oppo, D.W. and R.G. Fairbanks (1987) Variability in the deep and intermediate water circulation of the Atlantic Ocean during the past 25.000 years: Northern Hemisphere modulation of the Southern Ocean, *Earth Planet. Sci. Lett., 86,* 1-15, doi:10.1016/0012-821X(87)90183.

Paillard, D. (1998), The timing of Pleistocene glaciations from a simple multiple-state climate model. *Nature, 391,* 378–381, doi:10.1038/34891.

Palmer, M. R., (1985), Rare-Earth Elements in Foraminfera Tests. *Earth Planet. Sci. Lett., 73,* 285-298. doi: 10.1016/0012-821x(85)90077-9.

Palmer, M. R., and H. Elderfield (1985), Variations in the Nd Isotopic Composition of Foraminifera from Atlantic-Ocean Sediments. *Earth Planet. Sci. Lett., 73,* 299-305. doi: 10.1016/0012-821x(85)90078-0.

Palmer, M.R., and J.M. Edmond (1989), The strontium isotope budget of the modern ocean. *Earth Planet. Sci. Lett., 92,* 11-26, doi:10.1016/0012-821X(89)90017-4.

Peltier, W.R., G. Vettoretti, and M. Stastna (2006), Atlantic meridonal overturning and climate response to Arctic Ocean freshening. *Geophys. Res. Lett., 33,* L06713, doi:10.1029/2005GL025251.

Peterson, B. J., J. McClelland, R. Curry, R.M. Holmes, J.E. Walsh, and K. Aagaard (2006), Trajectory shifts in the Arctic and Subarctic freshwater cycle, *Science, 313,* 1061–1066, doi:10.1126/science.1122593.

Peucat, J.J., Y. Ohta, D.G. Gee, and J. Bernard-Griffith (1989), U-Pb, Sr and Nd evidence for Grenivillan and latest Proterozoic tectonothermal activity in the Spitsbergen Caldonides, Arctic Ocean, *Lithos, 22,* 275-285, doi:10.1016/0024-4937(89)90030-3.

Pfirman, S., R. Colony, D. Nürnberg, H. Eicken, and I. Rigor (1997), Reconstructing the origin and trajectory of drifting Arctic sea ice, *J. Geophys. Res., 102,* 12,575-12,586, doi:10.1029/96JC03980.

Piepgras, D.J., and G.J. Wasserburg (1987), Rare earth element transport in the western North Atlantic inferred from Nd isotopic observations, *Geochim. Cosmochim. Acta, 51,* 1257-1271, doi:10.1016/0016-7037(87)90217-1.

Piotrowski, A. M., S.L. Goldstein, S.R. Hemming, and R.G. Fairbanks (2005), Temporal relationships of carbon cycling and ocean circulation at glacial boundaries, *Science, 307,* 1933–1938, doi:10.1126/science.1104883.

Piotrowski, A.M., S.L. Goldstein, S.R. Hemming, R.G. Fairbanks, and D.R. Zylberberg (2008), Oscillating glacial northern and southern deep water formation from combined neodymium and carbon isotopes, *Earth Planet. Sci. Lett., 272,* 394–405, doi:10.1016/j.epsl.2008.05.011.

Piotrowski, A.M., V.K. Banakar, A.E. Scrivner, H. Elderfield, A. Galy, and A. Dennis (2009), Indian Ocean circulation and productivity during the last glacial cycle, *Earth Planet. Sci. Lett., 285,* 179 – 189, doi:10.1016/j.epsl.2009.06.007.

Pisias, N.G., and T.C. Moore (1981), The evolution of Pleistocene climate: a time series approach. *Geochim. Cosmochim. Acta, 73,* 2645-2659, doi:10.1016/j.gca.2008.11.046.

Pomies, C., G.R. Davies, and S.M.H. Conan (2002), Neodymium in Modern Foraminifera from the Indian Ocean: Implications for the Use of Foraminiferal Nd Isotope Compositions in Paleo-Oceanography. *Earth Planet. Sci. Lett., 203,* 1031-1045, doi: 10.1016/s0012-821x(02)00924.

Porcelli, D, P. Andersson, M. Baskaran, M. Frank, G. Björk and I. Semiletov (2009) The distribution of neodymium isotopes in Arctic Ocean basins, *Geochim. Cosmochim. Acta, 73,* 2645-2659, doi:10.1016/j.gca.2008.11.046

Qing, H., C.R. Barnes, D. Buhl, and J. Veizer (1998) The strontium isotopic composition of Ordovician and Silurian brachiopods and conodonts: relationships to geological events and implications for coeval seawater, *Geochim. Cosmochim. Acta, 62,* 1721-1733, doi:10.1016/S0016-7037(98)00104-5

Rahmstorf, S. (2002), Ocean circulation and climate during the past 120 000 years. *Nature, 419,* 207-214, doi:10.1038/nature01090.

Ravelo A.C., and D.H. Andreasen (2000), Enhanced circulation during a warm period, *Geophys. Res. Lett., 27,* 1001-1004, doi: 10.1029/1999GL007000.

Ravelo, A.C., D.H. Andreasen, M.Lyle, A.O. Lyle, and M.W. Wara (2004), Regional climate shifts caused by gradual global cooling in the Pliocene epoch. *Nature, 429,* 263 – 267, doi:10.1038/nature02567.

Raymo, M.E., W.F. Ruddiman, N.J. Shackleton, and D.W. Oppo (1990), Evolution of Atlantic-Pacific $\delta^{13}C$ gradients over the last 2.5 m.y., *Earth Planet. Sci. Lett., 97,* 353-368, doi:10.1016/0012-821X(90)90051-X.

Raymo, M.E., D. Hodell, and E. Jansen (1992), Response of deep ocean circulation to initiation of Northern Hemisphere Glaciation (3-2 Ma), *Paleoceanography, 7,* 645-672, doi:10.1029/92PA01609.

Raymo, M.E., and W.F. Ruddiman (1992), Tectonic forcing of late Cenozoic climate, *Nature, 359,* 117–122, doi:10.1038/359117a0.

Raymo, M.E. (1994), The Himalayas, organic carbon burial, and climate in the Miocene. Paleoceanographic currents, *Paleoceanography, 9*, 399–404, doi:10.1029/94PA00289.

Raymo, M.E. (1997), The timing of major climate termination. *Paleoceanography, 12*, 577–585, doi:10.1029/97PA01169.

Raymo, M.E., D.W. Oppo, B.P. Flower, D.A. Hodell, J.F. McManus, K.A. Venz, K.F. Kleiven, and K. McIntyre (2004), Stability of North Atlantic water masses in face of pronounced climate variability during the Pleistocene. *Paleoceanography, 19*, PA2008, doi:10.1029/2003PA000921.

Raymo, M.E., L.E. Lisiecki, and K.H. Nisancioglu, (2006), Plio – Pleistocene Ice volume, Antarctic Climate, and the global $\delta^{18}O$ record, *Science, 313*, 492–495, doi:10.1126/science.1123296.

Raymo, M.E., and P. Huybers (2008), Unlocking the mysteries of the ice ages. *Nature, 451*, 284-285, doi:10.1038/nature06589.

Rempfer, J., T.F. Stocker, F. Joos, J.-C. Dutay, and M. Siddall (2011), Modelling Nd-isotopes with a coarse resolution ocean circulation model: Sensitivities to model parameters and source/sink distributions, *Geochim. Cosmochim. Acta, 75*, 5927-5950, doi:10.1016/j.gca.2011.07.044.

Reimnitz, E., L. Marincovich Jr., M. McCormick, and W.M. Briggs (1992), Suspension freezing of bottom sediment and biota in the Northwest Passage and implications for Arctic Ocean sedimentation, *Can. J. Earth Sci., 29*, 693-703, doi:10.1139/e92-060.

Reynolds, B.C., M. Frank, and R.K. O'Nions (1999), Nd- and Pb- isotope time series from Atlantic ferromanganese crusts: Implications for changes in provenance and paleocirculation over the last 8 Myr, *Earth Planet. Sci. Lett., 173*, 381-396, doi:10.1016/S0012-821X(99)00243-5.

Roberts, N.L., A.M. Piotrowski, J.F. McManus, and L.D.Keigwin (2010), Synchronous Deglacial Overturning and water mass source changes, *Science, 327*, 75-78, doi:10.1126/science.1178068.

Robinson, M.M. (2009), New quantitative evidence of extreme warmth in the Pliocene Arctic, *Stratigraphy, 6*, 265-275.

Rudels, B. (1986), The Θ-S relations in the northern seas: Implications for the deep circulation. *Polar Res., 4*, 133-159, doi:10.1111/j.1751-8369.1986.tb00527.

Rudels, B. (1989), The formation of polar surface water, the ice export and the exchanges through the Fram Strait. *Prog. Oceanogr., 22*, 205–248, doi:10.1016/0079-6611(89)90013.

Rudels, B., E.P. Jones, L.G. Anderson and G. Kattner (1994) On the intermediate depth waters of the Arctic Ocean, In: *The role of the Polar Oceans in Shaping the Global Climate: The Nansen Centennial Volume.* Johannessen, O. M., Muench, R. D. & Overland, J. E. (eds.), pp. 33-46, Washington: American Geophysical Union.

Rudels, B., R. Meyer, E. Fahrbach, V.V. Ivanov, S. Østerhus, and D. Quadfasel (2000), Water mass distribution in Fram Strait and over the Yermak Plateau in summer 1997, *Ann. Geophys.*, *18*, 687-705, doi:10.1007/s00585-000-0687-5.

Rudels, B. E. Fahrbach, J. Meincke, G. Budéus, and P. Eriksson (2002), The East Greenland Current and its contribution to the Denmark Strait overflow. *ICES J. Mar. Sci., 59*, 1133–1154.

Rudels, B., G. Björk, J. Nilsson, P. Winsor, I. Lake, and C. Nohr (2005), The interaction between waters from the Arctic Ocean and the Nordic Seas north of Fram Strait and along the East Greenland Current: results from the Arctic Ocean-02 Oden expedition, *J. Mar. Sys., 55*, 1-30, doi:10.1016/j.jmarsys.2004.06.008.

Rutberg, R.L., S.R. Hemming, and S.L. Goldstein (2000), Reduced North Atlantic Deep Water flux to the glacial Southern Ocean inferred from neodymium isotope ratios. *Nature 405*, 935-938, doi:10.1038/35016049.

Sarnthein, M., E. Jansen, M. Weinelt, M. Arnold, J.C. Duplessy, H. Erlenkeuser, A. Flatøy, G. Johannessen, T. Johannessen, S. Jung, N. Koc, L. Labeyrie, M. Maslin, U. Pflaumann, and H. Schulz (1995), Variations in Atlantic Surface Ocean Paleoceanography, 50°-80°N: A Time-Slice Record of the Last 30,000 Years, *Paleoceanography, 10*, 1063-1094, doi:10.1029/95PA01453.

Sarnthein, M., G. Bartoli, M. Prange, A. Schmittner, B. Schneider, M. Weinelt, N. Andersen, and D. Garbe-Schönberg (2009), Mid-Pliocene shifts in ocean overturning circulation and the onset of Quaternary-style climates, *Climates of the Past, 5*, 269–283, doi:10.5194/cp-5-269-2009.

Saunders, P.M. (2001), The dense northern overflows. In: *Ocean Circulation and Climate: Observing and Modelling the Global Ocean*, Siedler, G., J. Church and J. Gould (eds.), pp. 401–417, London: Academic Press.

Schaule, B.K., and C.C. Patterson (1981), Lead concentrations in the northeast Pacific: evidence for global anthropogenic perturbations, *Earth Planet. Sci. Lett., 54*, 97-115, doi:10.1016/0012-821X(81)90072-8.

Schlichtholz, P., and I. Goszszko (2006), Interannual variability of the Atlantic water layer in the West Spitsbergen Current at 76.5°N in summer 1991–2003, *Deep-Sea Res. I, 53*, 608-626, doi:10.1016/j.dsr.2006.01.001.

Scrivner, A.E., D. Vance, and E.J. Rohling (2004), New neodymium isotope data quantify Nile involvement in Mediterranean anoxic episodes, *Geology, 32*, 565-568, doi: 10.1130/G20419.1.

Shackleton, N.J., and N.D. Opdyke (1976), Oxygen-isotope and paleomagnetic stratigraphy of Pacific core V28-239: Late Pliocene to latest Pleistocene. *Geological Society of America Memoir, 145*, 449–464, doi:10.1016/0033-5894(73)90052-5.

Shackleton, N.J., J. Backman, H. Zimmerman, D.V. Kent, M.A. Hall, D.G. Roberts, D. Schnitker, J.G. Baldauf, A. Desprairies, R. Homrighausen, P. Huddlestun, J.B. Keene, A.J. Kaltenback, K.A.O. Krumsiek, A.C. Morton, J.W. Murray, and J. Westberg-Smith (1984), Oxygen isotope calibration of the onset of ice-rafting and history of glaciation in the North Atlantic region, *Nature, 307*, 620–623, doi:10.1038/307620a0.

Shackleton, N.J. and M.A. Hall, and D.Pate (1995), Pliocene stable isotope stratigraphy of site 846. In: Pisias, N.G., L.A. Mayer, T.R. Janecek, A. Palmer-Julson, and T.H. van Andel (Eds.), *Proc. ODP Sci. Results, 138*, 337–355, Ocean Drilling Program, College Station, TX, USA.

Sharma, M., A.R. Basu, and G.V. Nesterenko (1992), Temporal Sr-, Nd- and Pb-isotopic variations in the Siberian flood basalts: Implications for the plume-source characteristics, *Earth Planet. Sci. Lett., 113*, 365-381, doi:10.1016/0012-821X(92)90139-M.

Shiklomanov, I.A., A.I. Shiklomanov, R.B. Lammers, B.J. Peterson, and C.J. Vörösmarty (2000), The dynamics of river water inflow to the Arctic Ocean. In: *The freshwater budget of the Arctic Ocean*, E.L. Lewis, E.P. Jones, P. Lemke, T.D. Prowse and P. Wadhams (eds.), vol.70, pp. 281–296, Kluwer Academics Publishers.

Simonsen, K., and P.M. Haugan (1996), Heat budgets of the Arctic Mediterranean and sea surface heat flux parameterizations for the Nordic Seas. *J. Geophys. Res., 101*, 6553–6576, doi:10.1029/95JC03305.

Smelror, M. (1999), Pliocene–Pleistocene and redeposited dinoflagellate cysts from the western Svalbard Margin (Site 986): biostratigraphy, paleoenvironments and sediment provenance. In: Raymo, M., E. Jansen, P. Blum, and T.D. Herbert (Eds.), *Proc. ODP Sci. Results, 162*, 83–97. Ocean Drilling Program, College Station, TX, USA.

Spielhagen, R.F., K.-H. Baumann, H. Erlenkeuser, N.R. Nowaczyk, N. Nørgaard-Pedersen, C. Vogt, and D. Weiel (2004), Arctic Ocean deep-sea record of northern Eurasian ice sheet history, *Quat. Sci. Rev., 23*, 1455 – 1483, doi:10.1016/j.quascirev.2003.12.015.

Spielhagen, R.F., K. Werner, S.A. Sørensen, K. Zamelczyk, E. Kandiano, G. Budeus, K. Husum, T.M. Marchitto, and M. Hald (2011), Enhanced modern heat transport to the Arctic by warm Atlantic water, *Science, 331*, 450, doi:10.1126/science.1197397.

Steiger, R.H., and E. Jäger (1977), Subcommission on geochronology: convention on the use of decay constants in geo- and cosmochronology, *Earth Planet. Sci. Lett., 36,* 359- 362, doi:10.1016/0012-821X(77)90060-7.

Stumpf, R., M. Frank, J. Schönberg, and B.A. Haley (2010), Late Quaternary variability of Mediterranean Outflow Water from radiogenic Nd and Pb isotopes, *Quat. Sci. Rev., 29,* 2462-2472, doi:10.1016/j.quascirev.2010.06.021.

Sun, Y., S.C. Clemens, Z. An, and Z. Yu (2006), Astronomical timescale and palaeoclimatic implication of stacked 3.6-Myr monsoon records from the Chinese Loess Plateau. *Quat. Sci. Rev., 25*, 33–48, doi:10.1016/j.quascirev.2005.07.005.

Swift, J.H., and K. Aagaard (1981), Seasonal transitions and water mass formation in the Iceland and Greenland seas, *Deep-Sea Res. I, 28,* 1107-1129, doi:10.1016/0198-0149(81)90050-9.

Swift, J.H., and K.P. Koltermann (1988), The origin of Norwegian Sea Deep Water, *J. Geophys. Res., Oceans, 93*, 3563 – 3569, doi:10.1029/JC093iC04p03563.

Tachikawa, K., C. Jeandel, and B. Dupré (1997) Distribution of rare earth elements and neodymium isotopes in settling particulate material of the tropical Atlantic Ocean (EUMELI site), *Deep Sea Res., Part I, 44*, 1769–1792, doi:10.1016/S0967-0637(97)00057-5.

Tachikawa, K., C. Jeandel, and M. Roy-Barman (1999), A new approach to the Nd residence time in the ocean: the role of atmospheric inputs, *Earth Planet. Sci. Lett., 170*, 433-446, doi:10.1016/S0012-821X(99)00127-2.

Tachikawa, K., V. Athias, and C. Jeandel (2003) Neodymium budget in the modern ocean and paleo-oceanographic implications, *J. Geophys. Res., 108,* 3254, doi:10.1029/1999JC000285

Tachikawa, K., M. Roy-Barman, A. Michard, D. Thouron, D. Yeghicheyan, C. Jeandel (2004), Neodymium isotopes in the Mediterranean Sea: comparison between seawater and sediment signal, *Geochim. Cosmochim. Acta, 68,* 3095-3106, doi:10.1016/j.gca.2004.01.024.

Tachikawa, K., T. Toyofuku, I. Basile-Doelsch, and T. Delhaye (2013), Microscale neodymium distribution in sedimentary planktonic foraminiferal tests and associated mineral phases, *Geochim. Cosmochim. Acta, 100,* 11-23, doi:10.1016/j.gca.2012.10.010.

Tanaka, T., S. Togashi, H. Kamioka, H. Amakawa, H. Kagami, T. Hamamoto, M. Yuhara, Y. Orihashi, S. Yoneda, H. Shimizu, T. Kunimaru, K. Takahashi, T. Yanagi, T. Nakano, H. Fujimaki, R. Shinjo, Y. Asahara, M. Tamimizu, and C. Dragusanu (2000), JNdi-1: a neodymium isotopic reference in consistency with LaJolla neodymium, *Chem. Geol., 168*, 279-281, doi:10.1016/S0009-2541(00)00198-4.

Taylor, P.N., F. Kalsbeek, and D. Bridgwater (1992), Discrepancies between neodymium, lead and strontium model ages from the Precambrian of southern East Greenland: Evidence for a Proterozoic granulite-facies event affecting Archaean gneisses, *Chem. Geol. (Isotope Geoscience Section), 94*, 28l-291, doi:10.1016/0168-9622(92)90003-S.

Tiedemann, R., M. Sarnthein, and N.J. Shackleton (1994), Astronomic timescale for the Pliocene Atlantic $\delta^{18}O$ and dust flux records of Ocean Drilling Program Site 659. *Paleoceanography, 9*, 619–638, doi:10.1029/94PA00208.

Thiede, J., A. Winkler, T. Wolf-Welling, O. Eldholm, A.M. Myhre, K.-H. Baumann, R. Henrich, and R. Stein (1998), Late Cenozoic history of the polar north Atlantic: Results from Ocean Drilling, *Quat. Sci. Rev., 17*, 185-208, doi:10.1016/S0277-3791(97)00076-0.

Tütken, T., A. Eisenhauer, B. Wiegand, and B.T. Hansen (2002), Glacial-interglacial cycles in Sr and Nd isotopic composition of Arctic marine sediments triggered by the Svalbard/Barents Sea ice sheet, *Mar. Geol., 182*, 351–372, doi:10.1016/S0025-3227(01)00248-1.

Vance, D., and K. Burton (1999), Neodymium Isotopes in Planktonic Foraminifera: A Record of the Response of Continental Weathering and Ocean Circulation Rates to Climate Change. *Earth Planet. Sci. Lett, 173*, 365-379, doi: 10.1016/s0012-821x(99)00244-7.

Vance, D., A. E. Scrivner, P. Beney, M. Staubwasser, G. M. Henderson, and N. C. Slowey (2004), The Use of Foraminifera as a Record of the Past Neodymium Isotope Composition of Seawater. *Paleoceanography, 19*, 17. Pa2009, doi: 10.1029/2003pa000957.

Venz, K.A., D.A. Hodell, C. Stanton, and D. Warnke (1999), A 1.0 Myr record of Glacial North Atlantic Intermediate Water variability from ODP Site 982 in the northeast Atlantic, *Paleoceanography*, 14, 42-52, doi:10.1029/1998PA900013.

Venz, K.A., and D.A. Hodell (2002), New evidence for changes in Plio-Pleistocene deep water circulation from Southern Ocean ODP Leg 177 Site 1090, *Palaeogeogr., Palaeoclimatol., Palaeoecol., 182*, 197-220, doi:10.1016/S0031-0182(01)00496-5.

Vinje, T. (2001), Anomalies and Trends of Sea ice Extent and Atmospheric Circulation in the Nordic Seas during the Period 1864-1998, *J. Clim., 14*, 255-267, doi:10.1175/1520-0442(2001)014.

von Blanckenburg, F., and T.F. Nägler (2001), Weathering versus circulation-controlled changes in radiogenic isotope tracer composition of the Labrador Sea and North Atlantic Deep Water, *Paleoceanography, 16*, 424-434, doi:10.1029/2000PA000550.

Vorontsov, A.A., V.V. Yarmolyuk, G.S. Fedoseev, A.V. Nikiforov, and G.P. Sandimirova (2010), Isotopic and Geochemical Zoning of Devonian Magmatism in the Altai–Sayan Rift System: Composition and Geodynamic Nature of Mantle Sources, *Petrology, 18*, 596-609, doi:10.1134/S0869591110060032.

Wahsner, M., C. Müller, R. Stein, G. Ivanov, M. Levitan, E. Shelekova, and G. Tarasov (1999), Clay-mineral distribution in surface sediments of the Eurasian Arctic Ocean and continental margin as indicator for source areas and transport pathways - a synthesis, *Boreas*, 28, 215-233, doi:10.1080/030094899421272.

Williams, D.F., J. Peck, E.B. Karabanov, A.A. Prokopenko, V. Kravchinsky, J. King, and M.I. Kuzmin (1997), Lake Baikal record of continental climate response to orbital insolation during the past 5 million years. *Science, 278,* 1114–1117, doi:10.1126/science.278.5340.1114.

Wilson, D.J., A.M. Piotrowski, A. Galy, and I.N. McCave (2012) A boundary exchange influence on deglacial neodymium isotope records from the deep western Indian Ocean, *Earth Planet. Sci. Lett, 341*, 35-47, doi: 10.1016/j.epsl.2012.06.009

Winter, B., C.M. Johnson, and D.L. Clark (1997), Strontium, neodymium and lead isotope variations of authigenic silicate sediment components from the late Cenozoic Arctic Ocean: Implications for sediment provenance and the source of trace metals in sea water, *Geochim. Cosmochim. Acta*, 61, 4181– 4200, doi:10.1016/S0016-7037(97)00215-9.

Wolf, T.C.W., and J. Thiede (1991), History of terrigenous sedimentation during the past 10 m.y. in the North Atlantic (ODP Legs 104 and 105 and DSDP Leg 81). *Mar. Geol., 101*, 83–102, doi:10.1016/0025-3227(91)90064-B.

Wolf-Welling, T.C.W., J. Thiede, A.M. Myhre and Leg 151 Shipboard scientific party, (1995), Bulk sediment parameter and coarse fraction analysis: Paleoceanographic implications of Fram Strait Sites 908 and 909, ODP Leg 151 (NAAG), *Eos Transactions, 76*, supplement, 166.

Appendix

Table A.1 (suppl. CHAPTER 2): ODP Site locations including water depth and carbonate content

	North Atlantic Ocean		**Nordic Seas**			
	Site 984	*Site 982*	*Site 907*	*Site 644*	*Site 986*	*Site 911*
Latitude, Longitude	61°25,517' N 24°04,949' W	57°30.992' N 15°52.001' W	69°14,989' N 12°41,894' W	66°40.700' N 04°34.600' E	77°20.431' N 09°04.664' E	80°28.466'N 08°13.640'E
Location	Bjørn Drift	Rockall Plateau	Icelandic Sea	Vøring Plateau	Svalbard shelf	Yermak Plateau
Water depth	1648m	1135m	1800m	1220m	2051m	906m
carbonate content	0.4% and 32.2%, with an average value of 8.0%	86%	26%-62%	1%-5% detrital carbonates 10%-25% detrital carbonate	0.7% to 10%	1% and 6%

Table A.2: Nordic Sea and North Atlantic Ocean down core leachate, bulk digest and foraminifera radiogenic isotope data

					carbonate fraction	*leach method A*		*leach method B*		*detrital fraction*		*cleaned benthic foraminifera*	*cleaned planktonic foraminifera*
Location	leg/**site**/core	**Core section**	**Depth [m]**	**Age [ka]**	ε_{Nd}	ε_{Nd}	$^{87}Sr/^{86}Sr$	ε_{Nd}	$^{87}Sr/^{86}Sr$	ε_{Nd}	$^{87}Sr/^{86}Sr$	ε_{Nd}	ε_{Nd}
Iceland Sea; 1800 m water depth; 69°14.989'N 12°41.894'W	151/**907**/A	1H-1/33-35	0.3	10.4	-8.84	-6.48	0.709305	-8.85	0.709130	-8.62	-	-8.84	-9.75
	162/**907**/C	3H-2/34-36	19.6	1022.6	-	-5.02	0.709617	-5.86	0.708785	-	-	-	-
	162/**907**/C	3H-2/63-65	19.9	1035.8	-	-5.70	-	-7.33	0.708646	-	-	-	-
	151/**907**/A	3H-4/142-144	22.7	1225.6	-	-1.25	0.709050	-	-	-	-	-	-
	151/**907**/A	3H-5/22-24	23.0	1240.1	-	-4.64	0.709211	-	-	-	-	-	-
	151/**907**/A	4H-1/73-75	27.0	1464.4	-	-3.45	0.709198	-5.28	0.708773	-	-	-	-
	151/**907**/A	4H-1/113-115	27.4	1485.1	-	1.11	0.708930	-0.66	0.708702	-	-	-	-
	151/**907**/A	4H-5/52-54	32.8	1732.2	-	-6.13	0.708973	-	-	-	-	-	-
	151/**907**/A	5H-3/15-17	39.0	2093.0	-	-2.23	-	-4.20	0.708694	-	-	-	-
	151/**907**/A	5H-3/46-48	39.3	2105.4	-	-4.93	-	-6.43	0.708646	-	-	-	-
	151/**907**/A	6H-3/3-5	48.3	2415.1	-	-3.37	0.709406	-2.98	0.708719	-	-	-	-
	151/**907**/A	6H-3/47-49	48.8	2423.6	-	-	-	-3.37	0.708748	-	-	-	-
	162/**907**/C	6H-4/45-47	51.6	2437.5	-	-4.94	0.709252	-5.12	0.708726	-	-	-	-
	151/**907**/A	6H-6/115-117	54.0	2655.6	-	4.48	0.708196	-0.20	0.708589	-	-	-	-
	151/**907**/A	6H-7/28-30	54.6	2675.3	-	-4.82	0.709281	-5.12	0.708744	-	-	-	-
	162/**907**/C	7H-3/117-119	61.8	2893.5	-	-0.67	-	-	-	-	-	-	-
	151/**907**/A	7H-3/115-117	59.0	2919.3	-	-4.63	0.709422	-	-	-	-	-	-

Table A.2 (continued)

					carbonate fraction	*leach fraction A*		*leach fraction B*		*detrital fraction*		*cleaned planktonic foraminifera*	*uncleaned planktonic foraminifera*
Location	leg/**site**/core	**Core section**	**Depth [m]**	**Age [ka]**	ε_{Nd}	ε_{Nd}	$^{87}Sr/^{86}Sr$	ε_{Nd}	$^{87}Sr/^{86}Sr$	ε_{Nd}	$^{87}Sr/^{86}Sr$	ε_{Nd}	ε_{Nd}
South of Iceland; 1648 m water depth 61°25.517'N 24°04.949' W	162/**984**/B	1H-1/3-5	0.03	0.0	-	3.85	0.709114	-	-	5.52	0.704834	-1.81	-
	162/**984**/B	1H-1/3-5	0.03	0.0	-	6.49	0.709147	-	-	5.28	0.704852	-	-
	162/**984**/B	1H-1/3-5	0.03	0.0	-	4.63	0.709099	-	-	5.56	0.704900	-	-
	162/**984**/B	1H-1/3-5	0.03	0.0	-	3.99	0.709090	-	-	5.36	0.705297	-	-
	162/**984**/B	14H-3/110-112	126.6	1028.8	0.66	4.79	0.708870	0.29	0.709097	-	-	1.18	-0.22
	162/**984**/B	14H-4/80-82	127.8	1038.0	-1.64	0.54	0.708783	-1.91	0.708999	-	-	-3.68	-3.53
	162/**984**/B	17H-7/34-36	160.3	1416.0	-0.40	1.97	0.708727	-0.45	-	-	-	-1.92	-1.94
	162/**984**/B	33X-3/99-101	305.8	2345.0	1.52	4.06	0.708709	1.68	0.708942	-	-	-0.37	-0.75
Western shelf of Svalbard; 2051 m water depth; 77°20.431' N 9°04.664' E	162/**986**/C	1H-1/0-2	0.0	0.0	-	-10.16	0.709656	-10.30	-	-11.31	0.720987	-	-
	162/**986**/C	6H-5/72-74	52.2	321.3	-	-8.66	0.708911	-11.55	-	-	-	-	-
	162/**986**/C	7H-3/74-76	58.0	356.9	-	-10.28	0.709908	-11.72	-	-	-	-	-
	162/**986**/C	8H-3/74-76	70.2	431.6	-	-10.35	-	-	-	-15.18	0.719432	-	-
	162/**986**/C	13X-4/74-76	114.7	705.6	-	-11.76	0.712575	-14.08	0.709383	-	-	-	-
	162/**986**/C	15X-4/74-76	133.5	845.4	-	-9.40	-	-	-	-11.75	0.725808	-	-
	162/**986**/D	6R-1/72-74	436.6	1457.3	-	-9.46	0.710397	-10.80	0.709515	-	-	-	-
	162/**986**/D	9R-1/23-25	464.9	1512.5	-	-10.44	0.711053	-11.04	0.709641	-14.05	0.728950	-	-
	162/**986**/C	34X-2/52-54	304.1	2030.1	-	-11.59	0.714148	-	-	-13.53	0.729752	-	-
	duplicate	*34X-2/52-54*	*304.1*	*2030.1*	-	*-12.16*	*0.714289*	-	-	-	-	-	-
	162/**986**/C	38X-3/120-122	344.8	2301.8	-	-10.86	0.712657	-11.85	0.711359	-	-	-	-
	162/**986**/C	39X-2/130-132	356.0	2376.7	-	-9.11	0.712474	-11.11	0.709648	-	-	-	-
	162/**986**/C	40X-2/23-25	361.5	2413.5	-	-11.07	0.712776	-11.64	0.710781	-15.23	0.726463	-	-

Table A.2 (continued)

					carbonate fraction	*leach fraction A*		*leach fraction B*		*detrital fraction*		*cleaned foraminifera*	*uncleaned foraminifera*
Location	leg/**site**/core	**Core section**	**Depth [m]**	**Age [ka]**	ε_{Nd}	ε_{Nd}	$^{87}Sr/^{86}Sr$	ε_{Nd}	$^{87}Sr/^{86}Sr$	ε_{Nd}	$^{87}Sr/^{86}Sr$	ε_{Nd}	ε_{Nd}
	162/**986**/D	51R-7/52-54	877.6	2691.2	-	-10.85	0.710381	-	-	-11.45	0.719824	-	-
	162/**986**/D	58R-1/74-76	936.4	3009.8	-10.78	-8.97	0.711382	-11.02	-	-	-	-	-
	duplicate	*58R-1/74-76*	*936.4*	*3009.8*	-	*-8.77*	*0.711942*	-	-	-	-	-	-
Vøring Plateau; Norwegian shelf; 1220 m water depth; 66°40.700'N 04°34.600'E	104/**644**/A	1H-1/2-6	0.0	0.0	-10.12	-9.59	-	-9.93	-	-11.26	0.721425	-	-
	104/**644**/A	8H-1/23-25	63.9	577.1	-	-11.12	-	-	-	-13.24	0.733083	-	-
	104/**644**/A	8H-6/22-24	71.4	644.9	-	-9.23	-	-10.24	0.709265	-	-	-	-
	104/**644**/A	10H-3/78-80	86.5	774.4	-	-6.92	-	-	-	-11.99	0.722602	-	-
	104/**644**/A	14H-3/60-62	123.3	1134.9	-12.35	-11.11	0.709772	-12.24	-	-15.25	0.725116	-	-
	104/**644**/A	14H-4/82-84	126.0	1167.7	-10.34	-7.37	0.709636	-10.29	-	-	-	-	-
	duplicate	*14H-4/82-84*	*126.0*	*1167.7*	-	*-8.19*	*0.709389*	-	-	-	-	-	-
	104/**644**/A	18H-3/42-44	162.1	1606.1	-	-9.47	-	-	-	-12.64	0.727102	-	-
	104/**644**/A	23H-5/120-122	201.3	2155.6	-11.17	-10.17	0.709428	-11.47	-	-	-	-	-
	104/**644**/A	24H-4/16-18	205.2	2207.4	-10.80	-9.73	0.709941	-10.92	0.709197	-12.66	-	-	-
	104/**644**/A	26H-2/62-64	212.6	2305.8	-	-7.20	-	-9.38	-	-	-	-	-
	104/**644**/A	34H-6/101-103	253.0	2842.3	-	-9.67	0.709062	-	-	-10.78	0.718474	-	-
	162/**982**/A	1H-1/0-2	0.0	0.0	-12.75	-10.99	0.709273	-12.55	-	-9.99	0.714350	-	-
	162/**982**/A	1H-3/134-136	4.3	217.0	-	-8.04	0.709449	-9.33	0.709181	-	-	-	-
	162/**982**/A	2H-1/82-84	9.0	395.0	-	-6.08	-	-	-	-9.42	0.717082	-	-
	duplicate	*2H-1/82-84*	*9.0*	*395.0*	-	*-6.52*	-	-	-	-	-	-	-
	162/**982**/A	4H-2/100-102	29.7	1172.0	-	-12.03	0.709164	-	-	-11.38	0.717431	-	-
	162/**982**/A	4H-5/85-87	34.1	1462.0	-12.92	-12.67	0.709135	-12.51	-	-9.11	0.709517	-	-
	duplicate	*4H-5/85-87*	*34.1*	*1462.0*	-	*-12.36*	*0.709085*	-	-	-	-	-	-
	162/**982**/A	4H-5/121-123	34.4	1490.0	-11.00	-10.74	0.709124	-10.78	-	-	-	-	-

Table A.2 (continued)

					carbonate fraction	*leach fraction A*		*leach fraction B*		*detrital fraction*		*cleaned foraminifera*	*uncleaned foraminifera*
Location	leg/**site**/core	**Core section**	**Depth [m]**	**Age [ka]**	ε_{Nd}	ε_{Nd}	$^{87}Sr/^{86}Sr$	ε_{Nd}	$^{87}Sr/^{86}Sr$	ε_{Nd}	$^{87}Sr/^{86}Sr$	ε_{Nd}	ε_{Nd}
	duplicate	*4H-5/121-123*	*34.4*	*1490.0*	-	*-10.51*	*0.709053*	-	-	-	-	-	-
	162/**982**/A	5H-2/6-8	38.3	1700.0	-	-9.57	0.709126	-	-	-4.09	0.712678	-	-
	162/**982**/A	5H-3/79-81	40.5	1795.0	-	-9.14	0.709098	-9.50	0.709075	-	-	-	-
	162/**982**/A	6H-3/29-31	49.5	2280.0	-10.98	-10.20	0.709047	-10.70	-	-	-	-	-
	162/**982**/A	6H-3/72-74	49.9	2305.0	-10.97	-10.96	0.709061	-10.90	-	-8.70	0.710014	-	-
	162/**982**/A	8H-1/49-51	65.7	2975.0	-9.97	-10.31	0.709015	-10.63	-	-	-	-	-
Yermak Plateau; N-W Svalbard; 906 m water depth; 80°28.466'N 8°13.640'E	151/**911**/A	1H-1/0-3	0.0	0.0	-	-9.72	0.710172	-11.04	0.709181	-	-	-	-
	151/**911**/A	2H-1/75-77	10.3	111.2	-	-	-	-12.11	-	-	0.724322	-	-
	151/**911**/A	4H-4/100-102	34.0	368.9	-	-9.87	0.712310	-11.68	0.709303	-12.16	0.722994	-	-
	151/**911**/A	5H-5/100-102	45.0	488.2	-	-8.54	0.710479	-10.36	0.710515	-	-	-	-
	151/**911**/A	6H-5/100-102	54.5	591.3	-	-9.22	-	-10.99	0.710529	-	-	-	-
	151/**911**/A	8H-1/75-77	66.0	715.5	-	-4.86	0.711392	-6.85	0.708907	-8.42	0.716076	-	-
	151/**911**/A	9H-3/100-102	77.8	847.8	-	-9.36	-	-10.14	-	-10.83	0.718050	-	-
	151/**911**/A	10H-5/100-102	91.2	997.2	-	-8.61	-	-11.36	0.710211	-	-	-	-
	151/**911**/A	12H-5/100-102	108.9	1113.4	-	-9.45	-	-11.02	0.710943	-	-	-	-
	151/**911**/A	13H-2/58-60	113.5	1137.4	-	-8.44	0.709350	-9.94	0.709024	-	-	-	-
	151/**911**/A	15H-2/99-101	132.9	1239.0	-	-	-	-10.76	-	-12.17	0.720313	-	-
	151/**911**/A	17X-3/100-102	153.4	1346.4	-	-8.24	-	-9.70	0.709673	-	-	-	-
	151/**911**/A	18X-5/100-102	165.6	1410.3	-	-9.65	-	-10.88	0.709961	-11.11	0.719787	-	-
	151/**911**/A	21X-4/100-102	193.4	1555.8	-	-8.70	0.712453	-11.24	0.712495	-	-	-	-
	151/**911**/A	24X-3/100-102	219.7	1693.5	-	-10.10	0.711542	-10.73	0.709425	-11.11	0.720894	-	-
	151/**911**/A	37X-6/12-14	349.0	2504.0	-	-8.65	0.710061	-10.00	0.709460	-10.66	0.720409	-	-
	151/**911**/A	38X-1/62-64	352.5	2528.0	-	-8.28	-	-9.71	0.709667	-	-	-	-
	151/**911**/A	38X-8/9-11	361.3	2589.3	-	-7.04	-	-8.75	0.709251	-	-	-	-

Table A.2 (continued)

					carbonate fraction	*leach fraction A*		*leach fraction B*		*detrital fraction*		*cleaned foraminifera*	*uncleaned foraminifera*
Location	leg/**site**/core	**Core section**	**Depth [m]**	**Age [ka]**	ε_{Nd}	ε_{Nd}	$^{87}Sr/^{86}Sr$	ε_{Nd}	$^{87}Sr/^{86}Sr$	ε_{Nd}	$^{87}Sr/^{86}Sr$	ε_{Nd}	ε_{Nd}
	151/**911**/A	39X-2/39-41	363.2	2601.3	-	-	-	-10.06	-	-10.90	0.719379	-	-
	151/**911**/A	40X-6/28-30	377.8	2692.5	-	-7.17	0.709477	-7.96	0.708993	-9.19	0.716004	-	-
	151/**911**/A	44X-3/28-30	412.6	3087.4	-	-9.69	0.710139	-10.97	0.709855	-12.90	0.718175	-	-

Table A.3 (suppl. Chapter 2): Nordic Sea and North Atlantic Ocean down core leachate and bulk digest Pb isotope data

					leach method A			*leach method B*			*detrital fraction*		
Location	leg/**site**/core	**Core section**	**Depth [m]**	**Age [ka]**	^{206}**Pb/^{204}Pb**	^{207}**Pb/^{204}Pb**	^{208}**Pb/^{204}Pb**	^{206}**Pb/^{204}Pb**	^{207}**Pb/^{204}Pb**	^{208}**Pb/^{204}Pb**	^{206}**Pb/^{204}Pb**	^{207}**Pb/^{204}Pb**	^{208}**Pb/^{204}Pb**
Iceland Sea; 1800 m water depth; 69°14.989'N 12°41.894'W	162/**907**/C	3H-2/34-36	0.3	10.4	18.678	15.580	38.670	18.666	15.585	38.661	-	-	-
	151/**907**/A	4H-1/73-75	19.6	1022.6	18.904	15.614	38.825	18.887	15.621	38.822	-	-	-
	151/**907**/A	4H-1/113-115	19.9	1035.8	18.885	15.611	38.788	18.880	15.607	38.767	-	-	-
	151/**907**/A	6H-3/3-5	22.7	1225.6	18.687	15.594	38.673	18.662	15.589	38.633	-	-	-
	162/**907**/C	6H-4/45-47	23.0	1240.1	18.669	15.590	38.688	18.659	15.591	38.663	-	-	-
	151/**907**/A	6H-6/115-117	27.0	1464.4	18.770	15.602	38.728	18.775	15.589	38.700	-	-	-
	151/**907**/A	6H-7/28-30	27.4	1485.1	18.728	15.598	38.752	18.716	15.593	38.714	-	-	-
South of Iceland; 1648 m water depth; 61°25.517'N 24°04.949'W	162/**984**/B	14H-3/110-112	137.5	1028.8	18.944	15.642	38.983	18.936	15.600	38.972	-	-	-
	162/**984**/B	14H-4/80-82	138.7	1038	18.791	15.623	38.796	18.768	15.607	38.742	-	-	-
	162/**984**/B	17H-7/34-36	174.2	1416	18.841	15.610	38.797	18.875	15.660	38.799	-	-	-
	162/**984**/B	33X-3/99-101	328.3	2345	18.729	15.620	38.709	18.690	15.584	38.608	-	-	-
Yermak Plateau; N-W Svalbard; 906 m water depth; 80°28.466'N 8°13.640'E	151/**911**/A	2H-1/75-77	10.3	271.8	-	-	-	19.064	15.645	38.999	19.038	15.634	39.012
	151/**911**/A	4H-4/100-102	34.0	430.7	19.145	15.652	38.991	19.133	15.656	38.993	19.016	15.638	38.961
	151/**911**/A	5H-5/100-102	45.0	504.3	18.872	15.619	38.830	18.851	15.620	38.794	-	-	-
	151/**911**/A	6H-5/100-102	54.5	567.9	18.959	15.648	38.939	18.925	15.630	38.850	-	-	-
	151/**911**/A	8H-1/75-77	65.9	644.5	18.650	15.583	38.538	-	-	-	18.711	15.593	38.896
	151/**911**/A	9H-3/100-102	77.8	723.7	18.757	15.602	38.736	18.754	15.610	38.749	18.754	15.595	38.756
	151/**911**/A	10H-5/100-102	91.2	813.4	18.999	15.637	38.876	18.984	15.638	38.856	-	-	-
	151/**911**/A	12H-5/100-102	108.9	931.8	18.988	15.638	39.011	18.972	15.637	38.982	-	-	-
	151/**911**/A	13H-2/58-60	113.5	962.4	18.644	15.591	38.691	18.627	15.586	38.633	-	-	-
	151/**911**/A	15H-2/99-101	132.9	1092.3	-	-	-	19.053	15.649	38.963	18.905	15.625	39.017
	151/**911**/A	17X-3/100-102	153.4	1229.5	18.679	15.593	38.699	18.655	15.582	38.634	-	-	-

Table A.3 (continued)

					leach method A			*leach method B*			*detrital fraction*		
Location	leg/**site**/core	**Core section**	**Depth [m]**	**Age [ka]**	$^{206}Pb/^{204}Pb$	$^{207}Pb/^{204}Pb$	$^{208}Pb/^{204}Pb$	$^{206}Pb/^{204}Pb$	$^{207}Pb/^{204}Pb$	$^{208}Pb/^{204}Pb$	$^{206}Pb/^{204}Pb$	$^{207}Pb/^{204}Pb$	$^{208}Pb/^{204}Pb$
	151/**911**/A	18X-5/100-102	165.6	1311.1	18.907	15.630	38.825	18.897	15.625	38.799	18.920	15.635	38.903
	151/**911**/A	21X-4/100-102	193.4	1497.1	18.926	15.619	38.880	18.910	15.618	38.855			
	151/**911**/A	24X-3/100-102	219.7	1673.1	18.672	15.584	38.679	18.680	15.600	38.726	18.747	15.598	38.822
	151/**911**/A	37X-6/12-14	349.0	2538.3	18.760	15.598	38.753	18.751	15.599	38.739	18.808	15.609	38.825
	151/**911**/A	38X-1/62-64	352.5	2561.6	18.718	15.595	38.699	18.728	15.616	38.731	-	-	-
	151/**911**/A	39X-2/39-41	363.2	2633.3	-	-	-	18.641	15.564	38.580	18.738	15.589	38.751
	151/**911**/A	40X-6/28-30	377.8	2730.9	18.569	15.576	38.567	18.612	15.601	38.589	18.615	15.588	38.608
	151/**911**/A	44X-3/28-30	412.6	3185.2	18.711	15.588	38.716	18.696	15.597	38.720	18.716	15.592	38.796
	151/**911**/A	2H-1/75-77	10.3	271.8	-	-	-	19.064	15.645	38.999	19.038	15.634	39.012
	151/**911**/A	4H-4/100-102	34.0	430.7	19.145	15.652	38.991	19.133	15.656	38.993	19.016	15.638	38.961
	151/**911**/A	5H-5/100-102	45.0	504.3	18.872	15.619	38.830	18.851	15.620	38.794	-	-	-
	151/**911**/A	6H-5/100-102	54.5	567.9	18.959	15.648	38.939	18.925	15.630	38.850	-	-	-
	151/**911**/A	8H-1/75-77	65.9	644.5	18.650	15.583	38.538	-	-	-	18.711	15.593	38.896
	151/**911**/A	9H-3/100-102	77.8	723.7	18.757	15.602	38.736	18.754	15.610	38.749	18.754	15.595	38.756
	151/**911**/A	10H-5/100-102	91.2	813.4	18.999	15.637	38.876	18.984	15.638	38.856	-	-	-
	151/**911**/A	12H-5/100-102	108.9	931.8	18.988	15.638	39.011	18.972	15.637	38.982	-	-	-
	151/**911**/A	13H-2/58-60	113.5	962.4	18.644	15.591	38.691	18.627	15.586	38.633	-	-	-
	151/**911**/A	15H-2/99-101	132.9	1092.3	-	-	-	19.053	15.649	38.963	18.905	15.625	39.017
	151/**911**/A	17X-3/100-102	153.4	1229.5	18.679	15.593	38.699	18.655	15.582	38.634	-	-	-
	151/**911**/A	18X-5/100-102	165.6	1311.1	18.907	15.630	38.825	18.897	15.625	38.799	18.920	15.635	38.903
	151/**911**/A	21X-4/100-102	193.4	1497.1	18.926	15.619	38.880	18.910	15.618	38.855	-	-	-
	151/**911**/A	24X-3/100-102	219.7	1673.1	18.672	15.584	38.679	18.680	15.600	38.726	18.747	15.598	38.822
	151/**911**/A	37X-6/12-14	349.0	2538.3	18.760	15.598	38.753	18.751	15.599	38.739	18.808	15.609	38.825

Table A.3 (continued)

					leach method A			*leach method B*			*detrital fraction*		
Location	leg/**site**/core	**Core section**	**Depth [m]**	**Age [ka]**	**$^{206}Pb/^{204}Pb$**	**$^{207}Pb/^{204}Pb$**	**$^{208}Pb/^{204}Pb$**	**$^{206}Pb/^{204}Pb$**	**$^{207}Pb/^{204}Pb$**	**$^{208}Pb/^{204}Pb$**	**$^{206}Pb/^{204}Pb$**	**$^{207}Pb/^{204}Pb$**	**$^{208}Pb/^{204}Pb$**
	151/**911**/A	38X-1/62-64	352.5	2561.6	18.718	15.595	38.699	18.728	15.616	38.731	-	-	-
	151/**911**/A	39X-2/39-41	363.2	2633.3	-	-	-	18.641	15.564	38.580	18.738	15.589	38.751
	151/**911**/A	40X-6/28-30	377.8	2730.9	18.569	15.576	38.567	18.612	15.601	38.589	18.615	15.588	38.608
	151/**911**/A	44X-3/28-30	412.6	3185.2	18.711	15.588	38.716	18.696	15.597	38.720	18.716	15.592	38.796
Western shelf of Svalbard; 2051 m water depth; 77°20.431' N 9°04.664' E	162/**986**/C	1H-1/0-2	0.0	0.0	18.783	15.643	38.694	-	-	-	18.847	15.633	38.799
	162/**986**/C	6H-5/72-74	52.2	321.3	18.686	15.597	38.710	18.748	15.597	38.709	-	-	-
	162/**986**/C	7H-3/74-76	58.0	356.9	18.965	15.630	38.858	18.950	15.631	38.843	-	-	-
	162/**986**/C	8H-7/74-76	70.2	431.6	18.519	15.576	38.742	-	-	-	18.752	15.576	39.293
	162/**986**/C	15X-3/74-76	132.0	830.6	19.189	15.664	39.138	19.207	15.678	38.981	-	-	-
	162/**986**/C	15X-4/74-76	133.5	845.4	18.980	15.641	38.922	19.219	15.657	38.957	18.897	15.622	38.840
	162/**986**/D	6R-1/72-74	436.6	1457.3	18.921	15.628	38.869	18.919	15.632	38.858	-	-	-
	162/**986**/D	9R-1/23-25	464.9	1512.5	18.783	15.596	38.754	18.853	15.600	38.698	18.923	15.608	39.074
	162/**986**/C	34X-2/52-54	304.1	2030.1	18.584	15.580	38.820	-	-	-	18.784	15.591	39.196
	duplicate	*34X-2/52-54*	*304.1*	*2030.1*	*18.695*	*15.596*	*38.863*	-	-	-	-	-	-
	162/**986**/C	39X-4/130-132	356.0	2376.7	18.907	15.617	38.870	18.917	15.626	38.836	-	-	-
	162/**986**/C	40X-2/23-25	361.5	2413.5	18.486	15.570	38.716	18.480	15.567	38.696	18.786	15.590	39.108
	162/**986**/D	51R-7/52-54	877.6	2691.2	18.798	15.600	38.756	-	-	-	18.640	15.576	38.634
	162/**986**/D	58R-1/74-76	936.4	3009.8	19.026	15.676	39.006	18.845	15.574	38.693	-	-	-
	duplicate	*58R-1/74-76*	*936.4*	*3009.8*	*19.008*	*15.676*	*38.963*	-	-	-	-	-	-
Vøring Plateau, Norwegian shelf; 1220 m water depth;	104/**644**/A	1H-1/2-6	0.0	0.0	18.950	15.668	38.792	-	-	-	18.884	15.638	38.686
	104/**644**/A	8H-1/23-25	63.9	577.1	19.661	15.730	39.218	-	-	-	19.380	15.687	39.011
	104/**644**/A	10H-3/78-80	86.5	774.4	18.823	15.617	38.721	-	-	-	18.808	15.613	38.749
	104/**644**/A	14H-3/60-62	123.3	1134.9	18.934	15.615	38.958	18.952	15.617	38.946	18.741	15.577	38.733
	104/**644**/A	14H-4/82-84	126.0	1167.7	19.225	15.681	39.008	19.207	15.678	38.981	-	-	-

Table A.3 (continued)

					leach method A			*leach method B*			*detrital fraction*		
Location	leg/**site**/core	**Core section**	**Depth [m]**	**Age [ka]**	**$^{206}Pb/^{204}Pb$**	**$^{207}Pb/^{204}Pb$**	**$^{208}Pb/^{204}Pb$**	**$^{206}Pb/^{204}Pb$**	**$^{207}Pb/^{204}Pb$**	**$^{208}Pb/^{204}Pb$**	**$^{206}Pb/^{204}Pb$**	**$^{207}Pb/^{204}Pb$**	**$^{208}Pb/^{204}Pb$**
66°40.700'N 04°34.600'E	*duplicate*	*14H-4/82-84*	*126.0*	*1167.7*	*19.215*	*15.673*	*38.984*	-	-	-	-	-	-
	104/**644**/A	18H-3/42-44	162.1	1606.1	19.316	15.683	39.045	-	-	-	19.103	15.647	38.880
	104/**644**/A	23H-5/120-122	201.3	2155.6	19.185	15.679	38.979	19.176	15.673	38.957	-	-	-
	104/**644**/A	24H-4/16-18	205.2	2207.4	19.240	15.674	39.020	19.219	15.657	38.957	19.107	15.659	38.894
	104/**644**/A	34H-6/100-104	253.0	2842.3	19.035	15.651	38.894	-	-	-	19.034	15.643	38.871

Table A.4 (suppl. Chapter 3): Nordic Sea down core leachate and bulk digest isotope data of Site 911

				leach fraction (leach method B)					*detrital fraction*				
Location	**Core section**	**Depth [m]**	**Age [ka]**	**ε_{Nd}**	**$^{87}Sr/^{86}Sr$**	**$^{206}Pb/^{204}Pb$**	**$^{207}Pb/^{204}Pb$**	**$^{208}Pb/^{204}Pb$**	**ε_{Nd}**	**$^{87}Sr/^{86}Sr$**	**$^{206}Pb/^{204}Pb$**	**$^{207}Pb/^{204}Pb$**	**$^{208}Pb/^{204}Pb$**
Yermak Plateau; N-W Svalbard; 906 m water depth; 80°28.466'N 8°13.640'E (leg/**site**/core 151/**911**/A)	1H-1/0-3	0.00	0.00	-11.04	0.709181	18.8506	15.6463	38.7545	-	-	-	-	-
	2H-1/75-77	10.26	111.24	-12.11	-	19.0640	15.6449	38.9995	-	0.724322	19.0382	15.6340	39.0120
	4H-4/100-102	34.01	368.91	-11.68	0.709303	19.1334	15.6563	38.9935	-12.16	0.722994	19.0160	15.6385	38.9610
	5H-5/100-102	45.01	488.23	-10.36	0.710515	18.8511	15.6196	38.7935	-	-	-	-	-
	6H-5/100-102	54.51	591.28	-10.99	0.710529	18.9247	15.6301	38.8502	-	-	-	-	-
	8H-1/75-77	65.96	715.48	-6.85	0.708907	-	-	-	-8.42	0.716076	18.7106	15.5928	38.8959
	8H-1/79.5-81.5	66.01	716.03	-9.90	-	18.6464	15.5907	38.6296	-	-	-	-	-
	8H-3/41-42.5	68.62	744.34	-9.05	0.709136	18.6258	15.5900	38.5931	-	-	-	-	-
	9H-3/100-102	77.81	847.78	-10.14	-	18.7544	15.6102	38.7488	-10.83	0.718050	18.7539	15.5953	38.7559
	10H-5/100-102	91.21	997.24	-11.36	0.710211	18.9836	15.6382	38.8562	-	-	-	-	-
	10H-CC/27.5-29	93.49	1014.64	-11.04	-	18.6918	15.6026	38.7058	-	-	-	-	-
	11H-4/124-126	100.45	1067.77	-11.53	-	18.8724	15.6220	38.8492	-	-	-	-	-
	12H-5/100-102	108.91	1113.41	-11.02	0.710943	18.9720	15.6372	38.9823	-	-	-	-	-
	13H-2/58-60	113.49	1137.39	-9.94	0.709024	18.6273	15.5856	38.6330	-	-	-	-	-
	15H-2/100-102	132.9	1239.02	-10.76	-	19.0525	15.6487	38.9629	-12.17	0.720313	18.9045	15.6248	39.0172
	15H-6/93-95	138.84	1270.12	-9.44	-	18.6591	15.5955	38.6495	-	-	-	-	-
	16X-1/91.5-93	140.83	1280.53	-10.65	-	18.7290	15.6054	38.7407	-	-	-	-	-
	16X-2/99-101	142.4	1288.75	-10.04	-	18.7937	15.6126	38.7693	-	-	-	-	-
	16X-2/126-127.5	142.67	1290.17	-10.56	0.709072	18.7350	15.6027	38.7223	-	-	-	-	-
	16X-4/18-19.5	144.59	1300.22	-7.81	-	18.7861	15.6109	38.5978	-	-	-	-	-
	16X-5/58-60	146.49	1310.17	-11.54	-	19.0514	15.6419	38.9185	-	-	-	-	-
	16X-CC/45-47	148.4	1320.17	-11.87	0.709243	18.9962	15.6371	38.9430	-	-	-	-	-
	17X-1/91-92.5	150.32	1330.22	-9.66	-	18.6129	15.5965	38.6168	-	-	-	-	-
	17X-2/131-132.5	152.23	1340.22	-9.09	-	18.6203	15.5876	38.6236	-	-	-	-	-

Table A.4 (continued)

Location	Core section	Depth [m]	Age [ka]	*leach fraction (leach method B)*					*detrital fraction*				
				ε_{Nd}	$^{87}Sr/^{86}Sr$	$^{206}Pb/^{204}Pb$	$^{207}Pb/^{204}Pb$	$^{208}Pb/^{204}Pb$	ε_{Nd}	$^{87}Sr/^{86}Sr$	$^{206}Pb/^{204}Pb$	$^{207}Pb/^{204}Pb$	$^{208}Pb/^{204}Pb$
	17X-3/100-102	153.41	1346.40	-9.70	0.709673	18.6554	15.5824	38.6339	-	-	-	-	-
	17X-4/25-26.5	154.16	1350.32	-9.39	0.709026	18.6363	15.5841	38.6268	-	-	-	-	-
	17X-CC/30-31.5	156.05	1360.22	-6.96	0.708916	18.6817	15.5969	-	-	-	-	-	-
	18X-1/0-2	157.96	1370.22	-11.00	-	18.9395	15.6374	38.9198	-	-	-	-	-
	18X-2/124-125.5	161.75	1390.06	-10.09	-	18.9964	15.6370	38.8247	-	-	-	-	-
	18X-4/45-47	163.69	1400.22	-10.91	0.709430	18.9029	15.6203	38.7507	-	-	-	-	-
	18X-5/99-100.5	165.59	1410.17	-10.50	-	18.7102	15.6029	38.7064	-	-	-	-	-
	18X-5/100-102	165.61	1410.27	-10.88	0.709961	18.8966	15.6246	38.7986	-11.11	0.719787	18.9204	15.6353	38.9031
	19X-1/85-86.5	169.46	1430.43	-11.46	-	18.8755	15.6195	38.8614	-	-	-	-	-
	20X-1/77-78.5	179.08	1480.80	-10.56	0.709365	18.8910	15.6340	38.8081	-	-	-	-	-
	21X-1/87-88.5	188.78	1531.58	-9.81	-	18.8310	15.6150	38.7725	-	-	-	-	-
	21X-4/100-102	193.41	1555.82	-11.24	0.712495	18.9095	15.6181	38.8546	-	-	-	-	-
	24X-3/100-102	219.71	1693.52	-10.73	0.709425	18.6801	15.6003	38.7259	-11.11	0.720894	18.7466	15.5984	38.8225
	27X-2/65-66	247.96	1840.29	-9.76	-	18.6947	15.5846	38.6516	-	-	-	-	-
	30X-5/65-66.5	281.26	2036.45	-11.14	-	18.8832	15.6193	38.8426	-	-	-	-	-
	31X-4/111-112	289.92	2096.17	-10.60	-	18.7094	15.5982	38.7117	-	-	-	-	-
	31X-6/69.5-71	292.51	2114.03	-9.41	0.709117	18.6998	15.5906	38.6632	-	-	-	-	-
	33X-3/108-109	307.69	2218.72	-9.48	-	18.5829	15.5861	38.6287	-	-	-	-	-
	35X-1/123-124	324.13	2332.10	-10.20	-	18.6603	15.5901	38.6650	-	-	-	-	-
	36X-1/68.5-70	333.3	2395.34	-6.80		18.6157	15.5769	38.4841	-	-	-	-	-
	37X-1/72-73.5	342.93	2461.76	-11.71		18.8202	15.6070	38.8036	-	-	-	-	-
	37X-6/12-14	349.05	2503.97	-10.00	0.709460	18.7514	15.5989	38.7393	-10.66	0.720409	18.8079	15.6090	38.8250
	38X-1/62-64	352.53	2527.97	-9.71	0.709667	18.7282	15.6161	38.7312	-	-	-	-	-
	38X-8/9-11	361.33	2589.31	-8.75	0.709251	-	-	-	-	-	-	-	-

Table A.4 (continued)

Location	Core section	Depth [m]	Age [ka]	*leach fraction (leach method B)*					*detrital fraction*				
				ε_{Nd}	$^{87}Sr/^{86}Sr$	$^{206}Pb/^{204}Pb$	$^{207}Pb/^{204}Pb$	$^{208}Pb/^{204}Pb$	ε_{Nd}	$^{87}Sr/^{86}Sr$	$^{206}Pb/^{204}Pb$	$^{207}Pb/^{204}Pb$	$^{208}Pb/^{204}Pb$
	39X-2/39-41	363.25	2601.31	-10.06	-	18.6412	15.5637	38.5803	-10.90	0.719379	18.7379	15.5889	38.7505
	40X-1/28-30	371.19	2650.94	-8.08	-	18.5553	15.5725	38.5432	-	-	-	-	-
	40X-6/28-30	377.84	2692.50	-7.96	0.708993	18.6125	15.6006	38.5887	-9.19	0.716004	18.6148	15.5881	38.6077
	41X-6/31-33	388.22	2757.38	-11.42	-	18.6969	15.5950	38.7177	-	-	-	-	-
	42X-7/82-84	397.86	2869.26	-11.14	-	18.7243	15.5908	38.7023	-	-	-	-	-
	43X-5/37-39	405.05	2975.74	-10.78	-	18.7554	15.6198	38.8067	-	-	-	-	-
	44X-3/28-30	412.59	3087.41	-10.97	0.709855	18.6955	15.5969	38.7204	-12.90	0.718175	18.7165	15.5917	38.7964
	45X-2/138-140	421.66	3221.73	-10.29	-	18.6024	15.5698	38.5876	-	-	-	-	-
	45X-5/105-107	425.48	3278.30	-11.02	-	18.7373	15.5975	38.7845	-	-	-	-	-
	46X-2/85-87	430.96	3359.46	-10.91	-	18.6872	15.5914	38.7473	-11.96	0.718576	18.6977	15.5877	38.7718
	46X-4/128-130	434.21	3407.59	-10.79	-	18.6208	15.5819	38.6408	-	-	-	-	-
	47X-2/64-66	440.35	3498.52	-9.00	-	18.6016	15.5771	38.5859	-	-	-	-	-
	47X-2/121-124	440.92	3506.96	-8.51	0.709125	-	-	-	-	-	-	-	-
	47X-7/26-29	446.56	3590.48	-10.83	-	18.6680	15.5920	38.6794	-	-	-	-	-
	48X-2/144-146	450.32	3749.89	-10.77	-	18.7351	15.6102	38.7649	-	-	-	-	-
	49X-2/74-76	459.75	4187.00	-9.09	-	18.5896	15.5774	38.5898	-	-	-	-	-
	50X-3/3-5	470.24	4653.75	-9.72	0.709732	18.6347	15.5866	38.6561	-11.41	0.716791	18.6720	15.5831	38.7447
	51X-1/145-147	478.26	4777.86	-9.96	-	18.6315	15.6113	38.7212	-	-	-	-	-
	51X-6/ 68.5-70	484.99	4882.02	-10.59	-	18.6718	15.5857	38.6764	-	-	-	-	-
	52X-3/28-30	489.04	4944.69	-11.41	-	18.7029	15.5964	38.7838	-	-	-	-	-
	52X-5/73-75	492.42	4997.00	-10.61	-	18.7240	15.6191	38.8212	-12.83	0.718896	18.7189	15.5830	38.9114
	52X-7/105-107	495.4	5055.43	-9.84	-	18.6477	15.5874	38.6739	-	-	-	-	-
	53X-1/41-43	496.62	5079.35	-9.73	0.710127	18.6856	15.5824	38.6837	-11.80	0.718673	18.5413	15.5640	38.6170
	53X-2/23-25	497.18	5090.33	-10.47	-	18.6737	15.5461	38.5680	-	-	-	-	-

Table A.4 (continued)

Location	Core section	Depth [m]	Age [ka]	*leach fraction (leach method B)*					*detrital fraction*				
				ε_{Nd}	$^{87}Sr/^{86}Sr$	$^{206}Pb/^{204}Pb$	$^{207}Pb/^{204}Pb$	$^{208}Pb/^{204}Pb$	ε_{Nd}	$^{87}Sr/^{86}Sr$	$^{206}Pb/^{204}Pb$	$^{207}Pb/^{204}Pb$	$^{208}Pb/^{204}Pb$
	53X-2/140-142	498.35	5113.27	-9.38	-	18.6833	15.6008	38.7404	-	-	-	-	-
	53X-3/39-41	498.84	5122.88	-11.54	-	18.7225	15.5993	38.7681	-	-	-	-	-
	53X-5/36-38	501.55	5176.02	-10.89	-	18.6800	15.5940	38.7715	-	-	-	-	-
	53X-6/65-67	503.21	5208.57	-9.73	-	18.6619	15.5774	38.6676	-	-	-	-	-
	53X-7/67-69	504.49	5233.67	-11.00	0.710144	18.7310	15.5619	38.6305	-12.38	0.718226	18.7323	15.5976	38.8083
	53X-8/37-39	505.65	5256.41	-10.92	-	18.6688	15.5771	38.6851	-	-	-	-	-

Table A.5 (suppl. Chapter 5): Nordic Sea and North Atlantic Ocean down core leachate and bulk digest isotope data of Site 986, 644 and 982

				leach fraction (leach method A)					*detrital fraction*				
Location	**Core section**	**Depth [m]**	**Age [ka]**	**ε_{Nd}**	**$^{87}Sr/^{86}Sr$**	**$^{206}Pb/^{204}Pb$**	**$^{207}Pb/^{204}Pb$**	**$^{208}Pb/^{204}Pb$**	**ε_{Nd}**	**$^{87}Sr/^{86}Sr$**	**$^{206}Pb/^{204}Pb$**	**$^{207}Pb/^{204}Pb$**	**$^{208}Pb/^{204}Pb$**
Western shelf of Svalbard; 2051 m water depth; 77°20.431' N 09°04.664' E leg/**site** 162/**986**	C/1H-1/0-2	0.0	0.0	-10.16	0.709656	18.7825	15.6427	38.6938	-11.31	0.720987	18.8473	15.6330	38.7989
	C/6H-5/72-74	52.2	321.3	-8.66	0.708911	18.6859	15.5975	38.7099	-	-	-	-	-
	C/7H-3/74-76	58.0	356.9	-10.28	0.709908	18.9653	15.6304	38.8576	-	-	-	-	-
	C/8H-7/74-76	70.2	431.6	-10.35	-	18.5188	15.5760	38.7421	-15.18	0.719432	18.7519	15.5758	39.2925
	C/10X-1/74-76	81.3	500.2	-9.76	0.712254	18.6279	15.5816	38.7283	-	-	-	-	-
	C/13X-4/74-76	114.7	705.6	-11.76	0.712575	20.1293	15.7613	39.5326	-	-	-	-	-
	C/14X-4/74-76	123.7	760.6	-10.30	-	19.2020	15.6690	38.9854	-	-	-	-	-
	C/15X-1/74-76	129.5	806.0	-10.04	0.710806	19.1179	15.6399	39.0960	-	-	-	-	-
	C/15X-3/74-76	132.0	830.6	-9.22	-	19.1891	15.6640	39.1384	-	-	-	-	-
	C/15X-4/74-76	133.5	845.4	-9.40	-	18.9799	15.6410	38.9220	-11.75	0.725808	18.8974	15.6220	38.8401
	C/16X-2/74-76	140.4	913.0	-9.79	-	19.1352	15.6440	39.0755	-	-	-	-	-
	C/16X-5/74-76	144.9	957.3	-11.20	0.710807	19.1810	15.6669	38.9844	-	-	-	-	-
	C/17X-2/74-76	150.3	1003.6	-8.46	0.709009	18.7488	15.6077	38.7532	-	-	-	-	-
	duplicate	*150.3*	*1003.6*	*-8.66*	*0.708966*	*18.7457*	*15.6071*	*38.7447*	-	-	-	-	-
	C/19X-2/74-76	169.6	1132.5	-8.79	-	18.8848	15.6196	38.8530	-	-	-	-	-
	duplicate	*169.6*	*1132.5*	*-8.79*	*0.709977*	*18.8876*	*15.6245*	*38.8663*	-	-	-	-	-
	C/20X-2/74-76	179.3	1197.2	-9.22	0.710603	19.1047	15.6522	39.0101	-	-	-	-	-
	D/6R-1/72-74	436.6	1457.3	-9.46	0.710397	18.9215	15.6279	38.8686	-	-	-	-	-
	D/9R-1/23-25	464.9	1512.5	-10.44	0.711053	18.7833	15.5959	38.7539	-14.05	0.728950	18.9226	15.6075	39.0742
	D/14R-4/74-76	517.9	1616.0	-10.07	-	18.9693	15.6382	38.9396	-	-	-	-	-
	D/16R-4/56-58	537.0	1653.1	-9.54	0.709213	18.5808	15.5774	38.6071	-	-	-	-	-
	D/17R-4/22-24	546.2	1671.2	-9.35	-	18.7213	15.5963	38.7368	-	-	-	-	-
	D/19R-2/53-55	562.7	1714.0	-10.96	0.710181	18.7334	15.5926	38.7559	-	-	-	-	-
	C/31X-1/28-30	273.5	1825.7	-10.06	-	19.0162	15.6400	38.9299	-	-	-	-	-

Table A.5 (continued)

Location	Core section	Depth [m]	Age [ka]	*leach fraction (leach method A)*					*detrital fraction*				
				ε_{Nd}	$^{87}Sr/^{86}Sr$	$^{206}Pb/^{204}Pb$	$^{207}Pb/^{204}Pb$	$^{208}Pb/^{204}Pb$	ε_{Nd}	$^{87}Sr/^{86}Sr$	$^{206}Pb/^{204}Pb$	$^{207}Pb/^{204}Pb$	$^{208}Pb/^{204}Pb$
	C/31X-5/28-30	279.5	1865.7	-9.72	0.711023	18.9951	15.6375	38.9262	-	-	-	-	-
	C/34X-2/52-54	304.1	2030.1	-11.59	0.714148	18.5845	15.5805	38.8196	-13.53	0.729752	18.7842	15.5910	39.1962
	duplicate	*304.1*	*2030.1*	*-12.16*	*0.714289*	*18.6950*	*15.5964*	*38.8629*	-	-	-	-	-
	C/35X-2/27-29	313.5	2092.8	-11.04	-	18.4210	15.5563	38.7467	-	-	-	-	-
	C/37X-5/24-26	336.0	2243.2	-9.89	-	18.8726	15.6237	38.9119	-	-	-	-	-
	C/38X-3/120-122	344.8	2301.8	-10.86	0.712657	18.4519	15.5611	38.6802	-	-	-	-	-
	C/39X-4/130-132	356.0	2376.7	-9.11	0.712474	18.9069			-	-	-	-	-
	C/40X-2/23-25	361.5	2413.5	-11.07	0.712776	18.4862	15.5697	38.7161	-15.23	0.726463	18.7855	15.5905	39.1082
	C/41X-5/23-25	375.6	2507.6	-10.28	0.710447	19.4313	15.6799	39.1632	-	-	-	-	-
	C/42X-1/72-74	379.8	2535.7	-10.63	0.711733	18.7180	15.5882	38.7506	-	-	-	-	-
	D/50R-5/74-76	865.5	2676.4	-10.16	-	18.8701	15.6030	38.8218	-	-	-	-	-
	D/51R-7/52-54	877.6	2691.2	-10.85	0.710381	18.7976	15.6001	38.7558	-11.45	0.719824	18.6404	15.5760	38.6335
	D/53R-5/123-125	894.8	2712.4	-10.74	-	18.7509	15.5969	38.7454	-	-	-	-	-
	duplicate	*894.8*	*2712.4*	*-10.47*	*0.710240*	*18.7520*	*15.5943*	*38.7407*	-	-	-	-	-
	D/55R-2/74-76	909.1	2730.0	-9.46	0.710381	18.8630	15.6141	38.8601	-	-	-	-	-
	D/58R-1/74-76	936.4	3009.8	-8.97	0.711382	19.0260	15.6757	39.0059	-	-	-	-	-
	duplicate	*936.4*	*3009.8*	*-8.77*	*0.711942*	*19.0076*	*15.6477*	*38.9626*	-	-	-	-	-
Vøring Plateau, Norwegian shelf; 1220 m water depth; 66°40.700'N 04°34.600'E	1H-1/2-6	0.0	0.0	-9.59	-	18.9497	15.6680	38.7915	-11.26	0.721425	18.8842	15.6379	38.6858
	4H-1/64-66	26.3	237.7	-8.35	0.709412	19.0209	15.6489	38.8411	-	-	-	-	-
	4H-1/102-104	26.7	241.3	-8.68	-	19.1225	15.6568	38.9163	-	-	-	-	-
	4H-1/142-144	27.1	244.9	-6.13	0.710648	19.3976	15.6888	39.0978	-	-	-	-	-
	5H-4/22-24	39.9	360.5	-11.18	0.710298	19.2011	15.6589	38.9197	-	-	-	-	-
	duplicate	*39.9*	*360.5*	*-11.48*	*0.710298*	*19.2123*	*15.6611*	*38.9262*	-	-	-	-	-
	6H-2/22-24	46.4	419.2	-10.55	0.710032	19.6921	15.7311	39.2545	-	-	-	-	-

Table A.5 (continued)

Location	Core section	Depth [m]	Age [ka]	*leach fraction (leach method A)*					*detrital fraction*				
				ε_{Nd}	$^{87}Sr/^{86}Sr$	$^{206}Pb/^{204}Pb$	$^{207}Pb/^{204}Pb$	$^{208}Pb/^{204}Pb$	ε_{Nd}	$^{87}Sr/^{86}Sr$	$^{206}Pb/^{204}Pb$	$^{207}Pb/^{204}Pb$	$^{208}Pb/^{204}Pb$
leg/**site**/core 104/**644**/A	8H-1/23-25	63.9	577.1	-11.12	0.708865	19.6605	15.7303	39.2176	-13.24	0.733083	19.3798	15.6875	39.0114
	duplicate	*63.9*	*577.1*	*-11.37*	*0.708865*	*19.5320*	*15.7144*	*39.1023*	-	-	-	-	-
	8H-2/40-42	65.6	592.4	-10.91	-	20.0143	15.7698	39.3924	-	-	-	-	-
	8H-6/22-24	71.4	644.9	-9.23	0.709265	19.3456	15.6894	39.0378	-	-	-	-	-
	10H-2/122-124	85.4	766.0	-8.42	0.709378	18.9582	15.6434	38.8184	-	-	-	-	-
	10H-3/78-80	86.5	774.4	-6.92	-	18.8229	15.6167	38.7207	-11.99	0.722602	18.8082	15.6131	38.7491
	duplicate	*86.5*	*774.4*	-	*0.709432*	*18.8303*	*15.6236*	*38.7350*	-	-	-	-	-
	11H-4/80-82	97.5	861.1	-9.62	-	19.4145	15.6828	39.0473	-	-	-	-	-
	11H-6/97-99	100.7	886.2	-7.67	0.709547	19.5385	15.7046	39.1445	-	-	-	-	-
	13H-4/42-44	116.1	1047.5	-8.41	0.709631	18.9184	15.6577	38.6487	-	-	-	-	-
	13H-6/62-64	119.3	1086.4	-9.32	-	19.3509	15.6895	39.0410	-	-	-	-	-
	14H-3/60-62	123.3	1134.9	-11.11	0.709772	18.9345	15.6152	38.9577	-15.25	0.725116	18.7412	15.5770	38.7330
	14H-4/82-84	126.0	1167.7	-7.37	0.709636	19.2252	15.6814	39.0080	-	-	-	-	-
	duplicate	*126.0*	*1167.7*	*-8.19*	*0.709390*	*19.2148*	*15.6727*	*38.9839*	-	-	-	-	-
	15H-1/12-14	131.4	1233.3	-6.82	0.709372	19.0860	15.6569	38.8955	-	-	-	-	-
	15H-3/122-124	134.2	1267.3	-8.36	-	19.1616	15.6601	38.9610	-	-	-	-	-
	16H-5/120-122	146.9	1421.5	-10.43	0.709294	19.1435	15.6709	38.9339	-	-	-	-	-
	duplicate	*146.9*	*1421.5*	*-10.08*	*0.709383*	*19.2565*	*15.6141*	*38.7645*	-	-	-	-	-
	17H-2/62-64	151.3	1474.9	-7.45	-	19.2775	15.6841	39.0302	-	-	-	-	-
	18H-1/142-144	159.9	1579.4	-8.92	-	19.0854	15.6480	38.9208	-	-	-	-	-
	18H-3/42-44	162.1	1606.1	-9.47	-	19.3160	15.6831	39.0455	-12.64	0.727102	19.1032	15.6472	38.8799
	19H-3/22-24	171.4	1736.4	-10.43	0.710093	19.9155	15.7544	39.3628	-	-	-	-	-
	19H-3/121-123	172.4	1751.8	-9.84	-	19.6656	15.7154	39.1951	-	-	-	-	-
	20H-3/82-84	181.3	1889.8	-8.58	0.709596	19.6671	15.7252	39.2469	-	-	-	-	-

Table A.5(continued)

Location	Core section	Depth [m]	Age [ka]	*leach fraction (leach method A)*					*detrital fraction*				
				ε_{Nd}	$^{87}Sr/^{86}Sr$	$^{206}Pb/^{204}Pb$	$^{207}Pb/^{204}Pb$	$^{208}Pb/^{204}Pb$	ε_{Nd}	$^{87}Sr/^{86}Sr$	$^{206}Pb/^{204}Pb$	$^{207}Pb/^{204}Pb$	$^{208}Pb/^{204}Pb$
	21H-1/22-24	184.6	1934.0	-	-	19.2254	15.6758	38.9664	-	-	-	-	-
	duplicate	*184.6*	*1934.0*	*-9.21*	*0.709115*	*19.2095*	*15.6681*	*38.9376*	-	-	-	-	-
	23H-2/42-44	196.0	2085.2	-9.71	0.709611	19.5458	15.7177	39.1697	-	-	-	-	-
	23H-5/120-122	201.3	2155.6	-10.17	0.709428	19.1849	15.6785	38.9787	-	-	-	-	-
	24H-4/16-18	205.2	2207.4	-9.73	0.709941	19.2400	15.6740	39.0205	-12.66	-	19.1073	15.6586	38.8935
	26H-2/62-64	212.6	2305.8	-7.20	0.709197	19.2186	15.6687	38.9918	-	-	-	-	-
	32H-1/102-104	239.1	2658.2	-6.30	-	18.9405	15.6295	38.7661	-	-	-	-	-
	33H-1/122-124	244.8	2733.9	-10.07	0.709059	18.9854	15.6401	38.8344	-	-	-	-	-
	34H-2/40-42	247.9	2774.8	-8.22	-	19.0406	15.6599	38.8761	-	-	-	-	-
	34H-6/100-102	253.0	2842.3	-9.67	0.709062	19.0347	15.6512	38.8936	-10.78	0.718474	19.0343	15.6433	38.8714
	34H- 6/122-124	253.2	2845.3	-9.75	0.709098	19.0247	15.6417	38.8795	-	-	-	-	-
Rockall Plateau; North Atlantic Ocean; 1135 m water depth; 57°30.992'N 15°52.001'W leg/**site**/core 162/**982**/A	1H-1/0-2	0.000	0	-10.99	0.709273	19.0421	15.6877	38.9471	-9.99	0.714350	18.9939	15.6744	38.8709
	1H-3/29-31	3.303	156	-8.35	-	19.2610	15.6791	39.0941	-	-	-	-	-
	1H-3/134-136	4.348	217	-8.04	0.709449	19.1914	15.6755	39.1971	-	-	-	-	-
	1H-6/38-40	7.887	365	-10.62	0.709045	20.0480	15.7697	39.4319	-	-	-	-	-
	2H-1/82-84	9.027	395	-6.08	-	19.4505	15.7039	39.1115	-9.42	0.717082	19.1514	15.6655	38.9281
	duplicate	*9.027*	*395*	*-6.52*	-	*19.2182*	*15.6740*	*39.2144*	-	-	-	-	-
	2H-5/31-33	14.512	548	-11.34	-	19.2202	15.6791	39.2447	-	-	-	-	-
	2H-5/84-86	15.040	575	-8.59	0.709411	18.9348	15.6346	38.9541	-	-	-	-	-
	3H-2/131-133	20.519	805	-10.95	0.709166	19.1195	15.6594	39.0722	-	-	-	-	-
	3H-3/134-136	22.048	850	-8.86	0.709213	19.4021	15.7055	39.3437	-	-	-	-	-
	3H-5/95-97	24.653	964	-10.53	-	19.1406	15.6770	39.1417	-	-	-	-	-
	3H-6/52-54	25.723	1022	-9.89	0.709326	19.1385	15.6738	39.1410	-	-	-	-	-
	duplicate	*25.723*	*1022*	*-9.93*	*0.709496*	*19.1319*	*15.6664*	*39.1152*	-	-	-	-	-

Table A.5 (continued)

Location	Core section	Depth [m]	Age [ka]	*leach fraction (leach method A)*					*detrital fraction*				
				ε_{Nd}	$^{87}Sr/^{86}Sr$	$^{206}Pb/^{204}Pb$	$^{207}Pb/^{204}Pb$	$^{208}Pb/^{204}Pb$	ε_{Nd}	$^{87}Sr/^{86}Sr$	$^{206}Pb/^{204}Pb$	$^{207}Pb/^{204}Pb$	$^{208}Pb/^{204}Pb$
	4H-1/7-9	27.274	1072	-10.25	-	19.7828	15.7437	39.3818	-	-	-	-	-
	4H-2/52-54	29.228	1135	-11.84	-	19.0376	15.6745	39.1504	-	-	-	-	-
	4H-2/100-102	29.706	1172	-12.03	0.709164	19.1304	15.6764	39.1943	-11.38	0.717431	18.8480	15.6294	38.9051
	4H-2/131-133	30.011	1198	-9.65	0.709372	19.2268	15.6806	39.2000	-	-	-	-	-
	4H-3/10-12	30.300	1234	-12.99	-	19.1833	15.6852	39.1973	-	-	-	-	-
	4H-5/85-87	34.059	1462	-12.67	0.709135	18.9497	15.6655	38.8795	-9.11	0.709517	18.9596	15.6646	38.9547
	duplicate	*34.059*	*1462*	*-12.36*	*0.709085*	*19.0217*	*15.6726*	*39.0757*	-	-	-	-	-
	4H-5/121-123	34.412	1490	-10.74	0.709124	19.0214	15.6739	39.0725	-	-	-	-	-
	duplicate	*34.412*	*1490*	*-10.51*	*0.709053*	*18.9497*	*15.6655*	*38.8795*	-	-	-	-	-
	5H-1/113-115	37.839	1670	-11.19	-	18.9863	15.6622	39.0857	-	-	-	-	-
	5H-2/6-8	38.268	1700	-9.57	0.709126	18.9328	15.6544	38.9667	-4.09	0.712678	18.7564	15.6229	38.7819
	5H-3/79-81	40.490	1795	-9.14	0.709098	18.9734	15.6629	38.9982	-	-	-	-	-
	5H-3/127-129	40.975	1830	-10.69	0.710420	18.9520	15.6379	38.9169	-	-	-	-	-
	5H-4/27-29	41.473	1862	-10.72	0.710201	18.8647	15.6333	38.8230	-	-	-	-	-
	5H-7/3-5	45.734	2065	-10.34	0.709111	18.9486	15.6451	38.9069	-	-	-	-	-
	6H-1/128-130	47.483	2135	-10.90	0.709034	18.8302	15.6237	38.7650	-	-	-	-	-
	6H-3/29-31	49.494	2280	-10.20	0.709047	19.0375	15.6621	39.0561	-	-	-	-	-
	6H-3/72-74	49.922	2305	-10.96	0.709061	18.9008	15.6399	38.8272	-8.70	0.710014	18.9306	15.6574	38.9153
	6H-4/138-140	52.083	2432	-11.38	0.709056	18.9787	15.6533	38.8720	-	-	-	-	-
	6H-5/62-64	52.827	2463	-9.88	0.709065	18.8942	15.6412	38.8307	-	-	-	-	-
	6H-6/78-80	54.485	2520	-11.08	0.708999	18.9618	15.6666	38.9190	-	-	-	-	-
	6H-7/18-20	55.375	2550	-10.62	-	18.9828	15.6735	38.9437	-	-	-	-	-
	7H-2/85-87	58.056	2645	-10.72	0.709039	18.6351	15.6388	38.5531	-	-	-	-	-
	7H-3/33-35	59.032	2680	-10.78	0.709036	19.0003	15.6714	38.9425	-	-	-	-	-

Table A.5 (continued)

Location	Core section	Depth [m]	Age [ka]	*leach fraction (leach method A)*					*detrital fraction*				
				ε_{Nd}	$^{87}Sr/^{86}Sr$	$^{206}Pb/^{204}Pb$	$^{207}Pb/^{204}Pb$	$^{208}Pb/^{204}Pb$	ε_{Nd}	$^{87}Sr/^{86}Sr$	$^{206}Pb/^{204}Pb$	$^{207}Pb/^{204}Pb$	$^{208}Pb/^{204}Pb$
	7H-4/3-5	60.249	2715	-9.43	-	18.8516	15.5528	38.5901	-	-	-	-	-
	duplicate	*60.249*	*2715*	*-9.80*	*0.709080*	*18.8225*	*15.4966*	*38.4581*	-	-	-	-	-
	7H-4/117-119	61.364	2743	-10.42	0.709202	18.9327	15.6328	38.8352	-	-	-	-	-
	8H-1/49-51	65.697	2975	-10.21	0.709019	18.9530	15.6532	38.8962	-	-	-	-	-

Danksagung

Zuerst möchte ich mich natürlich bei Prof. Dr. Martin Frank bedanken, dessen Tür immer für mich offen stand und auf dessen Rat ich mich stets verlassen konnte. Ich möchte dir dafür danken, dass du mich immer motivieren konntest, wenn ich mal das Ziel aus den Augen und den Mut verloren habe.

Brian A. Haley möchte ich dafür danken, dass er es mir ermöglicht hat in diesem Projekt zu arbeiten und natürlich immer mit guten, neuen Anregungen und Verbesserungsvorschlägen geholfen hat, wenn es auch über die Entfernung nicht immer ganz einfach war. Dr. Jochen Knies möchte danken für die Bereitstellung eines Teils der Proben und natürlich für die vielen hilfreichen Anmerkungen und Kommentare. Bei Prof. Dr. Anton Eisenhauer bedanke ich mich dafür, dass er sich meiner Arbeit als Zweitbetreuer angenommen hat.

Roland, Torben I, Paddy und Ed danke ich für die geduldigen Lehrstunden, die Hilfe im Labor sowie an der Maschine und natürlich für die schöne Zeit außerhalb des Geomars, auf Tagungen, im Urlaub, auf Ausfahrt und beim Bier (Glühwein) trinken. Kirstin und Torben II. danke ich für die aufschlussreichen Diskussionen über unser Lieblingsthema, die Fram Straße und die Nordic Seas. Danke natürlich auch an den Rest der Arbeitsgruppe: Janett, Moritz, Anne, Nabil, Tianyu und Jan, der mir gerade zum Ende sehr geholfen hat, und allen anderen, die ich nicht namentlich erwähnt habe.

Außerdem möchte ich mich bei Jutta bedanken. Egal was man für das Labor oder Büro benötigte, sie hat es entweder irgendwo gelagert, gefunden oder gebastelt. Und natürlich, dass sie einen immer mit Kaffee, Keksen oder anderen Kleinigkeiten versorgt, wenn es abends mal wieder später geworden ist.

Steffie und Claudia danke ich für die letzten zehn Jahre, die wir uns erst zusammen durchs Studium und dann durch die Doktorarbeit gekämpft haben, für die vielen leckeren Kuchen und die gute Zeit auf der Ausfahrt.

Besonderer Dank gilt Kristin, die während der letzten vier Jahre einen ganz besonderen Platz in meinem Leben eingenommen hat. Ohne dich hätte die Wissenschaft nur halb so viel Spaß gemacht. Danke für die gute Zeit auf der Ausfahrt, in Trinidad und Tobago und im Büro, wo wir uns so manchen Abend um die Ohren geschlagen haben!

Außerdem möchte ich meiner Familie danken, ohne deren Unterstützung und Liebe, ich bestimmt nicht so weit gekommen wäre. Danke, dass ihr mich immer ermutigt habt. Ihr seid die Besten!

Michi möchte dafür danken, dass er immer Verständnis gezeigt hat, mich unterstützt, mir zuhört, immer einen ehrlichen Rat für mich hat und dass er immer für mich da ist. Und natürlich für unsere kleine Räubertochter, die mich am Ende immer wieder neu motiviert hat und mich durch kleine Tritte zum Durchhalten ermutigt hat.

Vielen Dank!